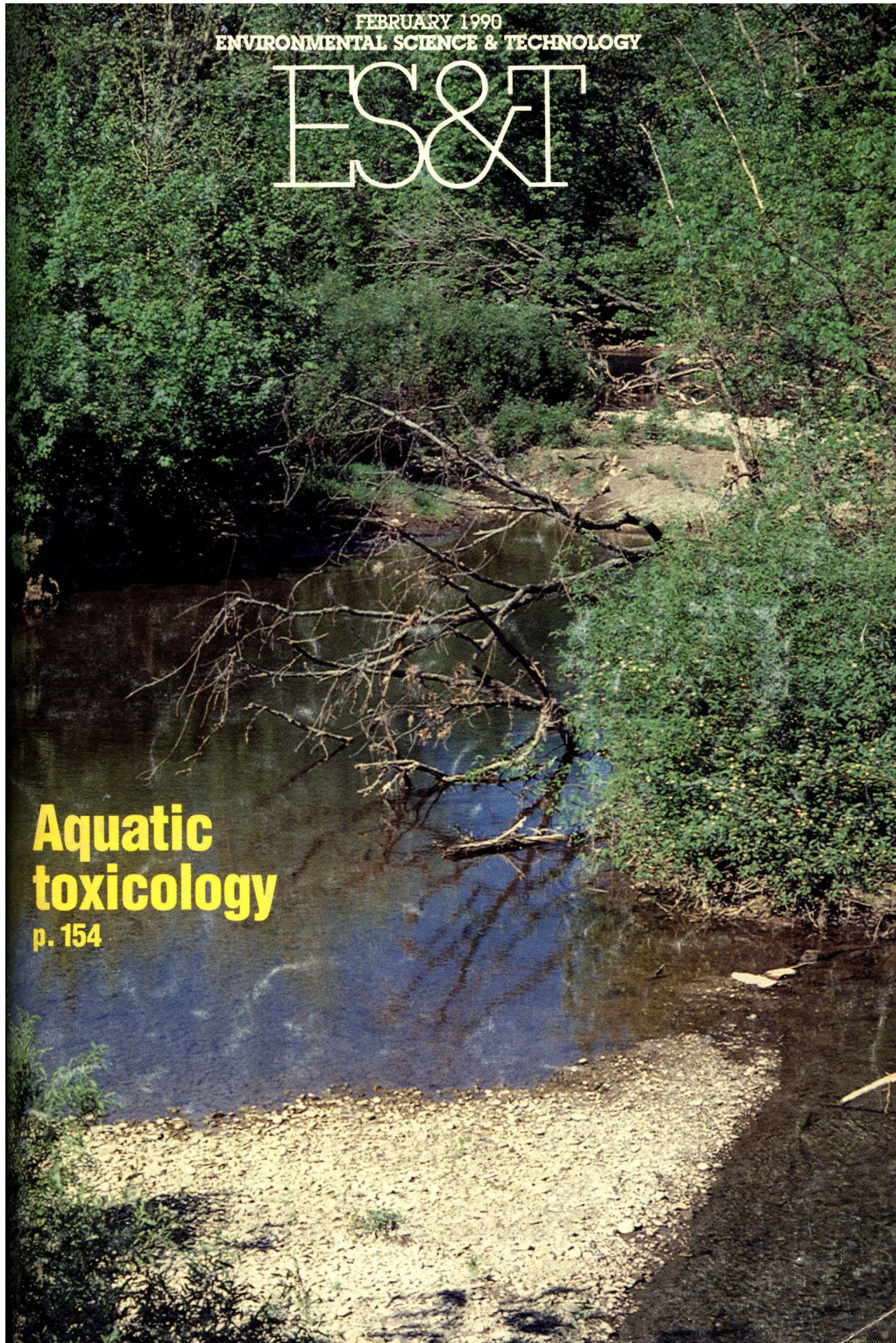


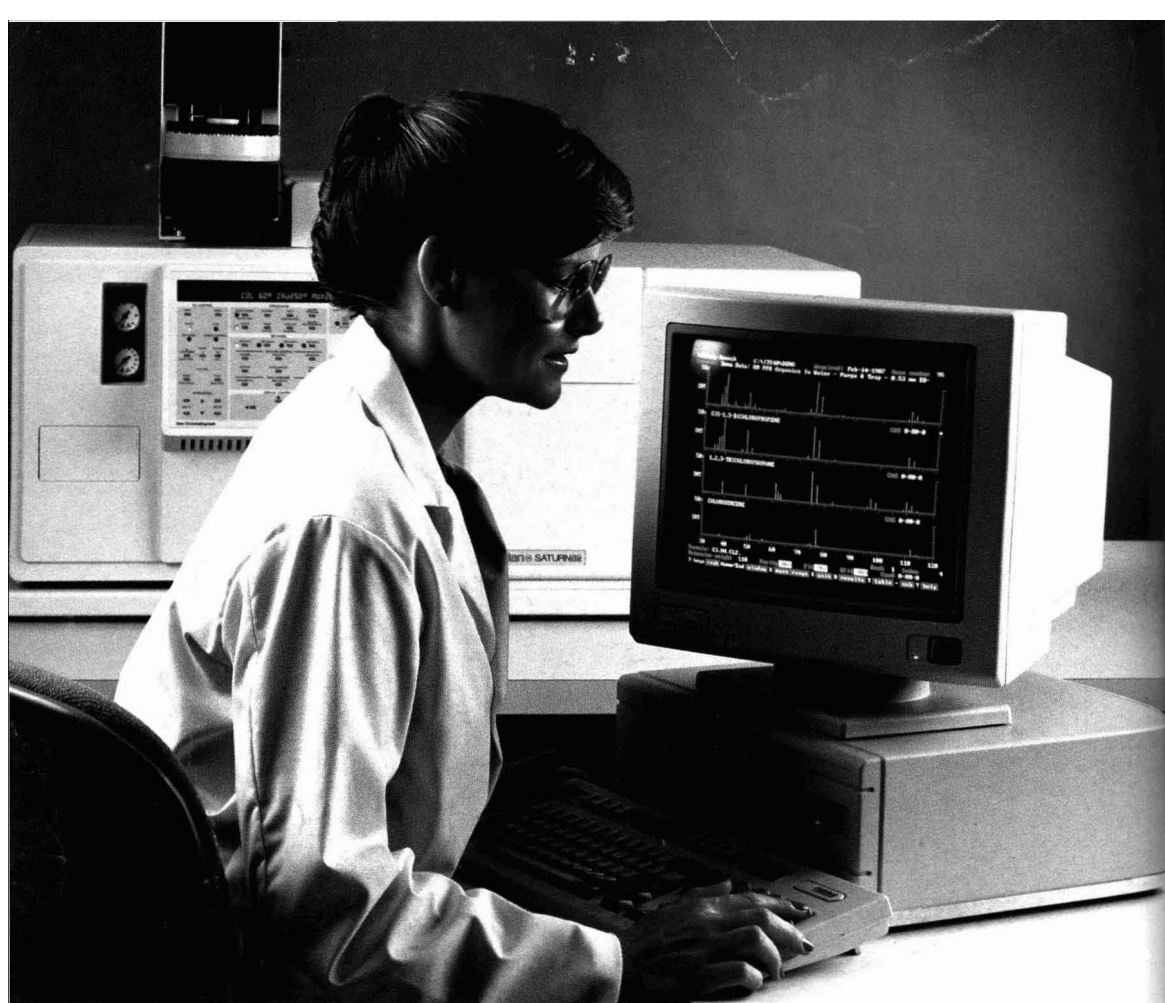
FEBRUARY 1990  
ENVIRONMENTAL SCIENCE & TECHNOLOGY

ES&T

**Aquatic  
toxicology**

p. 154





# THE FUTURE OF GC/MS IS WITH VARIAN.

The best GC/MS, now and in the future, starts with chromatographic excellence. After all, if you don't start with expert chromatographic techniques, how can you trust the final results? Look to the company known for its expertise — from sample handling to the most sensitive detection — Varian.

The combination of our proven 3400 Gas Chromatograph with second generation ion trap technology brings the most sensitive and reliable benchtop GC/MS to the market.

The new Varian Saturn GC/MS System gives picture perfect spectra even at picogram levels, a significant advantage over conventional benchtop quadrupoles. It's important to know that you can count on the Saturn GC/MS to give you the whole picture when you're confirming compounds, because you're doing scientific analyses that affect our environment, our health, the products we use, and must meet regulatory protocols.

Chromatographic excellence and the most sensitive mass spec detector, coupled with Varian's renowned service and support throughout the world, make this the GC/MS with a future.

Let us show you why you should invest your GC/MS future with Varian. For more information, call **800-231-8134**. In Canada, call **416-457-4130**.

**See you at Pittsburgh Conference, Booth 4736-4934 & 5042.**

CIRCLE 8 ON READER SERVICE CARD

GC WITH A FUTURE

**varian**®

Editor: William H. Glaze  
Associate Editors: Walter Giger, Ronald A. Hites, John H. Seinfeld, Philip C. Singer, Joseph Suflita

#### ADVISORY BOARD

Roger Atkinson, Joan M. Daisey, Fritz H. Frimmel, George R. Helz, Ralph Mitchell, Joseph M. Norbeck, Jerald L. Schnoor, Walter J. Weber, Jr., Alexander J. B. Zehnder, Richard G. Zopp

#### WASHINGTON EDITORIAL STAFF

Managing Editor: Stanton S. Miller  
Associate Editor: Julian Josephson

#### MANUSCRIPT REVIEWING

Manager: Yvonne D. Curry  
Associate Editor: Diane Scott  
Assistant Editor: Marie C. Wiggins  
Editorial Assistant: Bryan D. Tweedy

#### MANUSCRIPT EDITING

Journals Editing Manager: Mary E. Scanlan  
Associate Editor: Lorraine Gibb

Director, Operational Support:  
C. Michael Phillippe

#### GRAPHICS AND PRODUCTION

Head, Production Department: Leroy L. Corcoran

Art Director: Alan Kahan  
Designer: Peggy Corrigan  
Production Editor: Lennie Reinhardt

#### PUBLICATIONS DIVISION

Director: Robert H. Marks  
Head, Special Publications Department:  
Randall E. Wedin

Head, Journals Department: Charles R. Bertsch

#### ADVERTISING MANAGEMENT

Centcom, Ltd.

For officers and advertisers, see page 187.

Please send *research* manuscripts to Manuscript Reviewing, *feature* manuscripts to Managing Editor. For editorial policy, author's guide, and peer review policy, see the January 1990 issue, page 41, or write Yvonne D. Curry, Manuscript Reviewing Office, *ES&T*. A sample copyright transfer form, which may be copied, appears on the inside back cover of the January 1990 issue.

*Environmental Science & Technology*, *ES&T* (ISSN 0013-936X), is published monthly by the American Chemical Society at 1155 16th Street, N.W., Washington, D.C. 20036. Second-class postage paid at Washington, D.C., and at additional mailing offices. POSTMASTER: Send address changes to *Environmental Science & Technology*, Membership & Subscription Services, P.O. Box 3337, Columbus, Ohio 43210.

**SUBSCRIPTION PRICES 1990:** Members, \$36 per year; nonmembers (for personal use), \$67 per year; institutions, \$276 per year. Foreign postage, \$14 additional for Canada and Mexico, \$29 additional for Europe including air service, and \$36 additional for all other countries including air service. Single issues, \$23 for current year; \$24 for prior years. Back volumes, \$282 each. For foreign rates add \$3 for single issues and \$14 for back volumes. Rates above do not apply to nonmember subscribers in Japan, who must enter subscription orders with Maruzen Company Ltd., 3-10 Nihon bashi 2 chome, Chuo-ku, Tokyo 103, Japan. Tel: (03) 272-7211.

**COPYRIGHT PERMISSION:** An individual may make a single reprographic copy of an article in this publication for personal use. Reprographic copying beyond that permitted by Section 107 or 108 of the U.S. Copyright Law is allowed, provided that the appropriate per-copy fee is paid through the Copyright Clearance Center, Inc., 27 Congress St., Salem, Mass. 01970. For reprint permission, write Copyright Administrator, Publications Division, ACS, 1155 16th St., N.W., Washington, D.C. 20036.

**REGISTERED NAMES AND TRADEMARKS,** etc., used in this publication, even without specific indication thereof, are not to be considered unprotected by law.

**SUBSCRIPTION SERVICE:** Orders for new subscriptions, single issues, back volumes, and microform editions should be sent with payment to Office of the Treasurer, Financial Operations, ACS, 1155 16th St., N.W., Washington, D.C. 20036. Phone orders may be placed, using VISA, MasterCard, or American Express, by calling the ACS Sales Office at (614) 447-3776 or toll free (800) 333-9511 from anywhere in the continental U.S. (In the Washington, D.C., area call 872-4600.) Changes of address, subscription renewals, claims for missing issues, and inquiries concerning records and accounts should be directed to Manager, Membership and Subscription Services, ACS, P.O. Box 3337, Columbus, Ohio 43210. Changes of address should allow six weeks and be accompanied by old and new addresses and a recent mailing label. Claims for missing issues will not be allowed if loss was due to insufficient notice of change of address, if claim is dated more than 90 days after the issue date for North American subscribers or more than one year for foreign subscribers, or if the reason given is "missing from files."

The American Chemical Society assumes no responsibility for statements and opinions advanced by contributors to the publication. Views expressed in editorials are those of the author and do not necessarily represent an official position of the society.

# CONTENTS

Volume 24, Number 2, February 1990

## FEATURES



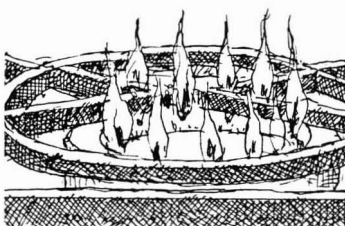
154

**Aquatic toxicology.** Part two of a four-part series on ecotoxicology. John Cairns, Jr., Virginia Polytechnic Institute and State University, Blacksburg, VA; and Donald I. Mount, EPA Environmental Research Laboratory, Duluth, MN.

162

**The role of genes in biological processes.** Part 2 of a two-part article. Barth F. Smets, Bruce E. Rittmann, and David A. Stahl, University of Illinois, Urbana, IL.

## VIEWS



170

**Slowing global warming.** Christopher Flavin discusses the current situation and proposed strategies.

172

**Investigation and remediation of VOCs in soil and groundwater.** James M. Kerr, Jr., presents an overview.

## REGULATORY FOCUS

177

**A unified approach to environmental quality.** Alvin L. Alm suggests ways to improve the current environmental control regime.

## DEPARTMENTS

149 Editorial

151 Currents

175 Environmental index

178 Products

183 Books

185 Classified

187 Consulting services directory

## UPCOMING

**Wildlife toxicology—the third article of a five-part series on ecotoxicology**  
**Using QSARs to determine chemical toxicity to aquatic species**

## RESEARCH

189

**Comparison of diesel engine exhaust using chromatographic profiling techniques.** Patricia A. Partridge,\* Francis J. Shala, Nicholas P. Cernansky, and Irwin H. Suffet

An analytical method, developed for examining changes in the intensity and number of chemical compounds in the odorless fraction of diesel exhaust, is applied to a variety of diesel engine systems.

■ 195

**Binding site analysis using linear programming.** Pierre Brassard, James R. Kramer,\* and Pamela V. Collins

Binding sites are ascertained by fitting a multiple mono-metal model to titration data using linear programming.

ESTHAG 24(2)147-268 (1990)  
ISSN 0013 936X

Cover: *ES&T*'s Julian Josephson

Credits: p. 164, J.A.W. Morgan, University of Liverpool, U.K.

201

**Enzymatic method for the determination of formaldehyde.** Mat H. Ho\* and Rex A. Richards

A sensitive method for the determination of formaldehyde using two sequential reactions catalyzed by two enzymes is described.

205

**Effect of some petroleum sulfonate surfactants on the apparent water solubility of organic compounds.** Daniel E. Kile, Cary T. Chou,\* and Robin S. Helburn

Commercial petroleum sulfonate surfactants as mixtures of sulfonated hydrocarbons and free mineral oils form stable emulsions in water that strongly enhance organic solute solubility.

208

**Sedimentary coprostanol as an index of sewage addition in Santa Monica Basin, southern California.** Mahalakshmi I. Venkatesan\* and Isaac R. Kaplan

Sediment cores from Santa Monica Basin and effluent from two major municipal wastewater dischargers in southern California are analyzed for sterols.

214

**Calcium molybdate solubility in spent oil shale and a preliminary evaluation of the association constants for the formation of  $\text{Ca-MoO}_4^0(\text{aq})$ ,  $\text{KMoO}_4^-(\text{aq})$ , and  $\text{Na-MoO}_4^-(\text{aq})$ .** Michael E. Essington

The results of this study are used to assess the occurrence of  $\text{CaMoO}_4$  (c) in spent oil shales and to evaluate the occurrence of various soluble molybdenum species.

220

**Binding of metal ions by particulate biomass derived from *Chlorella vulgaris* and *Scenedesmus quadricauda*.** Patricia O. Harris and Gerald J. Ramelow\*

Factors affecting the binding of silver, copper, cadmium, and zinc ions in aqueous solution by two strains of green algae are studied.

228

**Mobility of plutonium and americium through a shallow aquifer in a semiarid region.** William R. Penrose, Wilfred L. Polzer, Edward H. Essington, Donald M. Nelson, and Kent A. Orlandini\*

The subsurface transport of trace levels of actinides is shown to occur over kilometer distances and is correlated with the presence of aqueous colloidal materials.

234

**Kinetic approach to trace metal complexation in seawater: Application to zinc and cadmium.** François L. L. Muller and Dana R. Kester\*

The electrochemical and ion-exchange measurements of a metal in seawater are related to its speciation through the concept of "time of measurement."

242

**Kinetics of trace metal complexation: Ligand-exchange reactions.** Janet G. Hering and François M. M. Morel\*

Ligand-exchange reactions of humate-bound copper are compared with reactions of model ligands; the correspondence of equilibrium and kinetic constants is discussed.

252

**A conceptual model of organic chemical volatilization at waterfalls.** Michael McLachlan, Donald Mackay,\* and Philip H. Jones

A method for calculating volatilization rates at waterfalls is suggested.

258

**Characterization of mercury, arsenic, and selenium in the product streams of a bench-scale, inert-gas, oil shale retort.** K. B. Olsen,\* J. C. Evans, D. S. Sklarew, J. S. Fruchter, D. C. Girvin, and C. L. Nelson

A study to determine the concentrations of mercury, arsenic, and selenium in raw shale, spent shale, and product streams from an instrumented 6-kg laboratory-scale retort using both types of shales is undertaken.

264

**Effect of hydrogen peroxide on the alkaline hydrolysis of carbon disulfide.** Scott Elliott

The peroxide anion  $\text{HO}_2^-$  attacks carbon disulfide as a nucleophile, accelerating losses when hydrogen peroxide is added to alkaline  $\text{CS}_2$  solutions.

#### CORRESPONDENCE

268

**Comment on "Homogeneous hydrolysis rate constants for selected chlorinated methanes, ethanes, and propanes."** Jack E. Barbash\* and Martin Reinhard

\*To whom correspondence should be addressed.

■ This article contains supplementary material in microform. See ordering instructions at end of paper.

## Communities

One of the predominant trends of human civilization over the past few centuries has been urbanization. Since 1920, the population of the United States has shifted from predominantly rural to urban, and similar shifts are being seen in other developed and less developed nations of the world. A very large number of Earth's people now live in huge cities, some of which are larger than the entire population of countries in the not too distant past. The advantages of this type of community organization were apparent even to ancient cultures such as pre-Columbian Americans, and those advantages still prevail. Clearly, the development of cities gave industry the work force it needed to expand and caused commerce and culture to flourish. Technology—particularly in the areas of civil engineering, transportation, and energy distribution—made it possible for cities to grow larger and for modern amenities such as electric power, mass transportation systems, food distribution, treated drinking water, sewage systems, and garbage collection to be available to the masses.

It is now evident, however, that the unrestrained growth of cities and in part, the failure of political systems to keep pace, have resulted in significant new problems for cities including drug and crime proliferation, enhanced environmental degradation, and dehumanization of personal relationships. Urban neighborhoods that were once vital have become pockets of poverty, disease, and depravation. These and other factors have caused some flight away from the very large cities as more people who have the means move to smaller communities or rural areas to escape high social and financial costs. Industries, commercial organizations, government offices, and individuals are seeking relief from the strains of urban living. The dream is often now to escape from the city. This in turn has caused cities to lose tax revenues and for some to enter a downward spiral that may eventually result in bankruptcy.


The new federalism of the present and penultimate presidential administrations in the United States has exacerbated the problems of the cities and is causing new stresses on small communities. Congress and the administrative branch have deprived communities of funds to address some of their problems—paradoxically, just when external forces are compelling com-

munities to conform to increasingly complex regulations. Many of these are in the environmental arena, including new regulations on the disposal of solid wastes, treatment of sewage and drinking water, and control of urban air pollution, to name only a few. Communities are now forced to deal with these problems, not only because of the pressure from federal agencies but from local groups of activists.

Citizens of small and rural communities are now beginning to realize that they are not exempt from the stresses of modern life. Indeed, sewage and drinking-water treatment and waste management are significantly less efficient in decentralized communities than in large cities, at least in principle. There is an economy of scale in these technologies that is placing almost unbearable economic stresses on small communities.

The degradation of the quality of life in large cities and the concomitant stresses on suburban and rural communities cannot go unattended. Federal government assistance, enlightened leadership at the state level, and new approaches are all needed. The new era of peaceful coexistence that we now seem to be entering, with its decreased need for defense spending, presents a unique opportunity to address social and environmental needs in the communities of the world. Now is the time for new thinking. How can we use advanced technology to extend services to people in decentralized communities, organize small and large communities to minimize and recycle their wastes, and adopt new energy and transportation technologies to lower environmental costs? A renewed commitment for the solution of these problems is needed at every level of government.





# By the time you get regulatory information, is it too late?

*Let Regulated  
Chemicals Listing  
(CHEMLIST) help.*

***There's a lot of regulations to know  
about these days—***

PMN, CHIP, PAIR, CAIR, SNUR, FYI, Section 12B to mention a few. One way for your staff to find the information they need concerning regulations on commercial chemicals is to review every issue of key sources such as the EPA TSCA Inventory, the Federal Register, Chemical Regulation Reporter, TSCA Chemicals-in-Progress Bulletin, TSCATS (TSCA Unpublished Test Submissions), and Pesticide & Toxic Chemical News.

***A better solution is to search online***

A faster, easier solution is to have your staff access Regulated Chemicals Listing (CHEMLIST) online. We've already reviewed the important sources and input the data to our database. And your staff will get current information—in general—not more than two weeks old.

***To get additional details about how  
searching Regulated Chemicals  
Listing (CHEMLIST) online can help  
your staff comply with government  
regulations, write to***

Chemical Abstracts Service, Dept. 31790,  
P.O. Box 3012, Columbus, OH 43210.

Regulated Chemicals Listing is produced by the American Petroleum Institute; is marketed by Chemical Abstracts Service, and is available online only through STN International.

**REGULATORY AND  
ENVIRONMENTAL AFFAIRS**



**STN**  
INTERNATIONAL  
The Scientific & Technical  
Information Network

# ES&T CURRENTS

## INTERNATIONAL

**Britain will establish a Centre for Climate Change Prediction**, Prime Minister Margaret Thatcher told the U.N. General Assembly. Its mission will be to predict future climate change. The center's predictions would be used as a basis for developing policies to control the greenhouse effect, Thatcher said. She added that the British government will commit the equivalent of \$160 million over the next three years for bilateral aid to tropical forestry activity. The emphasis will be on reducing deforestation, promoting reforestation, and improving management of existing tropical forests.

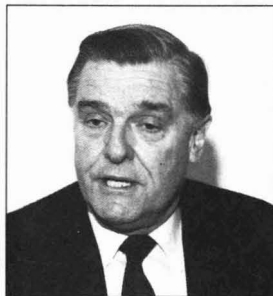
## FEDERAL

**EPA has referred 364 civil cases involving violations of environmental laws** to the Department of Justice (DOJ) during fiscal year 1989. This is slightly short of the all-time record of 372 cases sent to DOJ during FY 1988. In addition, EPA referred 60 criminal cases to DOJ during FY 1989. The mix of cases recently has shifted toward Superfund violations; the 153 cases referred to DOJ represent an increase of 34% over FY 1988. One reason for the increase is an enforcement-first policy EPA administrator William Reilly instituted last year. Enforcement actions under the Clean Water Act affected more municipal wastewater plants than in previous years (*Environ. Sci. Technol.* 1989, 23[12], 1436).

**The Food and Drug Administration (FDA) announced Dec. 13 that foods it surveyed contained no pesticides** or had pesticide residues well within legal limits. The survey was conducted during 1988. About 61% of more than 18,000 food products tested were found to be free of pesticides; another 34% showed pesticide content within permissible limits. Of the remainder, 4% were found to be not in compliance because of technical violations, and 1% contained pesticides above legal limits. This represents an improvement of about 5% over 1987, according to FDA spokespeople, who added that the agency's analytical

equipment can detect pesticides to levels as low as 10 ppb. Environmental advocates, however, say the survey technology and methods do not cover enough samples and are outdated.

**The Department of Energy is seeking "unique energy efficiency and renewable energy projects"** to complete its 1990 National Awards Program for Energy Innovation. Energy Secretary James Watkins emphasizes that the program's aim "is not only to recognize outstanding projects, but to transfer technologies to others who can use them." Local



Watkins: Wants technology shared

governments, school districts, corporations, small businesses, and individuals may compete for awards. To do so, they should contact their state energy offices for more information and an application form. The five projects deemed best by a state energy office will be sent to DOE for further evaluation. The program began in 1984. Since then, award-winning projects have involved waste-to-energy, better building design, and curbside recycling.

**EPA has proposed standards that aim at reducing emissions by as much as 90% overall** for municipal waste incinerators. Emission limits are set for toxic metals and organics and acid gases. Operating standards are proposed to ensure optimum combustion to reduce contaminants. Also, lead-acid batteries may not be burned, and reusable components of municipal trash must be separated. EPA expects toxic metal emissions to be reduced by 97-99%, organic chemical emissions by 99%, SO<sub>2</sub> and

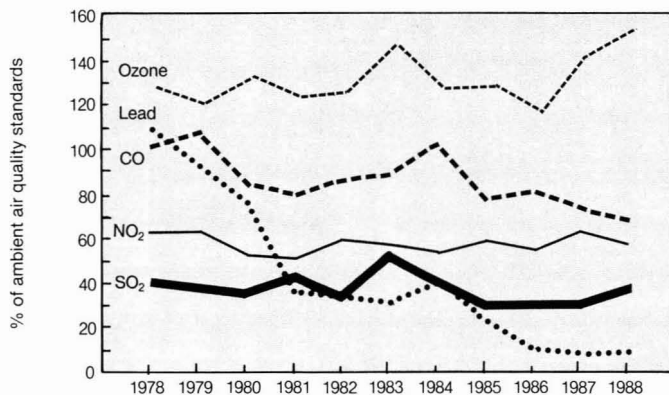
hydrogen chloride by 90-95%, and NO<sub>x</sub> by 40%. Moreover, the materials separation requirement is expected to reduce ash volume by more than 30%. The final regulations will apply to new incinerators and will serve as guidelines for states to apply to existing incinerators, as required by the Clean Air Act.

**EPA released on Dec. 7 a report, "Comparing Risks and Setting Environmental Priorities,"** which documents findings of a two-year study in three EPA regions. Among its findings is that radon, indoor air pollution other than radon, pesticides (primarily on food), and drinking-water contamination pose serious health risks. Moreover, indoor air pollution consistently causes high health risks, regardless of region. In addition, high ecological risks result from physical modification of habitats (for example, urbanization and destruction of wetlands) and nonpoint runoff of contaminated water. Although the study was conducted in Regions 1, 3, and 10, its findings are expected to be incorporated into strategic planning for all regions. For more information, contact Luke C. Hester at (202) 382-4383.

## STATES

**Four out of 10 New Jersey companies may not be complying with the state's right-to-know law**, advises attorney Albert Telsey of Margolis Chase (Verona, NJ). He warns that the state Department of Environmental Protection (DEP) will enforce the law strictly. Telsey notes that many New Jersey companies, including smaller businesses that regularly handle hazardous substances, have received a right-to-know inventory survey form (DEP 094). They must return the completed form to DEP by March 1, 1990. Failure to submit it may result in a \$1000/day penalty after the business receives a DEP order to submit the form. That fine is in addition to the usual \$100-\$2500 fines for noncompliance with DEP regulations. Telsey warns that DEP is expected to come down hard on smaller businesses such as gasoline stations, automobile dealerships, and dry cleaners.

### Maximum concentration of criteria pollutants in New Jersey\*



\*Methods of determining maximum vary by pollutant.  
Source: New Jersey Department of Environmental Protection.

Also in New Jersey, the DEP maintains a network of 26 continuous air monitoring stations that transmit data minute by minute to a computer in Trenton. Results for 1988 show that the state was in compliance with all of the primary national ambient air quality standards (NAAQS) except tropospheric ozone. DEP officials believe that controlling ozone sources only in New Jersey will not solve that problem and that controls must be imposed on a regional basis and include transportation controls. The above graph shows criteria pollutant levels, averaged from all monitoring sites, as a percentage of NAAQS.

Florida's Everglades National Park will be expanded by 107,600 acres under legislation signed Dec. 13 by President Bush. The President also ordered the U.S. Army Corps of Engineers to restore the natural flow of water to the park. The state of Florida will donate 35,000 acres; the rest must be purchased at an estimated cost of \$40 million, of which Florida has agreed to pay one-fifth. The Everglades is not only the second largest national park in the 48 contiguous states, but also the habitat of 13 endangered species.

As part of its quest for local energy resources, Hawaii will allow some rain forest to be cleared near Hawaii Volcanoes National Park. True Geothermal Energy (Casper, WY) has a permit to clear five acres to drill a geothermal steam test site and build a road. If the test is successful, the company plans to build a 25-MW geothermal power plant. Bill Paty, director of the Hawaii Department of

Land and Natural Resources, hopes that it will be possible to develop a 500-MW geothermal power plant and transmit much of that power by undersea cable to Honolulu. This plant, he believes, would sharply reduce Hawaii's dependence on fossil fuel, all of which must be imported. Answering critics who decry destruction of parts of the Wao Kele O Puna rain forest, Paty says, "We feel the trade-off of 500 acres out of 50,000 acres of rain forest in that area is a strong benefit to the state."

Iowa has become the first state to impose tight restrictions on the use of the herbicide atrazine on farms. Farmers have been allowed to apply four lb/acre annually. Beginning this spring, however, that limit is reduced to three lb/acre annually, and to as little as 1.5 lb/acre in 23 counties in which groundwater is especially susceptible to contamination. Moreover, atrazine may not be used within 50 ft of wells, lakes, and other sources of water. Iowa Agriculture Secretary Dale Cochran ordered these reductions because of groundwater contamination. Another reason, however, is that studies by the National Cancer Institute have detected a higher rate of cancer where herbicides are used heavily, although it has not been determined whether atrazine is a carcinogen.

### AWARDS

The 1989 Kirkpatrick Chemical Engineering Achievement Award goes to Union Carbide Industrial Gases for its oxygen-based technology that enhances the incineration of hazardous waste. The principle is to

use oxygen instead of air. If air, which is nearly 79% nitrogen, is used, the nitrogen must be heated as well as the waste; moreover, the nitrogen reduces processing capacity by more than 50%. Moreover, NO<sub>x</sub> emissions become a problem. The use of oxygen, introduced as high-velocity jets, reduces the amount of nitrogen in the system and thereby reduces fuel requirements by more than 50%. This increases the incinerator's processing capacity by up to 100%, according to company spokesmen. NO<sub>x</sub> emissions also are curtailed.

### SCIENCE

Carbon monoxide (CO) can accelerate the onset of myocardial ischemia and angina pectoris in persons who have coronary artery disease and who exercise after exposure to elevated levels of CO, according to results of a study sponsored by the Health Effects Institute (Cambridge, MA). In fact, exposure to CO at levels within current NAAQS standards could have the same effect. The study shows that carboxyhemoglobin—formed when CO combines with blood hemoglobin—reduces the oxygen-carrying capacity of blood beyond the point where a damaged heart can compensate by increasing blood flow to the heart. In healthy people, by contrast, the heart's need for more oxygen is met by increasing blood flow to the heart.

Greenhouse effect warming could occur in the Northern Hemisphere more rapidly than in the Southern Hemisphere, according to a computer model developed by the Geophysical Fluid Dynamics Laboratory at Princeton University and presented at the American Geophysical Union meeting in San Francisco Dec. 6. The model predicts that surface air temperatures in North America could increase by 3–7 °F by 2030 when greenhouse gas levels should be twice the 1958 levels. In the Southern Hemisphere, not only will the increase be slower, but over the Antarctic Ocean and Antarctica itself, air temperatures actually could cool by more than 7 °F, according to the model. Its results suggest that the role of the oceans in mitigating global warming needs much more study. One author of the study warns, however, that the estimates are not precise.

The greenhouse effect could be checked as well as enhanced by combustion gases, suggests Law-



rence Radke of the University of Washington (Seattle). Radke studies low-altitude marine stratocumulus clouds in the Pacific Ocean off southern California. These clouds cover about 33% of the ocean and reflect sunlight back to space. Some of them were unpolluted, but others contained pollutants from passing ships. Radke was surprised to find that the polluted clouds contained twice as much water as their unpolluted counterparts. Water particles in the polluted clouds could not coalesce into raindrops, so they were found to be longer-lived, and satellite photographs showed them to be more reflective of sunlight than were the unpolluted clouds. According to Radke, these clouds could chill the climate while greenhouse gases warm the climate.

## TECHNOLOGY

**A reagent can detect and measure ozone concentration and be used with a personal monitor**, according to three chemists at Kansas State and Kansas Wesleyan Universities. The reagent is on a badge of filter paper that turns red-violet in the presence of ozone. Other air pollutants do not interfere with the ozone detection. One possible application may be to place the badge as an indicator stripe on a jogging suit, says John Walters, director of the Kansas State University Research Foundation (Manhattan, KS). Another use may be in settings in which ozone is a by-product of a manufacturing process, he suggests. Walters observes that for people concerned about ozone in locations where no sophisticated equipment is monitoring smog, "we think an inexpensive personal tester would be very handy."

**More than 90% of SO<sub>x</sub> and NO<sub>x</sub> can be removed from coal-fired power plant emissions** by a process that converts NO<sub>x</sub> to nitrogen and SO<sub>x</sub> to hydrogen sulfide (H<sub>2</sub>S). The H<sub>2</sub>S subsequently is converted to marketable elemental sulfur. The first portion of the process is the Parsons Beavon Sulfur Removal Process, developed by The Ralph M. Parsons Company (Pasadena, CA). It works in conjunction with Exxon's Flexsorb SE Plus process to recover H<sub>2</sub>S quantitatively and with the Parsons/Unocal Recycle Selectox process to produce the sulfur. Parsons proposes to demonstrate the processes at the St. Marys Municipal Power Plant (St. Marys, OH) by processing 100% of the plant's flue gas for two years. The cost of the program is estimated at \$34 million, of which



### Wood chip burning power plant

\$17 million would be contributed by the Department of Energy if DOE approves the proposal.

### Up to 25 MW of commercial power is being generated by the burning of wood chips

in a 220,000-lb/h grate-type boiler in West Osipee, NH, operated by Pinetree Tower-Tamworth, Inc. The plant uses instrumentation for continuous emissions monitoring (CEM) and for automatic boiler control, designed by Westinghouse (Orrville, OH). The CEM system measures CO, NO<sub>x</sub>, stack oxygen, stack gas temperature and flow, and opacity, in keeping with EPA and New Hampshire regulations. The sampling probe contains a 0.5- $\mu$ m filter element. The gas analyzers are calibrated automatically every 24 h. The system has been operational since April 1988.

## BUSINESS

**Market forces could help abate air pollution**, according to the American Gas Association (Arlington, VA) (*The Natural Resource*, 1989, 3[2], 1). This market approach consists of a permit program that allows companies to buy, sell, and trade pollution credits. Robert Stavins of Harvard University suggests that this type of approach to acid deposition reduction could save as much as \$3 billion a year, compared with the cost of a dictated technological solution. Supporters of the market approach say that a similar program to improve air quality, part of an experiment begun by EPA in 1974, saved \$4 billion in control costs, even though the program was not widely carried out.

**A unique public-private partnership program that sets new standards for drinking-water products** will replace the Drinking Water Additives Program currently administered by EPA. Michael Cook, director of EPA's Office of Drinking Water, told the Pacificchem '89 Conference in Honolulu Dec. 20 that the new standards were developed in a partnership consisting of EPA, the

states, water utilities, private testing organizations, and the industries affected. Moreover, although EPA provided the incentive, the agency supplied only 12% of the financing necessary for the new program; the private sector paid the remaining costs.

**Costs of disposing of low-level radioactive waste (LLRW) will be 100-1000% higher** than current disposal costs, according to Environmental Information (Minneapolis, MN). The LLRW would be disposed of at 10 sites. One exists now (Richland, WA); others are expected to open between 1992 and 1995. Two other sites at Barnwell, SC, and Beatty, NV, currently manage LLRW, but they are scheduled to close at the end of 1992. The cost of each new facility is expected to range from \$29 million to \$75 million. The less expensive ones will use enhanced shallow land burial; the others will use above-grade concrete vaults. Disposal fees are expected to be \$85-\$450/ft<sup>3</sup>. Current minimum disposal fees are \$30-\$40/ft<sup>3</sup>. Nuclear power plants will be the most financially affected.

**Battelle will continue to monitor U.S. coastal waters for pollution and toxic materials** over the next five years. The National Oceanic and Atmospheric Administration (NOAA) has awarded \$11 million to Battelle to extend the National Status and Trends Mussel Watch Program through 1994. Under the program, Battelle researchers collect bivalves from the east and west coasts and from Alaskan and Hawaiian waters, as well as samples of sediment. They examine tissues of the bivalves for any abnormal or cancerous cells. Bivalves are well suited to this type of study because they feed off the ocean floor and ingest and concentrate contaminants such as pesticides, polychlorinated biphenyls, polycyclic aromatic hydrocarbons, and trace metals. They provide more concentrated and measurable levels of contaminants than seawater normally does.

# Aquatic toxicology

*Part 2 of a four-part series*

## Ecotoxicology series

Ecotoxicology is the study of the fate and effect of toxic agents in ecosystems. In the first part of this series John Bascietto, Dexter Hinkley, and colleagues provided an overview of applications of ecotoxicology through the various regulatory acts and programs of EPA. They reported that new directions within EPA reflect an increased emphasis on the role of sediments, biomarkers, and ecosystem assessments in regulating environmental pollutants. (See the January 1990 issue, p. 10.)

**John Cairns, Jr.**  
*Virginia Polytechnic Institute  
and State University  
Blacksburg, VA 24061*

**Donald I. Mount**  
*EPA Environmental Research  
Laboratory  
Duluth, MN 55804*

No instrument has yet been devised that will measure toxicity! Chemical concentration can be measured with an instrument, but only living material can be used to measure toxicity. Knowledge of the chemical concentration and toxicity under one set of conditions might expedite the prediction of toxicity under a variety of conditions. Unfortunately, environmental quality routinely influences how toxicity is manifested, and errors are made.

Nevertheless, chemical and physical measurements are an important part of any toxicity test because both the concentration of the toxicant and the environmental quality in which the toxicity was manifested must be known in order to determine how changes in quality will affect toxicity. When enough information is available, a robust predictive model can be developed. Because the goal is to protect organisms in ecosystems from damage, toxicity tests must necessarily be predictive.

The earliest toxicity tests, designed to protect humans, used surrogate species (e.g., monkeys, dogs, mice, rats). Surrogate species are physiologically different from humans in many respects; therefore, there is always some question about applicability in extrapolating from one species to another. Consequently, when a new drug is developed or a new chemical marketed, a



period of time is usually allotted when humans exposed to this material are carefully checked to see if the predictions of response based on surrogate species are correct. Even if a mammalian toxicity test is designed to determine effects on more than one species, the total number of species for which extrapolations are necessary is relatively small.

In contrast, extrapolations in aquatic toxicology tests are from a few species to an enormous number of species with an extraordinary taxonomic range (e.g., from diatoms to fish), spanning vast differences in size, physiology, life history, and geographic region. Furthermore, when one attempts to validate the predictions based on laboratory tests from single species, the end points may be quite different in ecosystems.

Despite these and other theoretical difficulties in developing predictive models for extrapolation, even the simplest toxicity tests, those low in environmental realism, have proven enormously helpful. The three most important reasons for this are

- Application factors (i.e., fractions or numbers) used with standard response thresholds (e.g., LC<sub>50</sub> or no-observable-effects level concentrations) are designed to compensate for uncertainties about the precise location of response thresholds;
- natural systems are resilient, transforming toxic materials, sequestering some of them into particular ecological compartments such as the sediments, or volatilizing them; and
- critical flows are set at the worst possible case level, providing an additional margin of safety.

The inability to measure more subtle damage except in exceedingly costly surveys may give a false sense of security. No matter how many toxicity tests are carried out, some uncertainty about the exact response of a complex system will exist because all the variables cannot possibly be covered.

The major questions in aquatic toxicology, then, are: What combination of tests will reduce the uncertainty to a tolerable level and what additional studies, if any, should be done to validate the estimate of uncertainty of the information obtained?

Over 9 million chemicals are listed on the Chemical Abstract Service's Registry of Chemicals, although only an estimated 76,000 are in daily use. Estimates of the total global number of species has risen from 5 million to between 30 and 50 million. A substantial number of these are aquatic. Of course, many species have a limited distribution, and comparatively few are likely to be found in a particular aquatic ecosystem at any particular time. Even so, aquatic toxicology routinely involves extrapolation from few to many species. Some of the other factors affecting uncertainty are discussed in the remainder of this paper.

#### Time span

For potentially hazardous substances, such as chlorine or some detergents that are quickly transformed in the environment to something less hazardous or are eliminated from the aquatic ecosystem, a short-term toxicity test will probably suffice except when the material is continuously discharged and concentrations persist near the outfall. However, many chemicals are persistent, and their exposure time in natural systems is likely to be much longer than is normally used in routine laboratory tests. Even when the laboratory test is carried out over a very long time, it is unlikely to match the period of exposure in natural systems for the most persistent nondegradable chemicals. Therefore, extrapolation from a shorter to a longer time is used.

One way to circumvent problems associated with this type of extrapolation is to use an organism such as *Ceriodaphnia* whose life stages are completed in a relatively short period of time. One can make a case for the theory that the time from the starting point of one generation to the starting point of another is a more important unit of time in determining the toxicological response than the actual clock time of the exposure. Of course, practical considerations, such as cost and availability of laboratory space and personnel, limit routine generational tests on long-lived organisms. Therefore, considera-

ble judgment must be exercised in determining which, if any, aquatic toxicity tests should be carried out on those organisms with relatively long life cycles. For example, can one extrapolate effectively from a *Ceriodaphnia* to a sturgeon?

A partial solution to this problem may be to extrapolate from a species with a very short life cycle to one with an intermediate life cycle, for example, from a *Ceriodaphnia* to a fathead minnow. Another way is to select a number of compounds for which predictions of long-term response have been made and that are being used routinely in natural systems, and to monitor these systems to see whether any unexpected events occur.

#### Coping with uncertainty

Figure 1 illustrates how a sound decision can be made even when uncertainty exists. As more tests are conducted and the data base increases (moving from left to right along the horizontal axis), the uncertainty about the response threshold is reduced. The same is true for the uncertainty about the environmental concentration of the chemical, which is dependent on factors such as transformation, environmental partitioning, and persistence.

In the case illustrated in Figure 1, an overlap exists at the outset and, therefore, the environmental concentration cannot be affirmed as being definitely below the no adverse response threshold. However, very shortly the uncertainty is reduced, and confidence that the concentration of the chemical is well below the concentration producing no adverse biological effects increases. Thus, an informed decision can be made even when there is uncertainty about both the toxicological threshold and the presumed environmental concentration (1, 2).

The goals of aquatic testing are to determine which types of toxicity tests will reduce uncertainty most cost effectively and to determine at what point the uncertainty has been sufficiently reduced to allow an informed professional judgment. [The Pellston series of books, which resulted from conferences on aquatic toxicity held near the University of Michigan Biological Station, furnish much information on hazard evaluation, including protocols, transformation processes, and a variety of other topics (2-7)].

#### Replicating conditions

An examination of the literature clearly demonstrates that water hardness, pH, suspended solids, total organic carbon (TOC), and temperature (to mention just a few characteristics) may markedly affect the expression of

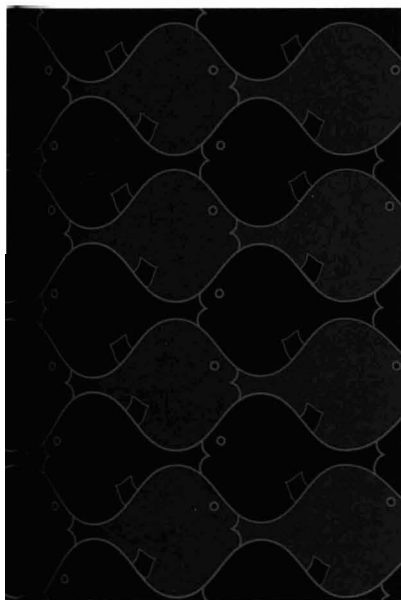
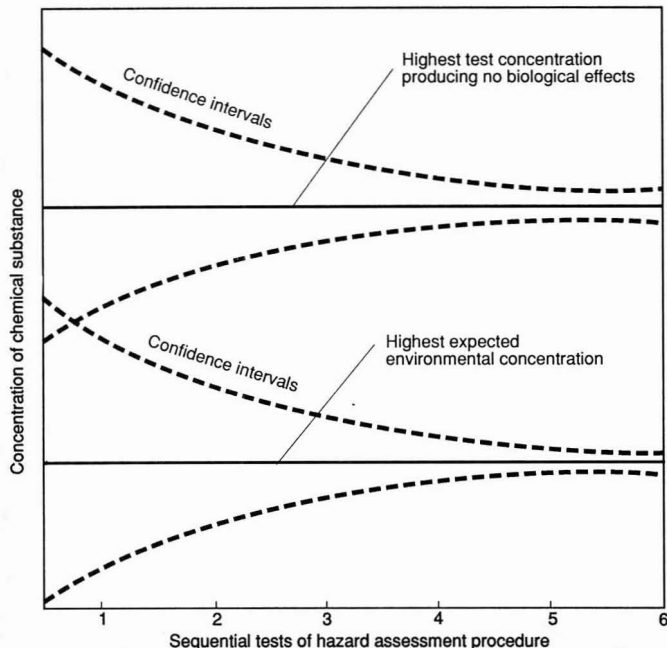


FIGURE 1

**Sequential hazard-assessment procedure demonstrating increasingly narrow confidence limits for estimates of no-biological-effect concentration and actual-expected-environmental concentration**



Source: Reference 2, reprinted with permission.

toxicity for a particular chemical compound. For example, the toxicity of zinc may be quite different in hard Texas water than it is in soft eastern coastal plain water.

The earliest toxicity tests (8) were done in approximately 18-liter glass containers as batch tests (the test solution was not renewed during the period of the test, usually 24, 48, or 96 hours). Flowing waters were more closely simulated by the proportional diluter (9), which enabled a frequent renewal of a portion of the test solution.

In aquatic toxicity testing, an effort is made to replicate the important qualities of a test water. A standardized or "artificial" water can be made by adding appropriate constituents to distilled water, or natural waters can be used from above the source of contamination. Use of natural water increases the difficulty of replication because natural waters vary considerably. Replication is always easier if the number of controlled variables is severely limited, but lack of environmental realism might cause a significant difference between the laboratory results and what actually happens in natural systems.

Figure 2 illustrates one case in which the clean water laboratory results show a close relationship between the envi-

ronmental concentration of the chemical and the no-adverse-biological-response threshold, although in the "real world" they are quite far apart. The reverse of this relationship is shown in Figure 3. This discussion does not distinguish between research projects and tests done for regulatory purposes. For the latter, however, there is merit in having a considerable degree of standardization.

The continuing effort to improve the predictive capability of aquatic toxicity testing requires that new types of tests be examined, as well as the effects of some components on the results, and the benefits and drawbacks of different methodologies. Routine tests should be sufficiently standardized so that technicians can conduct these tests with little or no change in the basic design.

This is not a call for a single all-purpose test, but for an array of standardized tests for regulatory purposes and for a continual effort from the research community to improve present methodology or to develop new methods. In short, it is inappropriate to require the exercise of judgment at every step in a toxicity testing procedure for regulatory purposes. Judgment is best utilized in the selection of the tests and in the interpretation of the results.

### Selection of test organisms

For many years a prime criterion for selecting organisms for toxicity testing was a high degree of sensitivity to chemical compounds. Unfortunately, the sensitivity of an array of species may vary quite strikingly from one chemical substance to another (10). Now with the attention on predictions of hazard, the emphasis is shifting to use of those organisms that are the most reliable predictors of the responses of other organisms or even of communities or ecosystems. Unfortunately, the data base for selecting such organisms (i.e., good predictors of other species' response) is limited.

Furthermore, only a relatively few species have been extensively used for aquatic toxicity testing. Many species that are extremely sensitive or have a high correspondence to the responses of other organisms are exceedingly difficult to keep alive or in good condition in the laboratory. For regulatory purposes, it is unquestionably sound to use test organisms that have been widely used for toxicity testing and whose strengths and weaknesses for this purpose are well known. At the same time, the information base on relative responses must be continually expanded (10).

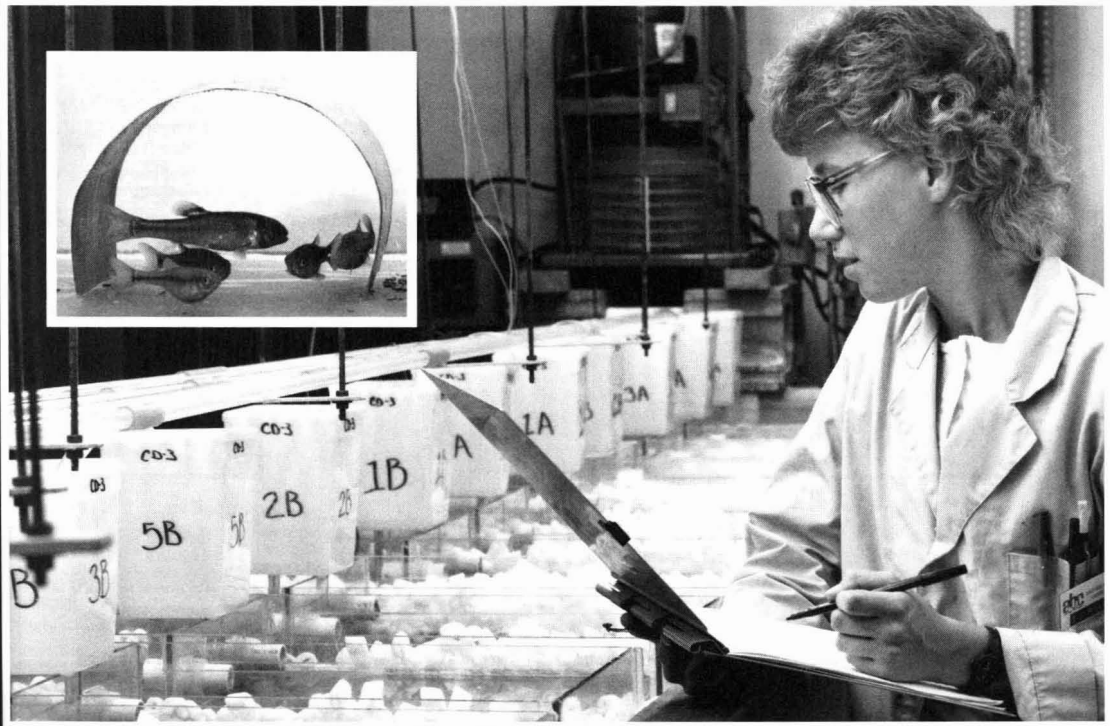
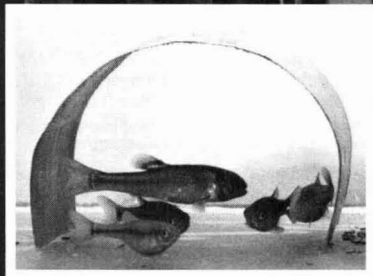
To develop methodology involving new toxicity testing organisms as an end in itself will probably not be productive. However, if it can be shown that there is a high correspondence with the response of many of other organisms or that the predictions are fairly easily validated in natural systems or surrogates thereof, a real contribution will have been made.

### Microcosms and mesocosms

There has been much in the news lately about the hostility of animal rights groups toward the use of animals in laboratory experiments (11). Some groups espouse a total ban on the use of experimental animals in the laboratory, including toxicity testing; more moderate groups call for greater control over the conditions in which such tests are carried out.

The organisms used for aquatic toxicity testing are not obtained from natural systems but are raised for this purpose under fairly well controlled conditions. (In this regard, the conditions for maintaining them in experimental laboratories are often much more rigorous than are the requirements for housing graduate students, technicians, and faculty.) Use of these organisms may save many millions or billions of others in natural systems.

In a very real sense, fish and other organisms raised for toxicity testing are better treated than the organisms raised



# **ABC - THE LEADER IN AQUATIC TOXICOLOGY TESTING SINCE 1976**

Analytical Bio-Chemistry Laboratories' Aquatic Toxicology group has been supplying aquatic bioassays and analytical support for product registration and environmental regulatory compliance since 1976.

Aquatic Bio-Assay studies include compliance data for:

- TSCA - industrial chemicals
- FIFRA - pesticide products
- NPDES - effluent guidelines
- USFDA - environmental assessments
- OECD - international guidelines

## **SPECIALLY DESIGNED FACILITIES**

Our Aquatic Toxicology labs are housed in three buildings designed especially for fish and invertebrate toxicity studies. This includes an environmentally-controlled lab for conducting full life-cycle tests with fish, and a facility especially for invertebrate and bioconcentration investigations.

Our bioassay labs are equipped with

culture facilities for cold and warm water fish and invertebrates, static and flow-through test systems; a complete analytical support lab. To insure test continuity our labs have back-up water and electrical systems.

In-house data and word processing systems expedite report preparation. Our independent QA unit assures that all tests are performed according to GLP's.

For a complete list of protocols and prices call 1-314-443-9021 or write:



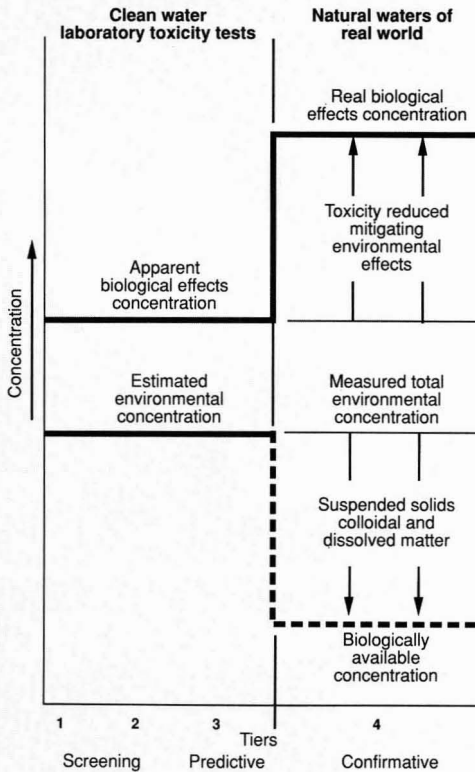
**ANALYTICAL  
BIO-CHEMISTRY  
LABORATORIES, INC.**

P.O. Box 1097, Columbia, MO 65205  
Phone: 314-443-9021 Telex: 821-814 FAX: 314-443-9033



FIGURE 2

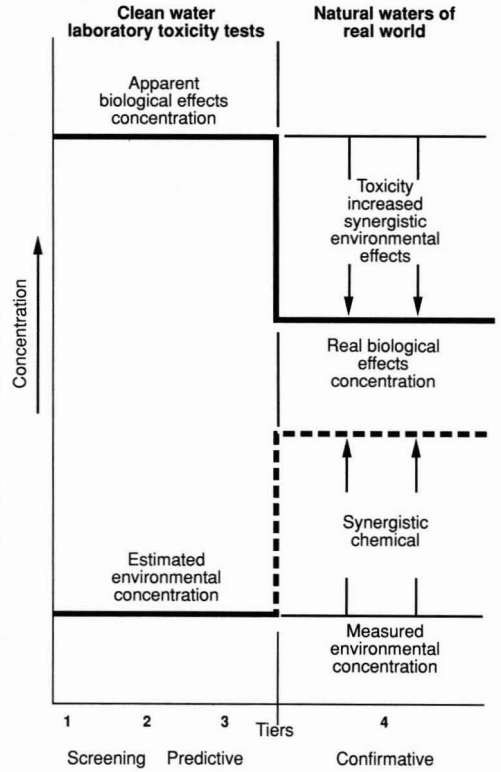
Hypothetical situation in which an apparently large margin of safety from clean water laboratory toxicity data is actually much greater because of mitigating effects of natural waters



Source: Reference 18.

FIGURE 3

Hypothetical situation in which an apparently small margin of safety from clean water laboratory toxicity data is actually much smaller because of synergistic effects of natural waters



Source: Reference 18.

for bait fishing or as food fish. Whether these considerations will persuade the animal rights groups is uncertain. It is possible that concerns about the ethics of animal tests will eventually limit the use not only of vertebrates, such as fish, but even macroinvertebrates as test organisms. The likely consequence will be increased surveillance and costs for such tests.

Therefore, aquatic toxicity testing using microorganisms may become much more common in the future. Many microbial species tests are carried out in microcosms, and, if either of the scenarios just mentioned develops, it is quite likely that these will be more commonly used. There is some persuasive, although not extensive, evidence that there is a high correspondence between the responses of microbial species and those of the more commonly used test species (12).

Another advantage to using microcosms is that they are more environmentally complex than the standard test systems and therefore more amenable to the simultaneous study of toxicity

and various chemical transformation and partitioning processes. Furthermore, a substantial number of the transformations are carried out by the biota, and the ability of biota to do so under various conditions is an important item of information.

Finally, because microcosms can monitor responses that are of direct concern in the natural environment, it may be easier to extrapolate to responses in natural systems. There is some evidence that this is the case (13, 14). Of course, the information base must be greatly expanded before there is solid evidence on this point.

Field studies that utilize natural or man-made ponds and enclosures are now commonly incorporated into testing programs for pesticide registration. The Pesticide Branch of the EPA Environmental Research Laboratory at Duluth, MN, has recently developed an aquatic field testing design and protocol using plastic-lined enclosures in natural aquatic systems (ponds and lakes). These littoral enclosures were designed to allow for true replications and con-

trols; to be more economical than larger mesocosms; to be conducive to accurate environmental chemistry studies of pesticides; to include all trophic levels and the natural undisturbed sediment, shoreline, and water column of the system being partitioned; and to be large enough to allow for sampling to characterize the parameters of interest without significantly disrupting the enclosed ecosystem.

Successful studies on the pesticides chlorpyrifos and fenvalerate have been completed. The protocol is being used as a field testing guidance document by EPA's Office of Pesticide Programs and is being refined for testing ecological effects models.

### Bioaccumulation

Chemicals that are persistent in aquatic environments, have low solubility in water, and have high solubility in fats and oils usually will occur in aquatic organisms at much higher concentrations than are found in the water. Thus, a trout living in a water concentration of 10 ng/L may have tissue con-

# Wastefilled Updates

Coming in May...

## Sanitary Landfilling

Process Technology and Environmental Impact

edited by

Thomas H. Christensen, Raffaello Cossu, and Rainer Stegmann

This work provides international updates on a variety of new developments, including landfill degradation processes, biogas, leachate, lining and drainage, environmental impacts, and design.

**Sanitary Landfilling** contains new contributions as well as edited papers from the First International Symposium on Sanitary Landfilling held in Cagliari, Italy, in October, 1987.

March 1990, 608 pages, \$110.00  
ISBN: 0-12-174255-5

Coming this Spring...

## Environmental Science

International Perspectives on Municipal Solid Wastes and Sanitary Landfilling

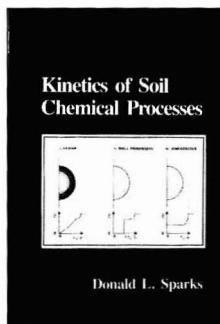
Joseph S. Carra and Raffaello Cossu

This volume looks at how different countries cope with the municipal solid waste problem politically, administratively, and technically, with a particular focus on sanitary landfilling.

Key Features:

- Highlights 15 countries approaches to municipal solid waste management
- Reports on the latest developments in the design and operation of sanitary landfills
- Explores future directions and policies for waste management and sanitary landfilling around the world

May 1990, c. 224 pages, \$59.00 (tentative)  
ISBN: 0-12-106355-0



## Kinetics of Soil Chemical Processes

Donald L. Sparks

To properly understand the fate of applied fertilizers, pesticides, and organic pollutants with time, and to thus improve nutrient availability and the quality of groundwater, one must study kinetics. This is the first comprehensive treatment of these subjects and as such will be a valuable reference for students and professionals in environmental engineering, soil science, geochemistry, and geology.

1989, 210 pages, \$34.95  
ISBN: 0-12-656440-X

New

## Nitrogen in Organic Wastes Applied to Soils

edited by

Jens Aa. Hansen and Kaj Henriksen

Organic wastes are traditionally applied to land to recover their fertilizer value, but the microbial turnover of such organic matter is often out of phase with the requirements of growing plants. Therefore, nutrients may be lost and may even act as potential pollutants of water and air. This treatise addresses both experimental and modeling methodologies of this problem.

Articles are based on material presented at a specialized seminar held under the auspices of ISWA and DAKOFA at Aalborg University, Denmark, in September, 1988.

December 1989, 400 pages, \$75.00  
ISBN: 0-12-323440-9

## Incineration of Municipal and Hazardous Solid Wastes

David A. Tillman, Amadeo J. Rossi, and Katherine M. Vick

This survey examines the principles and processes associated with the combustion of many materials discarded by society. It provides insight into the process of combustion and the application of that process to one of the leading problems confronting our lives. It focuses on first principles and the application of those principles by technology.

1989, 343 pages, \$42.95  
ISBN: 0-12-691245-9

## Geophysical Data Analysis

Discrete Inverse Theory  
Revised Edition

William Menke

From the Reviews of the First Edition:

*"I think that the value of the book is outstanding...It deserves a prominent place on the shelf of every scientist or engineer who has data to interpret."*

—GEOPHYSICS

August 1989, 289 pages, \$44.95  
ISBN: 0-12-490921-3

Order from your local bookseller  
or directly from



## ACADEMIC PRESS

Harcourt Brace Jovanovich, Publishers  
Book Marketing Department #23020  
1250 Sixth Avenue, San Diego, CA 92101

CALL TOLL FREE

**1-800-321-5068**

Quote this reference number for free postage and handling on your prepaid order — 23020

Prices subject to change without notice. ©1990 by Academic Press, Inc.  
All Rights Reserved. TJE:MDJ—23020.

CIRCLE 5 ON READER SERVICE CARD

centrations of 1 mg/kg. Some of this residue may be the result of direct water intake and some of food intake. The problems these residues cause are compounded when fish and other aquatic organisms are eaten by birds and mammals, but adverse effects—on predatory fish for example—have not been well documented.

The prediction of residue-forming potential, based on chemical and physical properties, has been much more successful. Recently, a draft protocol using HPLC to identify the presence of chemicals that will bioconcentrate in effluents has been developed at EPA.

#### Future needs

It is a pity that noted ecologists and ecotoxicologists interact only infrequently (15). The goal of aquatic toxicology or ecotoxicology is to protect natural systems and their inherent organisms. Because quality ecosystems are in short supply and ecosystems receiving anthropogenic wastes are difficult and expensive to study in terms of predictive modeling, it is clear that most of the toxicity tests for hazard evaluation should be done either in the laboratory or in artificial systems such as microcosms, mesocosms, and field enclosures.

Because new properties are added at each higher level of biological organization (i.e., cellular, whole organism, population, community, and ecosystem), predictive models generated in the laboratory or artificial system should be validated wherever possible in natural systems using end points characteristic of levels of biological organization higher than single species.

It is possible that functional attributes of very complex ecosystems (e.g., detritus processing) may be better indicators of overall stress for the system than are measurements made on components such as species. Theoretical ecologists have not been particularly helpful in providing end points for validating predictions of natural system response based on laboratory toxicity tests, either because they are unaware of the need or because it does not fit the traditional mode of research in theoretical ecology.

Nevertheless, Harper and Bradshaw are among the distinguished ecologists

who have criticized the lack of predictive modeling in the field of ecology (16, 17). It is clear that ecology could benefit from interaction with toxicologists interested in developing predictive models, because most systems undergo dramatic changes when exposed to toxicants.

At the same time, toxicologists could learn much from ecologists about dealing with complex systems with many uncontrolled variables. If environmental realism is to be an important component of aquatic toxicology, this development is essential.

Another important area is the determination of information redundancy. For example, how closely does the response of test species *X* correspond with the response of a large array of other species exposed under similar conditions? If areas of considerable information redundancy in aquatic toxicology can be identified, the number of tests could be markedly diminished without shrinking the information base.

Inevitably, ecosystems will be damaged by accidental spills of hazardous materials or by deliberate but misjudged releases. Toxicologists will have to become more knowledgeable about rehabilitation of damaged ecosystems, particularly where persistent toxicants are involved.

The decommissioning of hazardous-waste sites located in natural systems should be a good focus of interaction for toxicologists and ecologists, requiring from traditional aquatic toxicology more ecological emphasis. Although the sites might not be aquatic initially, there is ample evidence that materials from hazardous-waste storage sites regularly intrude into aquatic ecosystems. In these situations, neither discipline has a particular advantage because the knowledge base is inadequate.

With the recognition of global climate effects caused by ordinary gases such as CO<sub>2</sub>, the inevitable is becoming obvious. Matter is not destroyed in waste treatment, it is only converted to other forms. Our success in wastewater treatment has aggravated global climate problems. We are converting wastes to CO<sub>2</sub> and other gases and producing more greenhouse gases by using fossil fuel to provide energy for treatment plant operations. Regulators recognize

now that restrictions on wastewater discharges have caused waste generators to use underground injection and landfills as alternatives.

So what has this to do with aquatic toxicology? Thinking people now realize that to take matter out of water only forces it somewhere else, and we are now rapidly filling up the air, groundwater, and land surface.

The public will not readily change its consumption habits. Treatment and disposal will continue to be favored by society over reduced waste generation for some time to come. The comfortable margins of safety now used in water pollution regulation that have helped us so much in the past probably will disappear. If these margins of safety are eroded, aquatic toxicologists and ecologists will have to show marked improvement in the precision and accuracy of predictions in order to provide the defined response of aquatic communities without big margins of safety.

For the past century, our philosophy has been that it is better to put waste anywhere (in air, soil, groundwater) than into surface water such as streams and lakes. Although not openly stated, our decisions bear out our policy. In view of the other emerging problems, that policy must change, and, with it, aquatic toxicology.

#### Acknowledgments

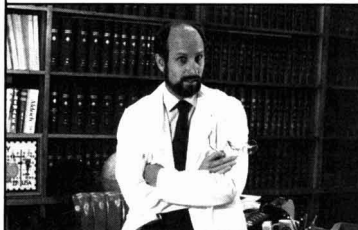
We are deeply indebted to Darla Donald, editorial assistant, University Center for Environmental and Hazardous Materials Studies, for manuscript preparation; to B. R. Niederlehner for bibliographic and other assistance; and to Teresa Moody for wordprocessing.

#### References

- (1) Cairns, J., Jr. *BioScience* 1980, 30(2), 101-7.
- (2) Cairns, J., Jr.; Dickson, K. L.; Maki, A. W., Eds.; *Estimating the Hazards of Chemical Substances to Aquatic Life*; STP657; American Society for Testing and Materials: Philadelphia, PA, 1978.
- (3) Dickson, K. L.; Cairns, J., Jr.; Maki, A. W., Eds.; *Analyzing the Hazard Evaluation Process*; American Fisheries Society: Washington, DC, 1979.
- (4) Dickson, K. L.; Maki, A. W.; Cairns, J., Jr., Eds.; *Modeling the Fate of Chemicals in the Aquatic Environment*; Ann Arbor Science Publishers: Ann Arbor, MI, 1982.
- (5) Dickson, K. L.; Maki, A. W.; Brungs, W. A., Eds.; *Fate and Effects of Sediment-Bound Chemicals in Aquatic Sys-*



# Me? Enroll in the ACS Employment Service?



## I'm head of a major research department!

Even for the successful chemist or scientist in an allied field, sometimes the best way to get ahead is to make a change.

The ACS Employment Service offers the opportunity to investigate the possibilities discreetly—and at very low cost. Our Employment Service is free to all ACS members. If you request confidentiality from current employers or other designated organizations there is a nominal charge.

For more information write,  
use coupon, or  
CALL TOLL FREE  
800-227-5558

**Employment Services Office,  
American Chemical Society  
1155 Sixteenth Street, NW,  
Washington, DC 20036**

Yes. I am a member of ACS and I would like to learn how the ACS Employment Service can help me advance my career.

Name (please print) \_\_\_\_\_

Membership # \_\_\_\_\_

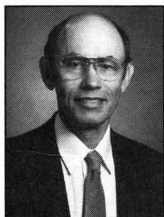
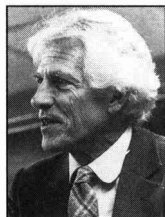
Address \_\_\_\_\_

City \_\_\_\_\_

State \_\_\_\_\_

ZIP \_\_\_\_\_

- tems; Pergamon Press: New York, 1987.
- (6) Maki, A. W.; Dickson, K. L.; Cairns, J., Jr., Eds.; *Biotransformation and Fate of Chemicals in the Aquatic Environment*; American Society for Microbiology: Washington, DC, 1980.
  - (7) Bergman, H. L.; Kimerle, R. A.; Maki, A. W., Eds.; *Environmental Hazard Assessment of Effluents*; Pergamon Press: New York, 1985.
  - (8) Hart, W. B.; Doudoroff, P.; Greenback, J. *The Evaluation of the Toxicity of Industrial Wastes, Chemicals and Other Substances to Freshwater Fishes*; Waste Control Laboratory, Atlantic Refining: Philadelphia, PA, 1945.
  - (9) Mount, D. I.; Brungs, W. A. *Water Res.* **1967**, *1*, 21-29.
  - (10) Mayer, F. L.; Ellersieck, M. L.; *Manual of Acute Toxicity: Interpretation and Data Base for 410 Chemicals and 66 Species of Freshwater Animals*; U.S. Department of Interior, Fish and Wildlife Service/Resource Publication 160; Washington, DC, 1986.
  - (11) *Newsweek* **1988**, Dec. 26, pp. 50-59.
  - (12) Niederlehner, B. R.; Pratt, J. R.; Buikema, A. L., Jr.; Cairns, J., Jr. In *Community Toxicity Testing*; Cairns, J., Jr., Ed.; American Society for Testing and Materials: Philadelphia, PA, 1986.
  - (13) Tolle, D. A.; McArthur, J. C.; Van Vorris, P. *Environ. Toxicol. Chem.* **1985**, *4*, 501-9.
  - (14) Livingston, R. J.; Diaz, R. J.; White, D. C.; *Field Validation of Laboratory-Derived Multispecies Aquatic Test Systems*; EPA 600/54-85-039; National Technical Information Service: Springfield, VA 1985.
  - (15) Brungs, W. A. *BioScience* **1986**, *36*(10), 677-78.
  - (16) Harper, J. L. In *The Plant Community as a Working Mechanism*; Newman, E. I., Ed.; Blackwell Scientific: London, 1982; pp. 11-25.
  - (17) Bradshaw, A. D. In *Restoration Ecology*; Jordan, W. R. III; Gilpin, M. E.; Aber, J. D., Eds.; Cambridge University Press: Cambridge, England, 1987; pp. 23-29.
  - (18) Kimerle, R. A. In *Workshop on Hazard Assessment*; Bratzel, M.P., Ed.; Great Lakes Water Quality Board of the International Joint Commission: Windsor, ON, Canada, 1979; pp. 221-30.



**John Cairns, Jr.** (l) is university distinguished professor in the Department of Biology and director of the University Center for Environmental and Hazardous Materials Studies at Virginia Polytechnic Institute and State University. He received Ph.D. and M.S. degrees from the University of Pennsylvania and an A.B. degree from Swarthmore College. He was curator of limnology at the Academy of Natural Sciences of Philadelphia for 18 years.

**Donald I. Mount** (r) is senior scientist at EPA Environmental Research Laboratory in Duluth, MN. He received B.S., M.S., and Ph.D. degrees from Ohio State University. He has worked for 30 years with EPA and its predecessor agencies in the water pollution field.

## NEW MICROWAVE DIGESTION BOMBS



PAT. PENDING

### Now in two sizes, 23 ml and 45 ml.

The speed and convenience of microwave heating can now be applied to the digestion of inorganic, organic, or biological materials in a Teflon Lined Bomb. The new Parr Microwave Digestion Bombs have been designed to combine the advantages of closed high-pressure and high temperature digestion with the requirements of microwave heating. Many samples can be dissolved or digested with less than one minute heating times. As with all Parr Digestion Vessels, careful design and testing effort have gone into the safety and sealing aspects of this unique vessel and operating environment.

Call or write for Bulletin 4781 with complete technical details.



**PARR  
INSTRUMENT  
COMPANY**

211 Fifty-third Street  
Moline, IL 61265

Phone: (309) 762-7716  
Telex: 270226

CIRCLE 3 ON READER SERVICE CARD

# The role of genes in biological processes

*Part 2 of a two-part article*

**Barth F. Smets**  
**Bruce E. Rittmann**  
**David A. Stahl**  
*University of Illinois*  
*at Urbana-Champaign*  
*Urbana, IL 61801-2397*

### Glossary of mathematical terms

- $b$  = biomass maintenance-decay coefficient ( $T^{-1}$ )
- $b_e$  = net decay coefficient for exogenous biomass ( $T^{-1}$ )
- $b_p$  = first-order plasmid-loss rate coefficient ( $T^{-1}$ )
- $D$  = concentration of donor cells ( $ML^{-3}$ )
- $K$  = half-maximum rate concentration ( $ML^{-3}$ )
- $k_{t1}$  = mixed second-order rate coefficient for transfer of plasmid from donor to recipient ( $L^3M^{-1}T^{-1}$ )
- $k_{t2}$  = mixed second-order rate coefficient for transfer of plasmid from transconjugant to recipient ( $L^3M^{-1}T^{-1}$ )
- $\rho$  = fraction of indigenous biomass that contains plasmid ( $ML^{-3}$ ); this fraction behaves as a transconjugant
- $q$  = specific rate of substrate utilization ( $MM^{-1}T^{-1}$ ); computed as  $\dot{q}S/(K + S)$
- $\dot{q}$  = maximum specific rate of substrate utilization ( $MM^{-1}T^{-1}$ )
- $Q$  = volumetric influent flow rate ( $L^3T^{-1}$ )
- $Q^e$  = volumetric effluent flow rate ( $L^3T^{-1}$ )
- $Q^w$  = volumetric flow rate of wasted sludge ( $L^3T^{-1}$ )
- $R$  = concentration of recipient cells ( $ML^{-3}$ )
- $r_d$  = rate of cell decay for maintenance ( $MT^{-1}$ )
- $r_{DR}$  = rate of transconjugant formation due to donor-to-recipient transfer ( $MT^{-1}$ )
- $r_{gr}$  = rate of cell growth ( $MT^{-1}$ )
- $r_L$  = rate of transconjugant loss due to plasmid loss ( $MT^{-1}$ )
- $r_{TR}$  = rate of transconjugant formation due to transconjugant-to-recipient transfer ( $MT^{-1}$ )
- $r_{ut}$  = rate of substrate accumulation due to utilization ( $MT^{-1}$ )
- $S$  = concentration of rate-limiting substrate ( $ML^{-3}$ )
- $S^o$  = influent concentration of rate-limiting substrate ( $ML^{-3}$ )
- $T$  = concentration of transconjugant cells ( $ML^{-3}$ )
- $V$  = liquid volume of reactor ( $L^3$ )
- $X$  = concentration of active cells ( $ML^{-3}$ )
- $X^e$  = effluent concentration of active cells ( $ML^{-3}$ )
- $X^w$  = concentration of active cells in wasted sludge ( $ML^{-3}$ )
- $X_e$  = concentration of plasmid-bearing exogenous cells ( $ML^{-3}$ )
- $X_e^o$  = input concentration of exogenous cells ( $ML^{-3}$ )
- $X_{min}$  = minimum active-cell concentration able to sustain a steady-state fraction of plasmid-containing transconjugants when no exogenous source of plasmid is present ( $ML^{-3}$ )
- $Y$  = true cell yield ( $MM^{-1}$ )
- $\theta$  = liquid detention time ( $T$ ); equals  $V/Q$
- $\theta_x$  = mean cell residence time ( $T$ ) (Equation 11)

The first part of this article (1) introduced the concept that the role of genes in biological processes is much more important than has been thought in the past. It described the transfer of plasmid DNA among the different bacteria present in a biological process and presented a method for modeling the kinetics of plasmid transfer.

In this second part of our article, the literature on plasmid transfer rates is analyzed critically. First, we estimate the plasmid transfer coefficients ( $k_{t1}$  for donor-to-recipient transfer,  $k_{t2}$  for transconjugant-to-recipient transfer, and  $b_p$  for plasmid loss by the transconjugant) and consolidate them from a variety of experimental results. Then, we combine these estimates with a simple biological-process model that includes plasmid content and transfers. We then use the model to evaluate the importance of plasmid transfer for controlling the action of the populations in a biological process. Finally, we suggest future research efforts involving plasmid transfer in biological processes.

### Evaluating transfer parameters

There are three transfer reactions: donor-to-recipient transfer to create a transconjugant ( $r_{DR}$ ), transconjugant-to-recipient transfer to create more transconjugants ( $r_{TR}$ ), and loss of the plasmid from the transconjugant ( $r_L$ ).

# Emerging Developments in Environmental Science



## ENVIRONMENTAL SCIENCE & TECHNOLOGY

Enter your own monthly subscription to ES&T and be among the first to get the most authoritative technical and scientific information on environmental issues.

**YES! I want my own one-year subscription to ENVIRONMENTAL SCIENCE & TECHNOLOGY at the rate checked below:**

1990 Published Monthly	U.S.	Canada & Mexico	Europe	All Other Countries
ACS members	<input type="checkbox"/> \$ 36	<input type="checkbox"/> \$ 50	<input type="checkbox"/> \$ 65	<input type="checkbox"/> \$ 72
Nonmembers Personal	<input type="checkbox"/> \$ 67	<input type="checkbox"/> \$ 81	<input type="checkbox"/> \$ 96	<input type="checkbox"/> \$103
Nonmembers-Institutional	<input type="checkbox"/> \$276	<input type="checkbox"/> \$290	<input type="checkbox"/> \$305	<input type="checkbox"/> \$312

Payment Enclosed (Payable to American Chemical Society)

Bill Me  Bill Company

Charge my  VISA/MasterCard

Diners Club/Carte Blanche

Card No. \_\_\_\_\_

Expires \_\_\_\_\_ Signature \_\_\_\_\_

Name \_\_\_\_\_

Title \_\_\_\_\_ Employer \_\_\_\_\_

Address  Home \_\_\_\_\_

Business \_\_\_\_\_

City, State, Zip \_\_\_\_\_

Employer's Business:  Manufacturing  Academic  Government

Other \_\_\_\_\_

Member rates are for personal use only.

Subscriptions outside the U.S., Canada, and Mexico are delivered via air service.

Foreign payment must be made in U.S. currency by international money order, UNESCO coupons, or U.S. bank draft. Orders accepted through your subscription agency. For nonmember rates in Japan, contact Maruzen Co., Ltd. Please allow 45 days for your first copy to be mailed.

Redeem until December 31, 1990.

880 MAIL THIS POSTAGE-PAID CARD TODAY! 5454J



(800) 227-5558 (U.S. only)



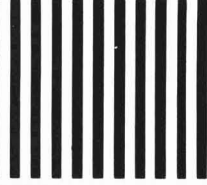
NO POSTAGE  
NECESSARY  
IF MAILED  
IN THE  
UNITED STATES

**BUSINESS REPLY MAIL**

FIRST CLASS PERMIT NO. 10094 WASHINGTON, D.C.

POSTAGE WILL BE PAID BY ADDRESSEE

**American Chemical Society**  
Marketing Communications Department  
1155 Sixteenth Street, N.W.  
Washington, D.C. 20077-5768



The top portion of Table 1 (Equations 1-3) summarizes the rate expressions and how they are related to the concentrations of donor ( $D$ ), recipient ( $R$ ), and transconjugant ( $T$ ). The remaining equations define rate expressions, mass balances, and steady-state solutions for substrates and cells.

Several experiments (2-7) were performed in batch or chemostat reactors specifically to evaluate the kinetics of plasmid transfer in liquid (broth) cultures. Table 2 summarizes, in common units, the kinetic parameters found through each of those experiments. Their values range from  $1.2 \times 10^{-6}$  to  $2.4 \times 10^3$  LgT/gD-gR-day for  $k_{11}$  and from  $1.2 \times 10^{-3}$  to  $1.1 \times 10^4$  L/gR-day for  $k_{12}$ .

Three aspects of these results are critical. First, the parameter values reflect the structure and assumptions of the model used to analyze the data; for instance,  $b_p$  was included explicitly in only one study (2), and  $k_{11}$  and  $k_{12}$  were assumed to be equal in two other studies (5, 7). These assumptions might have biased the parameter estimates. Second, the ranges of  $k_{11}$  and  $k_{12}$  values are very large—about nine and seven orders of magnitude, respectively. It is not possible to say whether these large ranges can be attributed to the use of different strains and plasmids or to errors in the model assumptions. Third, some of the values of  $k_{11}$  and  $k_{12}$  are relatively large. As will be illustrated below,  $k_{11}$  and  $k_{12}$  values larger than about 1 L/g-day should allow transfer rates that could affect the performance of biological processes significantly.

The loss of plasmids is not well quantified. A thorough literature search has revealed only one set of values of  $b_p$  (2), varying from 0.0024 to 0.24 day<sup>-1</sup>. Other methods of describing loss via segregation do not allow  $b_p$  to be estimated. Complicating the plasmid loss phenomenon is the loss of plasmids at different rates by the same strain (8, 9). Clearly, information on the kinetics of plasmid loss is limited.

There is a very large data base for the frequency of transconjugant formation during mating experiments. Mating experiments are a technique commonly used to test the relative ability of a specific donor strain to transfer a plasmid to a particular recipient strain. Mating experiments can be conducted in a liquid (i.e., broth) or on solid surfaces, such as agar plates and filter pads (10).

The mating frequency is the integration of the net rate of transconjugant formation during the incubation time. If the concentrations of donor and recipient are known or can be estimated as functions of time during the experiment, the kinetic parameters that give the final (integrated) mating frequency

TABLE 1  
Summary of kinetic expressions

Plasmid transfers to create transconjugants

$$\text{Donor-to-recipient} \quad r_{DR} = k_{11}DR \quad (1)$$

$$\text{Transconjugant-to-recipient} \quad r_{TR} = k_{12}TR \quad (2)$$

$$\text{Loss from transconjugant} \quad r_L = -b_p T \quad (3)$$

Conventional rate expressions for substrate and cells<sup>a</sup>

$$\text{Substrate utilization} \quad r_{ut} = -\frac{\dot{q}XS}{K+S} = -qX \quad (4)$$

$$\text{Cell growth} \quad r_{gr} = \frac{Y\dot{q}XS}{K+S} = YqX \quad (5)$$

$$\text{Cell decay} \quad r_d = -bX \quad (6)$$

Steady-state mass balances on substrate and cells<sup>b</sup>

$$\text{Substrate} \quad 0 = Q(S^0 - S) - \frac{\dot{q}XS}{K+S} \quad (7)$$

$$\text{Cells} \quad 0 = -X^e Q^e - X^w Q^w + \frac{Y\dot{q}SX}{K+S} - bXV \quad (8)$$

Steady-state solutions for S and X

$$\text{Substrate} \quad S = K \frac{1 + b\theta_x}{\theta_x \dot{q}Y - (1 + b\theta_x)} \quad (9)$$

$$\text{Cells} \quad X = \left(\frac{\theta_x}{\theta}\right) \frac{Y(S^0 - S)}{1 + b\theta_x} \quad (10)$$

where

$$\text{Mean cell retention time} \quad \theta_x = \frac{VX}{Q^e X^e + Q^w X^w} \quad (11)$$

Steady-state mass balance on plasmid-containing cells,  $pX^b$

$$0 = k_{12} pX(1 - p)X - b_p pX + (qY - b)pX - pX\theta_x \quad (12)$$

Steady-state solution for fraction of cells containing plasmid,  $p$

$$p = 1 - b_p/k_{12}X \quad (p \geq 0) \quad (13)$$

<sup>a</sup>All rate expressions are in units of ML<sup>-3</sup> T<sup>-1</sup>.

<sup>b</sup>All mass balance expressions are in units of MT<sup>-1</sup>.

TABLE 2  
Reported values of gene-transfer kinetic coefficients<sup>a</sup>

Organism	Plasmid	Parameters and values <sup>b</sup>	Reference
<i>E. coli</i> growing exponentially	F-lac	$k_{11} = 2.4\text{--}2400$ L-gT/gD-gR-day $b_p = 0.0024\text{--}0.24$ day <sup>-1</sup>	2
<i>E. coli</i> growing at $\mu = 0.12$ and $0.14$ h <sup>-1</sup>	R100; R100-1	$k_{12} = 1.05$ and $4.07$ L/gR-day, respectively	3
<i>E. coli</i> growing exponentially	F-lac; R1; R1 drd 19	$k_{11} = k_{12} = 0.11\text{--}0.37$ L/g-day	4
<i>E. coli</i> in lag phase	F-lac; R1; R1 drd 19	$k_{11} = k_{12} = 1.3\text{--}39$ L/g-day	
<i>E. coli</i> growing at $\mu = 0.2$ h <sup>-1</sup>	F-lac; R1; R1 drd 19	$k_{11} = k_{12} = 0.0066\text{--}0.44$ L/g-day	
<i>E. coli</i> growing at $\mu = 0.17$ h <sup>-1</sup>	R1; R1 drd 19	$k_{11} = 1.2 \times 10^{-6}\text{--}4.8$ L-gT/gD-gR-day $k_{12} = 48\text{--}1.1 \times 10^{-4}$ L/gR-day	5
<i>Pseudomonas cepacia</i>	R388:Tn 1721	$k_{11} = k_{12} = (1.2\text{--}1.3) \times 10^{-3}$ L/g-day	6

<sup>a</sup>Obtained by fitting experimental data to the respective model.

<sup>b</sup>Mass values were computed by assuming  $10^{12}$  cells per gram dry weight.

can be back-calculated. For example, sufficient information was available to make a reasonable back-calculation of  $k_{11}$  for the broth experiments listed in Table 3 and for the plate and filter experiments listed in Table 4. These tables give the estimated values of  $k_{11}$ , as

well as the experimental conditions and necessary assumptions. In all cases, the only transfer mechanism assumed to occur was donor-to-recipient transfer, because  $D$  and  $R$  concentrations usually were large compared with  $T$ .

The values of  $k_{11}$  in Tables 3 and 4

generally are lower than those shown in Table 2. The reasons for the differences could be related to different species, to poor mixing of the cells, or to a lack of accounting for plasmid loss. A second trend, shown in Table 3, is that lower temperature matings give higher  $k_{r1}$  values. The cause for this trend (if it is real) is not known, but one possibility is that  $b_p$  is reduced by low temperature, thereby making the apparent  $k_{r1}$  larger.

A third trend seen in Tables 3 and 4 is that the lowest values of  $k_{r1}$  are associated mainly with plate and filter matings. This finding is ironic, because it is well known that the highest mating frequencies usually occur for plate and filter matings (recall that frequency usually is defined as number of transconjugants per original number of donors) (11-13). The conventional wisdom is that filter matings have high frequencies partly because of the high cell densities obtainable. Although this concept is correct, when the actual concentrations are taken into account,  $k_{r1}$  appears to be lower for matings on solid surfaces. Again, the reasons are not clear, but a plausible hypothesis is that limited cell mobility on plates and filters reduces the opportunities for cell-to-cell contacts.

In summary, data for the quantification of plasmid transfer rates are limited. The results from studies designed to evaluate kinetics (Table 2) show a wide range of  $k_{r1}$  and  $k_{r2}$  values, but many of the values are large. The  $k_{r1}$  values computed from mating experiments (Tables 3 and 4) generally are lower than those derived from kinetic experiments. These values may be artificially low, however, because of poor mixing (especially likely for plate and filter matings) and failure to account for plasmid loss. Clearly, much more information is needed on plasmid transfer rates.

## Applications

**Plasmid content within an indigenous population.** Although quantitative data on the transfer coefficients are incomplete, enough information exists to make a good preliminary assessment of the effects of plasmid transfer on a biological process. That assessment is performed through the expansion of a conventional biological-process model to include plasmid content and plasmid transfers.

The model begins with the traditional relationships for substrate utilization, cell growth, cell decay, and input and output of substrate and cells. Rate equations for substrate utilization and cell growth and decay are tabulated in the second portion of Table 1. Nomenclature and definitions are given at the end of this article.

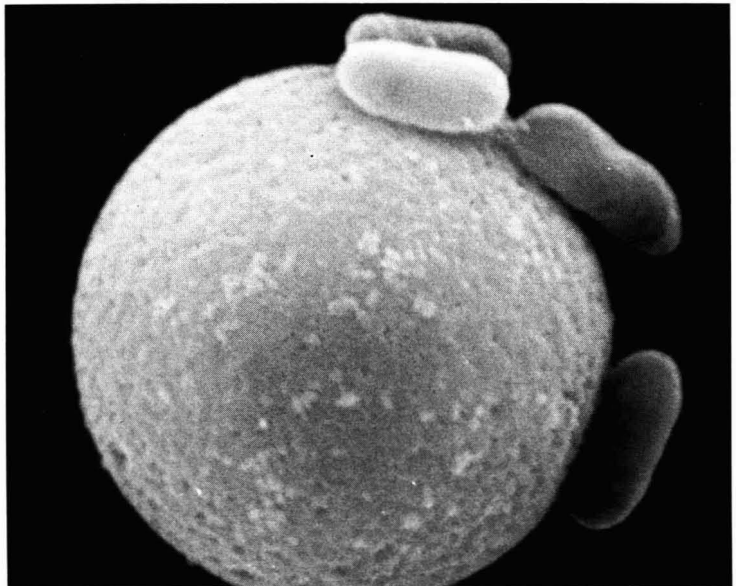
## General protocol for a mating experiment

- Known numbers of donor and recipient cells are mixed together and put into the appropriate incubation system (i.e., flask, plate, or filter).
- The cells are incubated for a set period of time under controlled conditions of temperature, pH, and nutrients.
- At the end of the incubation period, the cells are harvested, and the number of transconjugants formed is counted, usually by plating a dilution series on a selective medium and counting colonies.
- Finally, the mating frequency is computed, typically as the number of transconjugants formed divided by the original number of donor cells.

## The basis of the expanded model

The expanded model is based on the following assumptions:

- All the cells are dispersed, so that all cells have equal opportunity for substrate utilization and cell-to-cell contact.
- The total active biomass, at concentration  $X$ , is divided into two populations: the fraction  $p$  that contains the plasmid and the fraction  $1 - p$  that does not.  $pX$  corresponds to  $T$  (the transconjugant concentration), and  $(1 - p)X$  corresponds to  $R$  (the recipient concentration) for this two-population system.
- The transfer of plasmid is modeled as transconjugant-to-recipient transfer (see Equation 2, in which  $pX$  corresponds to  $T$  and  $(1 - p)X$  corresponds to  $R$ ). Thus, the plasmid could have originated from an exogenous donor that washed out of the system, from indigenous bacteria containing the plasmid, or from mutation within the indigenous population.
- Plasmid loss from  $pX$  is modeled by Equation 3, in which  $pX$  corresponds to  $T$ .
- The plasmid does not confer any growth advantage or disadvantage; thus,  $q$ ,  $K$ ,  $Y$ , and  $b$  are the same for both populations. Evidence exists that having a plasmid can confer an advantage or a disadvantage to cells, or have no effect on cells; in this case, the simplest scenario is assumed.
- The system is at steady state, in which  $\theta_x^{-1} = qY - b$ .
- The total biomass concentration,  $X$ , is controlled by the input substrate concentration,  $S^0$ , and the mean cell residence time,  $\theta_x$  (Equations 10 and 11).
- The influent contains no cells.



Polystyrene bead capturing bacteria.

TABLE 3  
Estimates of  $k_{t1}$  from batch mating experiments in liquid media

$k_{t1}$ , L-g <sup>-1</sup> g <sub>n</sub> -g <sub>o</sub> -day	Conditions and assumptions	Reference
$4.4 \times 10^{-5}$ at 29.5 °C $1.4 \times 10^{-2}$ at 22.5 °C	<i>E. coli</i> MA527 donated a 60MD R-plasmid pKK1 to <i>E. coli</i> MA728 in membrane diffusion chambers for 24 h at the noted temperature. No change in <i>D</i> or <i>R</i> was assumed.	14
Nutrient broth $1.4 \times 10^{-4}$ (97%) Sterile sewage $1.4 \times 10^{-4}$ (70%) I Clarifier $1.2 \times 10^{-1}$ (80%) II Clarifier $2.1 \times 10^{-1}$ (87%)	<i>Salmonella enteritidis</i> , <i>Proteus vulgaris</i> , or <i>E. coli</i> donated R plasmid to <i>Shigella sonnei</i> or another <i>E. coli</i> in nutrient broth or sterile sewage for 3 h at 37 °C. Exponential increase of <i>D</i> and <i>R</i> was assumed at 2.5 h <sup>-1</sup> , and $k_{t1}$ was calculated with the average <i>D</i> and <i>R</i> . In other experiments, diffusion chambers were equilibrated with sterile sewage in I and II clarifiers at 7.8–13.3 °C for 3 h. For these experiments, no growth of <i>R</i> and <i>D</i> was assumed. Reported are averages of observable transfer rates. In parentheses is percentage of experiments yielding positive results.	15
<i>Klebsiella pneumoniae</i> (R) to $\chi^{1997}$ $3.6 \times 10^{-4}$ – $3.8 \times 10^{-4}$ <i>Klebsiella pneumoniae</i> (R) to 343 $6.2 \times 10^{-5}$ – $9.9 \times 10^{-6}$ <i>E. coli</i> (R) to $\chi^{1997}$ $6.9 \times 10^{-1}$ – $7.0 \times 10^{-4}$ <i>E. coli</i> (R) to 343 $2.1 \times 10^{-1}$ – $1.7 \times 10^{-4}$	Strains isolated from sewage with R plasmid transferred to <i>E. coli</i> $\chi^{1997}$ (wastewater isolate) or <i>E. coli</i> 343 (lab isolate). Incubations were in spent medium (L-broth) for 25 h at 37 °C. Reported <i>R</i> and <i>D</i> values were assumed to be constant. <i>T</i> to <i>R</i> transfer might be important.	16
To <i>Enterobacter</i> $1.3 \times 10^{-2}$ to <i>E. coli</i> 191 $2.6 \times 10^{-3}$ to <i>E. coli</i> 1997 8.7	<i>E. coli</i> $\chi^{1784}$ donated plasmid R100-1 to other <i>E. coli</i> or to <i>Enterobacter cloacae</i> . Incubations were in spent medium for 25 h at 37 °C. <i>R</i> and <i>D</i> values are reported at time 0 and assumed constant. High final <i>T</i> concentrations might cause an overestimate of $k_{t1}$ .	17
Soil $7.5 \times 10^{-6}$ Water $1.7 \times 10^{-5}$	<i>E. coli</i> donated RP4 to a mixed population of <i>Pseudomonadaceae</i> and <i>Enterobacteriaceae</i> in soil and water at 37 °C for 24 h. Soil samples started with donors at 10 <sup>7</sup> and recipients at 10 <sup>9</sup> /mL, and water samples with donor at 10 <sup>8</sup> and recipients at 3 × 10 <sup>7</sup> /mL. No changes in <i>D</i> and <i>R</i> were assumed.	18
R68.45; spent medium $6.0 \times 10^{-2}$ R68.45; sterile lake water $3.6 \times 10^{-9}$ FP5; spent medium $1.1 \times 10^{-2}$ FP5; sterile lake water $1.2 \times 10^{-4}$ $1.7 \times 10^{-8}$ to $1.0 \times 10^{-4}$	Plasmids R68.45 and FP5 were transferred in <i>Pseudomonas aeruginosa</i> mating pairs, previously grown to exponential phase and resuspended in spent medium or sterile lake water. Matings occurred at 37 °C for 2 h, during which changes in <i>D</i> and <i>R</i> were assumed to be negligible.	19
	Antibiotic-resistant coliforms, isolated from porcine fecal waste transferred plasmid to a laboratory <i>E. coli</i> J 53 strain. Incubations were in nutrient broth at 37 °C. Growth quickly increased numbers of cells to 4 × 10 <sup>9</sup> /mL, which was used for computation. $k_{t1}$ values represent the range for transfer of resistances to tetracycline, ampicillin, and streptomycin.	12

Equation 12 in Table 1 defines the mass balance for transconjugants. Its solution requires prior knowledge of *S*, *X*, and  $\theta_x$  (from, for example, prior solution of Equations 9–11). The steady-state solution of Equation 12 is Equa-

tion 13, which shows that the fraction of plasmid-containing cells is proportional to *X* and  $k_{t2}$  and inversely proportional to  $b_p$ .

A useful manipulation of Equation 13 is to solve for *X* as *p* approaches zero.

The value is  $X_{min}$ , where

$$X_{min} = b_p/k_{t2} \quad (14)$$

$X_{min}$  is the minimum cell concentration required to sustain enough plasmid transfer to keep plasmid-containing cells in the reactor. Thus, when the cell concentration is lower than  $X_{min}$ , plasmids are “washed out” of the population. Stewart and Levin (2) obtained a similar result when they modeled plasmid behavior in a chemostat that had only *T* and *R*. For stable maintenance of plasmid in the population, a minimal cell number was required. The minimal cell number was directly proportional to the segregation rate (analogous to  $b_p$ ) and the transconjugants’ relative decrease in growth rate (not considered here), and inversely proportional to the plasmid transfer rate (analogous to  $k_{t2}$ ).

Figure 1 illustrates  $X_{min}$  for the range of  $k_{t2}$  values in Table 2 and a range of  $b_p$  values. Combinations of  $b_p$  and  $k_{t2}$  that give  $X_{min}$  values below about 5 g/L appear attainable for activated-sludge treatment, because 5 g/L is an upper limit of active-cell concentration that would make such treatment possible. Clearly, many such  $b_p$ ,  $k_{t2}$  pairs are available, especially when  $k_{t2}$  is larger than 1 L/g<sub>R</sub>-day. On the other hand, very low  $k_{t2}$  values (e.g., < 10<sup>-3</sup> L/g<sub>R</sub>-day) would require very low  $b_p$  values or very high *X* values to sustain plasmid content.

Figure 2 depicts values of *p* for combinations of  $k_{t2}$  and *X* in which  $X > X_{min}$  and  $b_p = 0.1 \text{ day}^{-1}$ . Because little is known about  $b_p$ , it has been selected near the upper end of the range reported by Stewart and Levin (2).

Figure 2 reveals two patterns. In the first pattern, *p* increases quickly when  $X > X_{min}$ . Second, significant *p* values can be achieved for  $k_{t2}$  values reported in Table 2. For example, when  $k_{t2} = 0.1 \text{ L/g}_R\text{-day}$  and  $X = 2 \text{ g/L}$  (typical for activated sludge), *p* equals 0.5. Thus, one-half of the population would have the potential to perform the reactions encoded by the plasmid.

**Plasmid content with bioaugmentation.** The expanded model evaluates the maintenance of a plasmid by transfer within the indigenous population. However,  $k_{t2}$  may be zero, or at least too small to sustain a steady-state fraction of plasmid-containing cells. In such cases, the addition of exogenous bacteria that contain and can donate the desired plasmid might be an effective means for enhancing process performance. Such a situation is an example of a *bioaugmentation* strategy, or the addition of specialized cells to augment the genetic capability of the indigenous population.

The basic model can be modified to include the effects of adding the exoge-

nous strain. The mass rate of addition of the exogenous strain is  $QX_c^\circ$ , where  $X_c^\circ$  is the input concentration of the exogenous strain. We can assume that the exogenous strain does not grow well in the biological process and has a net decay rate of  $-b_c X_c V$ . (Generally, bioaugmentation does not succeed by building up a large mass of the exogenous microorganisms, because they do not survive well in the treatment system, or their addition rate must be low for economic reasons.) The exogenous cells are lost from the reactor in proportion to their concentration in the reactor,  $-VX_c/\theta_x$ . Thus, the steady-state mass balance on  $X_c$  is

$$0 = QX_c^\circ - b_c X_c V - X_c V/\theta_x \quad (15)$$

which can be solved to yield  $X_c$ ,

$$X_c = \frac{\theta_x}{\theta} \frac{X_c^\circ}{1 + b_c \theta_x} \quad (16)$$

where  $\theta = V/Q$  = liquid detention time. For large  $b_c \theta_x$  (usually the norm), Equation 16 reduces to

$$X_c = \frac{X_c^\circ}{b_c \theta} \quad (17)$$

The steady-state mass balance on the fraction ( $p$ ) of the indigenous biomass ( $X$ ) that contains plasmid is similar to Equation 13 (Table 1), except that donor-to-recipient transfer from  $X_c$  to  $(1-p)X$  is used and  $T$  to  $R$  transfer is eliminated to accentuate the effects of the exogenous strain.

$$0 = k_{t1} X_c (1-p)X - b_p pX + (\hat{q}Y - b)pX - pX/\theta_x \quad (18)$$

Equations 17 and 18 can be solved for  $p$ :

$$p = \frac{1}{b_p b_c \theta + \frac{k_{t1} X_c^\circ}{\theta_x}} \quad (19)$$

Equation 19 shows that  $p$  can become a significant fraction when  $b_p$ ,  $b_c$ , and  $\theta$  are small and  $k_{t1}$  or  $X_c^\circ$  are large.

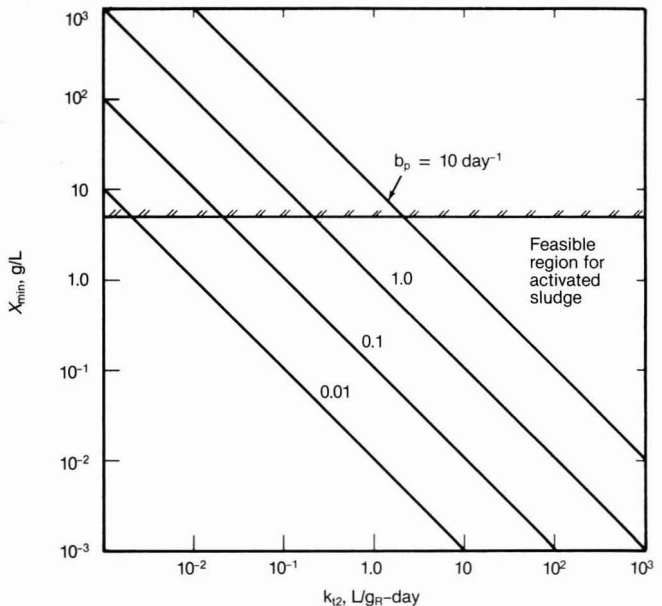
Figure 3 shows how  $p$  varies with  $k_{t1}$  and  $X_c^\circ$  when  $b_c$ ,  $b_p$ , and  $\theta$  are fixed. The value of  $b_p$  is selected as  $0.1 \text{ day}^{-1}$ , as in Figure 2. The value of  $b_c$ ,  $1.0 \text{ day}^{-1}$ , is representative of the exponential die-off observed when host cells that are potentially useful for genetic engineering are placed in sewage (21, 22) and sewage treatment processes (23). The trend in Figure 3 is clear: A significant portion of the indigenous biomass can contain the plasmid contributed by the exogenous strain, provided that  $X_c^\circ$  and  $k_{t1}$  are large enough.

In practice, however, bioaugmentation doses usually must be small, be-

TABLE 4  
Estimates of  $k_{t1}$  from filter and plate matings

$k_{t1}$ , L-g <sub>r</sub> /g <sub>b</sub> -g <sub>R</sub> -day	Conditions and assumptions	Reference
$10^{-9}$ to $10^{-8}$	<i>Bacteroides ruminicola</i> donated a tetracycline resistance plasmid to another strain of <i>B. ruminicola</i> on an agar surface for 16 h at 39 °C. <i>R</i> and <i>D</i> remained nearly constant during the incubation.	20
$5.5 \times 10^{-5}$ to $3.5 \times 10^{-3}$	<i>E. coli</i> donated the RP4 plasmid to several <i>Pseudomonadaceae</i> and <i>Enterobacteriaceae</i> isolated from soil or water. Tryptose agar plates with mixed suspensions of <i>D</i> and <i>R</i> were incubated at 37 °C for 24 h. No growth of <i>D</i> and <i>R</i> was assumed.	18
Plate $1.7 \times 10^{-6}$ to $1 \times 10^{-1}$ Filter $1.8 \times 10^{-5}$ to $3.1 \times 10^{-4}$	Antibiotic-resistant coliforms were isolated from porcine fecal waste and used as a donor to a laboratory <i>E. coli</i> strain (J53). Plate and filter matings on a MacConkey agar were carried out at 37 °C for 7 h. Rapid growth of <i>R</i> and <i>D</i> to $4 \times 10^9$ cells/mL was assumed and used for computation. Ranges of $k_{t1}$ reflect frequencies for transfer of resistance to tetracycline, ampicillin, and streptomycin.	12

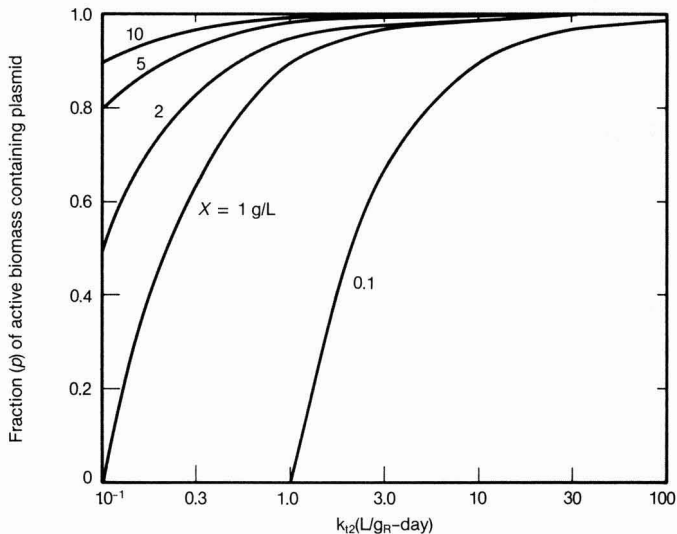
FIGURE 1  
How the activated-sludge operation becomes feasible<sup>a</sup>



<sup>a</sup> $X_{\min}$  decreases to make the activated-sludge operation feasible as  $k_{t2}$  increases and  $b_c$  decreases.

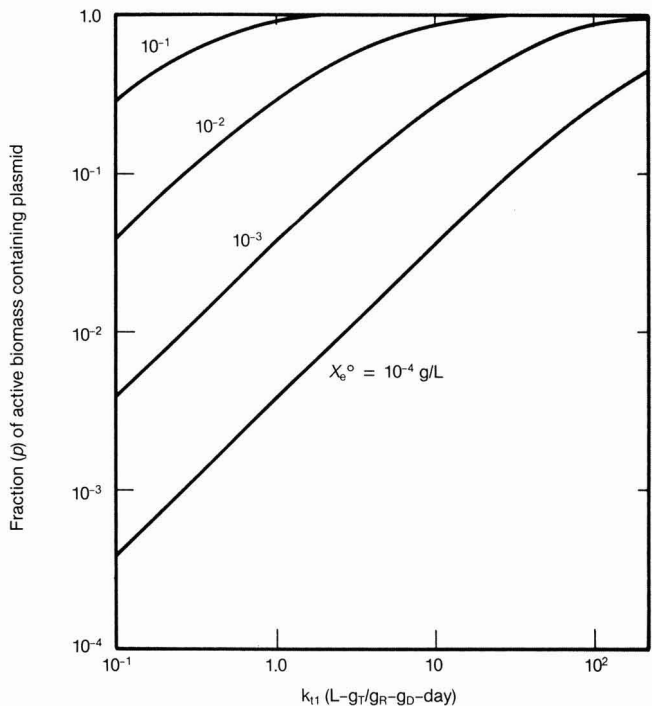


FIGURE 2  
Increasing the plasmid-containing fraction of biomass<sup>a</sup>



<sup>a</sup>The fraction ( $p$ ) of active biomass containing plasmid increases as  $k_{12}$  and  $X$  increase. Values are for  $b_p = 0.1 \text{ day}^{-1}$  and steady state.

FIGURE 3  
The transfer of plasmids in biomass<sup>a</sup>



<sup>a</sup>The fraction ( $p$ ) of active biomass containing plasmid increases with  $k_{11}$  and  $X_0$  when the only source of plasmid is transfer from an added exogenous strain ( $X_0$ ). Values are for  $b_p = 0.1 \text{ day}^{-1}$ ,  $b_c = 1.0 \text{ day}^{-1}$ , and  $\theta = 0.25 \text{ day}$ .

cause the specialized cells are expensive. Thus, we should expect actual  $X_c^\circ$  values to be at the low end of the  $X_c^\circ$  range in Figure 3. To compensate for the low  $X_c^\circ$  values, fairly large values of  $k_{11}$  (or compensatingly smaller values of  $b_p$  and  $b_c$ ) are needed to make a significant fraction of the biomass contain plasmid. However, when the degradation of a xenobiotic compound at low concentration is the goal, only a relatively small fraction of the cells, perhaps as low as 1%, need contain the plasmid to bring about noticeable removals (24).

In summary, a bioaugmentation strategy that adds a very small dose of exogenous microorganisms to a process already containing a large and stable indigenous population could successfully increase the indigenous population's genetic abilities to degrade a xenobiotic compound through plasmid transfer. Simple modeling analysis shows that the  $k_{11}$  value might need to be relatively large (e.g.,  $> 1 \text{ gT/gR-day}$ ) for plasmid transfer to be effective.

#### Future directions

The analyses presented here emphasize the need for quantitative information on the rates of plasmid transfer, particularly the kinetic parameters  $k_{11}$ ,  $k_{12}$ , and  $b_p$ . At this point, almost any quantification would be helpful. Over the long term, however, information must be gathered on genera and species that predominate in biological reactors (e.g., *Pseudomonas* and *Alcaligenes*) and on plasmids that encode functions useful for environmental control, such as degradation of xenobiotic compounds. A large portion of the information now available concerns enteric strains of medical importance and plasmids that encode resistance to antibiotics. Its relevance to environmental applications still is largely unknown.

Carefully controlled experiments that fulfill the needs for quantitative and environmentally relevant data await the development of new analytical techniques for the detection of specific DNA sequences and microbial strains. Selective culturing, which works so well for resistance to antibiotics, is of relatively little value when the plasmid encodes for a function that gives the microorganisms little or no advantage. Fortunately, promising new techniques from microbial molecular biology offer the opportunity to identify specific strains and to determine whether a strain contains DNA that will allow the cell to perform useful reactions.

Strain identification and DNA characterization can be accomplished through hybridization techniques that use small sequences of DNA to charac-

terize the microbial strain or the gene. Hybridization occurs when a small sequence of DNA, called the oligonucleotide probe, is exactly complementary (i.e., has exact base pairing) with a sequence of the cell's DNA or rRNA. The complementary sequences are linked through hydrogen bonding. Hence, the probe sequence is hybridized to, or bonded to, the cell's DNA or RNA. A cell contains the identifying DNA or RNA only when the probe hybridizes to and stays with the cell's DNA or RNA.

The identification of a microbial strain can be based on hybridization of an oligonucleotide probe with the cell's rRNA. Unique base sequences are present in two parts of each strain's rRNA: the 16S and 23S ribosomal RNAs, whose designations refer to the size of the rRNA. Oligonucleotide probes of 20–30 bases, complementary to unique regions in each strain's rRNA, generally provide excellent specificity (25). Because each cell contains thousands of ribosomes, sensitivity also is excellent.

The presence of a specific gene within a cell can be determined with oligonucleotide or longer probes that hybridize with DNA in the cell. Thus, the probe is complementary to a sequence within the gene of interest (e.g., encoding a catabolic function).

In principle, DNA probes for rRNA and DNA can be used to differentiate the strains that are present in a sample and to determine whether the strains contain the plasmid of interest. However, considerable development and testing are needed before hybridization can be widely used for analysis in biological processes. Once the experimental and analytical tools are fully developed, it will be possible to study the effects of plasmid content on the physiology of cells found in treatment processes. Particularly useful would be information on how having a plasmid affects the normal kinetic parameters  $\hat{q}$ ,  $K$ ,  $b$ , and  $Y$ . This information is especially interesting when the plasmid confers little or no advantage, such as for biodegradation of a compound whose concentration is at trace levels.

One more subject that requires research is the effect of cell aggregation on plasmid transfer. In real biological processes, almost all of the cells are aggregated as flocs or biofilms (26). As suggested by the results of Tables 2, 3, and 4, immobilization of cells seems to reduce the transfer rate,  $k_{11}$ , presumably because of reduced opportunities for cell-to-cell contacts. On the other hand, the high cell densities in most aggregates (5–100 g/L) tend to increase transfer rates. One possibility is that plasmid transfer in fixed or aggregated

### Methods for identifying strains and the presence of genes

The most versatile and general approach for identifying microbial strains is through hybridization of short synthesized sequences of nucleotide bases (oligonucleotide probes) to unique regions of the strains 16S or 23S of ribosomal RNAs (25, 27). The advantage of identifying different strains by their ribosomal RNA (rRNA) is that because all cells have rRNA, their RNAs generally can be differentiated by unique RNA sequences, and the DNA specifying the rRNA sequences is not transferred among cells (28). Thus, rRNA sequences are stable and unique markers for a given microorganism. Figure 4 illustrates that rRNA is made up of conserved (i.e., the same for all strains) and variable regions; hybridization to the variable regions allows identification of individual strains.

During hybridization, the DNA probe interacts with rRNA isolated from or within the cells. If the probe's sequence is complementary to the cell's rRNA, the two strands hybridize, and the probe RNA is kept with the cell's RNA. Usually, the rRNA is bound to a solid matrix so that the unhybridized probe is washed away, and the amount of retained, hybridized probe is used to measure the amount of the target rRNA. Normally, the oligonucleotides are labeled radioactively and measured by quantification of bound radioactivity. Nonradioactive labeling systems, such as enzymes and fluorescent dyes, are available, but they generally lack the sensitivity and accuracy of radiolabels. However, the development of nonradioactive labels is proceeding rapidly, and this technique eventually could replace radioactive detection systems. For example, probes labeled with fluorescent dyes currently are being used to identify single cells by microscopy.

There are two general approaches for determining the number of cells that have rRNA that hybridizes with a probe. The first approach involves extraction of total nucleic acid (mostly RNA) from the biomass, denaturing and immobilizing a portion of it on a membrane filter, and hybridizing it with a radiolabeled probe (25). The number of cells is determined by comparison with a reference standard containing a known number of the cells of interest. The second approach is based on hybridization of intact cells (29). The cell sample is fixed with formaldehyde or glutaraldehyde, and hybridization is performed under conditions similar to membrane hybridization. The cells then are collected and washed to remove unhybridized probes. Cells that contain hybridized radioactive probes are counted by exposing the hybridized cells to photographic film and using a microscope to count the images (autoradiography). Fluorescence microscopy is used when the probes are labeled with fluorescent materials.

Because there are many thousand copies of rRNA per cell, rRNA hybridization generally is the most sensitive technique for identifying strains. However, hybridization requires that the target strain first be isolated and purified, that the unique rRNA sequence be identified, and that probes complementary to unique sequences within the rRNA be synthesized. Thus, although RNA hybridization is a very powerful technique, it requires a substantial amount of preparatory work.

Specific DNA sequences, such as those that occur in a plasmid of interest, can be detected by DNA hybridization. This method is similar to RNA hybridization, except that the target sequences are sequences of DNA. Another variation is to use RNA as a probe for DNA. Nucleic-acid hybridization techniques now are standard tools of molecular genetics (30) and are being applied increasingly to the identification of specific genes in natural samples (31, 32).

environments is governed by a mechanism that resembles knocking down a row of dominoes (i.e., serial transfer through contiguous cells). In any case, the mechanisms and mathematical descriptions for plasmid transfer in aggregates eventually must be elucidated.

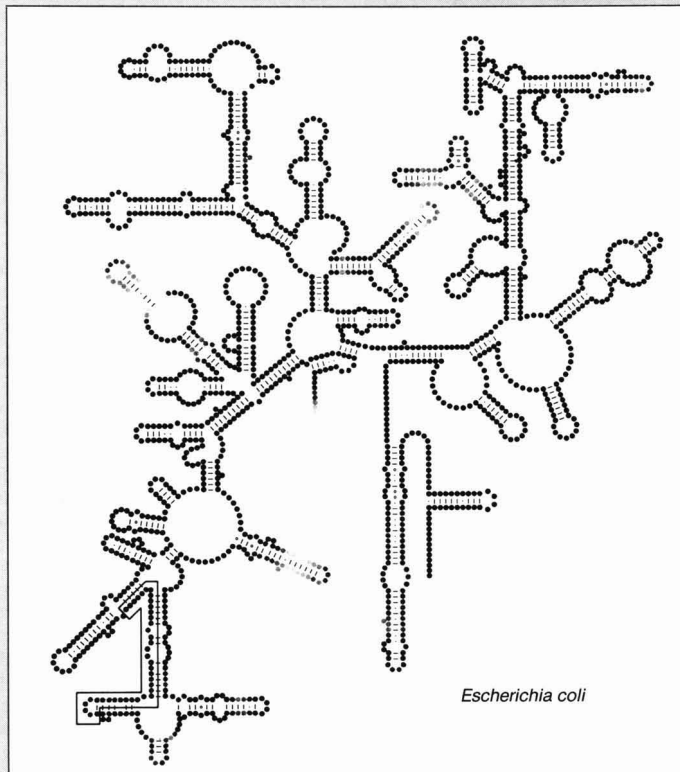
### Transfer rates must be quantified

For this second part of our article on the role of genes in biological processes we developed and applied a simple kinetic model for plasmid content and transfer in suspended-growth biological processes. Using transfer parameters

within the ranges observed from previous studies, the model suggests that plasmids could be stably maintained in biological processes if the parameter groups  $b_p/k_{12}X$  or  $b_p b_c \theta / (k_{11} X_c^2)$  are sufficiently small. However, confidence in values for  $b_p$ ,  $k_{11}$ ,  $k_{12}$ , and  $b_c$  is low, especially for strains and plasmids of interest for biological processes used for environmental control.

Therefore, major research advances are needed for quantifying transfer rate parameters. Carefully controlled kinetic studies and new analytical techniques must be employed to differenti-

FIGURE 4  
Secondary structure of eubacterial 16S ribosomal RNA\*



\*The secondary structure from 27 different eubacterial 16S rRNAs shows the degree of conserved and unique sequences. Each dot represents one ribonucleotide. Shading is proportional to the degree to which regions are conserved (invariant) for all the strains. Invariant regions are in black, and light gray regions differ for the different strains. The boxed region (lower left) illustrates an oligonucleotide-probe sequence.  
Source: Reference 33.

ate genetic transfers from other effects. Promising methods are available to accomplish the needed advances, but bringing them to fruition will require long-term, interdisciplinary research.

#### Acknowledgment

Valuable editorial assistance was provided by Jacqueline MacDonald. This research was funded wholly from funds provided by the United States Environmental Protection Agency through Cooperative Agreement CR-812582-03 to the Advanced Environmental Control Technology Research Center.

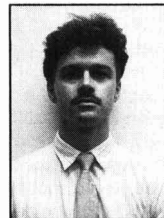
This article was reviewed for suitability as an *ES&T* feature by C. P. Leslie Grady, Clemson University, Clemson, SC 29634; and Gary Saylor, University of Tennessee, Knoxville, TN 37916.

#### References

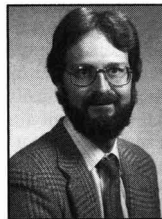
- (1) Rittmann, B. E. et al. *Environ. Sci. Technol.* **1990**, *24*, 23-29.
- (2) Stewart, F. M.; Levin, B. R. *Genetics* **1977**, *87*, 207-28.
- (3) Cullum, J. et al. *Plasmid* **1978**, *1*, 536-44.

- (4) Cullum, J. et al. *Plasmid* **1978**, *1*, 545-56.
- (5) Levin, B. R. et al. *Plasmid* **1989**, *2*, 247-60.
- (6) Freter, R. et al. *Infect. Immun.* **1983**, *39*, 60-84.
- (7) Knudsen, G. R. et al. *Appl. Environ. Microb.* **1988**, *54*, 343-47.
- (8) Jones, I. M. et al. *Molec. Gen. Genet.* **1980**, *180*, 579-84.
- (9) Godwin, D.; Slater, J. H. *J. Gen. Microb.* **1979**, *111*, 201-210.
- (10) Walter, M. V. et al. *Appl. Environ. Microb.* **1987**, *53*, 105-9.
- (11) Genthner, F. J. et al. *Appl. Environ. Microb.* **1988**, *54*, 115-17.
- (12) Abdul, P.; Venables, W. A. *Appl. Microb. Biotechnol.* **1986**, *24*, 149-52.
- (13) McKay, L. L. et al. *Appl. Environ. Microb.* **1980**, *40*, 84-91.
- (14) Altherr, M.; Kasweck, K. L. *Appl. Environ. Microb.* **1982**, *44*, 838-42.
- (15) Mach, P. A.; Grimes, D. J. *Appl. Environ. Microb.* **1982**, *44*, 1395-1403.
- (16) McPherson, P.; Gealt, M. A. *Appl. Environ. Microb.* **1986**, *51*, 904-9.
- (17) Gealt, M. A. et al. *Appl. Environ. Microb.* **1985**, *49*, 836-41.
- (18) Schilf, W.; Klingmuller, W. *Rec. DNA Techn. Bull.* **1983**, *6*, 101-2.
- (19) O'Morchoe, S. B. et al. *Appl. Environ. Microb.* **1988**, *54*, 1923-29.

- (20) Flint, H. F. et al. *Appl. Environ. Microb.* **1988**, *54*, 855-60.
- (21) Liang, L. et al. *Appl. Environ. Microb.* **1982**, *44*, 708-14.
- (22) Mallory, L. M. et al. *Rec. DNA Techn. Bull.* **1982**, *5*, 5-6.
- (23) Sagik, B. P.; Sorber, C. *Rec. DNA Techn. Bull.* **1979**, *2*, 55-61.
- (24) Namkung, B. E.; Rittmann, B. E. *J. Water Pollut. Contr. Fed.* **1987**, *56*, 670-78.
- (25) Stahl, D. A. et al. *Appl. Environ. Microb.* **1988**, *54*, 1079-84.
- (26) Rittmann, B. E. *Environ. Sci. Technol.* **1987**, *21*, 128-36.
- (27) Pace, N. R. et al. *Adv. Microb. Ecol.* **1986**, *9*, 1-55.
- (28) Woese, C. R. *Microbiol. Rev.* **1987**, *51*, 221-71.
- (29) Giovannoni, S. et al. *J. Bacteriology* **1988**, *170*, 720-26.
- (30) Maniatis, T. et al. In *Molecular Cloning: A Laboratory Manual*; Cold Springs Harbor Laboratory: Cold Springs Harbor, NY, 1982; p. 545.
- (31) Claus, P. et al. *Prog. Food Nutr. Sci.* **1983**, *7*, 139-42.
- (32) Saylor, G. S. et al. *Appl. Environ. Microb.* **1985**, *49*, 1295-1303.
- (33) Stahl, D. A. *Biotechnology* **1986**, *4*, 623-28.



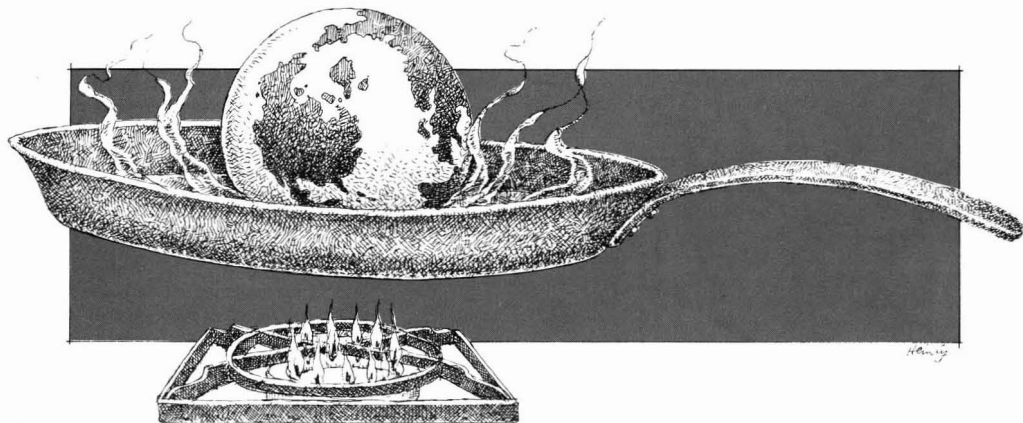
**Barth F. Smets** is a research assistant in environmental engineering at the University of Illinois. He is pursuing the Ph.D. degree in environmental engineering and science and has a strong interest in applied microbiology. Previously he obtained an M.S. degree in agricultural engineering at the State University of Ghent (Belgium).



**Bruce E. Rittmann** is professor of environmental engineering at the University of Illinois, Urbana, IL. Rittmann's research focuses on the biodegradation of low-concentration organic compounds, biofilm processes, and interdisciplinary research in environmental biotechnology.

**David Stahl** (r) is assistant professor of veterinary pathobiology and is affiliated with the Department of Microbiology at the University of Illinois at Urbana-Champaign. His research concerns the application of molecular ecology and phylogeny to the characterization of natural microbial communities.

# Slowing global warming



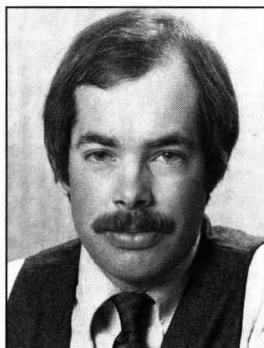
By Christopher Flavin

Global warming promises to be one of the central environmental issues of the nineties. After a decade of concern in the scientific community but neglect by the general population, there is now a growing political as well as scientific consensus that the world can no longer afford to procrastinate about this issue.

In November 1988,<sup>1</sup> representatives of 30 countries met in Geneva under the auspices of the United Nations Environment Programme (UNEP) and the World Meteorological Organization. Following a pattern established in arms control talks, these nations have formed an Intergovernmental Panel on Climate Change that meets periodically to forge an agreement. Plans call for the drafting of an international climate treaty in 1990 and for its formal adoption at a global environmental summit in 1992.

This action cannot come too soon. Changes to the Earth's atmosphere are global and—for all practical purposes—irreversible, not only in our lifetimes but in those of our children and grandchildren as well. Lending urgency to the problem is the fact that the chemical composition of the Earth's atmosphere is already quite different than it was just a century and a half ago. We have already committed ourselves to more climate change than many societies will be able to cope with.

Nitrogen and oxygen are still the



Christopher Flavin

main constituents of the atmosphere, but several more complex gases are building steadily: carbon dioxide (CO<sub>2</sub>) is up 25%, nitrous oxide 19%, and methane 100%. Chlorofluorocarbons (CFCs), a class of synthetic chemicals not normally found in the atmosphere, have added to this blanket of gases that allow sunlight in but trap the resulting heat.

Global average temperatures are now about 0.6 °C warmer than they were 100 years ago. No conclusive proof links this recent heating to the greenhouse effect, but circumstantial evidence has convinced many scientists that this is the cause. Of more concern, however, is the much faster warming that is predicted by a half-dozen computer models—reaching an increase of 2.5–5.5 °C late in the next century. The

difference between the warming of the past century and that expected in the decades ahead is like that between a mild day in April and a late-summer scorcher.

Although climate change is a young science and many aspects of it are uncertain, this is no excuse for delay: Societies invest in many programs, such as defense, to protect against an uncertain but potentially disastrous threat. Similarly, investing in strategies to slow global warming is a sort of insurance policy against catastrophes that have far greater odds of occurring than most events for which we buy insurance. And many of these programs are economical investments in their own right, cutting energy bills and air pollution as well as helping to restore the carbon balance.

Coping effectively with global warming will force societies to move rapidly into uncharted terrain, reversing powerful trends that have dominated the industrial age. This challenge cannot be met without a strong commitment on the part of individual consumers and governments alike. Unprecedented policy changes that have now become urgent regarding Earth's carbon balance include a new commitment to greater energy efficiency and renewable energy sources, a carbon tax on fossil fuels, a reversal of deforestation in tropical countries, and the rapid elimination of CFCs.

During 1988, some 5.66 billion tons

of carbon were released by the combustion of fossil fuels—more than a ton for each human being. Another 1–2 billion tons were released by the felling and burning of forests, mainly in tropical areas. Each ton of carbon emitted into the air results in 3.7 tons of carbon dioxide, the seemingly innocuous gas that is now one of the principal threats to humanity's future.

EPA has estimated that to stabilize atmospheric concentrations of CO<sub>2</sub> at the current level, carbon emissions must be cut 50–80%, back to the 1950s level. Scientists and policymakers meeting in Toronto in June 1988 offered a short-term goal: cut emissions 20% by 2005.

Any realistic strategy must start with the fact that one-fourth of the world's population accounts for nearly 70% of the fossil-fuel-based carbon emissions. This wealthy, energy-intensive quarter has an obvious responsibility to lead in the search for solutions. But the level of carbon emissions in developing countries remains an extraordinarily difficult issue.

In an effort to balance practicality and equity against the urgency of the problem, Worldwatch Institute has formulated reduction targets based on today's per capita carbon emissions levels (see Table 1). Countries such as the United States and the Soviet Union that currently produce carbon dioxide at a high rate would be required to reduce emissions by about 35% in the next 10 years, while nations such as India or Kenya could continue to increase emissions. Those with carbon emissions between these two extremes, such as Italy and Japan, would have to reduce them less rapidly than the high producers.

These targets can be met by pursuing the technologies and policies described earlier. The goals are designed to gradually narrow the disparities that now exist among national emissions levels. They are also practical, calling for a realizable 12% cut in global emissions by the year 2000. Under them, projected emissions of 6.4 billion tons are 38% below what they will be if the world continues on its current path. Although a 12% reduction would not by itself stabilize the climate, it would put the world on a course toward stabilization of global CO<sub>2</sub> concentrations by mid-century.

Because it is mainly deforestation that causes nations such as Brazil or Côte d'Ivoire to have such high per capita carbon emissions, these targets imply a major effort to slow forest clearing in these countries. A carbon reduction strategy can also begin to slow growth in Third World fossil fuel consumption, however—something that is essential if the planet is to avoid

TABLE 1  
Proposed carbon emission goals

Current carbon emissions level (tons/person)	Suggested emissions targets (percent/year)	Example countries
<0.5	+3.0	Kenya, India, Niger
0.5–1.0	+1.5	China, Nigeria, Philippines
1.0–1.5	0	Indonesia, Mexico, South Korea
1.5–2.0	–0.5	Italy, France, New Zealand
2.0–2.5	–1.0	Japan, Thailand, Peru
2.5–3.0	–2.0	Great Britain, West Germany, Brazil
>3.0	–3.0	Australia, United States, Soviet Union, Colombia, Côte d'Ivoire

Source: Adapted by Worldwatch Institute from Reference 1; Reference 2.

vast increases in carbon emissions in the decades ahead. China, for example, would need to cut its growth rate in coal use from 3.5% per year to 1.5%. This change alone would reduce emissions estimated for this decade's end by more than 200 million tons annually.

Scientists generally agree that the world needs to stabilize atmospheric concentrations of greenhouse gases by the middle of the 21st century, reducing net carbon emissions to a maximum of 2 billion tons per year. To get to this point, the world needs to end the production of CFCs and to cut global carbon emissions by 10–20% over the next decade, adopting country-specific targets based on the per capita figures described earlier. Within a year of signing a reduction agreement, each country would submit a plan to achieve the goals and then issue progress reports every two years. Negotiators, meanwhile, would consider the adoption of stricter goals to begin in 2000.

One issue that must be addressed is how to pay for massive investments in improving the energy efficiency of lighting, industrial motors, and transportation, as well as reforestation projects in developing countries that are strapped with huge debts. Many efficiency and forestry investments have broad economic and environmental value and can be justified on those grounds alone, but without sufficient capital they may be neglected. One important mechanism might be the carbon tax. Pledging 10% of the revenues from such a tax to Third World programs would create an annual fund of \$28 billion. Such a fund could be managed by the United Nations, which would make dispersal contingent on the implementation of credible climate stabilization plans. Programs to improve energy efficiency, manage forests, plant trees, slow population growth, develop renewable energy sources, and design CFC substitutes would be eligible for support. The World Bank and institutions such as the U.N. Development Programme could also play a role by

increasing their lending for such projects and by including climate stabilization as a consideration when reviewing loans.

As the scientific evidence mounts, the time has arrived for a global warming agreement—comprehensive, detailed, and prescriptive. Only a rapid turnaround in carbon emissions trends can begin to get the world on the path to a stable climate. Wholesale changes in energy, land use, and population policies are implied. Unless such action is taken in the next few years, the nineties will become a decade of increasing environmental instability, and we will relegate to the next generation a world less able to meet growing human needs. No other environmental problem has such an exponential and cumulative dimension to it, a fact that argues persuasively for the immediate adoption of strong policies.

The benefits of such an effort extend well beyond stabilization of the climate. Economies would be strengthened, new industries created, air pollution reduced, and forests preserved for their economic and recreational benefits. For humanity as a whole, it would be another step in the evolution of society, demonstrating the ability to work cooperatively as a world community. It would be an auspicious beginning to the new millennium.

## References

- (1) Marland, G. et al. *Estimates of CO<sub>2</sub> Emissions from Fossil Fuel Burning and Cement Manufacturing*; Oak Ridge National Laboratory: Oak Ridge, TN, 1989.
- (2) Houghton, R. A. et al. *Tellus* 1987, 39B, 122–39.

*Christopher Flavin is vice-president for research at the Worldwatch Institute, Washington, DC. The Worldwatch Institute is an independent nonprofit research organization created to analyze and focus attention on global problems. Worldwatch is funded by private foundations and various United Nations organizations. Its director is Lester R. Brown.*

# Investigation and remediation of VOCs in soil and groundwater

By James M. Kerr, Jr.

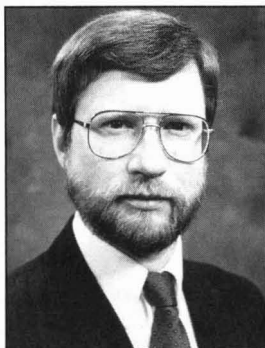
In the past several decades, the use of natural and synthetic volatile organic compounds (VOCs) has increased dramatically. Recently people have become more aware of contamination resulting from the poor or improper handling of these VOCs. When VOC contamination of soil or groundwater has occurred, the first step is to gather all available background data for use in determining the preliminary investigation and remediation objectives.

Background data are the key to determining the response when VOCs are released to the environment. Typically, three levels of data are evaluated: site-specific, local, and regional. By gathering these data, an understanding of the site and its environs is developed, making it less likely that any important factors will be overlooked during the subsequent investigation and remediation of the site.

Typical sources of site-specific data include title searches, aerial photos, site plans, site records, utility company records, and interviews with individuals who have lived near or worked at the site for an extended time.

Typical local information covers current and historical land uses in the area; other potential sources of contamination; and data about nearby wells, surface water bodies, subways, basements, underground utilities, schools, hospitals, and other potentially sensitive receptors.

Regional background data concerning the hydrogeology should include results of local, state, and federally sponsored studies, topographic maps, well records, and previous environmental investigations in the area. The regional data should give a rough esti-



James Kerr

mate of the depth to groundwater, the groundwater flow direction, and the types of materials that make up the unsaturated and saturated zones.

Results of the background data search are best presented by maps, tables, and a written summary. Site-specific data are presented on a site map extending just beyond the site boundaries and including all current and historical features of importance. Local background data are presented on a land use map showing the site and all land uses within a radius of at least 1000 feet.

Finally, the regional background data are presented on a topographic map that has a minimum radius of one mile. Information obtained during the background data search should be sufficient to determine the preliminary objectives, indicate techniques to be used during the investigative phase, provide insight into fate and transport mechanisms, delineate possible risks to human health and the environment, and provide a basic understanding of remedial goals based on local and regional land use.

## Preliminary objectives

Once all the background data have been obtained, the preliminary objectives of the investigation and remediation phases are then determined. This is important for determining the appropriate investigative techniques to use and the order in which they are performed. The preparation of a work plan should be done prior to commencement of site activities. There are different objectives for each phase of the work.

Objectives of the investigative phase typically include delineating the degree, nature, and extent of contamination; gaining an understanding of the transport of contaminants, including interactions and their fate; determining the risk to human health and the environment; and characterizing the subsurface environment sufficiently to determine the appropriate remedial approach.

The objectives of the remediation phase typically include minimizing or eliminating the risk to human health and the environment; minimizing the disruption of normal daily activities; and performing the optimum cleanup of contamination with a minimum expenditure of time and money.

Objectives of the remedial phase are achieved through one of three approaches: a no-action approach; a contamination and partial cleanup approach; or a total cleanup approach. The selection is based on the results of the background work and the information generated during the investigative phase.

## Investigative techniques

Once a contamination problem is known to exist and the objectives of the investigation have been determined, numerous investigative techniques are

available. The majority of these techniques are mechanical, geochemical, or geophysical. Mechanical techniques include hand augering, drilling, trenching, and hydraulic aquifer testing. Geochemical techniques include soil-gas surveys and chemical analyses of soil and water samples. Geophysical techniques include terrain conductivity, ground-penetrating radar, magnetic surveys, resistivity and seismic surveys, and various types of downhole logging.

Hand augering is appropriate for shallow sampling in loose unconsolidated sediments in open or confined spaces. Three main categories of drilling rigs are available for investigative work, but the auger drill rig has become the equipment of choice in most VOC investigations requiring representative soil samples. Trenching may be worthwhile and is relatively inexpensive. It is used on sites with water 10–20 feet deep. The trenching technique can supply information on site stratigraphy and soil type, depth to the water table, and initial extent of contamination.

Geochemical techniques range from simplistic to sophisticated. A simplistic technique of soil vapor surveys is using a hand-held photoionization detector (PID) or flame ionization detector (FID) to do head space analysis of soil and water samples. A more sophisticated technique is to drive an open-ended pipe into the ground and use a PID or FID to gather total VOC concentration data and delineate the area of contamination in the subsurface. The most sophisticated technique is using a field portable gas chromatograph to differentiate various VOCs and their spatial distribution in the subsurface.

Geophysical techniques used during VOC investigations are conductivity, resistivity, ground-penetrating radar (GPR), magnetic surveys, gravity, and seismic surveys in various types of downhole logging. One major drawback to most of these techniques is their susceptibility to cultural interference.

Several of these techniques may need to be combined to meet the objectives. Using multiple techniques can verify previous results and best delineate the degree and extent of contamination.

One example of an appropriate phased approach is the use of GPR to find abandoned underground storage tanks followed by: a soil-vapor survey to delineate the gross soil and water contamination around the tanks; the drilling of several soil borings to obtain soil samples; and the installation of monitoring wells in a minimum of three soil borings to obtain water samples, hydraulic gradient, and aquifer characteristics such as storativity and hydraulic conductivity. This approach will

supply information essential to developing an appropriate remedial plan.

### Remedial techniques

A properly conducted contamination investigation will provide sufficient information to develop a remedial plan, commonly referred to as a corrective action plan (CAP). The CAP may consist of the physical removal of the contaminant, in situ treatment of the contaminant, or a combination of the two. Physical removal of contaminants could include the excavation of contaminated soil or the pumping and treating of contaminated groundwater.

The pumping and treating of contaminated ground water, referred to as pump-and-treat, is probably the most commonly used remedial technique for water contaminated by VOCs. Pump-and-treat consists of one or more wells being pumped at a rate that captures most or all of the contaminated groundwater. The contaminated water is then run through a treatment system which may consist of phase separation, carbon filtration, air stripping, hydrogen peroxide, or a biological treatment system. Each of these technologies has its limitations based on flow rate, contaminant concentration, biological and mineral content of the influent water, site restrictions, and cost. Treated water can then be discharged to surface waters, storm sewers, sanitary sewers, or put back into the ground water system via infiltration galleries or injection wells.

The most common in situ techniques are bioremediation and soil venting, but others such as in situ vitrification have been tested. Physical and chemical characteristics of VOCs lend themselves to a combination of techniques such as pump-and-treat in conjunction with soil venting, excavation of contaminated soil with surface bioremediation, and numerous other combinations.

Although in situ bioremediation has been available for about two decades, its use is still not widespread. In situ bioremediation techniques may play a larger role in contaminant cleanup, but currently there are often options that are more effective in many situations.

In situ vitrification technology came about from studies of how to store low-level nuclear waste more safely. This technique does not appear viable for VOC contamination because of the very large power requirements and the volatilization of most if not all VOCs prior to vitrification.

The use of multiple cleanup techniques based on information gathered during the investigative phase shows real promise when compared to the single-technique approach most commonly used in the past. One example is the use of a pump-and-treat system in

conjunction with soil venting. The pump-and-treat system is used to contain the groundwater already affected by VOCs and to lower levels of contamination in the aquifer. Meanwhile, soil venting can remove contaminants from the unsaturated zone, which eliminates future groundwater contamination, volatilizes VOCs from the groundwater, and decreases the time the pump-and-treat system will be required to operate.

Excavation of contaminated soil coupled with surface bioremediation is another use of multiple cleanup techniques that has met with success in recent years. Excavated soil is stockpiled in lifts or is "thin spread" with appropriate VOC-digesting bacteria applied. When soil piles are used, vent pipes may be placed every couple of lifts to augment the oxygen supply and increase bacterial growth. When thin spreading is used, the contaminated soil must be turned and the VOC-digesting bacteria reapplied on a regular basis until targeted cleanup levels are reached.

The number of remedial techniques available for the treatment of soil and water contaminated with VOCs continues to grow. Most of the techniques are successful alone, but when used in combination they may become more cost- and time-effective. The decision about which technique or techniques to use should always be based on background and investigative data in order to obtain the best and most timely remediation of VOC contaminants.

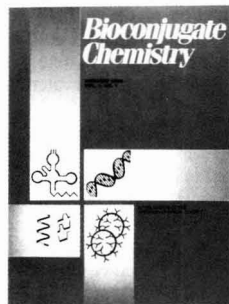
### The bottom line

Investigating and remediating VOCs can be accomplished in an environmentally sound manner with a minimal impact on daily activities and economics. Limited resources can be used best when the investigation and remediation of VOC contamination are based on sound data and realistic objectives.

---

*James M. Kerr, Jr., is a senior environmental geologist and a national technical advisor for Delta Environmental Consultants, Inc., Fort Collins, CO. Kerr has a B.S. degree in geology from Franklin and Marshall College and an M.S. in geology from Rutgers University, and is a registered professional geologist. His responsibilities include management of regional environmental projects and supervision of technical quality on a national level. He presented an expanded version of this paper at a recent U.S.-U.S.S.R. groundwater conference.*

**A long-awaited unifying medium for virtually any practitioner of conjugation chemistry**



# Bioconjugate Chemistry

Premiering January/February 1990.

**Editor:** Claude F. Meares,  
University of California, Davis

## Centralized Access Is Here!

In *bimonthly* issues, **Bioconjugate Chemistry** will bring together important research findings in the fast-developing discipline of conjugation chemistry. Now—in a single, time-saving source—you'll find information which otherwise might be scattered throughout broader-focus scholarly journals.

The central theme of **Bioconjugate Chemistry** is the joining of two different molecular functions by chemical or biological means. This includes:

### Conjugation of . . .

antibodies (and their fragments)  
nucleic acids and their analogs ( $\alpha$ -anomers, phosphonates, . . .)  
liposomal components  
other biologically active molecules (receptor-binding proteins, hormones, peptides, . . .)

### with each other or with any molecular groups that add useful properties . . .

drugs, radionuclides, toxins, fluorophores, photoprobes, inhibitors, enzymes, haptens, ligands, etc.

There is *no* journal with this precise focus published today.

## The Leading Edge In Biomedical Advances

**Bioconjugate Chemistry** will publish research at the core of many biotechnology enterprises, as well as of specific interest to biomedical firms, drug companies, and chemical laboratories.

Topics will emphasize the *chemical* aspects of conjugate preparation and characterization . . . *in vivo* applications of conjugate methodology . . . *molecular biological* aspects of antibodies, genetically engineered fragments, and other immunochemicals . . . and the relationships between conjugation chemistry and the biological properties of conjugates.

## Guided by a "Who's Who" in the Field

Editor: Claude F. Meares,  
Univ. of Calif., Davis

### 1990 Editorial Advisory Board

V. Alvarez, Cytogen Corp.  
L. Arnold, Gen-Probe  
R. W. Atcher, Argonne Natl. Labs  
R. W. Baldwin, Univ. of Nottingham, England  
T. Bumol, Eli Lilly & Co.  
K. Chang, Immunomedics  
G. David, Hybritech, Inc.  
P. B. Dervan, California Inst. of Tech.  
D. Dolphin, Univ. of British Columbia, Canada  
T. W. Doyle, Bristol-Myers  
R. E. Feeney, Univ. of California, Davis  
D. Fitzgerald, Natl. Inst. of Health  
J. M. Frincke, Hybritech, Inc.  
A. Fritzberg, NeoRx Corp.  
W. F. Goeckler, Dow Chemical Co.  
D. Goodwin, Stanford Univ.  
E. Haber, E.R. Squibb and Sons, Inc.  
T. Hara, Inst. for Biomedical Res., Japan  
R. Haugland, Molecular Probes, Inc.  
J. Hearst, Univ. of California, Berkeley  
N. Heindel, Lehigh Univ.  
C. Helene, Museum National D'Histoire Naturelle, France

E. Hurwitz, Weizmann Inst. of Science, Israel  
D. Johnson, Abbott Labs  
D. Kaplan, Dow Chemical Co.  
B. A. Khaw, Massachusetts Gen. Hospital  
K. Krohn, Univ. of Washington  
P. Miller, Johns Hopkins Univ.  
H. Nagasawa, Univ. of Minnesota, Minneapolis  
P. Nielsen, Univ. of Copenhagen, Denmark  
A. Oseroff, Tufts New England Medical Ctr.  
M. Ostrow, The Liposome Co., Inc.  
G. Pietersz, Univ. of Melbourne, Australia  
R. Reisfeld, Scripps Clinic & Res. Fnd.  
S. Rocklage, Salutar, Inc.  
J. Rodwell, Cytogen Corp.  
P. Schultz, Univ. of California, Berkeley  
P. Senter, Oncogen  
S. Srivastava, Brookhaven Natl. Lab.  
P. E. Thorpe, Imperial Cancer Res. Fund, England  
G. Tolman  
A. Tramontano, Scripps Clinic & Res. Fnd.  
J. Upešlacis, Lederle Lab.  
R. S. Vickers, Sterling Drug Co.  
E. S. Vitetta, Univ. of Texas, Dallas  
S. Wilbur, NeoRx Corp.  
M. Wilchek, Weizmann Inst. of Science, Israel  
M. Zalutsky, Duke Univ.

## Attention Prospective Contributors!

**With its exclusive, focused readership, Bioconjugate Chemistry will attract the specific audience of experts whom you want to reach, and is committed to prompt publication of manuscripts.**

**For information on submitting your original work, please contact Dr. Claude F. Meares, Department of Chemistry, University of California, Davis, CA 95616 (916/752-3360).**



# ENVIRONMENTAL INDEX

Number of carloads of hazardous materials transported by rail in the United States each year since 1985: more than 1 million

Number of times federal railroad inspectors cited shippers and railroads for violating regulations in 1984: 499

Number of times shippers and railroads were cited in 1988: 3,575

Number of people evacuated as a result of rail accidents involving hazardous materials in 1987 and 1988: 1,400

Decrease in number of B.S. degrees in chemistry awarded in the United States from 1978 to 1988: 3,600

Number of U.S. species that are endangered and threatened from all causes, as of August 4, 1989: 549

Number of endangered species added to EPA's list in 1988 and 1989: 47

Number of threatened species added to EPA's list in 1988 and 1989: 20

Number of disposable diapers entering U.S. landfills annually: 16 billion

Number of tons of disposable diapers entering the solid-waste stream annually: more than 3 million

*Sources are listed on p. 181.*

DEPARTMENT OF EDUCATION  
GRADUATE FELLOWSHIPS  
in  
CIVIL ENGINEERING  
and  
ENVIRONMENTAL ENGINEERING  
UNIVERSITY OF SOUTHERN CALIFORNIA

The University of Southern California Department of Civil Engineering is pleased to announce the availability of graduate fellowships in Civil and Environmental Engineering.

Beginning in Fall, 1990, seven fellowships will be provided to support graduate students enrolled in the Master's and Ph.D. programs. Each will provide a \$16,000 per year stipend, which will be paid over the nine months of the academic year. The fellowships include full-time tuition remission. \$600 per year will be available to pay for approved travel for academic purposes. The fellowships will be awarded for up to three years.

Eligibility is limited to U.S. citizens and permanent residents. Special efforts will be made to recruit students from traditionally underrepresented groups, such as minorities and women. Applications for the Environmental Engineering Program are invited from students with undergraduate degrees in Biology, Chemistry, Engineering, Geology, or other fields of science.

Funding is provided for the fellowships by the U.S. Department of Education program for Graduate Assistance in Areas of National Need. DOE provides \$123,000 per year, about 75% of total funding.

For further information and application materials, please write or call:

Dr. Joseph S. Devinny  
Environmental Engineering Program  
Civil Engineering Department KAP 224E  
University of Southern California  
Los Angeles, CA 90089-2531  
(213) 743-7866 or 743-0595

THE UNIVERSITY OF DAYTON RESEARCH INSTITUTE

## ENVIRONMENTAL SCIENCES

### ● TOXIC WASTE INCINERATION

INCINERABILITY TESTING  
BY-PRODUCT IDENTIFICATION  
TRIAL BURN SUPPORT

### ● THERMAL STABILITY

FIRE SAFETY  
EVOLVED GAS ANALYSIS  
LAB-SCALE PROCESS SIMULATION

### ● ANALYTICAL SERVICES

GC-FID/MS/FTIR  
CUSTOM ANALYSIS  
TGA



The University of Dayton  
ENVIRONMENTAL SCIENCES GROUP  
RESEARCH INSTITUTE  
300 College Park  
Dayton, Ohio 45469-0001  
(513) 229-2846

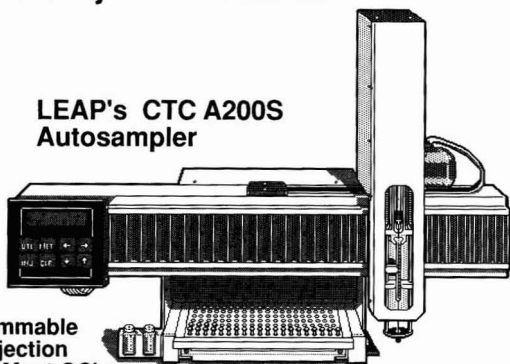
CIRCLE 2 ON READER SERVICE CARD

**Add Real Value  
to GC & GC/MS**  
**Automate Injection Methods**

Pittsburgh Conference

2  
4  
5  
3

**LEAP's CTC A200S  
Autosampler**



- Programmable
- Dual Injection
- Fits on Most GC's
- Variable Injection Rates



**Technologies**

P.O. Box 3220  
Chapel Hill, NC  
27515  
Tel 800 229-8814  
FAX 919 929-8956

CIRCLE 9 ON READER SERVICE CARD

**INDUSTRIAL &  
ENGINEERING  
CHEMISTRY  
RESEARCH**



**PUBLISHED MONTHLY**  
**Editor** Donald R. Paul  
*Univ. of Texas, Austin*

**Quality information that  
gives you the leading edge**

Each month I&EC RESEARCH will help you meet today's intense challenges in chemical technology with...new ideas...new techniques...new procedures...and innovative research that could prove crucial to you and your work.

**Don't miss a single issue!  
Subscribe today!**

**Call Toll free** in the U.S. at 1/800-227-5558 for credit card orders, or write:  
American Chemical Society  
Marketing Communications Dpt.  
1155 Sixteenth Street, NW  
Washington, DC 20036

**Telex:** 440159 ACSPIU or 892582 ACSPUBS  
**Cable address:** JEICHEM

*Get the whole picture from  
the world's most cited  
chemical publication*

**JOURNAL  
OF THE  
AMERICAN  
CHEMICAL  
SOCIETY**

**Editor: Allen J. Bard**  
**University of Texas**

Each biweekly issue of JACS gives you authoritative, original articles (plus concise communications hot off the press!) in *every key arena* of chemical research. What's more, JACS is *the most competitively priced* journal of its kind. Order your subscription today!

**Call Toll Free 1-800-227-5558**  
**Telex: 440159 ACSPIU or**  
**892582 ACSPUB**  
**Cable Address: JEICHEM**

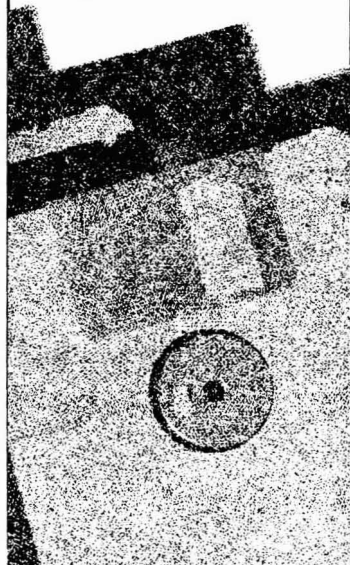
American Chemical Society  
1155 16th Street, NW,  
Washington, D.C. 20036  
202-872-4363

**ACS  
Software**

**High-quality soft-  
ware programs  
for the personal  
computer that  
meet the stand-  
ards you expect  
from the ACS**

For information about  
ACS SOFTWARE, call  
**TOLL FREE (800)**  
**227-5558** or write to:

American Chemical  
Society, Marketing  
Communications,  
1155 Sixteenth Street,  
N.W. Washington  
D.C. 20036



# A unified approach to environmental quality



Alvin L. Alm

In a recent speech to the Natural Resources Defense Council, EPA administrator William D. Reilly wisely called for a more comprehensive and strategic approach to environmental control efforts. He advocated focusing agency efforts on the most significant environmental and public health problems through a priority ranking system. He suggested that pollution prevention be the cornerstone of the environmental protection effort. He endorsed greater use of market incentives and recognized the need to reflect environmental priorities in energy, transportation, and agricultural policy.

Reilly reiterated a theme originally enunciated at the creation of EPA in 1970: the desirability of attacking environmental problems on a multimedia basis. He endorsed a draft bill developed by E. Clarence Davies, EPA Assistant Administrator for the Office of Policy and Program Evaluation, that would focus EPA work on functional lines—such as research and development, standard setting, and enforcement—rather than on media-specific problems.

I strongly applaud efforts to establish environmental priorities, pursue pollution prevention, use market incentives, and integrate environmental concerns into other government policies. I am less sanguine about the feasibility of breaking down the media orientation of EPA's programs.

Politically, the unified approach would require rejecting much of the environmental legislation of the last two decades. The detailed framework of

current laws would need to be jettisoned in favor of a simple and flexible structure. Otherwise, it would be impossible to establish and enforce standards on a unified basis.

Any movement toward a unified environmental statute involves dramatic shifts of power. A flexible statute would increase executive branch discretion at the expense of congressional control over the minute details of environmental programs. Congressional committees could begin to hold the agency accountable for broad program results, but such accountability could not justify the current legislative, oversight, and investigative superstructure.

Even if Congress were willing to devolve this power to the executive branch—an extremely remote possibility—there are real questions about how EPA could handle it. Prior to prescriptive legislation, EPA (and its predecessors) consistently missed statutory goals by a wide mark, partly because of its pioneering role, but largely because of its inability or unwillingness to make decisions and push for results.

At first, the sparse use of statutory deadlines did focus the agency and society on the most important objectives. Over time, statutory deadlines piled up, making them less useful in setting priorities. Nevertheless, they did force the agency to make decisions and OMB to free incarcerated regulations.

If EPA were relieved of all deadlines, an unprecedented amount of internal management discipline would be necessary to make decisions. Even if EPA could develop the management systems and the resolve, external pressures and deficiencies in data would make the decision-making process almost endless.

Dealing with environmental problems holistically is staggeringly complex. Instead of setting ambient and emission effluent standards by media, the holistic approach often requires either chemical-by-chemical controls or comprehensive controls by industry. The attempt to regulate individual chemicals has proven wholly inadequate,

and regulating contaminants by facility requires an immense amount of information and is inconsistent with federal, state, and local environmental laws.

If a comprehensive environmental control regime is not feasible, what can we do? First, EPA can and should establish strategic priorities based on risk to public health and the environment. The SAB "Relative Risk Project" can provide the factual basis for pursuing such priorities. Second, EPA needs to focus on the most efficacious tasks and jettison those that are peripheral. It needs to be more forthcoming on what can be accomplished given resource limitations. Finally, EPA needs to use unconventional, non-end-of-pipe approaches to achieve environmental objectives: for example, changing market signals to encourage energy and waste reduction. Information transfer programs can solve environmental problems more quickly, although less precisely, than regulatory approaches.

Ultimately, we will probably see the establishment of general ambient standards and waste reduction goals allowing technology and land-use patterns to adapt to these limitations. In the interim, we must address problems created in the past while we ensure that we do not create problems in the future. Specific-media, end-of-pipe, or other regulatory controls will still play the major role in achieving current statutory standards. But maintaining the gains from cleanup programs and solving intractable or new problems will require innovative approaches. A sensible mixed strategy, focusing on risk-based priorities, is the best we can hope for in the immediate future.

*Alvin L. Alm is a director and senior vice-president for energy and the environment for Science Applications International Corp., a supplier of high-technology products and services related to the environment, energy, health, and national security.*

# ES&T PRODUCTS

## AIR POLLUTION CONTROL

**Odor and pollutant removal.** BIOTON uses microorganisms as filters to remove more than 99% of odors and many pollutants found in industrial waste gas. The technique was invented in Holland. Ambient Engineering 112

**Opacity monitoring.** Models 4000 and 4500 opacity monitors are designed to monitor opacity in keeping with EPA regulations. The model 4500 can operate unattended for long periods of time. Land Combustion 113

**Engine exhaust analysis.** Sesam analyzer is designed to analyze several gases found in motor exhaust. It is based on Fourier-transform infrared spectroscopy. Siemens 114

**Asbestos filtration.** Super 25mm Cassette is designed to filter asbestos out of workplace air to meet the strict OSHA Method ID 160 specification that allows no more than 3 fibers per 100 field background. Enviroport 115

## HAZARDOUS MATERIALS

**Fluid waste recycling.** Company has systems to recycle contaminated fluid wastes from small generators such as dry-cleaners, auto body repair shops, and manufacturing plants. Safety-Kleen 116

**Waste incineration.** Aspiration burner introduces oxygen into combustion chamber by a patented method designed to double a mobile incinerator's capacity and reduce cost and waste residence time. Linde/Union Carbide 117

**Incinerator without refractories.** System is designed to burn wastes such as contaminated soil, hospital wastes, polychlorinated biphenyls (PCBs); it consists of concentric cylindrical housing and does not require refractory materials. Ecolo-Tech International 118

*Need more information about any items? If so, just circle the appropriate numbers on one of the reader service cards bound into this issue and mail in the card. No stamp is necessary.*



*Biofilter system removes odors and waste gas pollutants*

**Leachate treatment.** Sand filters and powdered activated carbon are used to treat as much as 30,000 gal/day of leachate to render it suitable for discharge. Zimpro/Passavant 119

## INSTRUMENTATION

**Animal breath analysis.** Product analyzes substances such as carbon dioxide and nitrous oxide from animal breath samples as small as 5 mL/min. Most such instruments require at least 150 mL/min. One application is pharmacology. Columbus Instruments International 120

**Underground leak detection.** Soil Sentry Twelve-X is designed to provide the fastest possible detection and location of leaks from underground storage tanks to soil. Device reportedly meets and better EPA's requirements. Arizona Instrument 121

**Detection of volatile chemicals.** D.L.E. Kit is designed to examine water samples quickly to determine the presence of volatile contaminants. National Draeger 122

**Formaldehyde monitoring.** TGM 555 air monitor is designed to monitor formaldehyde levels in the parts-per-

million range continuously. It uses the *pararosaniline* procedure. CEA Instruments 123

**Metals in groundwater.** Posi-Filter is designed to detect and measure metals dissolved in groundwater. It is made of Teflon and is reported to meet EPA's sampling guidelines. Norton-Performance Plastics 124

**Continuous-flow analyzer.** Analyzer uses EPA-approved chemical principles to determine up to 16 analytes automatically and simultaneously. Instrument software is easily mastered. Skalar/Seamark 125

**Chlorine and SO<sub>2</sub> detection.** Series 1650 Single Point chlorine and sulfur dioxide detectors present data from 10-40 ppm and are based on electrochemical redox sensors. Data can be analyzed and displayed on IBM-compatible personal computers. Capital Controls 126

*Companies interested in a listing in this department should send their release directly to Environmental Science and Technology, Attn: Products, 1155 16th St., N.W., Washington, DC 20036.*

**CIRCLE  
NUMBERS  
FOR FREE  
INQUIRY  
SERVICE**

**Please circle appropriate numbers to receive additional information**

READER SERVICE

1	2	3	4	5	6	7	8	9	10	11	12	13	14	15
16	17	18	19	20	21	22	23	24	25	26	27	28	29	30
31	32	33	34	35	36	37	38	39	40	41	42	43	44	45
46	47	48	49	50	51	52	53	54	55	56	57	58	59	60
61	62	63	64	65	66	67	68	69	70	71	72	73	74	75
76	77	78	79	80	81	82	83	84	85	86	87	88	89	90
91	92	93	94	95	96	97	98	99	100	101	102	103	104	105
106	107	108	109	110	111	112	113	114	115	116	117	118	119	120
121	122	123	124	125	126	127	128	129	130	131	132	133	134	135
136	137	138	139	140	141	142	143	144	145	146	147	148	149	150

**Principal product to which my work relates:**

- A. Oil/Gas/Petroleum
- B. Plastics/Resins
- C. Rubber
- D. Drugs/Cosmetics
- E. Food/Beverages
- F. Textile/Fiber
- G. Pulp/Paper/Wood
- H. Soaps/Cleaners
- I. Paint/Coating/Ink
- J. Agrichemicals
- K. Stone/Glass/Cement
- L. Metals/Mining

- M. Machinery
- N. Auto/Aircraft
- O. Instrument/Controls
- P. Inorganic Chemicals
- Q. Organic Chemicals
- R. Other Manufacturing
- S. Design/Construction
- T. Utilities
- U. Consulting Services
- V. Federal Government
- W. State Government
- X. Municipal Government
- Y. Education

NAME: \_\_\_\_\_

POSITION: \_\_\_\_\_

ORGANIZATION: \_\_\_\_\_

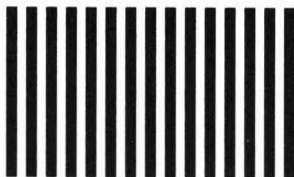
STREET: \_\_\_\_\_

CITY: \_\_\_\_\_

STATE: \_\_\_\_\_ ZIP: \_\_\_\_\_

TELEPHONE: ( \_\_\_\_\_ ) - \_\_\_\_\_ - \_\_\_\_\_

NO POSTAGE  
NECESSARY  
IF MAILED  
IN THE  
UNITED STATES



**BUSINESS REPLY MAIL**

FIRST CLASS PERMIT NO. 209 WESTPORT, CT

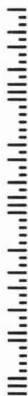
POSTAGE WILL BE PAID BY ADDRESSEE

**Environmental**  
Science & Technology

CENTCOM, LTD.

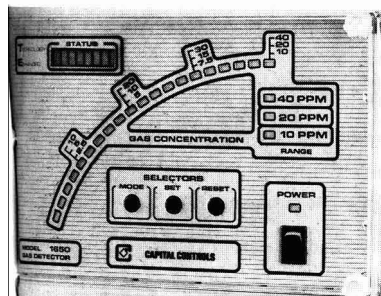
P.O. BOX 231

WESTPORT, CT 06881-9919



ES&T  
**Reader  
Service  
Reply Card**

It's computer  
processed  
for fast  
response  
to your  
inquiries  
**AND, IT'S  
FREE**



Chlorine and sulfur dioxide detector

**VOC measurement.** Century Organic Vapor Analyzer 128GC uses flame ionization to analyze volatile organic compounds in soil and groundwater. A gas chromatographic feature is optional. Foxboro 127

**Environmental analysis.** Company offers a complete line of instruments and ancillary supplies for environmental analysis that conforms to EPA methods for chromatography, titrimetry, and colorimetry. EM Science 128

**Dissolved oxygen analysis.** Model 9040 multi-channel dissolved oxygen analyzer offers a range of 0–100 mg/L  $\pm 0.1$  mg/L. Analysis is possible on four channels. Royce Instrument 129

## PUBLICATIONS

**Groundwater References.** *Groundwater References* is a listing of reference material on groundwater, available for loan or purchase from many public and private sources. Midwest Agricultural Chemicals Association 130

**Computer Usage in Engineering.** *ES&T* article series discusses trends and applications of computers, including artificial intelligence and the impact of computer use in environmental engineering. The report tells how personal computers will change the practice of environmental engineering in the future. ACS 131

**Wastewater Treatment.** *ES&T* article series reports on the processes for the treatment of wastewater, including removing particles and dissolved organic and inorganic contaminants, as well as aerobic treatment. ACS 132

## RISK ASSESSMENT

**Cancer Risk Assessment.** *ES&T* article series explores scientific topics of public concern regarding regulation of chemicals in the environment. Series reports on managing risk and communicating the results of risk assessment; also covered are exposure assessment

and being realistic about chemical carcinogenesis. ACS 133

## SERVICES

**Forensic analytical services.** Company provides laboratory services in the forensic and health sciences. Specialties are asbestos analysis and on-site exposure monitoring. Forensic Analytical Specialties 134

**Training for emergencies.** Company provides film and video training systems and services for personnel involved in chemical emergency response. Emergency Film Group 135

## SOFTWARE

**Plastics and solid waste.** Computer data base provides late-breaking news and legislative developments involving plastics and solid-waste management. Data base is available by subscription. The Council for Solid Waste Solutions 136

**Right-to-know reporting.** EnviroBase 313 Plus, Version 2.0 manages requirements of Superfund Section 313 Form R (right-to-know) submittals and performs other types of environmental tracking and evaluation. EnviroBase Systems 137

**Groundwater studies.** ModelCad helps design groundwater models, and AQTESOLV helps professionals analyze aquifer tests of many kinds. Geraghty & Miller 138

**Reporting of organics.** HP CLP PLUS software is written to simplify and speed the process of analyzing, reviewing, and reporting data on total organics required by EPA's Contract Laboratory Program. Hewlett-Packard 139

**Chemical risk analysis.** RISKPRO has been written to assess environmental impacts and cancer risks from chronic toxic chemical releases in a local community. Program is IBM-compatible. General Services 140

**Emergency response.** Emergency Plan Generator and Emergency Management Evaluation Toolkit are used to train for chemical emergencies in compliance with EPA and OSHA regulations and to evaluate such plans. Environmental Emergency Systems 141

**Chemical reporting.** TERMS Version 2.0 helps identify chemicals and prepare reports on them, as required by Superfund Title III and OSHA regulations (29 CFR 1910.1200). Data base includes list of 3800 reportable chemicals. Corbus 142

**High-speed data acquisition.** Data acquisition board allows high-speed data

acquisition in laboratories and at industrial sites; it can be put into high-speed computers using Extended Industry Standard Architecture. National Instruments 143

## STANDARDS

**GC analysis.** Full line of environmental standards and kits includes purgeable, surrogate, and calibration check compounds for gas chromatographic analysis of volatiles, base-neutral-acid extractables, and pesticides. J&W Scientific 144

**Standards for spectrometers.** Company offers line of PLASMA-PURE standards for ICP spectrometers, as well as accessories and training. Leeman Labs 145

**HPLC standards.** Company offers EPA method standards for use with high-performance liquid chromatography as well as several other techniques. PolyScience 146

**Contaminant standards.** Company offers extensive line of environmental contaminant standards, including unlabeled and labeled ( $^{13}\text{C}$  and  $^{37}\text{Cl}$ ) and tritiated dibenzo-*p*-dioxin and -furan congeners. Chemsyn Science Laboratories 147

## ENVIRONMENTAL INDEX SOURCE BOX

- (1) "Railroad Safety: DOT Should Better Manage Its Hazardous Materials Inspection Program"; U.S. General Accounting Office, November 1989, p. 22. (2, 3) Op. cit., p. 2. (4) Op. cit., p. 33. (5) Stevens, W. K. *The New York Times*, November 5, 1989; Sec. 4A, p. 46. (6-8) "Endangered Species Update"; EPA, Office of Pesticide Programs, Fall 1989. (9-10) American Public Health Association news release, Nov. 1, 1989, p. 2.

## WATER TREATMENT

**BOD prediction.** On-line wastewater respirometers are designed to give an accurate prediction of final biological oxygen demand (BOD) within 20–30 min. Tech-Line Instruments 148

**COD testing.** Chemical oxygen demand (COD) reactor is designed to give analysts more flexibility and versatility in performing digestions for COD analysis. Tests use EPA-approved methods. Hach 149

FOR A BROAD PERSPECTIVE IN THE SCIENCE OF NON- NUCLEAR FUELS . . .

# ENERGY & FUELS

Editor John W. Larsen, Lehigh University

Associate Editor Thomas R. Hughes, Chevron Research Company

## Ideas . . . Innovations . . . Discoveries . . .

ENERGY & FUELS is the bimonthly journal that delivers an abundance of highly readable reports on topics covering the transformation, utilization, formation, and production of fossil fuels.

Each issue features reports on all aspects of the chemistry of non-nuclear energy sources—including petroleum research, coal chemistry, oil shale, tar sands, C<sub>1</sub> chemistry, organic geochemistry and biomass research.

Plus, ENERGY & FUELS gives you a dynamic vision on how the field is developing. You'll find a wealth of information on . . .

- the formation of, exploration for, and production of fossil fuels
- the properties and structure or molecular composition of both raw fuels and refined products
- the chemistry involved in the processing and utilization of fuels
- the analytical and instrumental techniques used in energy and fuels investigations
- research on non-fuel substances that elucidates aspects of fuel chemistry
- and much more!

ENERGY & FUELS publishes more than research papers. You'll find Communications, Book Reviews, and invited feature essays by major figures in the field. In these, developments in active areas of research are made accessible to chemists involved in other branches of the discipline.

### Contributing Authors—

#### Look to ENERGY & FUELS for Rapid Publication!

The editors are working toward a timely turnaround from submission to publication. For further information on composition and submission of manuscripts write: John Larsen, Editor, ENERGY & FUELS, Department of Chemistry, Lehigh University, Bethlehem, PA 18015. Or call (215) 758-3489.

**In a hurry? Call Toll-Free 1-800-227-5558. In Washington, D.C. and outside the U.S. call 202-872-4363. Telex: 440159 ACSP UI or 89 2582 ACSPUBS. FAX: 202-872-4615.**

Editorial Advisory Board: T. Aczel, Exxon Res. & Eng. Co.; M.M. Boduszynski, Chevron Res. Co.; A.K. Burnham, Lawrence Livermore Natl. Lab; B. Cecil, U.S. Geological Survey; C.D. Chang, Mobil R&D Corp.; P. Griffiths, Univ. of California, Riverside; C. Horvath, Yale Univ.; J. Howard, Massachusetts Institute of Technology; L. Ignasiak, Alberta Res. Council; M. Lewan, Amoco Res. Ctr.; R. Liotta, Exxon Res. & Eng. Co.; L.J. Lynch, CSIRO, Australia; O.M. Mahajan, Amoco Res. Ctr.; J. McKay, Western Res. Inst.; H. Meuzelaar, Biomaterials Profiling Ctr.; H. H. Oelert, Chem. Tech. Univ., W. Germany; M. Poutsma, Oak Ridge Natl. Lab.; Y. Sarada, Hokkaido Univ., Japan; J. H. Shinn, Chevron Res. Co.; M. Siskin, Exxon Res. & Eng. Co.; L.M. Stock, Univ. of Chicago; I. Wender, Univ. of Pittsburgh; D.D. Whitehurst, Mobil Res. & Tech. Ctr.

1990 Subscription Information  
1990 Volume 4 ISSN: 0887-0624 Coden: ENFUEM

	ACS Members*		Non-member
	One Year	Two Years	One Year
U.S.	\$48	\$86	\$294
Canada & Mexico	\$ 55	\$100	\$301
Europe**	\$ 59	\$108	\$305
All Other Countries**	\$ 62	\$114	\$308

\* Member rate is for personal use only.  
\*\*Air service included.

ENERGY & FUELS is a journal of the American Chemical Society. For more information write: American Chemical Society, Marketing Communications Department, 1155 Sixteenth Street, NW, Washington, DC 20036

Foreign orders must be paid in U.S. currency by international money order, UNESCO coupons, or U.S. bank draft; or order through your subscription agency. For nonmember rates in Japan, contact Maruzen Co., Ltd.

This publication is available on microfilm, microfiche, and online through CJO on STN International.



**Chernobyl: The Long Shadow.** Chris C. Park. Routledge, London and New York, 1989. vii + 207 pages. \$39.95, cloth.

*Reviewed by Stanton S. Miller, Managing Editor of Environmental Science & Technology*

The Chernobyl accident was the worst in the history of nuclear power. This book offers a balanced account of what happened at Chernobyl on Saturday, April 26, 1986—and subsequently—from several viewpoints. The day after the accident, the Swedish National Defense Institute in Stockholm sounded the alarm and made the earliest radioactivity measurement. Author Chris C. Park states that according to Otto Huber, president of the Swiss Radioactivity Monitoring Commission, the significance of the Chernobyl accident is that it showed that fallout levels had by May 5 exceeded those from all previous atmospheric testing of nuclear weapons. Many countries measured fallout from the radioactive cloud blown from the U.S.S.R. But the International Atomic Energy Agency announced on April 30 that radiation levels appeared to pose no real threat to humans, certainly not to those outside the U.S.S.R.

The author, a lecturer in geography and principal of Furness College at the University of Lancaster in the U.K., explains how nuclear power stations work, radioactivity terms, and the effects of radioactivity on biological systems. He talks about the nuclear safety record, including other accidents such as the worst in the West at Windscale in 1957 and the worst in the United States at Three Mile Island in 1979.

Park discusses the struggle for containment after the accident. Evidence that the accident had happened was not concealed. After the report by the Swedish monitoring stations, a U.S. "spy in the sky" satellite five days later showed two bright red spots beneath a cloud of blue smoke.

Although the Chernobyl plant had been working since 1983 without any problems, its Number 4 reactor was operating at about 7% of capacity at the time of the accident. The Russian RBMK reactor was known to be unsta-

ble and difficult to control at low power; this may have been a significant factor in causing the disaster. The reactor site at Chernobyl was not covered until 12 days later, when it was sealed with sand, lead, and boron and then entombed in concrete to prevent any further release of radioactive material.

There was an immediate problem for humans. "One millisievert, which puts people dangerously close to the high risk category threatened with long-term cancers, could easily be accumulated by ordinary people going about their business in Pripyat [the nearest town of 49,000 people, about 14 km away from the accident site]," Park reports. He talks about the evacuation of people, and the delay of the exodus.

The immediate casualty toll of the Chernobyl accident was 31 dead and 200 hospitalized in Moscow with varying degrees of radiation poisoning. Some 135,000 people were evacuated.

Radiation affects human health. There is no safe level of radiation exposure, and there is always some background radiation. Park explains that humans receive an annual radiation budget from three sources: about two-thirds (67%) from natural background radiation; most of the rest (30.7%) from medical sources (like X-rays); and less than one sixtieth (a mere 1.7%) from all other sources, including the nuclear industry. Park includes explanations of the forms of radiation—alpha, beta, and gamma rays and neutrons—and their effects on humans and body organs. He explains radiation terms such as becquerels (activity), gray (absorbed dose), and sievert (dose equivalent expressing potential harm regardless of the source or type of radiation). But scientists still know relatively little about the long-term biological effects of exposure to small doses of radiation, according to Park.

Chapter 7 is truly revealing; it tells the Soviet report of what really happened. Experts in the West were impressed with the thoroughness of the Soviet report, its spirit of self-criticism, and the promptness with which it was prepared. The interim report on the disaster came two-and-a-half months after the accident. The basic design of the reactor was criticized as old-fashioned

and based on a safety factor that was completely unacceptable to the West. In the U.S.S.R. safety is based on operational control; in the United States safety is based on containment.

The accident was described "as the culmination of an almost incredible series of errors" by a group of unnamed technicians and involved six critical, deliberate actions by the technicians (including switching off the cooling water to make it possible to run a cooling experiment and to operate the reactor at low power). Human error was almost entirely to blame. The Soviet authorities were convinced that if any one of the six errors had not been committed, the accident would not have happened.

One chapter in the book takes a look at how Britain reacted to Chernobyl. Park reports that the radiation cloud reached Britain at the end of the first week. This country, like others in the path of the radioactive cloud, was unprepared for coping with public anxiety over the release of invisible radioactivity. Despite the fear in Britain over Chernobyl and its fallout, the long-term risk is very small, according to Park. Radiation levels in Britain were never high enough to put human health at direct risk, although a careful watch for contamination of milk, water, and foodstuffs was needed through May 1986. Data from the National Radiological Protection Board (at Didcot near Oxford) suggest that the average person in the U.K. was exposed to about 0.07 sievert of radiation from Chernobyl between May 1986 and April 1987. This would add over 3% to the average exposure received from natural background sources (2.15 millisieverts), according to Park.

The public is not always confident about nuclear power. But Park concludes, "By the end of 1985 a total of 374 nuclear plants around the world were producing about 15% of the world's electricity. That same year . . . 32 new reactors were brought into operation. A further 157 reactors were under construction." Park quotes seven heads of state who met in Tokyo in May 1986 as agreeing that, "Nuclear power is and will remain an increasingly widely used source of energy, provided that it is properly managed."

# The Best Source of Quantitative Numerical Data of Physics and Chemistry Published Today!

## JOURNAL OF PHYSICAL AND CHEMICAL REFERENCE DATA

Editor, David R. Lide  
National Institute of Standards and Technology

In response to the volume of quality work being done in this field, the *Journal of Physical and Chemical Reference* (JPCRD) is now being published BIMONTHLY. The American Chemical Society, the American Institute of Physics, and the National Institute of Standards and Technology jointly publish JPCRD, providing you with reliable up-to-date compilations and reviews.

Chemists, physicists, materials scientists, engineers, and information specialists can all benefit from the reliable information available in this journal. You'll find data on:

- Atomic and Molecular Science
- Chemical Kinetics
- Spectroscopy
- Thermodynamics
- Transport Phenomena
- Crystallography
- Materials Science
- And much more!

The *JOURNAL OF PHYSICAL AND CHEMICAL REFERENCE DATA* contains recommended values, uncertainty limits, critical commentary on methods of measurement, and full references to the original papers.

Join the thousands of professionals who rely on the *JOURNAL OF PHYSICAL AND CHEMICAL REFERENCE DATA* as a working tool for their research.

Backed by the ACS Guarantee, the *JOURNAL OF PHYSICAL AND CHEMICAL REFERENCE DATA* is guaranteed to be a reliable, up-to-date reference source—you won't want to miss a single issue!

### 1990 SUBSCRIPTION INFORMATION

*JOURNAL OF PHYSICAL AND CHEMICAL REFERENCE DATA* now published BIMONTHLY, one volume per year.  
Volume 19 (1990), ISSN: 0074-2689

	U.S.	Canada & Mexico	Europe, Mideast & N. Africa*	Asia & Oceania*
Members (ACS, AIP, and Affiliated Societies)	☐\$ 70	☐\$ 85	☐\$105	☐\$105
Nonmembers	☐\$325	☐\$340	☐\$360	☐\$360

Surface rates are \$85 (members) and \$340 (nonmembers) to all countries.

Member rates are for personal use only. \*Air service included.

To order your *JOURNAL OF PHYSICAL AND CHEMICAL REFERENCE DATA* subscription, call TOLL FREE 800-227-5558 and charge your order! (U.S. Only) In D.C. or outside the U.S. call (202) 872-4363, or write: American Chemical Society, Sales and Distribution Department, 1155 Sixteenth St., N.W. Washington, DC 20036

## HAZARDOUS WASTE PROFESSIONALS

Diversity, expertise, technology, and an environment for professional achievement. These are the hallmarks of The MITRE Corporation. We are a not-for-profit systems engineering corporation with major facilities in Bedford, MA and McLean, VA and with over 6,000 employees worldwide. For over 30 years, our highly respected scientists and engineers have specialized in the analysis, design, development, and acquisition of superior solutions to meet the advanced requirements of military and civilian agencies of the U.S. Government.

Our involvement in the area of hazardous waste is demanding yet exceptionally rewarding since it is designed to create workable solutions to a critical problem and make a positive impact on our nation's future. We have openings at MITRE facilities in San Antonio and McLean (a suburb of Washington, D.C.) for highly qualified individuals to assist Government agencies in identifying and evaluating hazardous waste sites throughout the United States. All positions offer significant levels of individual responsibility while working in a team context.

An advanced degree, five years' hazardous waste experience, and excellent communication skills are required. Some travel will be required to meet with regulatory officials and environmental consultants. We are especially interested in individuals in one or more of the following areas:

### McLean, VA —

Responsibilities include review of monitoring data and other technical information to determine the magnitude of threat posed by hazardous waste sites. Some of the openings require understanding of ground water systems, monitoring techniques, data interpretation, and transport and fate of environmental contaminants in aquifers. Knowledge of CERCLA, SARA and RCRA is desirable. Other positions require experience in hazardous waste work particularly related to air contaminant releases and surface water systems. Familiarity with sampling plans and techniques and the interpretation of environmental data is recommended. Familiarity with principles of risk assessment is also recommended.

### San Antonio, TX —

**Hydrogeology**—You will help assure the quality of hydrologic field studies at suspected hazardous waste sites. Responsibilities include developing specifications for well drilling and sampling; reviewing contractor plans; inspecting and evaluating contractor field activities; and assessing hydrologic data.

**Risk Assessment**—You will assist in assuring the quality of human health and environmental risk assessments performed by contractors. Responsibilities include developing guidance and specifications for conducting risk assessments; reviewing risk assessment data and documentation; and analyzing expected risk reduction.

**Remedial Design**—You will contribute to the development of clean up remedies at hazardous waste sites. Responsibilities include evaluating feasibility studies and decision documents; preparing specifications for remedial design/remedial action projects; and evaluating contractor plans and construction activities.

**Please send your resume to N.D. Scott, The MITRE Corporation, 7525 Colshire Drive, McLean, VA 22102. U.S. citizenship required. An Equal Opportunity/Affirmative Action Employer.**

# MITRE

## SENIOR-LEVEL FACULTY POSITION IN ENVIRONMENTAL ENGINEERING

The Civil Engineering Department at the University of Nevada, Reno invites applications for a tenure track faculty position at the rank of full Professor in Environmental Engineering starting August 1990. Salary will be consistent with the applicant's qualifications. The Civil Engineering Department is committed to excellence in both its undergraduate and graduate programs. A strong environmental engineering program is being developed with attendant external research funding. The Ph.D. program in the department is emerging, and the new faculty is expected to lead the program in his/her specialty area. A new ten million dollar engineering laboratory center is scheduled to open in mid 1991 to allow for the expansion of the environmental engineering program, among others. Only individuals with an outstanding record of scholarly publications and funded research with proven leadership abilities in their field are encouraged to apply.

A B.S. and a Ph.D. (or equivalent) in Civil/Environmental Engineering are required. Applications are accepted from all areas of environmental engineering, particularly biological processes, industrial waste treatment, groundwater pollution, and hazardous waste management. A proven record of interest and activities in the teaching aspects of academic programs in civil and environmental engineering is necessary. The candidate will be expected to conduct research and to support the teaching, research, and service goals of the department.

Letters of application, resumes and the names, addresses, and telephone numbers of five references should be sent to **Dr. M. Saidi, Chairman, Department of Civil Engineering, University of Nevada, Reno, Nevada 89557-0030.** The closing date for these applications will be March 15, 1990; however, if suitable candidates are not found, the deadline will be extended. Members of minority groups are especially encouraged to apply. The University of Nevada is an affirmative action/equal opportunity employer. The university employs only U.S. citizens and aliens lawfully authorized to work in the U.S.

## BROWARD COUNTY CIVIL SERVICE OPPORTUNITY

**ENGINEER II—(EOCB-Air Pollution Control)—\$31,556-\$42,599 per year.**

Requires graduation from an accredited four (4) year college or university with major course work in chemical or environmental engineering and two (2) years experience in professional engineering work involving toxic air pollutants.

Official application must be received by the Broward County Personnel Division by 5:00 p.m., February 23, 1990.

Official applications and additional information may be obtained from the Broward County Personnel Division, 115 S. Andrews Avenue, Ft. Lauderdale, Florida 33301. Phone (305) 357-6444.

EQUAL EMPLOYMENT OPPORTUNITY M/F/H/V

**GRADUATE STUDY IN ENVIRONMENTAL SCIENCE AND ENGINEERING** at the Oregon Graduate Center. Highly qualified, strongly motivated students sought for exciting research programs in transport and fate of organic and inorganic contaminants, atmospheric chemistry and physics, aquifer remediation, microbial ecology and physiology, biodegradation, biogeochemistry, analytical environmental chemistry, numerical modeling, estuarine and coastal studies, elemental cycling in terrestrial ecosystems. Intensive research experience, state-of-the-art instrumentation, maximal student-faculty interaction. Research assistantships with tuition remission available to qualified Ph.D. applicants. Write: **Carl D. Palmer, Department of Environmental Science and Engineering, 19600 N.W. von Neumann Dr., Beaverton, OR 97006, (503) 690-1196.** (Closing date 4/1/90). Affirmative Action/Equal Opportunity Employer.

## CLASSIFIED SECTION

### Senior Research Scientist

The Geochemistry section of Battelle, Pacific Northwest Laboratories seeks qualified individuals with backgrounds in soil chemistry, geochemistry, aquatic chemistry, or analytical chemistry.

The position entails interfacing with a multidisciplinary team of scientists investigating the behavior of contaminants in groundwaters, soils, and sediments. The senior scientist will direct original experimental research pertinent to the reactivity of inorganic/organic contaminant mixtures in subsurface environments and will also eventually assume program management, program development, and certain personnel management responsibilities. The successful candidate will have a strong publication record of original research, as well as experience in joint experimental and modeling studies.

The scientific focus of the research includes investigation of surface chemical reactions (i.e., sorption, transformation) on natural, heterogeneous mineral and organo-mineral surfaces that control the concentrations of organic molecules, radionuclides, and metal ions in groundwater; application of new spectroscopic techniques to investigate solute/solvent interactions at surfaces; studies of molecular scale interactions at mineral and organo-mineral surfaces responsible for the rates and magnitude of natural geochemical reactions.

Qualified individuals will possess a Ph.D. in a chemistry field with a minimum of 5 years experience, and be willing to tackle basic scientific questions involved in subsurface contaminant reactivity and transport. Those interested in applying basic chemical concepts to assist environmental restoration activities are also urged to apply.

Salary is commensurate with experience. Interested applicants should send their resume and the names and addresses of three references to: Mr. Larry Ranta, Battelle, Pacific Northwest Laboratories, P.O. Box 1406, Richland, WA 99352, or FAX (509) 376-9099. U.S. Citizenship required. An equal opportunity employer, M/F.



**Battelle**

Pacific Northwest Laboratories

### ASSISTANT PROFESSOR RESEARCHER

Responsible for generating research proposals and conducting and supervising research on marine pollution problems and waste management; research duties include developing methods for waste stabilization, performing trace metal analysis and metal leaching experiments; maintaining atomic absorption spectrophotometer; collating data and performing data analysis utilizing IBM PC/XT and Macintosh; preparing manuscripts for publication and preparing scientific presentations; supervising of assistants and graduate students in research activities and advising them on thesis preparation. M-F 8:00 a.m. to 5:00 p.m., \$41,400/year. Ph.D. in Oceanography/Chemical, one year experience in the position or one year experience as a Post-Doctoral Fellow Researcher required. Send resume only to Job Service of Florida, 3421 Lawton Road, Orlando, Florida 32803. Job Order # FLO208554.

**ATMOSPHERIC CHEMIST.** North Carolina State University invites applications for a tenure-track faculty position at the assistant or associate professor level for joint appointment in the Department of Chemistry and the Department of Marine, Earth and Atmospheric Sciences. Candidates should have a Ph.D. in Atmospheric Science, Chemistry, or a related discipline, preferably with postdoctoral or research experience. The successful applicant will be expected to develop interdisciplinary research and teaching programs associated with both departments. Priority will be given to those applicants with research interests in global/regional climate change, including (but not limited to) cloud and aerosol chemistry, gas phase reactions and kinetics, chemistry at the air-sea interface, modeling of the distribution of chemical species via atmospheric circulations, or related disciplines. Resources available include state-of-the-art analytical instrumentation, a wet chemistry laboratory atop Mount Mitchell, a Cray YMP supercomputer facility, and an opportunity for interactions with scientists and their research facilities in the Research Triangle Area. Participation in ongoing national/international research projects is encouraged. Interested applicants should send their curriculum vita, publication list, description of proposed research and the names of three references by March 1, 1990 to Professor Louis A. Jones, Co-Chair, Search Committee, Box 8204, North Carolina State University, Raleigh, NC 27695-8204. NCSU is an Affirmative Action/Equal Opportunity Employer.

### FACULTY POSITION IN INDUSTRIAL HYGIENE

The University of North Carolina at Chapel Hill, Department of Environmental Sciences and Engineering, seeks an assistant professor of industrial hygiene; appointment as associate professor will also be considered. Applicants for this tenure track appointment should have a doctorate in a field related to industrial hygiene and academic credentials in chemistry. Applicants must have commitments to developing a research program in the evaluation or control of workplace hazards, and to teaching graduate courses in industrial hygiene. Review of applications will begin 15 March 1990; applications will be considered until the position is filled. Please send c.v. to Prof. David Leith, Department of Environmental Sciences and Engineering CB 7400, University of North Carolina, Chapel Hill, NC 27599. The University of North Carolina at Chapel Hill is an Equal Opportunity/Affirmative Action Employer.

**GROUNDWATER CENTER/DIRECTOR OF RESEARCH.** The Academy of Natural Sciences of Philadelphia has an international reputation for conducting research on water resources. As part of a long-term commitment to environmental research, the Academy has established a new Groundwater Center and entered into cooperative arrangements with distinguished universities for collaborative groundwater research. We seek a Director for the Groundwater Center to recruit and lead a core of senior scientists from the groundwater community at large, as well as coordinate research with present Academy senior scientific staff. The candidate should have experience in designing multi-investigator programs and directing a diverse research team. The successful candidate should have professional experience in research concerning microbial attenuation of complex chemicals, organic chemistry or hydrology. A Ph.D. and a significant record of research accomplishments is required. Competitive salary dependent upon qualifications of candidate. Send curriculum vitae and 4 references with reply to: Dr. Sybil Zeltzinger, Division of Environmental Research, Academy of Natural Sciences, Philadelphia, PA 19103.

### AQUEOUS GEOCHEMISTRY University of California, Davis

The Department of Land, Air and Water Resources invites applications for an 11-month, tenure-track teaching and research position as Aqueous Geochemist at the Assistant Professor level. The successful candidate will be expected to contribute to the department undergraduate teaching program, develop and teach upper division and graduate courses in aqueous geochemistry, and participate in student advising. The appointee will establish an active research program in aqueous geochemistry with special emphasis on ground water quality.

A Ph.D. with emphasis in geochemistry and a strong background in aqueous low-temperature geochemistry and physical chemistry is required. Demonstrated knowledge and interest in kinetics of chemical weathering, isotope, trace element chemistry, and hydro-geochemical modeling and advanced analytical methods are desired. The position commences on or about July 1, 1990.

Applicants should submit a resume; academic transcripts; statement of research and teaching interests and experience; copies of publications, reports, and manuscripts; a summary or abstract of Ph.D. dissertation; and names, addresses and telephone numbers of at least four references should be postmarked by February 28, 1990, to:

Dr. James W. Biggar, Chair  
Aqueous Geochemist Search Committee  
Department of Land, Air and Water Resources  
University of California; Davis, CA 95616

THE UNIVERSITY OF CALIFORNIA IS AN AFFIRMATIVE ACTION/EQUAL OPPORTUNITY EMPLOYER.

### HEAD DEPARTMENT OF ENVIRONMENTAL HEALTH COLORADO STATE UNIVERSITY

The Department of Environmental Health seeks a dynamic, innovative leader to exploit growth opportunities in educational offerings, research and service with 14 faculty members specializing in epidemiology (veterinary and human), toxicology, water/waste water, occupational health, biostatistics, and vector-borne diseases. Unique opportunities exist to enhance educational offerings at the doctoral or master's (63 students) and bachelor's (100 students) levels with on-campus and off-campus offerings. Growth opportunities exist in toxicology, occupational health, hazardous materials and environmental risk assessment. Applicants must possess a Ph.D., M.D., D.V.M. or equivalent; demonstrated leadership/organizational ability; and scholarly/professional achievements appropriate for appointment to full professor. Qualified applicants from industry or government and especially women and minority group members are encouraged to apply. Send a letter of application, curriculum vitae and five references to: Dr. Rupert P. Amann, Head; Department of Physiology, Colorado State University, Fort Collins, CO 80523. Phone 303-491-6187. Applications will be accepted until March 23, 1990. Salary is negotiable. Colorado State University is an equal opportunity/affirmative action employer.

**ASSISTANT PROFESSOR, ENVIRONMENTAL SCIENCE.** Teaching/research tenure-track position for Fall semester 1990. Ph.D. required/Anticipated. Preference for expertise in water-related problems. Application deadline: April 1, 1990. Resume, three letters of recommendation, and inquiries directed to: Dr. George J. Fister, Environmental Science Search Committee, Department of Biological & Environmental Sciences, McNeese State University, P.O. Box 92000, Lake Charles, LA 70609-2000. McNeese State University is an equal opportunity employer.

# professional consulting services directory



"TREATMENT BY DESIGN"

**WE FOCUS ON SOIL & GROUNDWATER CLEAN-UP ON-SITE**

**Services including:**

- Bioremediation (BIOTA Division)
- Chemical Fixation (TOXCO Division)
- Vapor Extraction
- UV Ozonation
- Remedial Investigations
- Underground Tank Removals

**1-800-753-1818**



**staffing solutions**

Staffing Solutions specializes in NATIONWIDE recruitment and placement of professionals in the following disciplines:

- Environmental
- Risk Assessment
- Toxicology
- Chemical Engrg.
- Safety Engineers
- Permitting Specialist
- Hazardous Waste Mgmt.
- Incineration
- Hydrogeology
- Water/Waste Water
- Chemistry
- Industrial Hygienists
- Regulatory Compliance
- Civil Engineering

Contact Hank Scrivins, (503) 285-6560/FAX (503) 285-6150 or send resume to: 4505 N. Channel, Portland, OR 97217.

ALL FEES EMPLOYER PAID



**RMC Environmental and Analytical Laboratories**

- Leading researchers in chemical fixation, solidification/stabilization
  - Vast experience in treatability studies and incineration research
  - All types of leach studies such as EP TOX, TCLP, MEP, ANS 16.1, MCC-1, etc. for treated and untreated wastes
  - EPA audited lab
  - Major research projects funded by EPA
  - Short turnaround time, modest service charge
- For all your environmental and analytical needs, please call us.

214 West Main Plaza, West Plains, MD 65775  
Phone (417) 256-1101 Fax (417) 256-1103



Consulting Ground-Water Geologists and Engineers

- SARA RI/FS
- RCRA Compliance
- Property Transfers
- UST Management
- Pesticide Monitoring
- Remediation

**ROUX ASSOCIATES INC.**

Atlanta (708) 270-5145 New York (516) 673-7200  
Chicago (312) 571-0660 New Jersey (609) 346-3993  
Hartford (203) 653-8021 SF Bay Area (415) 370-2275

**THE CONSULTANT'S DIRECTORY**

UNIT	Six Issues	Twelve Issues
1" X 1 col.	\$60	\$55
1" X 2 col.	115	105
1" X 3 col.	170	145
2" X 1 col.	115	105
2" X 2 col.	210	190
4" X 1 col.	210	190

**ENVIRONMENTAL SCIENCE & TECHNOLOGY**  
500 Post Road East  
P.O. Box 231  
Westport, CT 06880  
FAX: (203) 454-9939

## INDEX TO THE ADVERTISERS IN THIS ISSUE

ADVERTISERS	PAGE NO.
Academic Press Inc. . . . .	159
Academic Advertising	
Analytical Bio-Chemistry Laboratories, Inc. . . . .	157
Bryan Donald, Inc.	
Analytical Products Group, Inc. . . . .	OBC
Bruel & Kjaer Instruments, Inc. . . . .	IBC
Space Advertising Agency ApS	
Leap Technologies . . . . .	176
Parr Instrument Company . . . . .	161
FBA Marketing Communications	
The University of Dayton Research Institute . . . . .	175
University of Southern California . . . .	175
Varian . . . . .	IFC
Lanig Associates	

Advertising Management for the American Chemical Society Publications

**CENTCOM, LTD.**

President

James A. Byrne

Executive Vice President

Benjamin W. Jones

Clay S. Holden, Vice President

Robert L. Voepel, Vice President

Joseph P. Stenza, Production Director

500 Post Road East  
P.O. Box 231  
Westport, Connecticut 06880  
(Area Code 203) 226-7131  
Telex No. 643310  
Fax No. (203) 454-9939

ADVERTISING SALES MANAGER

**Bruce Poorman**

ADVERTISING PRODUCTION MANAGER

**Jane F. Gatenby**

SALES REPRESENTATIVES

Philadelphia, Pa. . . . Patricia O'Donnell, CENTCOM, LTD., GSB Building, Suite 405, 1 Belmont Ave., Bala Cynwyd, Pa. 19004 (Area Code 215) 667-9666, FAX: (215) 667-9353

New York, N.Y. . . . John F. Raftery, CENTCOM, LTD., 60 E. 42nd Street, New York 10165 (Area Code 212) 972-9660

Westport, Ct. . . . Edward M. Black, CENTCOM, LTD., 500 Post Road East, P.O. Box 231, Westport, Ct 06880 (Area Code 203) 226-7131, FAX: (203) 454-9939.

Cleveland, OH. . . . Bruce Poorman, John Guyot, CENTCOM, LTD., 325 Front St., Berea, OH 44017 (Area Code 216) 234-1333, FAX: (216) 234-3425

Chicago, Ill. . . . Michael J. Pak, CENTCOM, LTD., 540 Frontage Rd., Northfield, Ill 60093 (Area Code 708) 441-6383, FAX: (708) 441-6382

Houston, Tx. . . . Michael J. Pak, CENTCOM, LTD., (Area Code 708) 441-6383

San Francisco, Ca. . . . Paul M. Butts, CENTCOM, LTD., Suite 1070, 2672 Bayshore Frontage Road, Mountainview, CA 94043 (Area Code 415) 969-4604

Los Angeles, Ca. . . . Clay S. Holden, CENTCOM, LTD., 3142 Pacific Coast Highway, Suite 200, Torrance, CA 90505 (Area Code 213) 325-1903

Boston, Ma. . . . Edward M. Black, CENTCOM, LTD., (Area Code 203) 226-7131

Allanta, Ga. . . . John F. Raftery, CENTCOM, LTD., (Area Code 212) 972-9660

Denver, Co. . . . Paul M. Butts, CENTCOM, LTD., (Area Code 415) 969-4604

Make your ideas heard! Learn how to design and give technical talks to any audience.....

# Effective Oral Presentations



A New Audio Course from the American Chemical Society

Special 30-day free examination offer for ACS members!

Did you ever see someone's good ideas get lost in a bad presentation? Make sure your ideas get the attention they deserve! Learn how to present your ideas clearly and convincingly with this new ACS Audio Course.

**Effective Oral Presentations** shows you just what goes into a successful presentation—and gives you the tools to make your's better. It offers a structured approach to designing and presenting a technical talk to any audience—from organizing your ideas. . .to preparing visual aids. . .to developing your personal style and delivery. In just a few short hours you'll gain skills that can help you give your presentations clarity and impact.....and make you a stand-out communicator on the job. You'll learn to:

- Decide what to say to an audience—and how to say it
- Prepare visual aids that both communicate your ideas and capture attention
- Overcome stage fright
- Use your personality and appearance to enhance your presentation

## Here's what you'll be able to do after taking this course:

- Analyze an audience to determine the organization and content that will work best
- Master the two most critical parts of a talk—the introduction and conclusion
- Project confidence and enthusiasm
- Critique and modify your own speaking voice
- Use visual aids that say just enough—but not too much

Raise your profile on-the-job! Become a convincing communicator when presenting technical material. Learn how with **Effective Oral Presentations**.

## Who Should Take This Course

Anyone who presents technical material—whether research seminars, progress reports, sales presentations, etc.—to a management or nontechnical audience can benefit from **Effective Oral Presentations**.

## Brief Course Outline

- **Text Preparation:** Selecting, Organizing, and Supporting Your Ideas; The Introduction; The Conclusion
- **Visual Aids:** Using Visual Aids; Types of Visual Aids; Criteria for Using; Transparencies and Slides
- **Personal Preparation, Delivery:** Personal Style; Voice and Diction; Barriers to Communication

## The Instructor

*W.F. (Fred) Oettle* works in industrial relations, training, and recruiting for E.I. du Pont de Nemours & Co.

## The Unit

**Effective Oral Presentations** consists of three cassettes (three hours of taped instruction) and a 50-page manual. It comes in one compact package, so that you can keep it with you to study when you want—at work, at home, or even while traveling.

From concept to delivery, **Effective Oral Presentations** can give your talks snap and polish—and make your ideas heard. To order, use the coupon below or call 1-800-227-5558.

## Order Form

Please send me **Effective Oral Presentations** (Catalog No. B3):

	US &			
	Qty.	Canada	Export	Total
Complete Course	_____	\$350	\$420	_____
Additional Manuals	_____	\$18	\$22	_____
		Total order		_____

## Payment Options:

1. Payment enclosed (make check payable to American Chemical Society).

2. Purchase order enclosed.

P.O. # \_\_\_\_\_

3. Charge my  MasterCard/VISA

AMEX  Diners Club/Carte Blanche

Account No \_\_\_\_\_

Name of cardholder \_\_\_\_\_

Expires \_\_\_\_\_

Signature \_\_\_\_\_

4. Send me my course to examine free for 30 days. I am an ACS member. ACS membership no. (above your name on your C&EN mailing label): \_\_\_\_\_

Signature \_\_\_\_\_

Ship to:

Name \_\_\_\_\_

Address \_\_\_\_\_

City \_\_\_\_\_

State, ZIP \_\_\_\_\_

Phone \_\_\_\_\_

Please allow 3-4 weeks for delivery. Prices quoted in U.S. dollars. Foreign payment must be in U.S. currency by international money order, UNESCO coupons, or U.S. bank draft.

Mail this order form to American Chemical Society, Distribution Office Dept. 15, P.O. Box 57136, West End Station, Washington, DC 20037.

## Comparison of Diesel Engine Exhaust Using Chromatographic Profiling Techniques

Patricia A. Partridge,<sup>\*,†</sup> Francis J. Shala,<sup>†</sup> Nicholas P. Cernansky,<sup>‡</sup> and Irwin H. Suffet<sup>†</sup>

Departments of Chemistry and Mechanical Engineering and The Environmental Studies Institute, Drexel University, Philadelphia, Pennsylvania 19104

■ An analytical method, developed for examining changes in the intensity and number of chemical compounds in the odor fraction of diesel exhaust, has been applied to a variety of diesel engine systems. Comparisons were made using the chromatographic computer profiles of samples collected with the Diesel Odor Analysis System (DOAS) and dilution tunnel sampling systems. The different engine systems showed several areas of common peak patterns, but with distinctly different overall patterns. The benzaldehyde-odor correlation developed in a previous study worked for the engine systems tested. The differences in the overall patterns are attributed to the specific diesel fuels used and to the specific engine configurations. Samples obtained from raw and diluted (with a dilution tunnel) exhaust were compared. Diluted exhaust sample profiles were shown to contain a greater number of peaks, probably due to postcombustion reactions occurring in the dilution tunnel.

### Introduction

Diesel exhaust has been characterized as a complex mixture of over a thousand compounds. Specific chemical analysis of all the odorants in the exhaust has been confounded by the complexity of the exhaust gas matrix (1). The only fully instrumental method of diesel exhaust odor analysis is the Diesel Odor Analysis System (DOAS) developed at Arthur D. Little, Inc. (2-4). The DOAS provides for liquid chromatographic measurement of the organics present in diesel odor samples that have been correlated to the total intensity of aroma (TIA) as perceived by human sensory panels.

In a previous study (5), a broad-spectrum analytical approach was used to investigate the DOAS oxygenate fraction and to determine which components are indicative of the overall odor. The combined application of a sample fractionation-gas chromatographic method with a chromatographic computer-profiling technique resulted in the development of a linear-log correlation between the DOAS odor system and a specific "character impact peak" (which is indicative of the significant differences between samples). The significant character impact peak was identified

**Table I. Comparison of Diesel Engines**

	Drexel	SwRI	AVL
manufacturer application type	Wakesha Fuels Research indirect injection CFR	Volkswagen Rabbit high swirl prechamber	AVL Mercedes direct injection <sup>a</sup>
compression ratio	17.4 and 23.0	23.5	21.5
cylinder no.	1	4	6
displacement, L	0.61	1.48	2.20

<sup>a</sup> Experimental, preproduction prototype.

**Table II. Physical Properties of Fuels**

fuel	gravity <sup>d</sup>	bp, °F		aromatics, wt %	cetane index (D976)
		initial	final		
Isopar-M <sup>a</sup>	49.0	410	495	0.4	29
diesel no. 1 <sup>a</sup>	41.6	374	518	1.0	45
diesel no. 2 <sup>b</sup>	36.1	368	596	29	50
AVL no. 93 <sup>c</sup>	36.1	343	649	26	44
AVL no. 97 <sup>c</sup>	28.9	433	739	28	42

<sup>a</sup>Drexel University. <sup>b</sup>SwRI. <sup>c</sup>AVL. <sup>d</sup>Degrees APoI at 60 °F.

as benzaldehyde (5). The quantitative relationship between exhaust odor as measured by TIA and the concentration of benzaldehyde in the exhaust was determined to be

$$\text{TIA} = 1.11 \log_{10} [\text{B}] + 4.10 \quad (1)$$

where [B] is the concentration of benzaldehyde in ppm in the exhaust, and TIA is an odor intensity scale as defined later.

It is the purpose of this study to ascertain whether this same correlation is applicable to diesel engine systems other than the single-cylinder engine used to develop the relationship. To this end, samples from two different diesel engine systems were obtained from Southwest Research Institute (SwRI) and AVL (Graz) for profile analysis, correlation testing, and comparison with the Drexel samples.

### Experimental Section

**Engine Systems.** Two automotive diesel engines and a laboratory research diesel engine were employed in this study. The Drexel Laboratory Research Engine was a Wakesha indirect-injection CFR diesel engine. The SwRI

\* Author to whom correspondence should be addressed: Department of Mechanical Engineering, Drexel University, 32nd and Chestnut Streets, Philadelphia, PA 19104.

<sup>†</sup>Department of Chemistry.

<sup>‡</sup>Department of Mechanical Engineering.

engine was a Volkswagen Rabbit high swirl prechamber diesel engine, and the AVL engine was a Mercedes direct-injection engine. The features of the engines used in this study are listed in Table I. The fuels used in this study were Isopar-M, diesel no. 1, diesel no. 2, AVL no. 93, and AVL no. 97. The Isopar-M and diesel no. 1 are low in aromatic content, while the diesel no. 2, AVL no. 93, and AVL no. 97 are much higher. Table II shows the physical properties of these fuels for reference purposes.

**DOAS Procedures.** The DOAS provides for liquid chromatographic measurement of organics present in diesel exhaust odor samples and has been correlated with human sensory panels. The overall methodology of the DOAS involves the use of an exhaust sampling system to trap odorous compounds on a Chromosorb 102 trap, elution with cyclohexane, and analysis of the eluate on a liquid chromatograph. The liquid chromatograph or "odormeter" separates the sample into two fractions: oxygenates (LCO) and aromatics (LCA). The fractions are quantified by their UV response at 254 nm and related to a total intensity of aroma (TIA) value. The relevant diesel exhaust odor has been attributed to the oxygenated species in the LCO fraction (2). On the basis of an odor panel correlation established at Arthur D. Little, Inc., TIA is given by

$$\text{TIA} = 1.0 + 1.0 \log_{10} (\text{LCO } (\mu\text{g/L})) \quad (2)$$

The numerical scale and intensity rating for the TIA scale ranges from 0.5 (threshold) to 3, which signifies strong odor. Reproducibility and duplicability for odormeter operation, sampling system operation, and experimental system operation was good, with all the data falling within  $\pm 0.1$  TIA unit of the mean at high odor levels (2.0 TIA) and within  $\pm 0.2$  TIA unit of the mean at low odor levels (1.5 TIA).

**Sample Analysis.** A total of 43 samples were used in this study for LCO profile analysis. Twenty-one odor samples were chosen from the past diesel odor work at Drexel University. Six odor samples were supplied by Southwest Research Institute (SwRI) and AVL supplied a series of 16 different exhaust samples (diluted and undiluted). The SwRI and AVL odor samples were collected onto Chromosorb 102 traps and the traps transported to Drexel for elution and chemical analysis.

Diesel exhaust odor samples were analyzed by our sample fractionation-gas chromatographic-computer-profiling method as mentioned above. The details of this method have been reported previously (5); thus, only the main features will be described here.

Each sample was separated into nonpolar and polar fractions by use of silica Sep-Pak (Waters) cartridges for gas chromatography preparation. The polar fraction (LCO), or oxygenates, contains the odorous compounds present in diesel exhaust. The LCO fraction was analyzed on a Varian Model 3700 gas chromatograph equipped with a flame ionization detector and a 60 m by 0.25 mm i.d. SE-30 glass capillary column (J&W Scientific, Inc.) was utilized for all analyses. For each run, 2.7  $\mu\text{L}$  of sample was injected with a split of 9.3:1 at initial temperature of 50 °C. The initial temperature was held for 10 min and then linearly programmed at 3 °C/min to 250 °C, where it was held for 25 min.

A Finnigan Model 4021 automated gas chromatograph/mass spectrometry system operated in the electron impact mode was used for compound separations and identifications. The GC employed a 60-m DB-1 fused-silica column (J&W) to produce a total ion chromatogram similar to the GC profiles.

Data reduction and computer profiling were performed on a Tektronix 4051 graphics system computer and in-

teractive digital plotter. Retention times and areas were transferred from a Spectra-Physics Model 4100 programmable integrator and stored on magnetic tapes. These data files were then used to generate computer profile spike plots representative of the original chromatograms. Relative retention times and areas were used to normalize each chromatographic spike plot for comparative purposes.

### Results and Discussion

**TIA Correlation.** Twenty-one odor samples were chosen from the indirect-injection CFR diesel engine work at Drexel University for LCO profile analysis. The range of sample odor values was from 1.08 to 3.26 TIA units or 1.2 to 186  $\mu\text{g/L}$  in LCO as measured by the DOAS. A series of sample profiles of increasing LCO value and a reference blank are shown in Figure 1. The reference blank contains hydrocarbon standards and polar solvent impurities accumulated from the cyclohexane elution solution as well as impurities from the silica Sep-Pak cartridge itself. The major impurity peak from each Sep-Pak cartridge was used as the reference time. Dodecane concentration was used to scale all the profiles equally. Peaks whose relative areas are increasing with increasing LCO are numbered. Of the numbered peaks, only peak no. 1 was consistently detected in all 21 samples. Since odor intensity is proportional to the log (concentration), the log of the peak area was used for TIA correlation (6). Therefore, a simple linear regression analysis was performed on the log of the area per microliter vs TIA for peak no. 1 in the set of 21 samples. The correlation given in eq 1, with a *R* value of 0.97, was obtained for the sample set. Benzaldehyde was identified as peak no. 1 by gas chromatography/mass spectrometry. Most of the other numbered peaks in Figure 1, consisting of primarily aldehydes and ketones, also followed the trend of increasing LCO; however, these peaks were only observed in the relatively few high LCO samples. Also, 12 of the 21 samples covering the range of LCO and engine conditions were spiked with *n*-alkane standards. These samples were rechromatographed and profiled to quantitatively verify correlations developed.

**Engine Exhaust Systems Analysis.** Odor samples taken in duplicate at three conditions were supplied by Southwest Research Institute (SwRI) from a high swirl prechamber Volkswagen Rabbit diesel engine for LCO profile analysis. The range of sample odor values was from 1.58 to 2.27 TIA units or 3.8 to 18.6  $\mu\text{g/L}$  in LCO as measured by the DOAS. Profiles of the LCO fractions of these samples are shown in Figure 2. The major impurity peak from each Sep-Pak cartridge was used as the reference time. Each successive group of two profiles are replicate samples. Figure 2 shows that peak no. 1 follows a trend similar to that of the LCO value. Also, it can be seen that at low LCO levels the relative peak area does not increase with increasing LCO. This is due to the scatter at low LCO values for the correlation. However, at higher LCO the relative peak areas does increase.

An additional factor to consider with these data is that the diesel Rabbit samples had a variable sample volume, with SwRI-W37 and SwRI-W4 being considerably larger than the fixed 25-L samples used in developing the benzaldehyde correlation. Since the sample volume collected for these diesel Rabbit samples varied from 41 to 121 L, a direct comparison with the fixed 25-L samples used in the benzaldehyde correlation may not be appropriate due to variations in TIA with sample volume effects (7). This effect predicts a reduction in odor with increasing sample volume. Benzaldehyde (peak no. 1) is a moderately polar compound and would adsorb more strongly than the



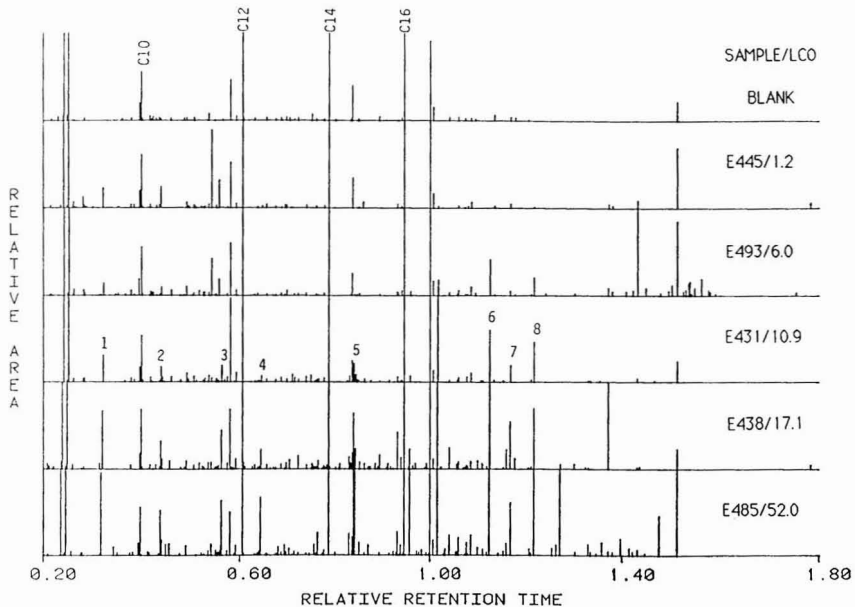


Figure 1. Chromatographic computer profiles of the LCO-1 fractions for engine exhaust samples with increasing LCO values ( $\mu\text{g/L}$ ) and a reference blank with hydrocarbon standards. Numbers in center profile denote character impact peaks (1 = benzaldehyde).

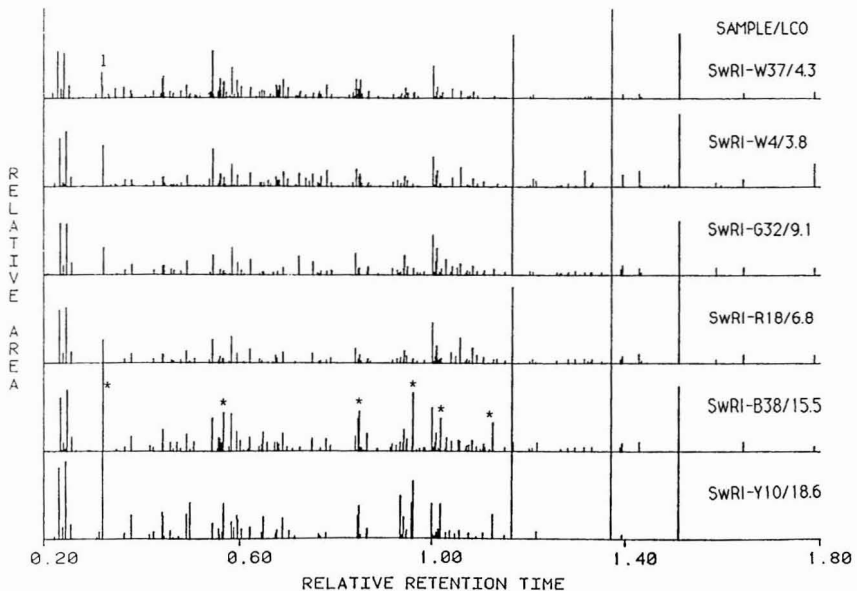


Figure 2. Chromatographic computer profiles of the LCO-1 fractions for SwRI engine exhaust samples with increasing LCO values ( $\mu\text{g/L}$ ) (1 = benzaldehyde).

odorous compounds onto the Chromosorb 102 surface and should not break through as readily as the odorous compounds. If this sample volume effect were significant for the two high-volume samples, SwRI-W37 and SwRI-W4, then their actual odor value relative to the other samples would be higher and the agreement with their predicted odor value also would be improved (see next section).

AVL supplied a series of 16 different exhaust samples, which were collected from an experimental Mercedes direct-injection diesel engine for LCO profile analysis. The range of sample odor values was from 1.54 to 2.41 TIA

units or 3.5 to 25.7  $\mu\text{g/L}$  in LCO as measured by the DOAS. The samples fall into two categories: diluted and undiluted. The undiluted samples were collected from the raw exhaust (the standard DOAS sampling procedure), whereas the diluted samples were collected from a dilution tunnel, where the exhaust is diluted with air before sampling. This is done so that the resulting exhaust may be sampled for particulates and PAH analysis (8, 9).

Each of the four engine operating conditions are represented by four exhaust samples, duplicate samples in both the diluted and undiluted exhaust forms. Figure 3

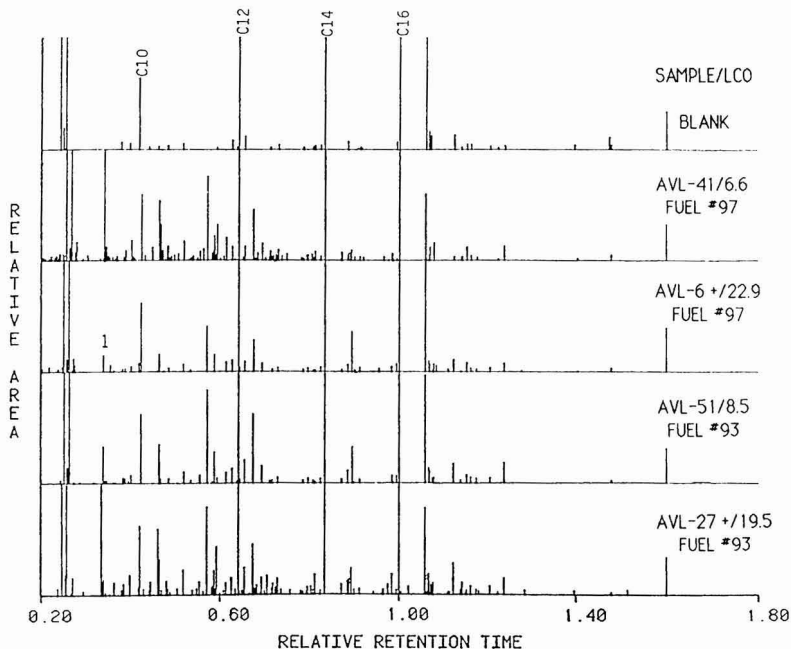


**Figure 3.** Chromatographic computer profiles of the LCO-1 fractions for AVL engine exhaust samples with LCO values ( $\mu\text{g/L}$ ) and a reference blank with hydrocarbon standards. Samples labeled + are dilution tunnel samples (1 = benzaldehyde).

shows the LCO profiles with the sample codes and associated LCO values in micrograms per liter of undiluted and diluted exhaust samples of both fuel types, thereby highlighting fuel characteristics and sample conditioning effects. The reference time of the *n*-hexadecane internal standard (50.5 min) was used to line the profiles up evenly for these samples, because of a switch to a new lot of Sep-Pak cartridges, which did not provide the previously used reference impurity peak. Note that all the AVL profiles yield the same general peak pattern as those of the SwRI and Drexel profiles. Also, there is a larger number of small peaks in the dilution tunnel samples than in the undiluted samples.

Overall, it appears that the increase in the character impact peak intensity deduced from chromatographic profiles follows the increase in odor level. A second indicator of odor level appears to be the total number of peaks observed. However, the number of peaks may just be a detectability problem for those samples in which the small peaks are not observed. What is needed is the processing of less concentrated samples to verify this conclusion.

**TIA Prediction Values.** As noted, a linear regression analysis was used to develop a correlation between the log of the concentration of benzaldehyde and the TIA exhaust odor value (eq 1). The minimum 95% prediction interval obtained was  $\pm 0.29$  TIA unit. This interval is largely due to the scatter at low LCO values for the correlation, as reported in an earlier paper (5). By use of this correlation, our new data can be tested to determine if it lies within the 95% prediction interval based on the benzaldehyde concentration. In the range of the benzaldehyde correlation, the 95% prediction interval is slightly higher at the ends of the bands than in the middle. Thus, for any measured benzaldehyde concentration, the predicted TIA level is assigned a corresponding  $\pm$  value to it, depending on where it lies in the range of the correlation. Each of the SwRI and AVL sample's TIA value (from the DOAS

analysis) was tested in this fashion, with the results tabulated in Table III. As can be seen, every TIA except that for AVL-45 is within the calculated 95% TIA prediction interval. This indicates that benzaldehyde may have general value in the prediction of diesel exhaust odor, given the correlations developed. It must be mentioned that benzaldehyde is only an indicator of odor and is not to be considered the cause of diesel odor.

The fact that only one of the 22 samples falls outside the 95% TIA prediction interval is a very supportive finding for the odor correlation, particularly in view of the widely different engine types, fuels, engine operating conditions, and exhaust dilution effects that were included in the statistical analysis.

**Operational Factors.** As noted above, large sample volumes of the raw exhaust have been found to result in LCO breakthrough and reductions in measured odor. A dilution tunnel effect on odor measurements can be observed from our data as well. Examining Table III and Figure 3, one observes that each dilution tunnel sample contains a larger number of small peaks and yields a higher odor TIA value than its corresponding undiluted counterpart. This is true for all cases and is independent of fuel type. The larger number of small peaks in the dilution tunnel samples may be due to one of two possibilities: further reactions (via oxidation or other means) of exhaust species in the tunnel to produce more compounds (10) or differential displacement of the adsorbed compounds on the Chromosorb 102 odor traps, although this latter possibility is not very likely. In any event, this increased number of odorous compounds is indicative of and contributes to the higher odor levels found in the dilution tunnel samples. The effect of engine load or air to fuel ratio (A/F) can be examined by using the AVL data where engine load was varied. As the load increases (A/F ratio decreases), the amount of fuel delivered to the engine increases and the level of odor might be expected to increase (11), although consistent behavior is not necessarily

**Table III. TIA Prediction Values for Diesel Odor Samples**

sample code	sample cond		A/F ratio	LCO, $\mu\text{g/L}$	TIA by DOAS	TIA predcn by peak 1
	vol, L	rate/min				
SwRI-W37	122	6.1	unknown	4.3	1.63	1.87 $\pm$ 0.31
SwRI-W4	85	4.3	unknown	3.8	1.58	1.88 $\pm$ 0.31
SwRI-G32	47	4.7	unknown	9.1	1.96	1.91 $\pm$ 0.31
SwRI-R18	48	4.8	unknown	6.8	1.83	1.91 $\pm$ 0.31
SwRI-B38	44	4.4	unknown	15.4	2.19	2.51 $\pm$ 0.32
SwRI-Y10	42	4.2	unknown	18.6	2.27	2.51 $\pm$ 0.32
AVL-23 <sup>a</sup>	25	<i>b</i>	103.7	6.3	1.80	1.94 $\pm$ 0.29
AVL-41	25	<i>b</i>	103.7	6.6	1.82	1.59 $\pm$ 0.29
AVL-6	25	<i>b</i>	103.7	22.9	2.36	2.44 $\pm$ 0.29
AVL-26	25	<i>b</i>	103.7	19.1	2.28	2.48 $\pm$ 0.29
AVL-51	25	<i>b</i>	109.6	8.5	1.93	1.94 $\pm$ 0.29
AVL-49	25	<i>b</i>	109.6	5.8	1.76	1.72 $\pm$ 0.29
AVL-27	25	<i>b</i>	109.6	19.5	2.29	2.46 $\pm$ 0.29
AVL-58	25	<i>b</i>	109.6	24.0	2.38	2.42 $\pm$ 0.29
AVL-43	25	<i>b</i>	43.2	7.2	1.86	1.81 $\pm$ 0.29
AVL-59	25	<i>b</i>	43.2	4.6	1.66	1.75 $\pm$ 0.29
AVL-25	25	<i>b</i>	43.2	17.4	2.24	2.42 $\pm$ 0.29
AVL-70	25	<i>b</i>	43.2	25.7	2.41	2.54 $\pm$ 0.30
AVL-45 <sup>d</sup>	25	<i>b</i>	24.1	7.2	1.86	1.45 $\pm$ 0.30
AVL-82	25	<i>b</i>	24.1	3.5	1.54	1.58 $\pm$ 0.29
AVL-35 <sup>c</sup>	25	<i>b</i>	24.1	18.2	2.26	2.17 $\pm$ 0.29
AVL-61 <sup>c</sup>	25	<i>b</i>	24.1	13.8	2.14	2.21 $\pm$ 0.29

<sup>a</sup>Fuel no. 97 was used for this set of four samples; otherwise, fuel no. 93 was used. <sup>b</sup>Sample flow rate range was 5.5–6.0 L/min. <sup>c</sup>Dilution tunnel samples. Sample volume represents total volume collected. <sup>d</sup>Sample that falls outside the prediction interval.

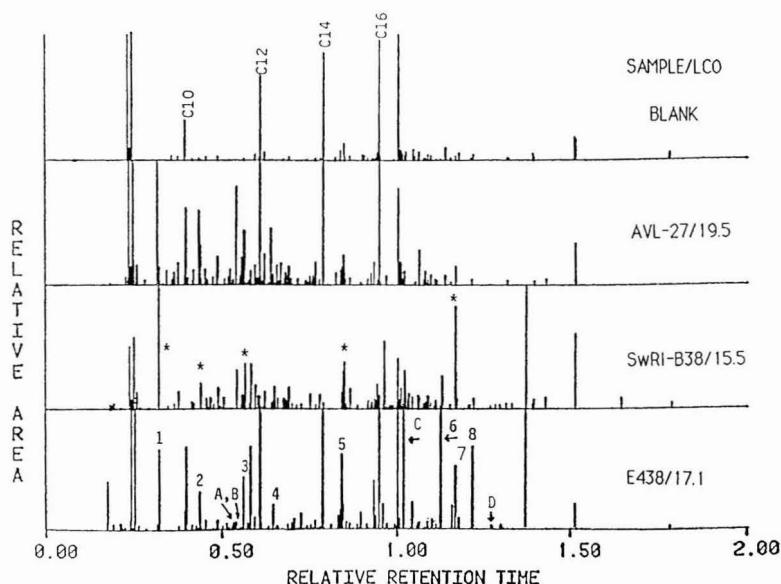


**Figure 4.** Chromatographic computer profiles of the LCO-1 fractions of the diesel engine exhaust samples. Asterisks denote common peak areas; letters and numbers are identified peaks.

expected (12). For the present data, the odor level decreases slightly with increasing fuel concentration for both the undiluted and diluted cases. Hence, the odor emissions behavior of the AVL engine is essentially independent of engine load.

**General Profile Comparisons.** Another application of the chromatographic profiling technique is the identification of differences and/or similarities between experimental combustion systems. The resulting profiles can indicate peak patterns that are distinctive of certain types of combustion systems as well as combustion mechanisms. It is appropriate, therefore, to compare the GC profiles of each engine type from the previous sections to determine and evaluate any similarities or differences that would be

indicative of the combustion process or system.

Figure 4 shows a representative profile of the LCO fraction of the exhaust from each engine type and a Sep-Pak blank (first batch) for reference. Samples E438, SwRI-B38, and AVL-27 represent the single-cylinder engine, the VW Rabbit engine, and the AVL engine, respectively. Sample SwRI-B38 does not contain alkane standards, so all the profiles are aligned by the major Sep-Pak impurity peak at 1.00 relative retention time. All the samples have approximately the same magnitude of odor (TIA  $\approx$  2.3).

Figure 4 shows that there is a similarity in the profiles in the engine samples. The asterisks in sample SwRI-B38 indicate areas of peaks or peak patterns common in all of

**Table IV. Compounds Identified in the Diesel Exhaust Odor Complex**

compound	ret reten time, <sup>a</sup> min	figure designation
benzaldehyde	0.320	1
methylbenzaldehyde isomer	0.438	2
C2-benzaldehyde isomer	0.538	A
3-phenylpropenal	0.556	B
cinnoline	0.563	3
1-indanone	0.646	4
1,1-diphenylethane <sup>b</sup>	0.840	5
9-fluorenone	1.02	C
benzo[c]cinnoline	1.13	6
c	1.18	7
pyrene	1.22	8
fluoranthene	1.30	D

<sup>a</sup>Reference time of 53.58 min for the major Sep-Pak impurity peak. <sup>b</sup>Tentative identification in a fused peak mix. <sup>c</sup>Figure designation no. 7 not positively identified.

the engine profiles. Variables that might affect the appearance of the profiles are the type of fuel used and the engine operating conditions. However, the engine operating conditions may not be or are not expected to significantly affect the shape of the profiles. This conclusion is based on the high degree of similarity in the peak pattern that was previously observed between the profiles of samples collected from the same engine type (13). Therefore, the significant variables affecting the profile pattern are either the fuel or engine type or both. Further experimentation should be made to study these variables. The labeled areas in sample E438 are for reference use in the following section.

**GC/MS Analysis.** The chromatographic profile approach precludes the need to identify all compounds present by allowing the selection of only the character impact peaks. These peaks then can be focused on for identification and interpretation purposes, such as determining their significance with respect to exhaust odor and combustion processes.

Gas chromatography/mass spectrometry can then be used to identify only the statistically significant character impact peaks. The most odor relevant peak, peak no. 1, was identified in all three samples as benzaldehyde. Benzaldehyde was found to yield an excellent correlation with odor as measured by the DOAS. Other compounds common to all engine systems are listed with their relative retention times on a 60-m SE-30 capillary column in Table IV. The reference number relates these compounds to the peaks in the sample E438 profile shown in Figure 4. It can be seen that most of these peaks are in areas common to all the engine-type profiles. This suggests that their formation may be linked to some aspect of the combustion process in all diesel engines.

### Summary

An analytical method that was developed to study the odorous fraction of diesel exhaust with respect to the DOAS method has been applied to three different diesel engine systems. Comparison of profiles between engine types showed areas of common peak patterns, but with distinctly different overall patterns. The benzaldehyde-odor correlation developed for an IDI laboratory research engine worked satisfactorily for the other engine systems tested, with only one of the 22 samples falling outside the 95% TIA prediction interval. This is a very supportive finding for the odor correlation in that widely different

engine types, fuels, engine operating conditions, and exhaust dilution effects were included in the statistical analysis. The differences in the overall peak patterns are thought to be due to the engine configuration and/or the type of fuel used. Comparisons between samples collected by the standard DOAS procedure and a dilution tunnel were made by examining their profiles. Dilution tunnel odor samples had higher overall odor values compared to the undiluted samples. The dilution tunnel profiles were similar to those of the standard sampling profiles, but included many additional small peaks. These peaks are probably due to increased postoxidative reactions occurring in the dilution tunnel. The above results also indicate the value of the profiling methodology in making data evaluations and interpretations.

**Registry No.** Benzaldehyde, 100-52-7; methylbenzaldehyde, 1334-78-7; 3-phenylpropenal, 104-55-2; cinnoline, 253-66-7; 1-indanone, 83-33-0; 9-fluorenone, 164-94-3; benzo[c]cinnoline, 230-17-1; pyrene, 129-00-0; fluoranthene, 206-44-0.

### Literature Cited

- (1) Daudel, H. L.; Fieber, M. J.; Hardenberg, H. O. Progress in Instrumental Analysis of Exhaust Odorants. SAE Paper 830117; SAE: Warrendale, PA, 1983.
- (2) Levins, P. L.; Kendall, D. A.; Caragay, A. B.; Leonardos, G.; Oberholtzer, J. E. Chemical Analysis of Diesel Exhaust Odor Species. SAE Paper 740216; SAE: Warrendale, PA, 1974.
- (3) Hames, R. J.; Slone, R. J.; Perez, J. M.; Johnson, J. H. Cooperative Evaluation of Techniques for Measuring Diesel Exhaust Odor Using the Diesel Odor Analysis System (DOAS). SAE Paper 800422, SAE: Warrendale, PA, 1980.
- (4) Chemical Analysis of Odor Compounds in Diesel Exhaust. Final Report, Coordinating Research Council Project CAPE-7-68; EPA Contract 68-02-0087, Arthur D. Little, Inc.: Cambridge MA, 1973.
- (5) Partridge, P. A.; Shala, F. J.; Cernansky, N. P.; Suffet, I. H. *Environ. Sci. Technol.* 1987, 21, 403-408.
- (6) National Academy of Sciences Report by the Committee on Odors from Stationary and Mobile Sources; National Academy of Sciences: Washington, DC, January 1979.
- (7) Cernansky, N. P.; Savery, C. W.; Suffet, I. H.; Cohen, R. S. Diesel Odor Sampling and Analysis Using the Diesel Odor Analysis System. SAE Paper 780223; SAE: Warrendale, PA, 1978.
- (8) Black, F.; High, L. Methodology for Determining Particulate and Gaseous Diesel Hydrocarbon Emissions. SAE Paper 790422; SAE: Warrendale, PA, 1979.
- (9) Trayser, D. A.; Peterson, B. A. Development of Dilution and Sampling Methodologies for PNA Measurement in Diesel Exhaust Particulates. Presented at the Chemical Characterization of Diesel Exhaust Emissions Workshop, Dearborn MI, 1981.
- (10) Daudel, H. L.; Fieber, M. J.; Murthy, D. M.; Hardenberg, H. O. Detection and Instrumentation Analysis of Diesel Engine Exhaust Gas Odorants—A New Approach to an Old Problem. SAE Paper 790489; SAE: Warrendale, PA, 1979.
- (11) Petrow, E. D.; Savliwala, M. N.; Hsieh, F. T.; Cernansky, N. P.; Cohen R. S. An Investigation of Diesel Odor in an Air Aspirated Spray Burner and a CFR Diesel Engine. SAE Paper 780632; SAE: Warrendale, PA, 1978.
- (12) Cernansky, N. P.; Petrow, E. D. A Comparison of the Odorous Emissions from a Direct Injection and an Indirect Injection Diesel Engine. *Int. J. Vehicle Des.* 1985, 6, 183-198.
- (13) Shala, F. J. Characterization and Analysis of Diesel Exhaust Odor. Ph.D. Dissertation, Drexel University, Philadelphia, PA, June 1983.

Received for review August 22, 1988. Revised manuscript received August 14, 1989. Accepted September 1, 1989.

# Binding Site Analysis Using Linear Programming

Pierre Brassard, James R. Kramer,\* and Pamela V. Collins

Department of Geology, McMaster University, Hamilton, Ontario, Canada L8S 4M1

■ Estimation of binding site concentrations and equilibrium constants is achieved by using a linear programming technique configured to a multiple-site monometal model. Simulated and actual titration data are used to test the procedure. The calculation is robust and can discriminate multiple pKs with extremely variable concentrations. For acid/base titrations, acid neutralizing capacity is determined as part of the procedure. The method works when the assumption for Gran's analysis is violated. The resolution of titration curves by this method is only limited by the quality of the data.

## Introduction

There are many complexation reactions that can occur among metals, ligands, and surfaces in aquatic environments. These reactions are often inferred by resolution of titration curves into concentration-pK spectra. Yet determination of more than three to four equilibrium constants is apparently difficult. Dzombak et al. (1) and Fish et al. (2) argued that the profile of a titration is controlled by a few sites of highest affinity, while the remaining sites of lesser importance have little influence on the determination. Indeed, with an analysis of variance (*F* test) as criterion, two to four pK values are sufficient to characterize the titration curve (3), which amounts to about one ligand for each order of magnitude (1).

Limitations to a few resolvable sites need not be caused by the model itself, but also by the numerical method used to approximate it, as is the case for the continuous affinity spectrum of Shuman et al. (4), which also requires smoothing techniques. Similar limitations may come from the optimization procedure used to find the solution. For example, in the case of FITTEQL (5), a preset number of parameters are adjusted according to numerical differentiation of the model equation so as to minimize the least-squares error. Since least-squares estimates are biased toward the larger differences, the contribution of small peaks will tend to be ignored in the final solution.

The resolution of titration data for environmental samples on the one hand seems quite limited. This limitation is not unpredictable, however, if one considers that the *F* test [as used by Dzombak et al. (1)] deals only with the overall variance. Thus, the *F* test is similar to a principal component analysis, i.e., to find the least number of variables that would explain, say, 95% of the total variance in the titration curve. By design, the *F* test will exclude small peaks and give a conservative signature to the sample. Although it is possible that the overall shape of a titration curve can be described by only three or four binding constants, it is desirable to know if this limitation arises from the true titration signature or from an artifact of the data reduction method.

The potential clearly exists to resolve more than three binding sites from the many tens of data points that can be obtained for a titration profile. Here we assess the problem by using a linear programming (LP) approach on simulated titration data and on actual acid/base titrations. In contrast to the preceding discussion, the LP approach emphasizes peaks and maximizes zero concentrations.

In the following, titration data and dissociation constants are considered at constant temperature and constant ionic

strength, and concentrations are represented in the text by brackets. The ion balance expression can then be written for the unreacted protolyte [ligand<sub>*i*</sub>], acid neutralizing capacity [ANC], carbonates [carb] = ([HCO<sub>3</sub><sup>-</sup>] + 2[CO<sub>3</sub><sup>2-</sup>]), base [base], and acid [acid] titrants as

$$\sum[\text{ligand}_i] - [\text{ANC}] = [\text{base}] - [\text{acid}] - [\text{carb}] + [\text{H}^+] - [\text{OH}^-] \quad (1)$$

[carb] can be obtained from dissolved inorganic carbon (DIC) - pH measurements. Alternately, [carb] may be resolved as part of [ligand<sub>*i*</sub>]. ANC is defined as the sum of all nonreacting cations minus nonreacting anions (6). Equation 1 shows that ANC is equal to alkalinity ([carb] - H<sup>+</sup> + OH<sup>-</sup>) in the special case when only carbonates are present as ligands. Otherwise ANC is always greater than alkalinity.

ANC is usually determined independently either by Gran's method (7) or by total ion balance (8), but both methods have their biases. In Gran's method, the sample is titrated with acid to the low portion of the pH range, where all possible "weak" acids are expected to be protonated. In this range, the increase of H<sup>+</sup> ion in the solution should solely be due to the addition of titrant. The difference between the H<sup>+</sup> ions predicted by titrant addition and the one actually measured is therefore the sum of remaining "strong" ions and, therefore, ANC. In Gran's method, errors can be introduced if a site concentration similar to H<sup>+</sup>-ion concentration exists with a pK value in the low pH range.

We propose the determination of ANC as an additional term in the discrete monoprotic distribution model. Then eq 1 becomes

$$[\text{base}] - [\text{acid}] - [\text{carb}] + [\text{H}] - [\text{OH}] = \sum C_j \alpha_{ij} - C_{\text{anc}} \quad \text{for } i = 1, m \quad (2)$$

where  $\alpha_{ij} = K_j / (K_j + [\text{H}])$ ,  $K = 10^{-\text{pK}}$ ,  $K_j$  is the conditional product at a given ionic strength and temperature,  $C_j$  is the total concentration in the *j*th protolyte ( $j = 1, n$ ), and  $C_{\text{anc}}$  is the ANC determined in the equation. The problem is then treated as a set of *m* multiple linear equations, one for each titration step *i*. Each equation is linear because it is assumed that the titration profile of the ligands arises from the sum of *n* monoprotic sites, with constants ranging from  $K_1$  to  $K_n$ . The error introduced by diprotic terms is small (9, 10). Biases brought about by possible multiprotic terms using the present LP approach are discussed further on.

Suppose now that the estimates of [ligand<sub>*i*</sub>] - [ANC] are error free. If each titration step is nonredundant, exactly *n* + 1 titration steps are required to fully define each  $C_j$  and  $C_{\text{anc}}$ .  $C_j$  and  $C_{\text{anc}}$  are the unknowns, and  $K_j$ s are preset to cover the range of the model in *n* equal pK intervals. Equation 2 then becomes a multilinear equation with the condition that  $C_j \geq 0$ . In reality, more than *n* + 1 titration steps are required to compensate for the loss of degrees of freedom due to measurement errors, for redundancy, and for the fact that the values of  $K_j$ s for the model are chosen a priori and only approximate the  $K_j$ s of the sample. In addition, losses may occur if the titration pH range is not wide enough. In spite of these conditions, we show that the titration profile contains enough information to

yield the complete spectrum and ANC.

This paper first describes the LP analysis. Then simulated and actual titration data are used to test the robustness, pK resolution, and precision of the technique.

### Materials and Methods

**(a) The Linear Programming (LP) Solution.** The purpose of LP is to find an optimal solution to a linear multivariate equation from a finite number of possible solutions. Assuming that the system can be solved, the number of solutions is kept finite because both the number of simultaneous equations and the number of variables are finite. This number is further reduced by the implicit constraint that all variables are positive and by any number of explicit constraints imposed by the user upon the system. The set of such linear solutions is called the feasible set, and the optimal solution is chosen by evaluating an objective function. The solution that scores best on the objective function is the desired one.

The LP method thus requires a matrix containing the objective function, the set of linear equations, and the constraints to limit the scope of the solution. This problem is referred to as the PRIMAL and its solution is the PRIMAL solution. The problem can also be recast in the DUAL form by taking more or less the transposed PRIMAL matrix, which leads to the DUAL solution. The duality theorem (11) ensures that for any problem with a primal solution there is a unique dual solution. Furthermore, the dual solution of a dual problem returns the primal solution. This apparent detour is convenient to minimize matrix size and to gain speed and precision.

The LP approach we use is similar in concept to that of Tobler and Engel (12). The differences are as follows:

(1) The number of terms ( $n$ ) in the equation is variable.

(2) The optimization problem is presented as its dual to reduce the size of the matrix and improve the stability of the algorithm.

(3) We use the FORTRAN77 revised simplex algorithm of Best and Ritter (13), which solves for both dual and primal forms and where the observed values need not be entered as positive integers.

(4) Double-precision arithmetic eliminates the separation of single pK peaks into two separate ones, as found by Tobler and Engel. Such doublets result from truncation of  $\alpha_{ij}$ s to 0 or 1 with single-precision calculations.

(5) The values for  $C_j$  are forced positive in the primal problem, even if this condition is implicit in the algorithm. By solving simulated spectra, we found that rounding errors in the dual solution are less important when this condition is applied.

The PRIMAL problem is

Minimize Absolute  $\{\sum E_i\}$  such that (3)

$$E_i + \sum C_j \alpha_{ij} - C_{anc} \geq \text{ligand}_i - \text{ANC} \quad i = 1, m$$

$$E_i - \sum C_j \alpha_{ij} + C_{anc} \geq -\text{ligand}_i + \text{ANC} \quad i = 1, m$$

$$C_j \geq 0 \quad j = 1, n$$

where  $E_i$  is the error for the  $i$ th term and  $(C_j \dots C_{anc})$  is the required solution vector.

After some simplification, the DUAL problem is

Maximize Absolute  $\{\sum (\text{ligand}_i - \text{ANC})\}$  such that (4)

$$\sum U_i \alpha_{ij} + \frac{1}{2} W_j = \frac{1}{2} \sum \alpha_{ij} \quad j = 1, n$$

$$\sum U_i = m/2 \quad j = n + 1$$

where  $(U_i \dots W_j)$  is the solution vector.

By the duality theorem, the dual solution of this dual problem is the primal solution, i.e.,  $(C_j \dots C_{anc})$ .

**(b) Artificial Titration Data.** Profiles of pH vs titrant were generated for a distribution of up to 10 discrete monoprotic ligands, using the ion balance equation corrected for volume dilution. The first pH value at zero titrant addition (equivalence pH) was determined by solving the ion balance equation iteratively. Subsequent additions were found by solving the equation with up to 51 preset pH values covering the titration range in equal steps. Profiles were generated with different ANCs and different pK distributions. Random deviation (noise) was also added to data to evaluate the robustness of the method to recover the original spectrum. Goodness of fit was estimated as the root mean square (rms) difference between the  $C_j$  concentrations found by the model and the original known distribution. Three sources of bias were examined.

(1) Interference of "strong" and "weak" ligands (14): Simulated data were analyzed for ANC by the LP method and Gran's method. Acid titration data were generated with a fixed ANC and two ligands, one fixed at a pK = 10 and another with decreasing pK.

(2) The effect of incomplete data: Wide (11 ligands), intermediate (7 ligands), and narrow (3 ligands) profiles were produced at varied pH ranges to simulate the situation when either the titration range or the model range do not include all of the ligand sites. All simulations were done at the same interval of 0.2 pH unit.

(3) Noise sensitivity of the method: The effect of adding a random error of up to  $\pm 0.032$  unit on the pH term was simulated for a site distribution with pKs at 3, 5, 7, 9, and 11, each of equal concentration. The test was made for concentrations of 40, 100, and 200  $\mu\text{equiv/L}$ .

We then assessed the LP procedure to obtain pKs for metal-ligand complexes. For this assessment, a mass balance equation for bound sites was used:

$$[\text{met-titr}] - [M_i] = \sum C_j \frac{[M_i]}{[M_i] + K_j} \quad (5)$$

$[\text{met-titr}]$  is the metal titrant and  $[M_i]$  is the unreacted metal concentration. We generated synthetic titration spectra for the six-site model proposed by Fish et al. (2), both for a perfect data set and for a data set with random error added to the pM value. Seventy data points were generated for a pM range of 2–16 (e.g., 0.2 interval). The LP solution was obtained for the pK range of 2–16 at 0.5 pK interval. Due to the coarse pK interval of 0.5, we represent adjacent peaks by only one peak. The pK for the adjacent peaks was calculated as the concentration-weighted average. The concentration was the sum of the adjacent concentrations.

**(c) Real Titrations.** All titrations were carried out in a constant-temperature/pressure variable volume airtight reactor to eliminate the transfer of volatiles (e.g.,  $\text{CO}_2$ ) during the course of the titration. Ionic strength was kept at 0.04 equiv/L. Variable-volume, constant pH interval titrations were obtained with a programmed automated titrator that tracked the buffer capacity of the solution. First known mixtures of sodium carbonate, sodium citrate, and sodium acetate solutions were titrated in 0.1 pH steps from equilibrium pH down to pH 3 with acid. For citric acid, a back-titration with base followed to pH 11 in order to cover the full titration range of 3–11.

A commercial humic acid (Aldrich) was also titrated to a pH of 3 and then to a pH of 11. To evaluate reversibility of the titration, the samples were also titrated to a pH of 11 and then to a pH of 3.

Table I. Simulated Titration Profiles To Evaluate Recovery of Data<sup>a</sup>

no.	ligand sites, pK	titration range, pH		model range, pH		rms, ( $\mu\text{equiv/L}$ )
		min	max	min	max	
1a	4, 5, 6, 7, 8, 9, 10	2	12	4	10	0.127
1b	6, 7, 8	4	10	2	12	0.017
1c	4, 5, 6, 7, 8, 9, 10	2	12	2	12	0.141
1d	6, 7, 8	2	12	4	10	0.025
1e	2, 3, 4, 5, 6, 7, 8 9, 10, 11, 12	2	12	2	12	0.269
2a	4, 5, 6, 7, 8, 9, 10	2	12	6	8	817
2b	2, 3, 4, 5, 6, 7, 8 9, 10, 11, 12	2	12	4	10	692
2c	2, 3, 4, 5, 6, 7, 8 9, 10, 11, 12	4	10	6	8	1490
3a	2, 3, 4, 5, 6, 7, 8 9, 10, 11, 12	6	8	4	10	1095
3b	2, 3, 4, 5, 6, 7, 8 9, 10, 11, 12	4	10	2	12	1021
3c	4, 5, 6, 7, 8, 9, 10	6	8	2	12	416
4a	2, 3, 4, 5, 6, 7, 8 9, 10, 11, 12	4	10	4	10	589

<sup>a</sup> All discrete ligand site concentrations are the same and equal to 1000  $\mu\text{equiv/L}$ . All titration and analysis points occur at 0.2 logarithmic intervals.

The term  $([\text{ligand}] - [\text{ANC}])$  was calculated from the titration data, by use of eq 1, and analyzed by LP using a pK range of 3–11 with a 0.2 pK interval. In the case of separate titrations for the humic acid, the term  $([\text{ligand}] - [\text{ANC}])$  was calculated for both acid and base titrations. Also, the first portions of each titration were joined and analyzed. In all cases, a Gran analysis was made on the acid portion of the titration profile.

### Results and Discussion

The set of simultaneous monoprotic equations cannot be solved correctly by using multiple linear regression because the solution has to be restricted to  $C_j \geq 0$ . Although nonlinear methods have been used to exclude negative values of  $C_j$  (15), convergence to a solution is not assured and depends on a good choice of seed values. The LP procedure is different from other fitting procedures for three reasons. First, and contrary to normal regression, LP minimizes the absolute of the error ( $L_1$  norm), not its square ( $L_2$  norm). The  $L_1$  norm (11) is more robust for erratic data (16) because it assigns an equal weight to all elements of the equation. Second, the revised simplex algorithm (11) always converges if there is at least one feasible solution. No seed values are required. Third, the algorithm is stable because the number of solutions is finite and the algorithm to find them does so directly without using approximation methods to converge, for example, as in FITEQL (5). The tradeoff for this stability is to impose a preset value to the pKs examined by the algorithm. Although this potentially limits the precision of pK determination to the chosen interval, the interval can be chosen very small, with an increase in time for calculation.

**(a) Redundancy of Data.** The solution found by LP can be biased when an inadequate titration data set is used. This occurs either because the monoprotic model is not given enough information or because the model is inflexible. Some basic rules can be deduced by looking at the monoprotic equation (eq 2). In order to find an adequate solution, the titration data must have at least the same number of points as the number of unknowns ( $C_s + C_{\text{anc}}$ ) in the model. Furthermore, to be significant, each of these points must have pH values near different pKs. In reality, this occurs rarely and two limiting cases of redundancy arise. First, if pH values lie to far above or below the model

range, the calculated values for all values of  $\alpha_{ij}$  are equal to either zero or 1. Thus, all such titration points give identical equations and are therefore redundant. Second, if the pH of several titration data points is clustered around the same value, the resulting equations are replicates within experimental error. The total minimum number of titration points should, therefore, equal the number of unknowns (including the ANC term) plus any redundant points arising from the above cases.

The first case of redundancy can be examined by testing for all possible ordinal combinations between titration, model, and sample ranges. Given a (simulated) sample with a defined distribution, we limit the performance of the method by restricting the model or the titration to a set of pK or pH values well below the distribution range of the sample. To simplify matters, we choose to start and end all ranges with whole numbers, and an uniform 0.2-unit increment is used for all intermediate values.

Table I shows the results of simulations in four groups. In the first group, where the titration and model ranges are greater than the sample range, the fit is good, with root mean square (rms) difference of expected and fitted (rms) values below 1  $\mu\text{equiv/L}$ . This is expected since the whole distribution is covered. Interestingly, the titration does not have to exceed the sample range, even if the effects of a pK sitting at the end point of the titration does influence the profile by a further 1–1.5 pH units. In the second group, the model range is shorter than the others and no spectrum (all zero values) is recovered. In this case the model is too inflexible to fit the available data set. With an unknown sample, an empty spectrum is therefore the indicative of an inadequate model. An intermediate condition is reached in the third group where the titration range is the shortest. The recovered spectrum appears to be a random assortment of peaks, as the model tries to accommodate insufficient information from the titration data. Except for a high rms, this case is not easily discernible from a true sample with a similar randomlike distribution. In the only example of the fourth group, both titration and model ranges are smaller than the sample range. A bad fit is expected, as this is the worst case possible.

The correct resolution of the spectrum depends then upon what pK ranges and data ranges are used. Clearly,

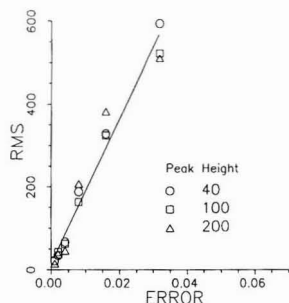


**Figure 1.** Error in spectrum recovery caused by electrode noise. Noise was added to simulated titration of a five-site distribution ( $pK = 3, 5, 7, 9, 11$ ), each of equal concentration. Spectrum analysis and rms calculations were done at the three concentration levels shown. All values of rms and peak height are in  $\mu\text{equiv/L}$ . Errors are in pH units.

the only acceptable experimental conditions are from the first group, and a biased spectrum will result if the sample distribution is not covered by either titration or model ranges. Since the sample is unknown, the analysis should be done with a model range equal to the titration and then reduced to the actual range of the sample so that a finer increment can be used. The size of computer memory and time are the limiting factors, as the constraint matrix in the LP algorithm has a dimension of  $(n + 1)(m + n + 1)$  (including the ANC term). For the maximum of 210 titration points ( $m$ ) and 60  $pK$  values in the model ( $n$ ), the compiled version requires  $\sim 350$  kilobytes and can run on a "386" computer with coprocessor in  $\sim 1$  min. Titrations rarely require this number of points. Fifty points and 25  $pK$  values are more common and run in a part of a minute.

The second source of redundancy comes mostly from electrode precision, as the volume of titrant dispensed in the reactor is usually well controlled. Figure 1 shows the extent of simulated noise on the recovery of a five-site distribution at three concentrations. For an error of up to  $\pm 0.32$  pH unit, the distortion on the spectrum is a linear function with a slope of 4.25 mequiv/pH, independent of concentration. In other terms, the expected rms for a realistic electrode noise of  $\pm 0.005$  is 21.3  $\mu\text{equiv/L}$  over the whole distribution. Thus, a quality data set is required especially when low concentration samples are analyzed.

An attribute of this approach is that no extraneous concentrations are generated if the above rules are followed. Even when electrode error is added to the simulation, the form of the distribution is maintained although  $pK$ s and concentrations may be changed somewhat. To amplify upon this point in a different manner, we have determined the resolution of three adjacent  $pK$ s of markedly different concentrations. For a perfect simulation of three  $pK$ s differing from each other by 0.2 and with concentrations of 1,000, 10, and 100  $\mu\text{equiv/L}$ , respectively, we recover the  $pK$ s exactly and the concentrations exactly for the high concentrations and within a few percent for the low concentrations (Table II).

**(b) Acid Neutralizing Capacity.** The difference in ANC determinations by Gran's method and our method lies in the assumptions made. Gran's method assumes that past a certain value, the response of the pH sensor is due solely to titrant addition. In the LP approach, we remove all weak acids from the ion balance by fitting them to the model; what remains is the sum of all strong ions (unreacted with  $H^+$  ion), which is the ANC. Although the basic concept for ANC is the same for the two methods, different assumptions and procedures lead to different biases. Figure 2 shows that the LP procedure recovers

**Table II. Resolution of Adjacent  $pK$ s Using Linear Programming<sup>a</sup>**

$pK$	input	concn recovered, $\mu\text{equiv/L}$	diff, %
3.6	0	0.12	
3.8	1000	1000	0.0
4.0	10	10.3	3.5
4.2	100	99.9	0.1
6.6	0	0.13	
6.8	1000	999.5	0.0
7.0	10	10.7	7.0
7.2	100	99.5	0.5
7.4	0	0.13	
9.8	1000	1000	0.0
10.0	10	10.3	2.7
10.2	100	100	0.2
10.4	0	0.07	

<sup>a</sup> Recovery of spectra for simulated titration data with three  $pK$ s near 4 (3.8, 4.0, 4.2), 7 (6.8, 7.0, 7.2), and 10 (9.8, 10, 10.2) and concentrations of 100, 10, and 1000  $\mu\text{equiv/L}$  for each cluster. All other  $pK$ s have zero concentrations.

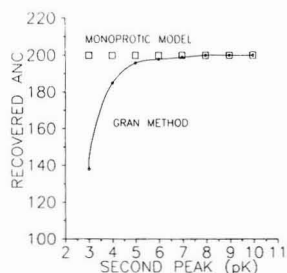


**Figure 2.** Recovery of ANC by the LP procedure compared to Gran's method. The simulated distribution has two sites, one is fixed at  $pK = 10$ , the second peak travels from 10 to 3 at unit interval. Concentration of each site is 100  $\mu\text{M}$ , [ANC] = 200  $\mu\text{equiv/L}$ . The simulated data are error free.

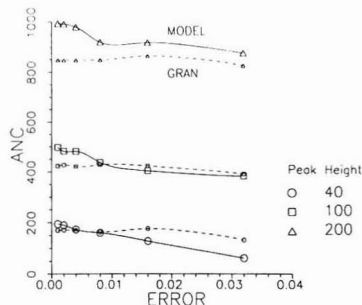


**Figure 3.** Recovery of ANC from simulated noisy titrations compared to Gran's method. Conditions are as in Figure 2. All values of ANC and peak height are in  $\mu\text{equiv/L}$ . Errors are in pH units.

ANC exactly, whereas there is a major bias in Gran's method when a peak is brought closer to the acid end of the titration.

Figure 3 shows, however, that the LP method can give incorrect ANC values when noise is introduced in the data. As the error on the pH term is increased, the ANC estimate decreases to the point where it becomes lower than that obtained by Gran's method. At low concentrations ( $\sim 200$   $\mu\text{equiv/L}$ ), the error where the bias is the same is about  $\pm 0.008$  pH unit. For Gran's analysis, the presence of a  $pK$  site of high concentration in the acid range causes ANC to be underestimated. But the estimate tends to be stable because it is derived from the end of the titration



**Table III. Comparison of Results of Different Simulations for a Six-Site Metal Complexation Model (2)<sup>a</sup>**

analysis	pKs concn					
	1	2	3	4	5	6
model spectra (2)						
pK	15.0	10.8	8.8	6.5	4.0	3.0
-log C <sub>j</sub>	10.0	7.0	6.2	5.2	5.0	5.3
perfect simulation of data <sup>b</sup>						
pK	15.5	10.8	8.8	6.5	4.0	3.0
-log C <sub>j</sub>	10.0	7.1	6.2	5.2	5.0	5.3
random error pM = 0.05 put on data <sup>c</sup>						
pK	15.0	11.0	8.8	6.6	5.5	2.5
-log C <sub>j</sub>	10.1	7.1	6.2	5.3	5.7	3.3
random error pM = 0.1 put on data <sup>d</sup>						
pK	15.5	10.6	8.6	6.6	3.6	
-log C <sub>j</sub>	10.1	43	6.1	5.1	3.9	
pM data truncated to X.XXX <sup>e</sup>						
pK	16.0	11.5	8.7	6.4	4.0	3.5
-log C <sub>j</sub>	10.2	7.1	6.2	5.3	5.2	5.1

<sup>a</sup> Metal titrant-pM data were generated for 70 equal pM intervals from 2 to 16. LP analysis was carried out for an equal pK interval of 0.5. <sup>b</sup> Results obtained for a perfect simulation. <sup>c</sup> Results obtained when a random error of 0.05 pM was added. <sup>d</sup> When a random error of 0.1 pM was added. <sup>e</sup> When pM data were truncated to three significant figures beyond the decimal. <sup>f</sup> Adjacent pKs were averaged by weighting concentrations, and concentrations were obtained by addition of adjacent peaks.

**Table IV. Concentration Recovery of Sodium Carbonate and Citric-Acetic Acid Mixture from Titration Data<sup>a</sup>**

	concn, $\mu$ equiv/L			diff, %
	expected	recovered	after multiprotic correctn	
	Sodium Carbonate			
ANC	997	903		1.71
nC <sub>1</sub>	500	501	504	0.60
C <sub>2</sub>	500	451	451	10.9
	Citric Acid plus Acetic Acid			
ANC	4157	4117		0.97
C <sub>1</sub>	4943	4769	4857	1.76
C <sub>2</sub>	9100	8631	8662	5.05
C <sub>3</sub>	4943	5003	5006	0.04

<sup>a</sup> Ionic strength, 0.04 N; t, 20.3 °C. Comparison of the second and third columns of numbers indicates the error possible when analyzing multiprotic acids and assuming a monoprotic system.

where, due to high H<sup>+</sup>-ion concentration, the buffer capacity is high. Weaknesses in both procedures tend to underestimate ANC. Therefore, to obtain the best estimate for ANC in the case of noisy data, both methods should be used and the more positive value accepted.

(c) **The Six-Site Model of Fish et al.** Similar conclusions can be made for metal-ligand data when analyzed for pKs by using eq 3. Table III shows that the six-site model (with pKs from 3 to 15) of Fish et al. (2) is recovered exactly by use of the LP technique on perfectly simulated data. Even when a random error of pM = 0.1 is added to the data (c), the shape of the distribution is maintained. The effect of error and truncation, in general, is to reproduce the middle portion of the spectrum and introduce error on the extremes. The end effect is not unexpected when one considers that the spectral fit is made over 14 orders of magnitude difference in K. LP analysis of the perfect data with pM data truncated (three figures beyond the decimal analogous to "good" data from a research-grade pH meter) gives results similar to introduction of random error. Thus, we can expect limitations in analysis over 10+ orders of magnitude of K due to the limitation in measurement of the metal concentration, especially for the largest and smallest pKs. By comparison, other models (Scatchard, FITQL, continuous affinity spectrum, continuous stability, and normal distribution) examined by Fish et al. (2) would recover the three main sites at most.

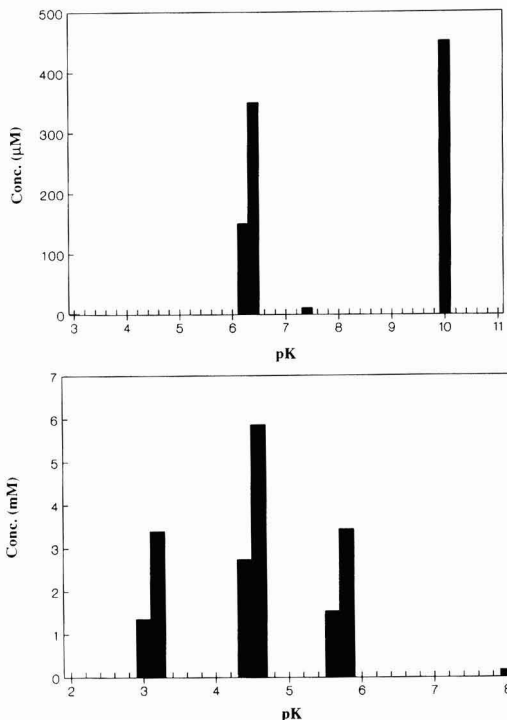


**Figure 4.** Linear programming analysis of (A, top) sodium carbonate and (B, bottom) citric acid plus sodium acetate. Details in Table IV.

(d) **Real Samples.** The titration of real samples shows that the LP method adequately recovers the original signature of simple compounds and is only limited by the precision of the data. Figure 4 shows the LP spectra resolved for a carbonate and a citrate with acetate solutions. Table IV summarizes these analyses and shows the calculated effect of the diprotic terms. Sensitivity analysis shows that differences in expected and calculated results can be due to an error of  $\leq 1\%$  in titrant standardization.

The monoprotic assumption for multiprotic sites gives a negligible error in these cases. The difference between columns 2 and 3 of Table IV shows the diprotic effect. The effect of using a monoprotic model on a multiprotic acid

was estimated as follows. Simms (10) has shown the error between the two occurs as a small shift in  $pK$  with no effect on concentration. In our case, however, the values of  $pK$  are fixed into the model so that some of the error has to be transferred to the concentration. We estimated the correction by running a simulation of the multiprotic citric acid and carbonate free acid ligands and compared it to their monoprotic counterpart, using the same  $pK$  values. The ratio of the first to the second taken at the point where the contribution of the respective  $pK$  is maximum, i.e.,  $pH = pK$ , is the multiprotic correction given in Table IV.

In the case of carbonate, the error with the  $pK = 10$  peak is due to the restricted titration range (up to 9.9). Figure 4 shows that all  $pK$ s are accurately recovered for carbonate and citrate with acetate solutions. Zero concentrations between adjacent peaks are also recovered for the ranges shown. The double peaks displayed occur because the true  $pK$  of the sample falls at an intermediate position between the two adjacent  $pK$  intervals of the model. Either another LP analysis with a finer  $pK$  interval or determination of a concentration-weighted average  $pK$  gives a correct  $pK$  for known and simulated data (e.g., Tables III and IV, Figure 4). For example, adjacent peaks for the acetic acid-citric acid mixture were averaged by concentration weighing to give  $pK$ s of 3.13, 4.53, and 5.73. These results fit literature data (17), interpolated for ionic strength and temperature, within 0.1  $pK$  unit. The second concentration array includes acetic acid and the second dissociation of citric acid. A small extraneous peak at  $pK = 8$  is also resolved in the analysis. The carbonate spectrum shows that the 6.33  $pK$  is recovered precisely whereas the single  $pK = 10$  peak results from the titration terminating at 10.1. A small concentration of 11  $\mu\text{equiv/L}$  at  $pK = 7$  resulted from inaccuracy in sensor response or a contaminant in the solution.

Obtaining the spectrum of a complex substance presents more problems mainly because the site distribution may be altered irreversibly due to pH changes, by changes in sample concentration, and by surface coatings of electrodes (e.g., humic acid) altering the calibration. Several analyses of Aldrich humic acid at various concentrations were carried out to test if the same spectrum could be obtained with an acid-then-base and a base-then-acid titration. Figure 5 shows a representative result. Figure 5c is the "control", which is the LP result obtained on the combination of separate first portions of the acid and base titrations. If the system is reversible, all plots should be the same. This analysis displays three major peaks and a minor one. Figure 5a (acid-then-base) displays two supplementary peaks and an overall reduction in concentrations compared to the combined first titrations (Figure 5c). The sample titrated with base first (Figure 5b) does not differ as much when compared to Figure 5c; concentrations are closer to the control except for  $pK$  7.6, which is greater. Overall, only the major peaks at  $pK$  4.2, 7.6, and 9.7 appear to be stable, although some loss in concentration occurs with an acid titration first. The peaks at  $pK$  4.2 and 9.6 correspond to carboxylic and phenolic sites (18). There is also a middle group of peaks, which are not often found in other analyses. These peaks are resolved because of equal pH titration intervals. The position of some peaks ( $pK$  9.6) is also shifted from the control by 0.2 unit. Although this shift may be real, it is too close to the precision of the titration to be significant. Other causes of shift can be traced to the standardization of the titrant concentration and the change in  $pK_w$  (at high pH) due to reactor temperature.

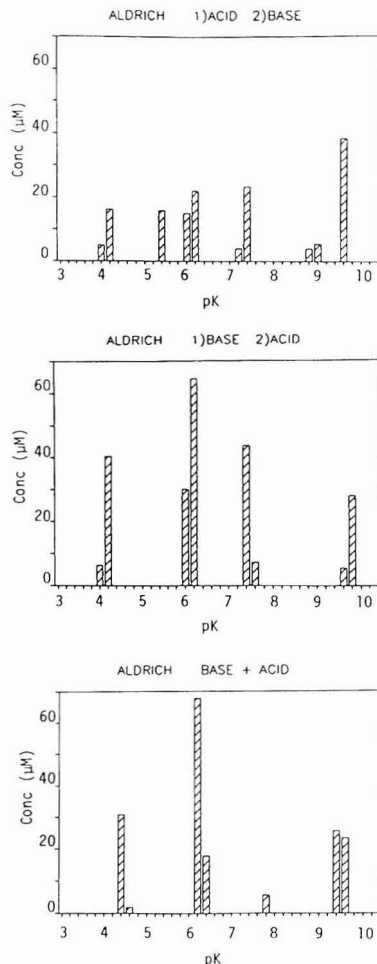


**Figure 5.** Effect of acid/base titrant addition order on the  $pK$  distribution found for Aldrich humic acid. Order of addition is shown by numbers (1, first titrant; 2, back-titration) [(a) = 1 then 2; (b) = 2 then 1]. Base + acid (c) are results obtained by combining the first portions of the above titrations. Ionic strength, 0.04 N;  $t$ , 22.0 °C; humic acid concentration, 30 mg/L.

Raw data for real samples are available as supplementary material.

### Conclusion

The advantage of fitting a monoprotic model by use of LP is that multiple sites and sites of low concentration are resolved. These attributes are particularly useful for heterogeneous systems such as humic substances and particle surfaces. The optimal solution will occur if, and only if, the range of both titration and model is greater or equal to the  $pK$  distribution of the sample. The analyses show that multiple peaks are recovered from titration data if the redundancy is kept low. Otherwise, as noise increases, the number of peaks needed to fit the profile decrease until the noise is so great that the best spectrum is achieved by a single constant (ANC) with no peaks at all. Thus, the limiting number of  $pK$ s that can be resolved by LP analysis of titration data for a multiple-site substance depends only on the precision of the experiment, requiring only equal intervals of pH or pM data. However elaborate the method for reducing titration profiles, the

resulting spectrum cannot be made better than the quality of the original data.

The same general conclusions are relevant for the LP determination of pK spectra for a metal-ligand model. Thus, the range of model and data must be equal to or exceed the spectral range, and the accuracy of the results is limited mostly by the quality of data.

Inclusion of the ANC term in a discrete pK model provides for an unbiased estimate of its true value. The presence of low ANC and errors in the electrode readings can decrease the ANC estimate. At high noise levels (for pH > 0.01) and low ANC (<200 µequiv/L), the resulting LP estimate can be worse than found by Gran's method.

*Supplementary Material Available*

Titration data for the spectra presented (6 pages) will appear following these pages in the microfilm edition of this volume of the journal. Photocopies of the supplementary material from this paper or microfiche (105 × 148 mm, 24× reduction, negatives) may be obtained from Microforms Office, American Chemical Society, 1155 16th St., N.W., Washington, DC 20036. Full bibliographic citation (journal, title of article, authors' names, inclusive pagination, volume number, and issue number) and prepayment, check or money order for \$14.50 for photocopy (\$16.50 foreign) or \$10.00 for microfiche (\$11.00 foreign), are required.

*Literature Cited*

(1) Dzombak, D. A.; Fish, W.; Morel, F. M. M. *Environ. Sci. Technol.* **1986**, *20*, 669.  
 (2) Fish, W.; Dzombak, D. A.; Morel, F. M. M. *Environ. Sci. Technol.* **1986**, *20*, 676.  
 (3) Sunda, W. G.; Hanson, P. J. In *Chemical Modeling of Aqueous Systems: Speciation, Sorption, Solubility, Kinetics*; Jenne, E., Ed.; ACS Symposium Series 93; American Chemical Society: Washington, DC, 1979; pp 147-180.

(4) Shuman, M. S.; Collins, B. J.; Fitzgerald, P. J.; Olson, D. L. In *Aquatic and Terrestrial Humic Materials*; Christman, R. F.; Gjessing, E. T., Eds.; Ann Arbor Science: Ann Arbor, MI, 1983; pp 349-370.  
 (5) Westall, J. C. *FITEQL, A Program for the Determination of Chemical Equilibrium Constants from Experimental Data. Version 2.0*; Chemistry Dept., Oregon State University: Corvallis, OR, 1984.  
 (6) Stumm, W.; Morgan, J. J. *Aquatic Chemistry*, 2nd ed.; Wiley-Interscience: New York, 1980; p 163.  
 (7) Gran, G. *Analyst* **1952**, *77*, 661.  
 (8) McQuaker, N. R.; Sandberg, D. K. *Environ. Sci. Technol.* **1988**, *22*, 590.  
 (9) Ricci, J. E. *Hydrogen Ion Concentration*; Princeton University Press: Princeton, NJ, 1952.  
 (10) Simms, H. S. *J. Am. Chem. Soc.* **1926**, *48*, 1239.  
 (11) Chvátal, V. In *Linear Programming*; Klee, V., Ed.; W.H. Freeman and Co.: New York, 1983.  
 (12) Tobler, H. J.; Engel, G. *Naunyn-Schmiedeberg's Arch. Pharmacol.* **1983**, *322*, 183.  
 (13) Best, M. J.; Ritter, K. *Linear Programming. Active Set and Computer Programs*; Prentice Hall Inc.: Englewood Cliffs, NJ, 1985.  
 (14) Kortelainen, P.; Mannio, J.; Mäkinen, I. *Aqua Fenn.* **1986**, *16*, 221.  
 (15) Di Toro, D. M.; Padula, J. E.; Watkins, J. P. *Proc. Am. Soc. Civil Eng., Environ. Eng. Div.* **1981**, *107*, 251.  
 (16) Claerbout, J. F.; Muir, F. *Geophysics* **1973**, *38*, 826.  
 (17) Martell, A. E.; Smith, R. M. *Critical Stability Constants*; Plenum Press: New York, 1977; Vol. 3, pp 3, 161.  
 (18) Perdue, E. M.; Reuter, J. H.; Parrish, R. S. *Geochim. Cosmochim. Acta* **1984**, *48*, 1257.

Received for review October 17, 1988. Revised manuscript received June 26, 1989. Accepted August 30, 1989. This work was supported in part by operating and strategic grants from the Natural Sciences and Engineering Research Council of Canada.

## Enzymatic Method for the Determination of Formaldehyde

Mat H. Ho\* and Rex A. Richards

Department of Chemistry, University of Alabama at Birmingham, Birmingham, Alabama 35294

■ This paper describes a sensitive method for the determination of formaldehyde using two sequential reactions catalyzed by two enzymes, formaldehyde dehydrogenase and diaphorase. The principle of this method is based on the quantitative oxidation of formaldehyde, in the presence of formaldehyde dehydrogenase and oxidized nicotinamide adenine dinucleotide (NAD<sup>+</sup>), to produce formic acid and the reduced dinucleotide (NADH). The NADH produced then reacts with oxidized 2-(4-iodophenyl)-3-(4-nitrophenyl)-5-phenyltetrazolium (INT), in the presence of diaphorase, to produce formazan, a highly chromogenic compound. The formazan formed is measured spectrophotometrically at 500 nm and will be directly proportional to the amount of formaldehyde in the assay solution. As low as 0.05 µg/mL (1.6 × 10<sup>-6</sup> M) formaldehyde concentration can be determined, and the linear range was up to 3 µg/mL (1.0 × 10<sup>-4</sup> M). This enzymatic method is simple, sensitive, selective and can be used for the determination of formaldehyde in air, particularly in indoor environments.

*Introduction*

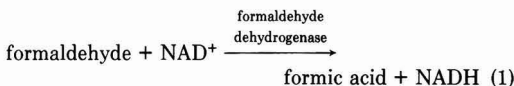
Formaldehyde is recognized as an important air pollutant in a variety of industrial and domestic environments.

It is used extensively in a myriad of consumer products, building materials (i.e., particle board and plywood), and in urea-formaldehyde foam insulation (1). Conclusive evidence has been compiled indicating that these materials can release formaldehyde into the air of residences, mobile homes, and office buildings, resulting in exposure of inhabitants and workers (1, 2).

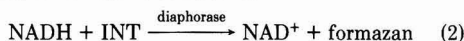
Along with the widespread use of formaldehyde, reports of its adverse effects on health and its potential carcinogenicity have created great concern, prompting the development of methods that control and monitor exposure to formaldehyde, both in industrial and nonindustrial environments (3, 4). Sensitive and selective formaldehyde monitoring, from near-ambient levels up to approximately 10 ppm (µg/mL), under a variety of environmental conditions, is a recognized need. Existing methods for formaldehyde determination include the use of chromotropic acid (5, 6), pararosaniline (7, 8), fluorescence (9), gas chromatography (10), high-performance liquid chromatography (11-18), ion chromatography (19, 20), and polarography (21).

During the past decade, enzymes have become increasingly useful as analytical reagents due to their specificity. However, most of their applications are in clinical

and bioanalytical chemistry (22). Recently, we showed that the enzyme formaldehyde dehydrogenase can be used as an analytical reagent for the determination of formaldehyde (23). This formaldehyde dehydrogenase is a non-glutathione-dependent enzyme; however, it requires nicotinamide adenine dinucleotide as a cofactor. One of the outstanding properties of this biological catalyst is its specificity toward formaldehyde. In this paper, we describe a sensitive method for formaldehyde determination using two enzymes, formaldehyde dehydrogenase and diaphorase. The principle of this method is based on the quantitative oxidation of formaldehyde in the presence of formaldehyde dehydrogenase and oxidized nicotinamide adenine dinucleotide (NAD<sup>+</sup>) to produce formic acid and the reduced dinucleotide (NADH).



The NADH produced then reacts with oxidized 2-(4-iodophenyl)-3-(4-nitrophenyl)-5-phenyltetrazolium chloride (INT), in the presence of diaphorase, to produce formazan, a highly chromogenic compound.



The absorbance of formazan is measured at 500 nm and is directly proportional to the concentration of formaldehyde in the sample.

#### Experimental Section

**Reagents.** Oxidized nicotinamide adenine dinucleotide ( $\beta$ -NAD<sup>+</sup>), formaldehyde dehydrogenase (EC 1.2.1.46, from *Pseudomonas putida*), and diaphorase (EC 1.6.4.3, from *Clostridium kluyveri*) were obtained from Sigma Chemical Co., St. Louis, MO.  $\beta$ -NAD<sup>+</sup> solution, 5 mg/mL, was prepared with deionized water. Formaldehyde dehydrogenase solution, 10 units/mL, and diaphorase solution, 72 units/mL, were prepared in 0.1 M phosphate buffer (pH 7.5).  $\beta$ -NAD<sup>+</sup>, formaldehyde dehydrogenase, and diaphorase solutions were prepared fresh daily. INT (Aldrich Chemical Co., Milwaukee, WI) solution, 2 mg/mL, was prepared with deionized water.

Formaldehyde stock solution, approximately 5 mg/mL, was prepared from formalin solution with deionized water; this solution was standardized by using the sulfite method (6, 24) to obtain the exact concentration. Formalin solution (37%) was ACS reagent grade and obtained from Fisher Scientific Co., Pittsburgh, PA. The formaldehyde stock solution remained stable for 3 months. Formaldehyde standard solutions were prepared daily from the stock solution by appropriate dilutions with deionized water.

The deionized water used for solution preparations was obtained from the Filterite Deionized Water System (Filterite Corp., Timonium, MD). Other chemicals for formaldehyde standardization, buffer preparations, and interferent studies were analytical reagents.

**Procedure.** A Beckman Model 26 spectrophotometer (Beckman Instruments, Inc., Fullerton, CA) was used in this study. Temperature of the sample and reference cuvettes was controlled with a Haake-Buchler thermostated water bath circulator (Fisher, Springfield, NJ). Absorbance versus time was recorded with a potentiometric recorder.

Glycine buffer (1 mL of 0.1 M, pH 9.5) was placed into a sample cuvette and then 125  $\mu$ L of formaldehyde dehydrogenase, 50  $\mu$ L of NAD<sup>+</sup>, 50  $\mu$ L of diaphorase, and 150  $\mu$ L of INT were added. The mixture was mixed thoroughly for 5 s before placing the cuvette into the cell compartment

thermostated at 35 °C. A stable base line was obtained and absorbance was then adjusted to zero against a buffer solution in the reference cuvette. To start the reaction, 500  $\mu$ L of formaldehyde standard solution or sample was added to the sample cuvette and the absorbance was measured at 500 nm. The change in absorbance versus time was recorded on the recorder and the steady-state absorbance and initial rate were obtained. The absorbance was stable up to 10 min after the steady state has been achieved. Initial rates were measured manually by determining the slope of the absorbance versus time curves within the initially linear region. This procedure was used for the optimization of NAD<sup>+</sup>, formaldehyde dehydrogenase, diaphorase, INT, and pH and for the study of linear range and limit of detection, as well as calibration. In the optimization studies, various concentrations of formaldehyde dehydrogenase, NAD<sup>+</sup>, diaphorase, and INT were obtained by varying the volumes of these reagents. Phosphate buffers (pH 7-8.5) and glycine buffer (pH 8.5-9.5) were used for the study of the effects of pH.

Another procedure was also employed for calibration. In this procedure, the reaction was stopped at a specific time by placing the mixture in boiling water to inactivate the enzymes. The same amounts of buffer, formaldehyde dehydrogenase, NAD<sup>+</sup>, diaphorase, and INT were used as described above except that two small test tubes were employed for reference and sample, and 500  $\mu$ L of buffer was added to the reference tube instead of formaldehyde. The mixtures were incubated at 35 °C for 10 min in order to achieve the steady state and then immersed in boiling water for another 3 min. After being cooled to room temperature, these solutions were transferred to the reference and sample cuvettes, respectively, and the absorbance was measured.

#### Results and Discussions

Two sequentially enzymatic reactions are employed in this method. The NADH formed, which is related to formaldehyde concentration, can be measured at 340 nm if only reaction 1 is used. In coupling with reaction 2, the formazan formed can be measured at 500 nm. Since the molar absorptivity of formazan is higher than that of NADH, the second approach is more sensitive. The oxidation of NADH, and thereby re-forming more NAD<sup>+</sup>, also has the net effect of improving the steady state and reaction rate of this method by maintaining the NAD<sup>+</sup> concentration relatively constant and suppressing the NADH concentration. These effects are shown in Figure 1. At their respective optimal NAD<sup>+</sup> concentrations, the steady-state absorbance of 4.2  $\mu$ g/mL formaldehyde with both reactions 1 and 2 is still higher than that of 6.8  $\mu$ g/mL of formaldehyde when only reaction 1 is used. Figure 1 also shows the effect of NAD<sup>+</sup> concentration on the sensitivity of the method. If only reaction 1 is employed, both the steady-state absorbance and reaction rate increased with the increase in NAD<sup>+</sup> concentrations. However, the steady state and initial rate decreased as NAD<sup>+</sup> increased above 0.3 mg/mL if both reactions 1 and 2 are employed. This may be due to the fact that if a large amount of NAD<sup>+</sup> were used, the equilibrium of eq 2 would be shifted to the left, thereby decreasing formazan concentration. NAD<sup>+</sup> concentration also affects the time required to reach steady state. This time increases as the concentration of NAD<sup>+</sup> increases above 0.4 mg/mL. These results indicate that the optimal concentration of NAD<sup>+</sup> is in the range from 0.13 to 0.26 mg/mL. We decided to use 0.13 mg/mL NAD<sup>+</sup> for this study.

The effects of formaldehyde dehydrogenase concentration on both the steady state and reaction rate were also

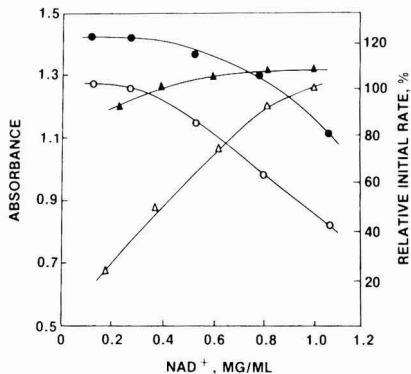


**Figure 1.** Effect of  $\text{NAD}^+$  concentration. Conditions: formaldehyde dehydrogenase, 0.70 unit/mL; diaphorase, 1.47 units/mL; INT, 0.053 mg/mL; buffer, 0.053 M phosphate pH 7.5; temperature, 25 °C. ●, steady-state absorbance with two reactions and 4.2  $\mu\text{g/mL}$  formaldehyde; ○, initial rate with two reactions and 4.2  $\mu\text{g/mL}$  formaldehyde; ▲, steady-state absorbance with only reaction 1 and 6.8  $\mu\text{g/mL}$  formaldehyde; Δ, initial rate with only reaction 1 and 1.6  $\mu\text{g/mL}$  formaldehyde.

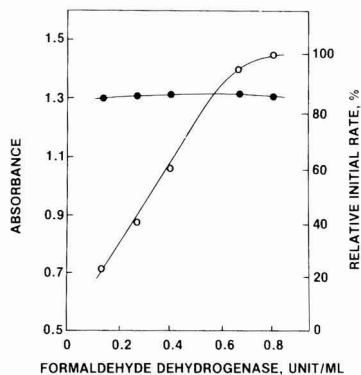


**Figure 2.** Effect of formaldehyde dehydrogenase concentration (●, steady-state absorbance; ○, initial rate). Conditions:  $\text{NAD}^+$ , 0.13 mg/mL; diaphorase, 1.47 units/mL; INT, 0.053 mg/mL; formaldehyde, 4.2  $\mu\text{g/mL}$ ; buffer, 0.053 M phosphate, pH 7.5; temperature, 25 °C.

investigated, and the results are shown in Figure 2. The result indicated that varying the concentration of formaldehyde dehydrogenase from 0.13 to 0.80 unit/mL did not affect the steady-state absorbance; however, the reaction time required to reach the steady state decreased sharply with increase in the enzyme concentration. The time decreased from 60 to 18 min as the concentrations of formaldehyde dehydrogenase increased from 0.13 to 0.40 unit/mL. Further increase in the enzyme concentration did not affect the time significantly. The initial rate of the reaction was also shown to be a function of formaldehyde dehydrogenase concentration. This is to be expected since an increase in enzyme concentration will increase the rate of the reaction. However, at concentrations higher than 0.70 unit/mL the initial rate is no longer proportional to the total enzyme concentration and further increase in formaldehyde dehydrogenase did not affect the rate of the reaction significantly. From these results, the final formaldehyde dehydrogenase concentration was then chosen to be 0.70 unit/mL.

The effects of diaphorase concentration on steady state and initial rate are shown in Figure 3. Increasing the concentration of diaphorase from 1 to 1.80 units/mL did not affect the steady-state absorbance significantly.

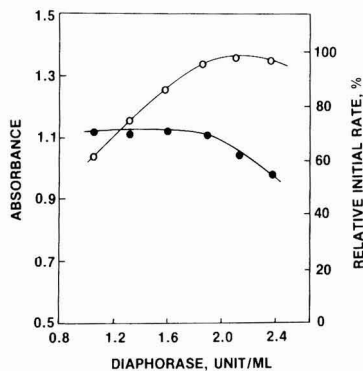


**Figure 3.** Effect of diaphorase concentration (●, steady-state absorbance; ○, initial rate). Conditions: formaldehyde dehydrogenase, 0.70 unit/mL;  $\text{NAD}^+$ , 0.13 mg/mL; INT, 0.053 mg/mL; formaldehyde, 4.0  $\mu\text{g/mL}$ ; buffer, 0.053 M phosphate, pH 7.5; temperature, 25 °C.

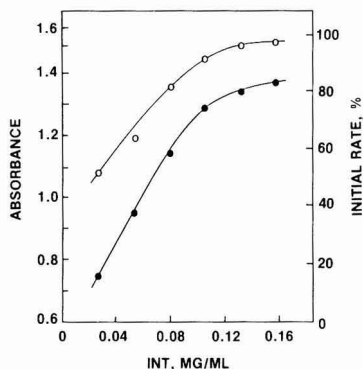


**Figure 4.** Effect of INT concentration (●, steady-state absorbance; ○, initial rate). Conditions: formaldehyde dehydrogenase, 0.70 unit/mL;  $\text{NAD}^+$ , 0.13 mg/mL; diaphorase, 1.80 units/mL; formaldehyde, 3.60  $\mu\text{g/mL}$ ; buffer, 0.053 M phosphate, pH 7.5; temperature, 25 °C.

However, the absorbance decreased with further increase in diaphorase concentrations above 1.80 units/mL. This may be due to the fact that if a large amount of enzyme is used, coenzyme  $\text{NAD}^+$  may be bound to the enzyme and not be available for reaction. Initial rate and reaction time were also functions of diaphorase concentration. As the concentration of diaphorase increased up to 1.80 units/mL, the initial rate increased and time required to reach steady state decreased sharply. At 1.80 units/mL of diaphorase concentration it required ~6 min to reach the steady state while 16 min is required at 1 unit/mL diaphorase. The initial rate started to level off at 2.0 units/mL and then decreased slightly at higher concentrations of diaphorase. Thus, the optimal concentration of diaphorase was chosen to be 1.80 units/mL.

The concentration of INT required for each determination was investigated. The effects of INT concentration on steady state and initial rate are shown in Figure 4. These results indicated that 0.16 mg/mL is an optimal concentration for INT.

Using the optimized concentrations of formaldehyde dehydrogenase,  $\text{NAD}^+$ , diaphorase, and INT thus determined, we investigated the effect of pH since all enzyme-catalyzed reactions have an optimal pH range. Two types of buffer were used, 0.053 M phosphate (for pH from 7 to 8.5) and 0.053 M glycine (for pH from 8.5 to 9.5). The results are shown in Figure 5. It should be pointed out that there is a difference in pH optima between the oxi-

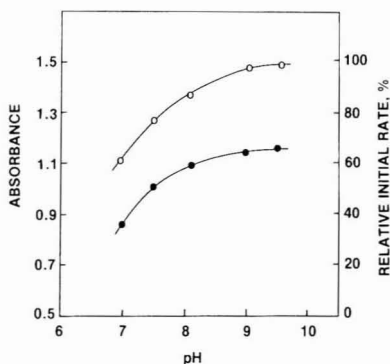


**Figure 5.** Effect of pH (●, steady-state absorbance; O, initial rate). Conditions: formaldehyde dehydrogenase, 0.70 unit/mL; diaphorase, 1.80 units/mL;  $\text{NAD}^+$ , 0.13 mg/mL; INT, 0.16 mg/mL; formaldehyde, 2.10  $\mu\text{g/mL}$ ; buffer, phosphate, pH 7–8.5, and glycine, pH 8.5–9.5; temperature, 25 °C.

dation of formaldehyde catalyzed by formaldehyde dehydrogenase and the coupling of two sequential reactions using both formaldehyde dehydrogenase and diaphorase. It has been shown that formaldehyde dehydrogenase was most active at pH 8–9 for formaldehyde (23, 25). However, the optimal pH for reaction 1 is not necessarily the optimum for reaction 2. The rate of formazan formation was found to be faster as the pH increased from 7 to 9.5. Absorbance at steady state also increased when pH was varied from 7 to 9. The optimal pH was chosen to be 9.5.

The calibration curve was obtained with the optimized concentration of formaldehyde dehydrogenase,  $\text{NAD}^+$ , diaphorase, and INT, as well as the pH of buffer. The calibration curve of this method fits the equation  $Y = 0.530X + 0.035$  where  $Y$  is the absorbance at steady state and  $X$  is formaldehyde concentration ( $\mu\text{g/mL}$ ). The linear range was from 0.05 to 3  $\mu\text{g/mL}$  ( $1.6 \times 10^{-6}$ – $1.0 \times 10^{-4}$  M) of formaldehyde. If the absorbance of NADH is measured directly at 340 nm without the use of the indicator reaction (reaction 2), the calibration line fits the equation  $Y = 0.216X + 0.002$  and the linear range was from 0.3 to 8  $\mu\text{g/mL}$  ( $1.0 \times 10^{-5}$ – $2.7 \times 10^{-4}$  M). The coupling of formaldehyde dehydrogenase with reaction 2 lowers the detection limit by a factor of almost 10 and provides more than twice as sensitive a method as compared to the direct measurement of NADH. The high sensitivity and lower detection limit of this enzymatic method will have potential applications in the determination of formaldehyde in air, particularly in indoor environments, since the sampling time can be reduced. The kinetic method can also be used for calibration by plotting the initial rate versus formaldehyde concentration; however, we found that this approach gave poor reproducibility.

With the steady-state method, the relative standard deviations were 2.4% and 3.2% with five repetitive measurements at concentrations of 3 and 0.5  $\mu\text{g/mL}$ , respec-

tively. The reproducibility of the calibration curve was also investigated and the slope of  $0.530 \pm 0.018$ , at the 95% confidence level, was obtained with four calibration plots.

**Registry No.** INT, 146-68-9;  $\beta\text{-NAD}^+$ , 53-84-9; formic acid, 64-18-6; formazan, 504-65-4; formaldehyde, 50-00-0; formaldehyde dehydrogenase, 9028-84-6; diaphorase, 9001-18-7.

#### Literature Cited

- (1) Meyer, B.; Andrews, B. A. K.; Reinhardt, R. M. *Formaldehyde Release from Wood Products*; ACS Symposium Series 316; American Chemical Society: Washington, DC, 1986.
- (2) U.S. Consumer Product Safety Commission *Formaldehyde in Indoor Air: Sources and Toxicity*; Government Printing Office: Washington, DC, 1981.
- (3) WHO International Agency for Research on Cancer *IARC Monographs on the Evaluation of the Carcinogenic Risk of Chemicals to Humans*, World Health Organization: Geneva, Switzerland, 1982; Vol. 29, pp 345–390.
- (4) Turoski, V., Ed. *Formaldehyde: Analytical Chemistry and Toxicology*, Advances in Chemistry Series 210; American Chemical Society: Washington, DC, 1985.
- (5) Altshuler, A. P.; Leng, L. J.; Wartburg, A. F. *Air Water Pollut.* **1962**, 6, 381.
- (6) Katz, M., Ed. *Methods of Air Sampling and Analysis*, 2nd ed.; American Public Health Association: Washington, DC, 1977; pp 303–307.
- (7) Lyles, G. R.; Dowling, F. B.; Blanchard, V. J. *J. Air Pollut. Control Assoc.* **1965**, 15, 106.
- (8) Miksch, R. R.; Anthon, D. W.; Fanning, L. Z.; Hollowell, C. D.; Revzan, K.; Glanville, J. *Anal. Chem.* **1981**, 53, 2118.
- (9) Möhlmann, G. R. *Appl. Spectrosc.* **1985**, 39, 98.
- (10) Dumas, T. *J. Chromatogr.* **1982**, 247, 289.
- (11) Van Langenhove, H. R.; Van Acker, M.; Schamp, N. M. *Analyst* **1983**, 108, 329.
- (12) Grosjean, D. *Environ. Sci. Technol.* **1982**, 16, 254.
- (13) Tanner, R. L.; Meng, Z. *Environ. Sci. Technol.* **1984**, 18, 723.
- (14) Lipari, F.; Swarin, S. *J. Environ. Sci. Technol.* **1985**, 19, 70.
- (15) Mopper, K.; Stahovec, W. L. *J. Chromatogr.* **1983**, 256, 243.
- (16) Chiavari, G.; Facchini, M. C. *J. Chromatogr.* **1985**, 333, 262.
- (17) Mann, B.; Grayeski, M. L. *J. Chromatogr.* **1987**, 386, 149.
- (18) Noda, H.; Minemoto, M.; Noda, A.; Ushio, T. *Chem. Pharm. Bull.* **1986**, 34, 3499.
- (19) Kim, W. S.; Geraci, C. L.; Kupel, R. E. *Am. Ind. Hyg. Assoc. J.* **1980**, 41, 334.
- (20) Lorrain, J. M.; Fortune, C. R.; Dellinger, B. *Anal. Chem.* **1981**, 53, 1302.
- (21) Septon, J. C.; Ku, J. C. *Am. Ind. Hyg. Assoc. J.* **1982**, 43, 845.
- (22) Guibault, G. G. *Analytical Uses of Immobilized Enzymes*; Marcel Dekker: New York, 1984.
- (23) Ho, M. H.; Samanifar, M. *Anal. Chim. Acta* **1988**, 215, 249.
- (24) Walker, J. K. *Formaldehyde*; Reinhold: New York, 1975; pp 486–487.
- (25) Ogushi, S.; Ando, M.; Tsuru, D. *Agric. Biol. Chem.* **1984**, 48, 597.

Received for review September 12, 1989. Accepted September 29, 1989.

# Effect of Some Petroleum Sulfonate Surfactants on the Apparent Water Solubility of Organic Compounds

Daniel E. Kile and Cary T. Chiou\*

U.S. Geological Survey, Box 25046, MS 408, Denver Federal Center, Denver, Colorado 80225

Robin S. Helburn

Department of Chemistry and Geochemistry, Colorado School of Mines, Golden, Colorado 80401

Water solubility enhancements of 1,1-bis(*p*-chlorophenyl)-2,2,2-trichloroethane (DDT) and 1,2,3-trichlorobenzene (TCB) by some commercial petroleum sulfonates (Petronate L, Petronate HL, and Pyronate 40) were studied at room temperature. Unlike conventional surfactants, the petroleum sulfonate surfactants are mixtures of sulfonated hydrocarbons and free mineral oils, which form stable emulsions in water and thus behave much like a bulk organic phase in concentrating organic solutes. The extent of solubility enhancement is linearly proportional to the concentration of the petroleum sulfonate-oil (PSO) emulsion, in contrast with the effect of a conventional surfactant in which a sharp inflection occurs in the vicinity of the critical micelle concentration (CMC). The enhancement effect of the PSO surfactant is 1.5-3 orders of magnitude greater than that of ordinary surfactant monomers below the CMC. The partition coefficient of the solute between the emulsified PSO phase and water ( $K_{em}$ ) is closely related to the nonpolar content of the PSO surfactant; the normalized  $K_{em}$  values are about the same order of magnitude as the solvent (octanol)-water partition coefficients of the solutes. The data suggest the potential impact of an emulsified phase on the transport and fate of organic contaminants in situations where spilled or waste oils may be emulsified by surfactants.

## Introduction

In earlier studies we investigated the cause of the water-solubility enhancement of sparingly soluble organic compounds by dissolved organic matter (DOM) such as natural humic substances and some surfactants (1-3); the resulting data provide a basis for assessing the impact of DOM on the mobility and behavior of organic solutes. The observed enhancement effect was accounted for by a partitionlike interaction between the DOM and solute, in which the degree of enhancement is closely related to the molecular size and composition of the DOM and to the intrinsic water solubility of the solute. In the case of humic and fulvic acids as DOM, the extent of solubility enhancement of a solute is a linear function of the DOM concentration. By contrast, the enhancement caused by dissolved surfactants exhibits a distinct inflection in the vicinity of the critical micelle concentration (CMC) of the surfactant. This discontinuity is attributed to aggregate (i.e., micelle) formation of the surfactant above the CMC, which results in a marked increase in the solubilization power of the surfactant because the micelle, in effect, provides an organic environment for the much smaller solute molecules (3-5).

The strong effect of surfactant aggregation on solubility enhancement led to the present investigation of commercial "petroleum sulfonate surfactants", which differ from relatively homogeneous conventional surfactants by being mixtures of sulfonated alkyl-aryl petroleum products and free mineral oils. These materials are used as emulsifying and dispersing agents in various applications that may lead to their potential introduction into the envi-

**Table I. Composition and Properties of Commercial Petronate and Pyronate Surfactants (Data Provided by Witco Chemical Corp.)**

composition/property	Petronate L	Petronate HL	Pyronate 40
% petroleum sulfonate	62	62	41
fraction as hydrocarbon	46.9	48.0	28.6
fraction as -SO <sub>3</sub> Na	15.1	14.0	12.4
% free mineral oil	33.0	32.5	12.0
% inorganic salts	0.5	0.5	8.5
% water	4.5	4.5	38.5
MW of petroleum sulfonate	415-430	440-470	330-350
% hydrocarbon in water-free sample <sup>a</sup>	83.7	84.3	66.0

<sup>a</sup>Total of hydrocarbon in petroleum sulfonate and free mineral oil; calculated from data provided by Witco Chemical Corp.

ronment, such as in oil-well drilling muds, tertiary oil recovery, and ore flotation, and as detergent additives in automotive lubrication oils. They form stable emulsions in water as a result of oils being emulsified by the sulfonated hydrocarbons. Although they effectively reduce the surface tension of water, plots of the surface tension as a function of the logarithm of surfactant concentration do not display any distinct inflection, contrary to the case for conventional micelle-forming surfactants (4-8). In this sense, the petroleum sulfonate surfactants exist as a separate phase even at very low concentrations. One would therefore expect the emulsion formed by the petroleum sulfonate and mineral oil to be far more effective in enhancing solute solubility at low concentrations than would conventional surfactants as monomers below their CMCs. Furthermore, since the emulsified phase should approximate a bulk organic phase in its solvency, a comparison of partition data between the emulsion system and the micellar phase would provide further insight into the efficiency of the micellar environment for solute solubilization. The present study gives an account of the effect of some emulsified systems of petroleum sulfonates and free mineral oils on the apparent water solubility of organic contaminants, using *p,p'*-DDT and 1,2,3-trichlorobenzene as model solutes. The results provide a conceptual basis for assessing the potential impact of oil emulsions on the behavior of organic contaminants in natural systems.

## Experimental Section

The petroleum sulfonate surfactants (Petronate L, Petronate HL, Pyronate 40) were obtained from Witco Chemical Corp. and used as received. The bulk materials are dark brown, highly viscous liquids. The compositions of these petroleum sulfonates as commercial products are given in Table I. These surfactants are mixtures of petroleum sulfonates and free mineral oils that form stable emulsions in water. They are manufactured by treating selected petroleum stocks with sulfuric acid, a process whereby the aromatic components of the petroleum are

sulfonated, leaving the straight-chain hydrocarbons as free mineral oils. Stock solutions of the Petronate surfactants, at concentrations of 5000 mg/L, show a high degree of emulsion (as measured by light scattering) because of their substantial mineral oil contents; they are light brown and have an opalescent appearance. By comparison, the stock solution of Pyronate 40, at 5000 mg/L, is a distinct dark brown and shows less light scattering than the Petronate solutions. At concentrations less than 500 mg/L, the opalescence of these surfactants is not apparent. For clarity in the following text, the heterogeneous surfactants as mixtures of petroleum sulfonates and mineral oils will here be referred to as PSO surfactants (to be distinguished from petroleum sulfonates as a component of the mixture) and the emulsions formed in water as PSO emulsions. Test solutes, *p,p'*-DDT (DDT) and 1,2,3-trichlorobenzene (TCB), were obtained as reagent-grade chemicals (purity of 99% or greater) from Aldrich Chemical Co. and used without further purification. *n*-Hexane, used for sample extraction and standards preparation, was obtained as a UV-grade solvent from American Burdick and Jackson, and deionized water was obtained from a Sybron/Barnstead Nanopure II water treatment system.

Surface tension was measured by using a Fisher Scientific Model 20 tensiometer that operates on the DuNouy principle (by which the force, in dyn/cm, necessary to pull a platinum-iridium ring free of a surface film is measured); surface tension values at given concentrations of the PSO surfactant were plotted when stable readings were obtained from a series of consecutive measurements.

Procedures for sample equilibration and solubility determination were the same as reported earlier (1-3). A series of concentrations was prepared for each PSO surfactant and placed in 25-mL Corex centrifuge tubes with Teflon cap liners; the test solute (DDT or TCB) was added to each tube in an amount slightly more than required to saturate the solution. Triplicate samples were prepared for each PSO surfactant concentration, equilibrated on a reciprocating shaker for approximately 48 h at  $24 \pm 1^\circ\text{C}$ , and subsequently centrifuged at 5000 rpm (2987*g*) for 1 h to separate the undissolved solute. Solute particles adhering to the glass walls were removed with a cotton swab, and the meniscus was subsequently aspirated to remove any particles suspended on the surface. This centrifugation/cleaning procedure was repeated twice more. An aliquot of supernatant was volumetrically withdrawn and extracted in a volume of *n*-hexane required to bring the solute into a detectable concentration range. A pure water blank was run with each sample set as a check on analytical accuracy and to assure adequate equilibration.

The analysis of test solutes was done by gas chromatography using a cross-linked methyl silicone (0.88- $\mu\text{m}$  film thickness) megabore capillary column (30 m  $\times$  0.53 mm) with a  $^{63}\text{Ni}$  electron-capture detector for DDT, and a cross-linked 5% phenyl methyl silicone (0.88- $\mu\text{m}$  film thickness) megabore capillary column (30 m  $\times$  0.53 mm) with a flame-ionization detector for TCB.

### Results and Discussion

Figure 1 shows a plot of the surface tension as a function of the log concentration of the PSO surfactant for Petronate L, Petronate HL, and Pyronate 40 at room temperature ( $24 \pm 1^\circ\text{C}$ ). No inflection was detected in the plot for all three surfactants with concentrations extended to  $\sim 1000$  mg/L.

Figure 2 shows a plot of the apparent DDT solubility as a function of the PSO concentration at room temperature. A similar plot for the dependence of the TCB solubility on PSO concentration is shown in Figure 3. The

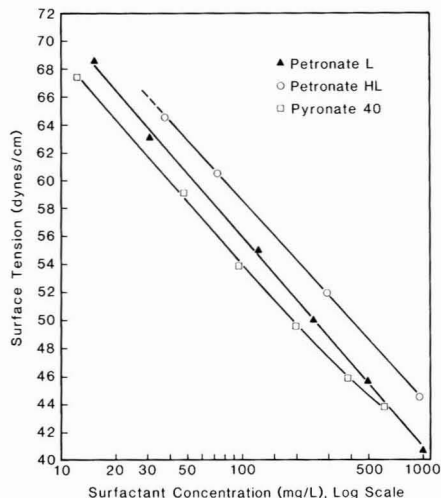


Figure 1. Plot of the surface tension as a function of the log concentrations of Petronate L, Petronate HL, and Pyronate 40.

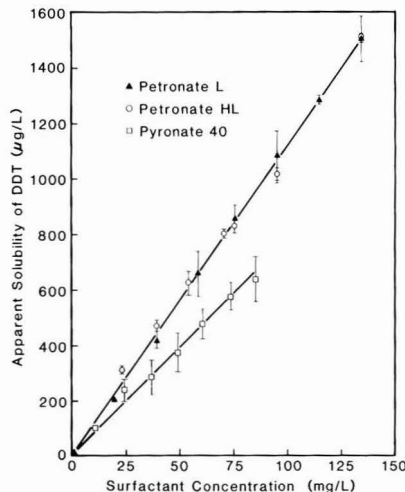
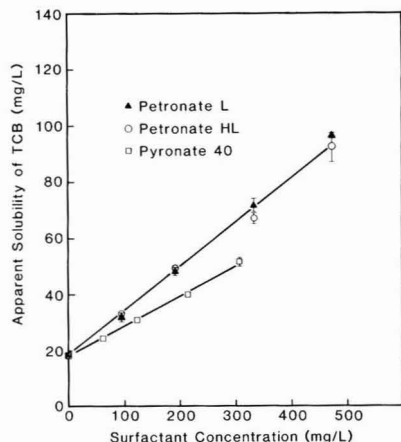


Figure 2. Dependence of the apparent water solubility of *p,p'*-DDT on the concentrations of Petronate L, Petronate HL, and Pyronate 40.

expressed PSO concentration has been corrected for the amount of water in each sample. To improve the accuracy of the data, higher PSO concentrations were used for the study of TCB because of its lower sensitivity to DOM. A linear relation is observed between the apparent solute solubility and PSO concentration, throughout the range of PSO concentrations studied. This relation is consistent with the surface tension vs PSO surfactant concentration curve that shows no inflection, indicating the absence of monomer-micelle characteristics. Based on these results, the emulsified PSO system is much like a separate bulk phase at all concentrations; this is in contrast to the behavior of a conventional (micelle-forming) surfactant that shows a distinct break in the solubility enhancement (or surface tension) plot in the vicinity of the measured CMC (3).

The linear solubility enhancement of the solute by the PSO emulsion can be accounted for by a partition equilibrium of the solute between the emulsified phase and water, in analogy to the enhancement effect by dissolved





**Figure 3.** Dependence of the apparent water solubility of 1,2,3-TCB on the concentrations of Petronate L, Petronate HL, and Pyronate 40.

natural humic substances (1, 2), which can be expressed as

$$S_w^* = S_w (1 + XK_{em}) \quad (1)$$

where  $S_w^*$  is the apparent solute solubility in water,  $S_w$  is the intrinsic water solubility of the solute,  $X$  is the concentration of the PSO emulsion (on a water-free basis), and  $K_{em}$  is the partition coefficient of the solute between the emulsified PSO phase and water. With the quantity of  $X$  expressed in g/mL in the solution and solute concentrations in both water and PSO emulsified phases expressed in the same weight-to-weight basis, the resulting  $K_{em}$  is a dimensionless quantity. The plot of  $S_w^*$  as a function of  $X$  gives a slope of  $S_w K_{em}$  and an intercept of  $S_w$ , from which the  $K_{em}$  value can be calculated for each solute with each emulsified system. DDT and TCB as test solutes give solubility in pure water as 5.5  $\mu\text{g/L}$  and 18 mg/L, respectively, at 25 °C (1, 2). These values are used for determining the extent of solubility enhancement.

Table II shows the calculated  $K_{em}$  values for DDT and TCB on a water-free, total PSO weight basis and on a normalized weight basis of the total hydrocarbon content (i.e., the sum of hydrocarbons in sulfonated petroleum and free mineral oil). Also included in Table II for comparison are the corresponding solute partition coefficients with micelles ( $K_{mc}$ ) and monomers ( $K_{mn}$ ) of some surfactants from an earlier study (3), in which  $K_{mc}$  and  $K_{mn}$  have been similarly defined. The difference in the magnitude of solubility enhancement between DDT and TCB is the same as found with natural humic substances and other surfactants in earlier studies (1-3), the  $K_{em}$  for DDT being more than 2 orders of magnitude greater than that for TCB. This difference is characteristic of equilibrium partitioning of solutes between organic phases and water, in which the equilibrium partition constant is inversely related to the solute solubility in water (9, 10). On a total weight basis, the  $K_{em}$  values of solutes with Petronate L and Petronate HL are greater than values with Pyronate 40, in keeping with the higher hydrocarbon content of the former. However, the difference is minimized by normalization of the  $K_{em}$  values for the total (nonpolar) hydrocarbon content of the PSO surfactant, manifesting that the hydrocarbon moiety is mainly responsible for solute solubilization. Similar results were found in earlier studies with other surfactants above the CMC (3).

In view of the unique composition of the PSO surfactants, it is of interest to compare the  $K_{em}$  values of solutes

**Table II.** Comparison of Solute Partition Coefficients with Commercial Surfactants (on Water-Free Basis)

surfactant	1,2,3-TCB		<i>p,p'</i> -DDT	
	log $K_{em}$	log $K_{em}^*$ <sup>a</sup>	log $K_{em}$	log $K_{em}^*$ <sup>a</sup>
Petronate L	3.94	4.02	6.32	6.40
Petronate HL	3.94	4.01	6.32	6.39
Pyronate 40	3.77	3.95	6.14	6.32
	log $K_{mc}$	log $K_{mc}^*$ <sup>a</sup>	log $K_{mc}$	log $K_{mc}^*$ <sup>a</sup>
CTAB <sup>b,c</sup>	3.80	4.01	5.88	6.09
sodium dodecyl sulfate <sup>c</sup>	3.54	3.77	5.38	5.61
Triton X-100 <sup>c</sup>	3.82	4.34	6.15	6.67
Triton X-114 <sup>c</sup>	3.95	4.40	6.18	6.64
	log $K_{mn}$	log $K_{mn}^*$ <sup>a</sup>	log $K_{mn}$	log $K_{mn}^*$ <sup>a</sup>
CTAB <sup>b,c</sup>	ND <sup>d</sup>	ND	3.54	3.75
sodium dodecyl sulfate <sup>c</sup>	ND	ND	2.68	2.91
Triton X-100 <sup>c</sup>	ND	ND	4.26	4.78
Triton X-114 <sup>c</sup>	ND	ND	4.59	5.05

<sup>a</sup> Partition coefficients normalized to nonpolar hydrocarbon contents. <sup>b</sup> CTAB, cetyltrimethylammonium bromide. <sup>c</sup> Partition coefficients with micelles and monomers from Kile and Chiou (3). <sup>d</sup> ND, not detectable; enhancement is too low to be accurately quantified.

from this study and the corresponding partition coefficients with other surfactants as monomers ( $K_{mn}$ ) and micelles ( $K_{mc}$ ) from the earlier work (3). For DDT, the  $K_{em}$  values on a water-free basis are nearly 3 orders of magnitude greater than  $K_{mn}$  values for sodium dodecyl sulfate (SDS) and cetyltrimethylammonium bromide (CTAB), and  $\sim 1.5$ -2 orders of magnitude greater than  $K_{mn}$  values for Triton X-100 and Triton X-114, although these differences are reduced slightly with  $K_{em}$  and  $K_{mn}$  values normalized to nonpolar hydrocarbon contents of the surfactants. (The  $K_{mn}$  values for the Triton surfactants were obtained from the linear slopes at concentrations far below the nominal CMC, as these octylphenol polyethoxylates are not molecularly homogeneous because of variable ethylene oxide chain lengths in the monomers.) In contrast, the  $K_{em}$  values for DDT and TCB are comparable to the  $K_{mc}$  values for Triton surfactants; they are moderately greater than  $K_{mc}$  values for CTAB and SDS (the lower  $K_{mc}$  values for the SDS relative to the  $K_{em}$  values for PSO emulsions could be due to the greater impact of the sulfate-group hydration on the partition efficiency of the shorter dodecyl chain of SDS; however, this point has to be further investigated). On the other hand, the enhancement effect by the emulsified PSO systems of this study is  $\sim 1.5$ -2 orders of magnitude greater than that by aquatic humic and fulvic acids on a total water-free weight basis (1, 2). Thus, the present emulsified system at low concentrations exhibits enormously greater power to enhance the solute solubility than do monomeric surfactants or aquatic humic substances. The contention that the emulsified system approximates a bulk organic phase is further supported by the similarity of  $K_{em}$  values to the octanol-water partition coefficients ( $K_{ow}$ ) of the solutes. The log  $K_{ow}$  for DDT and TCB are 6.73 and 4.20, respectively, based on corrected solute concentrations in pure water as assumed in eq 1; the measured log  $K_{ow}$  values based on solute concentrations in octanol-saturated water are 6.36 and 4.14, respectively (3).

By the above data, the relative solubility enhancement effects by various types of dissolved and emulsified organic matters can now be placed in perspective. The enhancement effects of aquatic humic substances and conventional surfactant monomers are relatively small and comparable and would have significant impacts on solute solubility

only for extremely water-insoluble compounds such as DDT. The weak effect is much a result of the small size of the surfactant monomer and of the large polar group content of aquatic humic and fulvic acids. By comparison, the enhancement effect by micelles and oil emulsions is greater by ~1.5-3 orders of magnitude because of their relatively large aggregate size, which makes them behave like a bulk organic phase. Accordingly, oil emulsions may be expected to exhibit much more pronounced and broader impacts than other dissolved organic matter at low concentrations on the transport and fate of organic pollutants, including many relatively water-soluble solutes such as TCB.

In summary, the results of this study indicate that the emulsified solution of sulfonated hydrocarbons and free mineral oils can greatly enhance the water solubility of relatively water-insoluble compounds. The enhancement effect by such an oil emulsion approximates that by a relatively nonpolar organic solvent on a unit weight, water-free basis. Calculation of the partition coefficient with the emulsified system is facilitated by knowledge of the nonpolar hydrocarbon content of the emulsion and the solvent (octanol)-water partition coefficient of the solute. From the environmental standpoint, the results from this study illustrate the potential impact of oil emulsions on solute transport and fate in situations where spilled or waste oils may be emulsified by surfactants in natural waters, at landfill sites, and possibly in waste waters generated from oil-well drilling and tertiary oil recovery operations.

## Sedimentary Coprostanol as an Index of Sewage Addition in Santa Monica Basin, Southern California<sup>†</sup>

Mahalakshmi I. Venkatesan\* and Isaac R. Kaplan

Institute of Geophysics and Planetary Physics, University of California, Los Angeles, California 90024-1567

■ Sediment cores from Santa Monica Basin and effluent from two major municipal wastewater dischargers in southern California were analyzed for sterols. Specifically, the fecal sterols, coprostanols (coprostanol and epicoprostanol), were quantitated to determine the degree of sewage addition to the sediment. Although coprostanols are distributed throughout the Santa Monica Basin sediments in association with fine particles, some stations contain elevated levels, either due to their proximity to the outfalls or because of preferential advection of fine-grained sediments into their location where anoxicity aids in better preservation. The progressive seaward decline of coprostanols relative to total sterols from the outfalls represents dilution of sewage by biogenic sterols. The ratio of coprostanols to dinosterol appears to be a better indicator of the degree of sewage addition. A rapid increase in content of coprostanols from about 1935 coincides with the start of offshore wastewater discharge by JWPCP, the Los Angeles County Sanitation Districts on Palos Verdes Shelf. It is estimated that wastewater treatment plants release into southern California Bight 260 metric tons/yr of fecal sterols and  $5 \times 10^4$  metric tons/yr of sewage carbon.

With growing population density in coastal urban centers, the need for disposal of sewage containing fecal wastes

**Registry No.** DDT, 50-29-3; TCB, 87-61-6; water, 7732-18-5; Petronate L, 63952-44-3; Petronate HL, 39412-55-0; Pyronate 40, 63952-48-7.

### Literature Cited

- (1) Chiou, C. T.; Malcolm, R. L.; Brinton, T. I.; Kile, D. E. *Environ. Sci. Technol.* **1986**, *20*, 502.
- (2) Chiou, C. T.; Kile, D. E.; Brinton, T. I.; Malcolm, R. L.; Leenheer, J. A.; MacCarthy, P. *Environ. Sci. Technol.* **1987**, *21*, 1231.
- (3) Kile, D. E.; Chiou, C. T. *Environ. Sci. Technol.* **1989**, *23*, 832.
- (4) McBain, J. W.; Richards, P. H. *Ind. Eng. Chem.* **1946**, *38*, 642.
- (5) Shinoda, K.; Hutchinson, E. *J. Phys. Chem.* **1962**, *66*, 577.
- (6) Mukerjee, P.; Mysel, K. J. *Critical Micelle Concentrations of Aqueous Surfactant Systems*; NSRDS-NBS 36; U.S. Dept. of Commerce: Washington, DC, 1971.
- (7) Schwartz, A. W.; Perry, J. W. *Surface Active Agents—Their Chemistry and Technology*; Robert E. Krieger Publishing Co.; Huntington, NY, 1978.
- (8) Rosen, M. J. *Surfactants and Interfacial Phenomena*; John Wiley and Sons; New York, 1978.
- (9) Chiou, C. T.; Peters, L. J.; Freed, V. H. *Science (Washington, D.C.)* **1979**, *206*, 831.
- (10) Chiou, C. T.; Schmedding, D. W.; Manes, M. *Environ. Sci. Technol.* **1982**, *16*, 4.

Received for review March 27, 1989. Revised manuscript received August 28, 1989. Accepted October 3, 1989. The use of trade or product names in this paper is for identification purposes only and does not constitute endorsement by the U.S. Geological Survey.

increases. Municipal wastes are often discharged into the marine environment and it therefore becomes important to determine the distribution and fate of these contaminants in the aquatic systems. Various reports have demonstrated that coprostanol (5 $\beta$ -cholestan-3 $\beta$ -ol), a fecal sterol of higher animals, can be used as a quantitative indicator of the presence of fecal material (ref 1-3 and references therein). Coprostanol concentration is unaffected by various treatments such as chlorination (1) or aeration of overlying water (4) and it persists in anoxic sediments (2, 5, 6). For the above reasons coprostanol can be a useful tracer of fecal pollution in the ocean or brackish waters where other tracers fail (3).

This paper describes our investigations on the spatial and depth distribution of coprostanol in the sediments of Southern California Bight, with the main focus on the Santa Monica Basin. The Bight includes a network of continental shelf basins close to shore (7), which serve as efficient sediment traps. Because coprostanol can become associated with organic-rich solids (8), it can be easily deposited in nearshore basins and incorporated into (fine-grained) sediments. The onshore/offshore Santa Monica Basin is a target area for intense use by the large industrial and residential population. With the termination of sludge discharge from the Hyperion 7-mile plant as of November 1987, a decrease in the contaminant input levels from the outfalls is expected, and the present work should establish a benchmark for further comparisons in

<sup>†</sup>Institute of Geophysics and Planetary Physics Contribution No. 3199.

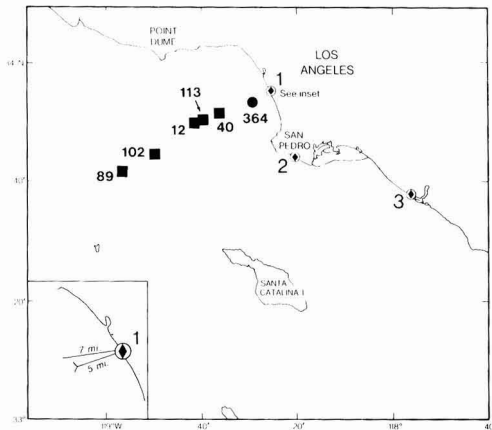


**Figure 1.** Surface sediment and core locations in the Santa Monica Basin. ■, Box core (Cross I, BC); ●, surface sediment (BLM); 1, Hyperion, 2, JWPCP, and 3, Orange County sewage outfalls.

the future. Our goal is therefore to determine the seaward transport of anthropogenic contaminants, from sewage outfalls.

In view of our recent finding (9) that the ratio of coprostanol to its epimer epicoprostanol (5 $\beta$ -cholestan-3 $\alpha$ -ol) is an important factor in differentiating human waste from marine mammalian feces, we also determined the concentration of epicoprostanol. The ratio of coprostanol to epicoprostanol in the Santa Monica Basin sediments is very similar to that from sewage sludge but quite different from those measured in feces from marine animals such as toothed and baleen whales, pinnipeds, and penguin (9). Therefore, any contribution from marine mammalian feces, i.e., from cetaceans (10) and pinnipeds, in the Basin must be trivial. These observations suggest that sewage effluents are the major source of fecal sterols in the Basin (9). The two isomers together will be referred to as coprostanols in the report.

Several cores were examined for coprostanols to identify the principal areas of sewage contamination and to trace the historic record of sewage input in Santa Monica Basin. Sewage sludge as well as effluent filtrates from Los Angeles County and City Sanitation Districts wastewater dischargers (JWPCP and Hyperion, respectively) were also analyzed to relate to the sterol composition of sediments and to estimate the mass emission rates of sewage sterols and carbon into the Bight. The inputs from these two outfalls are the major sources of anthropogenic waste contaminants into the study area (11).

### Methods

**Sample Location and Characteristics.** Glass tube subcores were obtained from Soutar-type box cores, collected during Cross I cruise of October 1985 from Santa Monica Basin (Figure 1) along the northeast to southwest transect, onboard the R.V. New Horizon as part of the DOE CaBS (California Basin Study) program. Cores were stored frozen until the start of analysis. Surface sediment sample from station 364 is from a 1976 BLM cruise and was also stored frozen.

The center of the Basin is ~30 km from land and the maximum water depth is 910 m. The bottom water is anoxic below the sill depth of ~730 m. The dominant particle sizes are in the fine silt range (5–10  $\mu$ m in diameter) and the silt fraction can be as high as 60–70% of the sediment. Surface sediments from station 364 contain

coarse sand, while those from stations BC 40 and 113 contain fine sand (D. Gorsline, personal communication, 1989). Basin slope sediments (stations 40, 113, and 12) are dark green and coarser than the deep basin sediments (stations 102 and 89). Clay percentages generally increase offshore (ref 12 and 13; D. Gorsline, personal communication, 1989). A general decrease in grain size away from shore toward the center of the basins, following the increasing water depth contours, is noted (7).

Surface sediments (stations H5 and H7) at the 5-mile (Hyperion, primary and secondary treatment) and 7-mile (digested sludge and secondary treatment) pipeline outlets, respectively, were obtained from the City of Los Angeles, Bureau of Sanitation. Effluent sludge (H7S) entering the 7-mile pipeline was collected on a day different from H5 and H7 collection. Twenty-four-hour composite treated effluent (JWPCPS, advanced and primary treatment) from the Los Angeles County Sanitation District was also analyzed for comparison with H7S.

**Analytical Procedures.** Frozen sediment cores were partially thawed and discrete horizons (2–4 cm) were subsampled for lipid and total organic carbon (TOC) analysis. Sludge from effluents (4–16 L) were filtered on precombusted glass fiber (Whatman GF/A). Sediment samples and sludge were extracted with methanol and then methylene chloride in a Virtis homogenizer. The methanol, after dilution with nanopure water, was back-extracted into hexane, which was then combined with the methylene chloride phase. Extraction and subsequent fractionation into alcohol/sterol and other different compound classes were carried out according to the methods of Venkatesan et al. (14). Filtrates from effluents and an unfiltered effluent from Hyperion 5-mile were extracted three times with methylene chloride and analyzed for coprostanol as above. Only sterol profiles are discussed in this report. Derivatization into trimethylsilyl (TMS) ethers with BSTFA and quantitation by gas chromatography (GC) and GC/mass spectrometry (GC/MS) identification are the same as previously described (6).

An external sterol standard mixture comprising coprostanol, epicoprostanol, cholesterol, cholestanol, campesterol, and  $\beta$ -sitosterol was used in GC quantitation and GC/MS identification. Recoveries of these sterols ranged from 80 to 92% in the current procedure. Selected TMS ethers were also coinjected with derivatized coprostanol or epicoprostanol to confirm the identification.

The following GC conditions were employed: HP 5840 gas chromatograph equipped with Grob-type splitless injector was used; 30-m DB5 (0.25-mm i.d., 0.25- $\mu$ m film thickness) fused silica column was programmed from 40 °C at 4 °C/min up to 280 °C and 2 °C thereafter to 310 °C. Helium was the carrier gas at a flow rate of 20 cm/s. GC/MS (Finnigan 4000) conditions were the same as above with electron energy, 70 eV; source temperature, 240 °C; scan speed, 2 s scan<sup>-1</sup> from 50 to 550 amu.

### Results and Discussion

**General Observations.** The following sterols were measured in the Basin sediments: cholesterol, campesterol,  $\beta$ -sitosterol, dinosterol, coprostanol, epicoprostanol, cholestanol, and  $\beta$ -sitostanol. With the exception of coprostanols (coprostanol + epicoprostanol), all others are common in uncontaminated marine sediments (see ref 14–16, among others). Excluding dinosterol, all the sterols are also present in sewage sludge samples but in different proportions than in the sediments. The total sterols range in concentration from 1 to 81  $\mu$ g/g (Table I) in the cores with the highest concentrations in the top 4 cm of deep water stations 102 and 89, in the anoxic zone. The sewage

**Table I. Coprostanols, Total Sterols, Dinosterol, and TOC Contents of Santa Monica Basin Sediments and Sewage Effluents (Concentration Based on Dry Sediment Weight)**

sample	TOC, <sup>a</sup> %	concn, $\mu\text{g/g}$		
		copro- stanols <sup>b</sup>	total sterols <sup>c</sup>	dino- sterol
BC 40 (398 m) <sup>d</sup>				
0-2 <sup>e</sup>	1.36	1.6 (119) <sup>f</sup>	6.6(487) <sup>f</sup>	0.8
2-4	1.20	0.8 (70)	7.6 (631)	0.8
10-12	1.15	0.12 (10)	1.2 (104)	0.2
16-21	1.13	0.05 (5)	0.9 (79)	0.2
BC 113 (572 m)				
0-2	2.52	1.7 (67)	12.4 (491)	2.9
2-4	2.61	1.2 (46)	11.1 (425)	2.0
12-14	2.26	0.17 (8)	7.0 (309)	2.0
20-23.5	2.27	0.17 (8)	4.8 (212)	1.4
BC 12 (750 m)				
0-2	2.65	1.2 (45)	9.2 (599)	2.0
2-4	2.76	0.5 (18)	20.2 (732)	3.3
12-14	2.92	0.3 (10)	13.1 (449)	3.5
21-24.5	2.50	tr (tr) <sup>g</sup>	6.9 (277)	1.2
BC 102 (910 m)				
0-2	4.07	1.7 (41)	48 (1184)	13.7
2-4	4.76	4.3 (91)	77 (1624)	19.5
14-16	3.52	0.2 (6)	12 (324)	3.4
22-25	2.52	tr (tr)	7.7 (306)	1.7
BC 89 (908 m)				
0-2	4.18	5.1 (123)	81 (1938)	21.8
2-4	4.63	1.1 (24)	47 (1004)	12.5
12-14	3.70	0.1 (4)	12 (332)	5.4
22-27.5	1.21	tr (tr)	3 (236)	0.4
BLM 364 (57 m)				
0-2	0.5	0.5 (100)	1.0 (200)	0.03
sewage effluents				
H5 (sediment, 6/87) <sup>h</sup>	NA	33	47	0.6
H7 (sediment, 6/87)	6.92	1302	1850	tr
H7S (sludge, 7/87)	19.71	1374	2077	ND <sup>i</sup>
JWPCPS (sludge, 11/87)	25.3	947	1950	ND
H5 (effluent, 6/87)	NA	158 $\mu\text{g/L}$	459 $\mu\text{g/L}$	ND
H7 (EF, 6/87) <sup>j</sup>	NA	140 $\mu\text{g/L}$	298 $\mu\text{g/L}$	ND
JWPCP (EF, 11/87)	NA	29 $\mu\text{g/L}$	63 $\mu\text{g/L}$	ND

<sup>a</sup> Percent dry weight. <sup>b</sup> Coprostanol + epicoprostanol. <sup>c</sup> Sum of cholesterol, campesterol,  $\beta$ -sitosterol, dinosterol, coprostanol, epicoprostanol, cholesterol, and  $\beta$ -sitosterol. <sup>d</sup> Water depth in meters. <sup>e</sup> Centimeters depth in the core. <sup>f</sup> Microgram per gram of organic carbon ( $\mu\text{g/g}$  of OC) given in parentheses. <sup>g</sup> Trace amounts detected but too low to be integrated. <sup>h</sup> Collection date in parentheses. <sup>i</sup> Not detected. <sup>j</sup> Effluent filtrate.

sludge and the Hyperion 7-mile sediment samples contain total sterols as high as 2 mg/g of dry weight where coprostanols constitute a very high percentage of the total sterols (50-70%).

**Coprostanols in Surficial Sediments.** The coprostanols content in the Santa Monica Basin surficial sediments is presented in Table I. Concentrations range from 1.1 to 5.1  $\mu\text{g/g}$  of dry sediment weight, which is comparable to that found in the heavily polluted New York Bight (2). Concentrations of coprostanols in surface sediments are generally similar throughout the region sampled. Lowest coprostanols concentration in 0-2-cm sediments is found at station 364, closest to the outfall, and the highest concentration is observed in station 89, farthest from the outfall. However, the ratio of coprostanols to other organic components does vary from station to station. When the concentration of coprostanols is expressed based on total organic carbon (Table I), highest concentrations of fecal sterols are exhibited in stations 364 and 40 adjacent to the sewage outfall and in station 89 in the deeper waters. High values in shallow waters reflect the deposition of sewage outfall materials, which cause black streaking among coarse or fine sands at these stations. The high concentration of

**Table II. Grain Size Characteristics of Surface Sediments from Santa Monica Basin<sup>a</sup>**

station	concn, %			
	sand	silt	clay	silt/clay
BLM 364 (57 m)	40	55	5	11
Seawatch BC 2 (297 m) <sup>b</sup> (=BC 40)	38	51	11	4.6
Seawatch BC 4 (490 m) <sup>b</sup> (=BC 113)	2	65	33	2
Seawatch BC 5 (750 m) <sup>b</sup> (=BC 12)	1	62	38	1.6
CaBS 7 BC 1 (~900 m) <sup>b</sup> (=BC 102)	<1	50	50	1
CaBS 7 BC 2 (~900 m) <sup>b</sup> (=BC 89)	<1	49	51	0.96

<sup>a</sup> Data from D. Gorsline (personal communication from CaBS data, 1989). <sup>b</sup> The exact station location of these samples may be separated by as much as 1 km from those reported for BC samples in the current study. These samples were collected in October and November of 1987, 2 years later than our BC samples listed in Table I.

coprostanols in the deep basin is associated with advected fine-grained sediments, which tend to adsorb organic carbon.

The concentration of coprostanols from 0-2-cm horizon correlates reasonably well with TOC among all the stations including BLM 364 ( $r = 0.69$  at the 87% confidence level). The amounts of fine-grained silt trapped between the sandy grains most likely determine the TOC of sandy sediments (2). Various other pollutants also concentrate on surfaces of fine-grained particles (17) and clay (18), which are transported long distances offshore. The grain size distributions of the surface sediments are presented in Table II. Sample 364 contains the highest percentage of sand and silt/clay ratio and, therefore, the lowest % TOC and coprostanols content (cf. Table I). By contrast, all the BC samples exhibit similar silt/clay ratios, which are an order of magnitude less than for BLM 364, although BC 40 contains a considerably high percentage of sand. Note that all BC samples also contain much higher concentrations of coprostanols than BLM 364. Very good correlation is exhibited between % TOC and (i) % sand ( $r = -0.88$ ) and (ii) silt/clay ratios ( $r = -0.87$ ). However, the content of coprostanols is less strongly correlated to percent sand ( $r = -0.46$ ) and to the silt/clay ratio ( $r = -0.54$ ) in all the samples, including BLM 364. Note that coprostanols content is better correlated to the silt/clay ratio than to the sand percentage. This trend is stronger when data from BC 89 are excluded in the linear regression (coprostanols vs silt/clay,  $r = -0.85$ ). It is therefore not unexpected to see relatively high concentrations of coprostanol in the deeper basin where silt and clay fractions dominate (ref 12, 13, and 19; D. Gorsline, personal communication, 1989). The advective transport of fine particles as well as better preservation of organic matter in anoxic deeper waters is reflected in the very high coprostanols content of station 89. Total sterols (Table I), fatty acids, and other classes of compounds in the lipid fraction were also found to be highest in station 89 (Venkatesan, unpublished data).

It is probably more meaningful to relate coprostanols to total sterols content, so as to eliminate the grain size dependency of coprostanol. The resulting parameter (percent coprostanols in total sterols) should reflect the degree of sewage contamination in the marine sediments (2). The percent coprostanols relative to total sterols (listed above) is plotted for surface sediments, along with sediments at the Hyperion pipeline outlets (Figure 2).

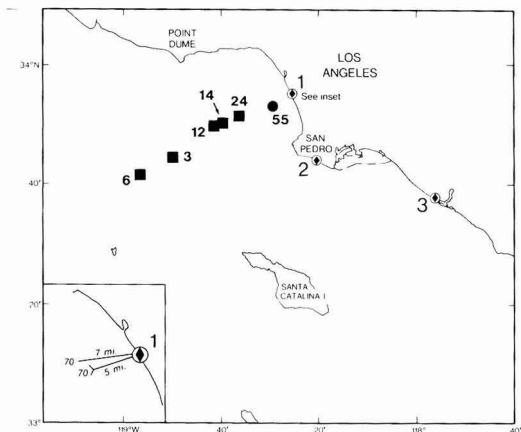


**Figure 2.** Percent coprostanols (percent of total sterols) distribution in surficial sediments of Santa Monica Basin. Percent coprostanols in the sediments at the pipeline outlets are indicated in the inset. See text for sludge data.

Coprostanols of H7S and JWPCPS are 66 and 49% of total sterols, respectively, whereas the coprostanols content in the two sediments at the outfall (H7 and H5) represent 70% of total sterols. The sewage effluents generally contain coprostanol in the range 50–80% of total sterols (3, 20). Considering this range in the data, it is reasonable to assume that the coprostanols/total sterol ratio of 70% at Stations H7 and H5 reflects the maximum degree of sewage contamination in the sediments. A progressive decline in percent coprostanols seaward from the outfall sites was noticed. The decrease is sharp from 57 to 398 m water depth, after which it tapers off only gradually to 910 m, at which depth the sewage-derived sterols comprise ~6% of the total sedimentary sterols. Near-bottom transport of particles plays a significant role in supplying materials to the deeper basins, as reported from studies on sediments and sediment traps in the Bight (12, 21, 22). Consequently, other anthropogenic indicators, i.e., DDT metabolites, have also been detected in sediment trap material (23) and sediment cores off San Nicolas Basin (24) farther offshore.

#### Core Profiles as Historic Record of Sewage Input.

The concentrations of coprostanols relative to the total organic carbon content are plotted in Figure 3. A sampling gap between sediment sections from 10 to 16 cm (corresponding to ~1890s) and 2 to 4 cm (more recent horizons in the approximate 1950s) is noticeable here. This was intentionally done because of the knowledge from previous studies showing increases in anthropogenic pollutants at about 1935 (25–27) and from information on population dynamics in southern California showing rapid growth beginning in the 1930s (28). For example, population in Los Angeles County was ~937 000 in 1920, it more than doubled to 2.2 million by 1930, and in 1950 it was 4.2 million (29). Since then, a steady increase in population has been noted and in 1980 it had climbed to 7.5 million. The discharge of chemical contaminants from the outfall also exhibited a concomitant increase from 1937 to 1971 and then decreased to 1987 (26). The decrease is due to the improved wastewater treatment.

An onset of rapid increase in the content of coprostanols is observed beginning around 1935 corresponding to the age determinations by  $^{210}\text{Pb}$  and  $^{239}\text{Pu}$  (Figure 3). This decade probably marks the start of the boom in population growth in the California coastal urban areas (29).

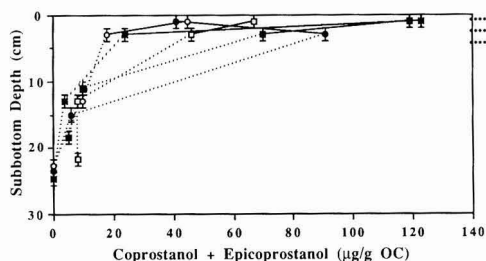


**Figure 3.** Depth profiles of coprostanols from Santa Monica Basin cores (micrograms per gram of organic carbon). ■, BC 40; □, BC 113; ○, BC 12; ●, BC 102, and ▣, BC 89. Ages of the sediment horizons, based on  $^{239}\text{Pu}$  and  $^{210}\text{Pb}$  chronology from ref 3 and 21 corresponding to BC 102 and 89, are indicated. Although the declining trend is expected, lines below 4 cm are broken to indicate the sampling gaps.

Wastewater discharges off JWPCP offshore on Palos Verdes Shelf via a 152-cm submarine pipe began in 1937 (26). This wastewater flow increased with growth in the county from 1937 to 1970 (28, 29). A subsurface maximum is also noted for station 102 at 2–4 cm, at the same depth as that observed for trace metal profiles of cores from Basin I-LBC1 (close to station 102) and from station 12 (27). The decrease in coprostanols above 2 cm may be attributed to the major improvements in wastewater treatment technologies introduced in 1960s to 1970s (26), which considerably increased the efficiency in solids removal (28). Because most of the coprostanol is associated with the solid phase of the effluent, a concomitant decrease in its level is not surprising with the decrease in solids output from the dischargers. This historic record has apparently been preserved in the anoxic sediments at station 102. It is not clear why a similar trend is not obvious at station 89, which is also anoxic and where both cores exhibit maxima for total organic carbon at this interval. All cores reach background levels below 5–10 cm, comparable to the trace metal data of Finney and Huh (27).

The lack of subsurface maxima in most of the cores is consistent with the following observation. An increase in the suspended solids load from Hyperion 5-mile has been noted commensurate with the increase in flow from the 1960s to (211–377)  $\times 10^3$  lb/day during 1970–1986]. The termination of usage of the Hyperion 5-mile outflow for solid waste in 1987 resulted in a considerable decrease in the suspended solids load in the last 2 years to (182–185)  $\times 10^3$  lb/day (J. Dorsey, personal communication, 1988). This change has not yet been observed in the cores. On the contrary, a significant reduction in suspended solids output, despite the increase in flow from the 1970s, has been reported off JWPCP outfalls (28) due to improvements in the wastewater treatment process. The enhanced coprostanols level in Santa Monica Basin in the last two decades, therefore, apparently reflects a mixed input from both the major sewage dischargers. The less distinct subsurface maximum in the shallow water could also be a result of bioturbation.

The stanols/stenols ratios (0.3–1.1) fluctuate down the cores, thus implying that rapid hydrogenation of stenols, which could lead to the conversion of cholesterol to coprostanol at depth, does not play a major role in these sediments. If this were the case, a steady increase in ratio with depth would have been noticed (30). Coprostanols obviously originate from sewage outfalls in the area. Future monitoring for coprostanol on a finer scale should

**Table III. Mass Emission Rate of Coprostanol + Epicoprostanol from the Sewage Outfalls into Southern California Bight**

I	coprostanols in effluent filtrate Hyp 7-mi	140 $\mu\text{g/L}$
	total effluent flow	15 ML/day <sup>a</sup>
	total coprostanols in Hyp 7-mi effluent filtrate	2.1 kg/day
II	coprostanols in effluent Hyp 5-mi	158 $\mu\text{g/L}$
	total effluent flow	1453 ML/day <sup>a</sup>
	total coprostanols in Hyp 5-mi effluent	230 kg/day
III	coprostanols in Hyp 7-mi sludge	1374 $\mu\text{g/g}$
	1 L of effluent	4.266 g of sludge
	$\therefore$ 1374 $\mu\text{g/g}$ of coprostanols	5.86 mg/L of effluent
	total effluent flow	18 ML/day
	coprostanols in the sludge	105.5 kg/day
	total coprostanols from the effluents	
	Hyp 5-mi and 7-mi	337.5 kg/day
	mass emission rate of wastewater coprostanols	
	from Hyp outfall in 1987	123 metric tons/yr
IV	total coprostanols from effluent filtrate and sludge from JWPCP	100 $\mu\text{g/L}$
	average flow	1385 ML/day <sup>b</sup>
	total coprostanols from JWPCP	138.5 kg/day =
		50.6 metric tons/yr
V	assuming the same proportion as that from Hyp 5-mi effluent also comes from OCSD <sup>c</sup> (Orange County), CSD (City of San Diego), SERRA, Encina, and Oxnard wastewater outfalls, for the total effluent flow of 1500 ML/day from the five outfalls, the mass emission rate of coprostanols	86.5 metric tons/yr
	mass emission rate of coprostanol + epicoprostanol from all seven outfalls	260 metric tons/yr

<sup>a</sup>Based on July 1987 average (data from Los Angeles, city). <sup>b</sup>Based on average flow for the year 1987 (data from Los Angeles, County). <sup>c</sup>Data from Schafer (17) for OCSD and the following three outfalls.

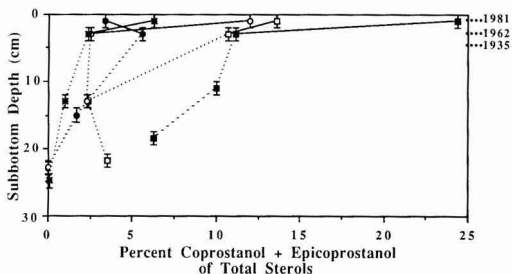


**Figure 4.** Depth profiles of percent coprostanols from Santa Monica Basin sediments. For core identification and other details, refer to Figure 3.

reveal the favorable impact on this ecosystem from the advanced waste treatment technology and the recent termination of the sludge input from the Hyperion 7-mile plant.

For comparison, the downcore variation of the percent coprostanols of total sterols is illustrated in Figure 4. The sewage impact is again clearly demonstrated in the basin slope stations 40, 113, and 12 in the top 4 cm, where it is more dominant than in the deep basin stations. As expected, there is a steady decline in the degree of sewage contamination, which generally levels off to  $\leq 4\%$ , at depths below 10 cm, with the exception of station 40, where it is  $\sim 6\%$ . This enhanced background level may be due to greater bioturbation at this shallow station.

We have also plotted the ratio of coprostanols to dinosterol vs depth of the core (Figure 5). This parameter could serve as a better indicator of degree of sewage contamination than normalizing coprostanol to total sterols, which includes cholesterol. Cholesterol is nonspecific to sewage. It is produced in the marine environment and is also present in fecal sterols at the level of  $\sim 10\%$  (20). In sewage sludge it occurs at the level of 9 (H7S) to 20% (JWPCPS) of total sterols. In contrast, dinosterol is not detected in sewage effluents and is apparently exclusively produced by marine phytoplankton, for example, from dinoflagellates (31). Figure 5 clearly demonstrates that the basin slope sediments, especially station 40, are impacted by sewage much more than the deep basin samples.

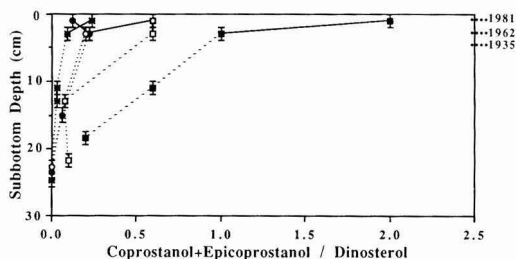


**Figure 5.** Downcore distribution of the coprostanols/dinosterol ratios. For core identification and other details, refer to Figure 3.

Although this parameter yields profiles very similar to that from percent coprostanols (Figure 4), the background values below 10 cm in this data set are more consistent with the absolute concentrations of coprostanols (Figure 3), as expected, than the former approach of percent coprostanols. For practical purposes, it appears that both approaches can be used interchangeably to estimate the degree of sewage contamination.

**Mass Emission Rates.** One of the main aims of this study was to compute mass emission rates of sewage coprostanols and carbon into the southern California Bight. The estimates presented here are based upon relatively few measurements from sewage effluents. When the available data, i.e., flow, suspended solids, oil, and grease are compared, it is clear that the monthly and annual variations in these parameters during the last decade is not significant (ref 11; Stull, personal communication, 1988). The few measurements on coprostanols, reported here for the first time, can therefore be assumed to be representative of the sewage impact on the Bight sediments, which can be used for comparison with known current inputs.

Table III illustrates the computation of mass emission rates of coprostanols into the Bight. The contribution of coprostanols from the effluent filtrate is less by an order of magnitude compared to that from solid sludge (Table I). However, coprostanols constitute nearly 30% of total sterols in the filtrate and the volume of effluent flow is significantly large. Therefore, transport of large mass of coprostanols via aqueous medium is likely in addition to

**Table IV. Mass Emission Rate of Sewage Carbon from the Outfalls into Southern California Bight**

coprostanols in Hyp 7-mi sludge	1374 $\mu\text{g/g}$
coprostanols in JWPCP sludge	947.2 $\mu\text{g/g}$
average coprostanols in the sludge	1161 $\mu\text{g/g}$
from % TOC of Hyp 7-mi and JWPCP	
from Table I, average % TOC in sludge	22.54
coprostanols in the sludge from the above averages	5.15 $\text{mg/g}$ of OC
therefore, organic carbon to coprostanols in sewage	1000:5.15 = 194:1
mass emission rate of sewage carbon into the Bight (from Table III)	$5 \times 10^4$ metric tons/yr

that from the sediment + sludge outfall. Consequently, the coprostanols content of the filtrate was also included in the estimate. Note that the coprostanols data have been extrapolated from the Hyperion 5-mile data to the five remaining minor dischargers, which discharge either primary or secondary effluents, or both. The extrapolated data are therefore approximate and can only be used for comparative purposes. The mass emission rate of sewage coprostanols is  $\sim 2$  orders of magnitude less than that of total hydrocarbons reported earlier (32).

Table IV illustrates the computation of mass emission rates of sewage carbon into the Bight. This estimate agrees remarkably well with another computation made by multiplying the organic carbon (25%) data of Eganhouse and Kaplan (33) with the suspended solids load equivalent to 200 000 metric tons/yr (average values for the years from 1984 through 1986 taken from ref 34). The mass emission rate of sewage carbon amounts to  $5 \times 10^4$  metric tons/yr. Note that only sludge coprostanols content is considered here and that coprostanols from water (filtrate) is omitted for lack of dissolved organic carbon data. We estimate that this flux of sewage carbon is  $\sim 3$  orders of magnitude less than the organic carbon flux from primary productivity [(1.1–1.6)  $\times 10^7$  metric tons/yr] in the Bight [based on primary productivity 0.39  $\text{g of C m}^{-2} \text{ day}^{-1}$  (35) and 0.46–0.56  $\text{g of C m}^{-2} \text{ day}^{-1}$  (36) and assuming the area of the Bight to be 78 000  $\text{km}^2$  (7)]. This comparison implies that the sewage carbon input is still a small percentage of the natural, biogenic inputs, although the local effects of discharges could impact the Bight environment.

### Conclusions

This work has shown that the presence of coprostanols denote fecal (sewage) pollution in the Santa Monica Basin and Bay. Despite the lengthy analytical procedures, this method is advantageous in tracing the cumulative load of fecal pollution. The data demonstrate that sewage-derived materials from the discharges are spread throughout the study area (and probably beyond) by the current system and by sediment creep down basin slopes. Deeper basin sites, approximately 50–60 km from the sewage outfall, are accumulating sewage carbon as well as marine biogenic components. Coprostanol analyses, in conjunction with water current movements and sediment dynamics, should prove very useful in designating condemnation zones. Periodic measurements of coprostanols could provide useful information of input assessments and sewage distribution in the Bight.

### Acknowledgments

We thank E. Ruth for GC/MS data acquisition, Nam-woo Kim and C. Santiago for technical assistance, H. Schafer for helpful discussions, and the following individuals for supplying samples and relevant data: Hyperion, J. Dorsey; JWPCP, J. Stull, G. Horner, and W. Holtz. R.

Jahnke collected the box cores (Cross I cruise) and D. Gorsline provided a BLM sediment and relevant data.

### Literature Cited

- (1) Kirchmer, C. J. Ph.D. Thesis: University of Florida, Gainesville, FL, 1971.
- (2) Hatcher, P. G.; McGillivray, P. A. *Environ. Sci. Technol.* **1979**, *13*, 1225–1229.
- (3) Walker, R. W.; Wun, C. K.; Litsky, W. *CRC Crit. Rev. Environ. Control* **1982**, *12*, 91–112.
- (4) Bartlett, P. D. *Mar. Pollut. Bull.* **1987**, *18*, 27–29.
- (5) Müller, G.; Kanazawa, A.; Teshima, S. *Naturwissenschaften* **1979**, *66*, 520–522.
- (6) Venkatesan, M. I.; Ruth, E.; Kaplan, I. R. *Mar. Pollut. Bull.* **1986**, *12*, 554–557.
- (7) Emery, K. O. *The Sea Off Southern California: A Modern Habitat of Petroleum*; John Wiley & Sons, Inc.: New York, 1960; p 366.
- (8) Wun, C.; Walker, R. W.; Litsky, W. *Water Res.* **1976**, *10*, 955–959.
- (9) Venkatesan, M. I.; Santiago, C. A. *Mar. Biol.* **1989**, *102*, 431–437.
- (10) Smith, R. C.; Dustan, P.; Au, D.; Baker, K. S.; Dunlap, E. A. *Mar. Biol.* **1986**, *91*, 385–402.
- (11) Schafer, H. A. In *Southern California Coastal Water Research Project Biennial Report, 1983–1984*; Bascom, W., Ed.; Southern California Coastal Water Research Project: Long Beach, CA, 1984; pp 11–19.
- (12) Malouta, D. N.; Gorsline, D. S.; Thornton, S. E. *J. Sediment. Petrol.* **1981**, *51*, 1077–1095.
- (13) Gorsline, D. S. In *Depositional Processes in Active Margin Basins: Pacific Section, Society of Economic Paleontologists and Mineralogists Short Course*; Colburn, L., Douglas, R., Gorsline, D. S., Eds.; 1984; pp 39–60.
- (14) Venkatesan, M. I.; Ruth, E.; Steinberg, S.; Kaplan, I. R. *Mar. Chem.* **1987**, *21*, 267–299.
- (15) Lee, C.; Farrington, J. W.; Gagosian, R. B. *Geochim. Cosmochim. Acta* **1979**, *43*, 35–46.
- (16) Huang, W. Y.; Meinschein, W. G. *Geochim. Cosmochim. Acta* **1976**, *40*, 323–330.
- (17) Wade, T. L.; Quinn, J. G. *Org. Geochem.* **1979**, *1*, 157–167.
- (18) Karickhoff, S. A.; Brown, D. S.; Scott, T. A. *Water Res.* **1979**, *13*, 241–248.
- (19) Brown, R. C.; Wade, T. L. *Water Res.* **1984**, *18*, 621–632.
- (20) Perezou, J.; Gouffier, E.; Coste, T.; Chevallier, F. *Digestion* **1978**, *18*, 201–212.
- (21) Huh, C.-A.; Zahnle, D. L.; Small, L. F.; Noshkin, V. E. *Geochim. Cosmochim. Acta* **1987**, *51*, 1743–1754.
- (22) Nelson, J. R.; Beers, J. R.; Eppley, R. W.; Jackson, G. A.; McCarthy, J. J.; Soutar, A. *Continental Shelf Res.* **1987**, *7*, 307–328.
- (23) Crisp, P. T.; Brenner, S.; Venkatesan, M. I.; Ruth, E.; Kaplan, I. R. *Geochim. Cosmochim. Acta* **1979**, *43*, 1791–1801.
- (24) Venkatesan, M. I.; Brenner, S.; Ruth, E.; Bonilla, J.; Kaplan, I. R. *Geochim. Cosmochim. Acta* **1980**, *44*, 789–802.
- (25) Bruland, K. W.; Bertine, K.; Koide, M.; Goldberg, E. D. *Environ. Sci. Technol.* **1974**, *8*, 425–432.
- (26) Stull, J. K.; Baird, R. B.; Heesen, T. C. *J.—Water Pollut. Control Fed.* **1986**, *58*, 985–991.
- (27) Finney, B.; Huh, C. A. *Environ. Sci. Technol.* **1989**, *23*, 294–303.
- (28) Stull, J. K.; Haydock, C. I. In *Proceedings, Symposium on Managing Inflows to California's Bays and Estuaries*; Bay Institute of San Francisco, 1988; pp 44–49.
- (29) U.S. Department of Commerce, U.S. Bureau of Census 1890–1980. *Census of the U.S. Population, Characteristics of Population, Vol. 1*; U.S. Government Printing Office.
- (30) Gaskell, S. J.; Eglinton, G. *Nature* **1975**, *254*, 209–211.
- (31) Boon, J. J.; Rijpsma, W. I. C.; deLange, F.; deLeeuw, J. W.; Yoshioka, M.; Shimizu, Y. *Nature* **1979**, *277*, 125–127.
- (32) Eganhouse, R. P.; Kaplan, I. R. *Environ. Sci. Technol.* **1982**, *16*, 180–186.
- (33) Eganhouse, R. P.; Kaplan, I. R. *Mar. Chem.* **1988**, *24*, 163–191.

- (34) SCCWRP 1987 Annual Report; Long Beach, CA, 1987; pp 5-12.
- (35) Eppley, R. W.; Holm-Hansen, O. In *Lecture Notes on Coastal and Estuarine Studies: Plankton Dynamics of the Southern California Bight*; Eppley, R. W., Ed.; Springer-Verlag: New York, 1986; Chapter 5.
- (36) Smith, R. C.; Baker, K. S. *Mar. Biol.* 1982, 66, 269-279.
- (37) Noshkin, V. E.; Wong, K. M.; Eagle, R. J. In *West Coast Environmental Studies: California Basin Study (CaBS)*;

Received for review December 12, 1988. Revised manuscript received June 26, 1989. Accepted October 3, 1989. Financial assistance was provided by the Department of Energy, OHER, Ecological Research Division, under Grant No. DE-FG03-85-ER60338. Data from surface sediments (percent coprostanols) presented at the 8th International Symposium of Environmental Biogeochemistry, Nancy, France, September 14-18, 1987.

## Calcium Molybdate Solubility in Spent Oil Shale and a Preliminary Evaluation of the Association Constants for the Formation of $\text{CaMoO}_4^0(\text{aq})$ , $\text{KMoO}_4^-(\text{aq})$ , and $\text{NaMoO}_4^-(\text{aq})$

Michael E. Essington

Division of Environmental Technology, Western Research Institute, University of Wyoming Research Corporation, P.O. Box 3395, University Station, Laramie, Wyoming 82071

■ In order to better understand the fate and behavior of molybdenum in spent oil shale disposal environments, the equilibrium solubility of  $\text{CaMoO}_4(\text{c})$ , powellite) in deionized-distilled water, potassium nitrate solutions, and spent oil shale leachates was determined. The calculated  $\log K_{\text{sp}}$  for the dissolution of  $\text{CaMoO}_4(\text{c})$  is  $-8.05$ . The ion association constants for the formation of  $\text{CaMoO}_4^0(\text{aq})$  and  $\text{KMoO}_4^-(\text{aq})$  were also determined by using an iterative estimation technique. The estimate of  $\log Q$  for the formation of  $\text{CaMoO}_4^0(\text{aq})$  is 3.09. Similarly, an estimate of  $\log Q$  for the formation of  $\text{KMoO}_4^-(\text{aq})$  is 1.29. Calcium molybdate solubility in  $\text{CaMoO}_4(\text{c})$ -spiked and nonspiked spent oil shale equilibrium solutions was evaluated. The  $\text{CaMoO}_4(\text{c})$ -spiked spent oil shale solutions were initially evaluated as supersaturated with respect to  $\text{CaMoO}_4(\text{c})$ . Evaluation of the data indicated that the  $\text{NaMoO}_4^-(\text{aq})$  ion pair may significantly contribute to total soluble molybdenum. The spiked spent oil shale solution data are used to generate a  $\log Q$  of 1.66 for the formation of  $\text{NaMoO}_4^-(\text{aq})$ . Inclusion of this species in the geochemical model analyses of the spiked spent oil shale solutions suggests that the solutions are in equilibrium with  $\text{CaMoO}_4(\text{c})$ . Geochemical model analyses show that  $\text{CaMoO}_4(\text{c})$  does not control molybdenum concentrations in the spent oil shale (nonspiked) equilibrium solutions. Further, these data suggest that  $\text{CaMoO}_4(\text{c})$  may not occur in spent oil shales.

### Introduction

The uptake and accumulation of molybdenum by plants and the subsequent ingestion by wildlife is one concern associated with the surface disposal of spent oil shale. The concentrations of molybdenum and Cu/Mo ratios in plants grown on spent oil shale indicate that molybdenosis could be expected in grazing livestock (1, 2). Reddy and Lindsay (3) postulated that the recarbonation of spent oil shale to reduce leachate alkalinity, and correspondingly decrease soluble molybdenum, would promote the establishment of a beneficial vegetative disposal pile cover. However, they found plant uptake of molybdenum to increase with recarbonation. Further, Reddy et al. (4) could not document a consistent reduction in soluble molybdenum with recarbonation.

In order to understand the chemistry of molybdenum in spent oil shale disposal environments, predict fate and behavior, and assess the effectiveness of proposed miti-

gation techniques (e.g., recarbonation), the solid-phase chemistry of molybdenum must be characterized. Analysis of spent oil shale solids using selective dissolution techniques shows that molybdenum resides in solids that are highly resistant to chemical attack (5, 6), such as iron oxide, sulfides, and silicate phases. Molybdenum partitioned into the less than 2- $\mu\text{m}$  size fraction and the light and heavy density fractions of spent oil shales (5, 7). However, molybdenum could not be concentrated into any specific density fraction of a recarbonated retorted oil shale (7). A statistical analysis of the partitioning of molybdenum into spent oil shale particle size, density, and magnetic separates shows that molybdenum is associated with cobalt, chromium, copper, iron, lead, lithium, nickel, sulfur, vanadium, and zinc (8).

Despite the indications that molybdenum may reside in relatively stable solids, molybdenum exhibits mobility in and from spent oil shales (9, 10). Equilibrium solubility analysis of spent oil shale leachate data strongly suggests that soluble molybdenum concentrations are controlled by the precipitation of calcium molybdate,  $\text{CaMoO}_4(\text{c})$ , powellite). Stollenwerk and Runnells (9) observed that the calculated saturation index ( $\log \text{IAP} - \log K_{\text{sp}}$ , using  $\log K_{\text{sp}} = -8.36$ ) for  $\text{CaMoO}_4(\text{c})$  was close to zero for the first pore volume of spent oil shale leachate. This suggests that  $\text{CaMoO}_4(\text{c})$  controls soluble molybdenum concentrations. However, Essington et al. (5) and Essington and Spackman (7) observed that calculated  $\text{CaMoO}_4(\text{c})$  saturation index values ( $\log K_{\text{sp}} = -7.72$ ) range from  $-0.18$  (saturation) to  $-2.94$  (undersaturation) for spent oil shale leachates as a function of spent oil shale type, solid/solution ratio, carbon dioxide partial pressure, and solid-water contact times. Calculated  $\text{CaMoO}_4(\text{c})$  saturation index values ( $\log K_{\text{sp}} = -7.94$ ) range from  $-0.83$  to  $-1.82$  for directly retorted and combusted oil shale (5). Indirectly retorted spent oil shale leachates were calculated to be highly undersaturated with respect to  $\text{CaMoO}_4(\text{c})$ . In general, the calculated saturation index values grow more negative as the spent oil shale-water contact times increase, indirectly retorted oil shale leachates were undersaturated to the greatest extent, and carbon dioxide partial pressure did not significantly influence the calculated saturation index values (5, 7).

Literature values for the equilibrium solubility ( $\log K_{\text{sp}}$ ) of  $\text{CaMoO}_4(\text{c})$  are highly variable. Reported  $\log K_{\text{sp}}$  values include  $-7.02$  (11),  $-8.50$  (12),  $-8.51$  (13),  $-8.0$  (14),  $-7.19$  to  $-8.50$  (15),  $-7.95$  (16),  $-7.83$  (17), and  $-7.41$  to  $8.36$  (18).



Such variability in an equilibrium solubility product constant can significantly influence data interpretations. The objective of this study was to reevaluate the equilibrium solubility of  $\text{CaMoO}_4(\text{c})$ . The solubility experiments were performed under four different ionic strength conditions, and equilibrium was approached from undersaturated and supersaturated initial conditions. In addition, the solubility of  $\text{CaMoO}_4(\text{c})$  in spent oil shale-water systems was evaluated. The results of this study were used to assess the occurrence of  $\text{CaMoO}_4(\text{c})$  in spent oil shales and to evaluate the occurrence of various soluble molybdenum species.

### Materials and Methods

Calcium molybdate [ $\text{CaMoO}_4(\text{c})$ ] was prepared by mixing 1 M  $\text{Ca}(\text{NO}_3)_2 \cdot 4\text{H}_2\text{O}$  and 1 M  $\text{Na}_2\text{MoO}_4 \cdot 2\text{H}_2\text{O}$  solutions in equal Ca to  $\text{MoO}_4$  molar proportions. A white precipitate was obtained upon mixing. The suspension was allowed to react by constant mixing at ambient temperatures for 24 h. The white precipitate was removed from solution by vacuum filtration and washed with copious amounts of deionized-distilled water followed by absolute ethanol. The solid was oven-dried at 115 °C for 24 h. The precipitate was analyzed by X-ray diffraction (random sample orientation, Ni-filtered Cu  $K\alpha$  radiation, 45 kV and 40 mA,  $2^\circ 2\theta \text{ min}^{-1}$ ) and the diffractogram was compared to Joint Committee on Powder Diffraction Standards (JCPDS) files for solid-phase identification. X-ray diffraction identified the precipitate as  $\text{CaMoO}_4(\text{c})$  (powellite). No impurities were detected by X-ray diffraction analysis.

The solubility experiments were conducted in much the same manner as those used to determine the equilibrium solubility of magnesite,  $\text{MgCO}_3$  (19), and barium arsenate,  $\text{Ba}_3(\text{AsO}_4)_2$  (20). The equilibrium solubility experiments were conducted under four different ionic strength conditions, and equilibrium was approached from both undersaturated and supersaturated initial conditions. All equilibrium solubility systems were replicated 3-fold.

Samples of  $\text{CaMoO}_4(\text{c})$  (2 g) were placed in 50-mL polypropylene centrifuge tubes. For the undersaturated initial condition experiments, 20 mL of 0.01, 0.05, or 0.10 M  $\text{CO}_2$ -free  $\text{KNO}_3$  solution or 20 mL of deionized-distilled water was added to each tube. The tubes were capped and placed in a temperature-controlled water bath ( $298 \pm 0.1$  K) in a  $\text{CO}_2$ -free glovebox. The  $\text{CO}_2$ -free environment of the glovebox was maintained by bubbling laboratory compressed air through 1 M NaOH. The samples were equilibrated, with periodic shaking, for times that varied from 7 to 113 days.

Prior to supersaturated initial condition experiments, 2-g samples of  $\text{CaMoO}_4(\text{c})$  were placed into each of three 250-mL polypropylene bottles. To each bottle, 140 mL of either 0.01, 0.05, or 0.10 M  $\text{CO}_2$ -free  $\text{KNO}_3$  was added. The bottles were placed in a 60 °C water bath and equilibrated, with periodic shaking. The production of the supersaturated solutions in this manner is based on the results of Zelikman and Prosenkova (11). They found  $\text{CaMoO}_4(\text{c})$  solubility to increase with increasing solution temperature. Following a 7-day equilibration period, 20 mL of each supersaturated solution was combined with 2-g samples of  $\text{CaMoO}_4(\text{c})$  in 50-mL polypropylene centrifuge tubes. These samples were equilibrated under  $298 \pm 0.1$  K,  $\text{CO}_2$ -free conditions with periodic shaking for 14, 56, and 106 days.

After equilibration, the aqueous phase was extracted from the centrifuge tube and pressure filtered through a 0.45- $\mu\text{m}$  Millipore filter. Aqueous-phase pH was determined with a standardized (pH 7 and 10) combination pH

**Table I. Ion Pair Formation Reactions and Ion Association Constants Used by PHREEQE and GEOCHEM**

	reaction	log Q	source
PHREEQE			
1	$\text{Ca}^{2+} + \text{H}_2\text{O}(\text{l}) = \text{CaOH}^+ + \text{H}^+$	-12.60	24
2	$\text{Ca}^{2+} + \text{NO}_3^- = \text{CaNO}_3^-$	0.70	14
3	$\text{Ca}^{2+} + 2\text{NO}_3^- = \text{Ca}(\text{NO}_3)_2^0$	0.60	14
4	$\text{Ca}^{2+} + \text{MoO}_4^{2-} = \text{CaMoO}_4^0$	3.09	a
5	$\text{H}^+ + \text{MoO}_4^{2-} = \text{HMoO}_4^-$	4.23	18
6	$2\text{H}^+ + \text{MoO}_4^{2-} = \text{H}_2\text{MoO}_4^0$	8.23	18
7	$3\text{H}^+ + \text{MoO}_4^{2-} = \text{MoO}_3(\text{OH})^+ + \text{H}_2\text{O}(\text{l})$	8.17	18
8	$\text{K}^+ + \text{H}_2\text{O}(\text{l}) = \text{KOH}^0 + \text{H}^+$	-14.46	25
9	$\text{K}^+ + \text{NO}_3^- = \text{KNO}_3^0$	-0.15	14
10	$\text{K}^+ + \text{MoO}_4^{2-} = \text{KMoo}_4^-$	1.29	a
GEOCHEM			
11	$\text{Ca}^{2+} + \text{H}_2\text{O}(\text{l}) = \text{CaOH}^+ + \text{H}^+$	-12.6	24
12	$\text{Ca}^{2+} + \text{CO}_3^{2-} = \text{CaCO}_3^0$	3.2	26
13	$\text{Ca}^{2+} + \text{H}^+ + \text{CO}_3^{2-} = \text{CaHCO}_3^+$	11.4	26
14	$\text{Ca}^{2+} + \text{SO}_4^{2-} = \text{CaSO}_4^0$	2.3	26
15	$\text{Ca}^{2+} + \text{Cl}^- = \text{CaCl}^+$	0.3	26
16	$\text{Ca}^{2+} + \text{F}^- = \text{CaF}^+$	1.1	18
17	$\text{Ca}^{2+} + \text{H}_2\text{SiO}_4^{2-} = \text{CaH}_2\text{SiO}_4^0$	4.7	27
18	$\text{Ca}^{2+} + \text{H}^+ + \text{H}_2\text{SiO}_4^{2-} = \text{CaH}_3\text{SiO}_4^+$	14.4	27
19	$\text{Ca}^{2+} + 2\text{H}^+ + 2\text{H}_2\text{SiO}_4^{2-} = \text{Ca}(\text{H}_2\text{SiO}_4)_2^0$	35.6	27
20	$\text{Ca}^{2+} + \text{S}_2\text{O}_3^{2-} = \text{CaS}_2\text{O}_3^0$	1.9	14
21	$\text{Ca}^{2+} + \text{NO}_3^- = \text{CaNO}_3^+$	0.7	14
22	$\text{Ca}^{2+} + 2\text{NO}_3^- = \text{Ca}(\text{NO}_3)_2^0$	0.6	14
23	$\text{Ca}^{2+} + \text{MoO}_4^{2-} = \text{CaMoO}_4^0$	3.1	a
24	$\text{H}^+ + \text{MoO}_4^{2-} = \text{HMoO}_4^-$	4.2	26
25	$2\text{H}^+ + \text{MoO}_4^{2-} = \text{H}_2\text{MoO}_4^0$	8.2	26
26	$3\text{H}^+ + \text{MoO}_4^{2-} = \text{MoO}_3(\text{OH})^+ + \text{H}_2\text{O}(\text{l})$	8.2	18
27	$4\text{H}^+ + \text{MoO}_4^{2-} = \text{MoO}_2^{2+} + 2\text{H}_2\text{O}(\text{l})$	8.6	18
28	$\text{K}^+ + \text{MoO}_4^{2-} = \text{KMoo}_4^-$	1.3	a
29	$\text{Na}^+ + \text{MoO}_4^{2-} = \text{NaMoO}_4^-$	1.7	a

<sup>a</sup> Determined from solubility data.

electrode and a Corning Model 155 pH/ion meter. The aqueous phase was then acidified with  $\text{HNO}_3$  to approximately pH 2. The remaining solid was resuspended in 20 mL of the appropriate solution and allowed to reequilibrate. The acidified aqueous extracts were simultaneously analyzed for total Ca, Mo, and K by inductively coupled argon plasma spectroscopy (ICAP) using a Jarrell-Ash 1100. Standard solutions were prepared from  $\text{CaCO}_3$ ,  $(\text{NH}_4)_2\text{MoO}_4$ , and KCl and verified against EPA7 and EPA19 standard reference solutions. The prepared standards, over the duration of the study, were within +3% and -2% for Ca, +2% and -2% for Mo, and +16% and -7% for K of the standard reference solution values. Spectral interference and background correction factors were verified by spike recovery analyses and analyses of diluted samples. Spiked and diluted samples were within +6.7% and -7.8% for Ca, +5.5% and -2.9% for Mo, and +14% and +0.5% for K of the sample results. Because  $\text{NO}_3^-$  was not added to the systems in excess of what was required for ionic strength control,  $\text{NO}_3^-$  concentrations (on a molar basis) were assumed to equal K concentrations.

The fractions of total soluble Ca occurring as  $\text{Ca}^{2+}(\text{aq})$  and of total soluble Mo occurring as  $\text{MoO}_4^{2-}(\text{aq})$  were calculated by use of the chemical equilibrium computer model PHREEQE (21). The aqueous species considered for total soluble Ca in the calculations were  $\text{Ca}^{2+}$ ,  $\text{CaOH}^+$ ,  $\text{CaNO}_3^+$ , and  $\text{Ca}(\text{NO}_3)_2^0$ . For total soluble Mo, the species considered were  $\text{MoO}_4^{2-}$ ,  $\text{HMoO}_4^-$ , and  $\text{H}_2\text{MoO}_4^0$ . The ion association reactions, and the association constants used in the calculations, are listed in Table I.

Green River Formation oil shale from the Piceance Creek Basin was obtained from the Exxon Colony Oil Shale Mine at Parachute, CO. The oil shale was directly retorted under conditions typical of the Paraho process

and combusted in an inclined fluid bed. The directly retorted oil shale (designated PPP4) was produced by using recycled process gas and air at an average maximum temperature of 1075 °C and a heating rate of 14 °C min<sup>-1</sup>. The combusted oil shale (designated TR8) was produced in a fluid bed reactor that used air as the process gas, a maximum temperature of 760–930 °C, and a heating rate of 667 °C min<sup>-1</sup>. The retorting and combustion processes and the basic physical, chemical, and mineralogical properties of the spent oil shale samples are described elsewhere (5, 22).

The equilibrium solubility of CaMoO<sub>4</sub>(c) in spent Green River Formation oil shale was examined by comparing CaMoO<sub>4</sub>(c) ion activity products in equilibrium extracts of spent oil shale to ion activity products in extracts of CaMoO<sub>4</sub>(c)-spiked spent oil shale. Samples (10 g) of either PPP4 or TR8 were placed in 125-mL polypropylene bottles. For the CaMoO<sub>4</sub>(c)-spiked systems, 0.5 g of CaMoO<sub>4</sub>(c) was added to each bottle. To each bottle was added 100 mL of deionized-distilled water. The bottles were capped and placed in a temperature-controlled water bath (298 ± 0.1 K). The samples were equilibrated, in triplicate and with periodic shaking, for 28 and 56 days.

After equilibration, the aqueous phase was extracted from the centrifuge tubes and pressure filtered (for TR8) or vacuum filtered (for PPP4) through a 0.45-μm Millipore filter. Aqueous-phase pH was determined with a standardized (pH 7 and 10) combination pH electrode and a Corning Model 255 pH/ion meter. The filtered extract was split, and a subsample was analyzed by ion chromatography for F<sup>-</sup>, Cl<sup>-</sup>, NO<sub>3</sub><sup>-</sup>, SO<sub>4</sub><sup>2-</sup>, and S<sub>2</sub>O<sub>3</sub><sup>2-</sup> with a Dionex Model 4040i dual-channel ion chromatograph equipped with a Model CHA-6 valve module, a 100-μL sample injection loop, an HPIC-AS4A analytical column, an HPIC-AG4A guard column, and a suppressed conductivity detector. For F<sup>-</sup>, Cl<sup>-</sup>, NO<sub>3</sub><sup>-</sup>, and SO<sub>4</sub><sup>2-</sup> analyses, a 1 mM Na<sub>2</sub>CO<sub>3</sub>/0.9 mM NaHCO<sub>3</sub> eluent and a flow rate of 2 mL min<sup>-1</sup> were used. A 10 mM Na<sub>2</sub>CO<sub>3</sub> eluent and a flow rate of 2 mL min<sup>-1</sup> were used for S<sub>2</sub>O<sub>3</sub><sup>2-</sup>. Standard solutions were prepared from NaF, NaCl, NaNO<sub>3</sub>, K<sub>2</sub>SO<sub>4</sub>, and Na<sub>2</sub>S<sub>2</sub>O<sub>3</sub>·5H<sub>2</sub>O. For any given anion, the coefficient of variation for multiple analyses of a single sample was within 10%. Inorganic carbon was determined by coulometric titration. However, due to the limited sample size, multiple analyses for inorganic carbon in a single sample could not be performed.

The remaining subsample was acidified with HNO<sub>3</sub> to approximately pH 2 and analyzed for Al, Ba, Ca, K, Mg, Mo, Na, Si, and Sr by ICAP. Standard solutions were prepared from Al-metal, BaCl<sub>2</sub>, CaCO<sub>3</sub>, KCl, MgO, (NH<sub>4</sub>)<sub>2</sub>MoO<sub>4</sub>, NaCl, Na<sub>2</sub>SiO<sub>3</sub>·9H<sub>2</sub>O, and SrCO<sub>3</sub> and verified against EPA7 and EPA19 standard reference solutions. Over the duration of the study, the prepared standards were within ±3% of the standard reference solution values. Spiked and diluted sample concentration analyses were within ±4% of the sample results for the elements analyzed. The fractions of the total soluble Ca that occurs as Ca<sup>2+</sup>(aq) and of the total soluble Mo that occurs as MoO<sub>4</sub><sup>2-</sup>(aq) were calculated by use of the chemical equilibrium computer model GEOCHEM (23). The GEOCHEM model was chosen over the PHREEQE model to describe the spent oil shale leachates because of the greater number of ion association reactions considered, ease of use for multicomponent systems, and ability to consider or input specific species (e.g., S<sub>2</sub>O<sub>3</sub><sup>2-</sup>) to the model. Ion association reactions that involve calcium and molybdenum, and the corresponding association constants that were used in the calculations, are listed in Table I.

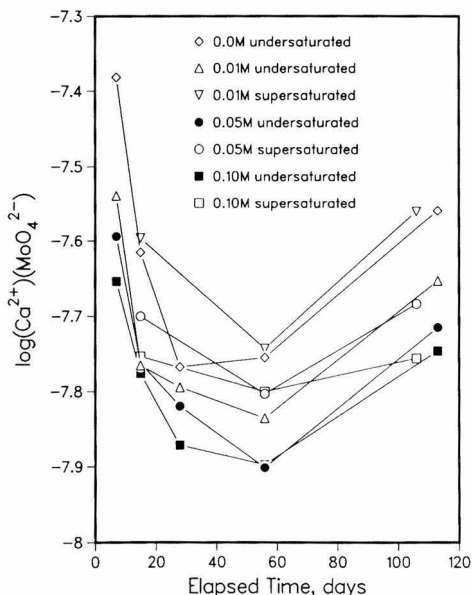
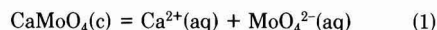


Figure 1. Calculated ion activity products as a function of elapsed time for the CaMoO<sub>4</sub>(c) solubility experiments. The ion pairs CaMoO<sub>4</sub><sup>0</sup>(aq) and KMoO<sub>4</sub>(aq) are not considered in the calculations.

### Results and Discussion

The dissolution of CaMoO<sub>4</sub>(c) can be described by the following reaction:



Assuming equilibrium and unit activity of the solid phase

$$\log K_{\text{sp}} = \log (\text{Ca}^{2+}) + \log (\text{MoO}_4^{2-}) \quad (2)$$

where  $K_{\text{sp}}$  is the equilibrium constant of dissolution for the reaction in eq 1, and the parentheses denote the thermodynamic activity of the species enclosed. The right side of eq 2 may also be defined as the logarithm of the ion activity product (log IAP). This definition is not contingent upon the existence of equilibrium. If it can be ascertained that CaMoO<sub>4</sub>(c) is in equilibrium with the aqueous solution, and that the solid is in its standard state, the measured log IAP = log  $K_{\text{sp}}$ .

Measured log IAP values for the CaMoO<sub>4</sub>(c) solubility experiments are plotted as a function of elapsed time in Figure 1. The log IAP values vary as a function of time and background electrolyte concentration. In general, CaMoO<sub>4</sub>(c) decreases in solubility with increasing background electrolyte concentrations. Further, minimum CaMoO<sub>4</sub>(c) solubility occurs at an elapsed time of 56 days. The variability in IAP with time and background electrolyte concentration (Figure 1) suggests that significant ion pairs containing Ca<sup>2+</sup> and MoO<sub>4</sub><sup>2-</sup> have not been properly considered in the calculations. Possible soluble species that should be included in the calculations are CaMoO<sub>4</sub><sup>0</sup>(aq) and KMoO<sub>4</sub>(aq). The fact that CaMoO<sub>4</sub>(c) has the greatest solubility in the deionized-distilled water system, in which Ca and Mo are the only components, indicates that the ion pair CaMoO<sub>4</sub><sup>0</sup>(aq) must be considered. This adjustment would effectively reduce the activities of both Ca<sup>2+</sup>(aq) and MoO<sub>4</sub><sup>2-</sup>(aq) and reduce log IAP. Further, it may also be necessary to consider the formation of the KMoO<sub>4</sub>(aq) species, because  $K$  is a component of the background electrolyte. A preliminary evaluation of the solubility data included the CaMoO<sub>4</sub><sup>0</sup>(aq)

**Table II. Analysis of Variance for the Multiple Linear Regression Analysis of eq 10**

$$\sum \text{Ca} \sum \text{Mo} = K_{\text{sp}} X_1 + Q_2 K_{\text{sp}} X_2 + Q_1 K_{\text{sp}} X_4 + Q_1 Q_2 K_{\text{sp}} X_5 + \epsilon$$

predictor	coeff	SD	t ratio <sup>a</sup>
$\epsilon$	$4.097 \times 10^{-9}$	$5.187 \times 10^{-9}$	0.79
$X_1$	$8.706 \times 10^{-9}$	$2.599 \times 10^{-9}$	3.35**
$X_2$	$1.708 \times 10^{-7}$	$7.000 \times 10^{-8}$	2.44*
$X_4$	$1.626 \times 10^{-5}$	$1.165 \times 10^{-6}$	9.12**
$X_5$	$3.548 \times 10^{-4}$	$6.313 \times 10^{-5}$	5.62**

$$R^2 = 0.977$$

source	df <sup>b</sup>	SS <sup>b</sup>	MS <sup>b</sup>	F <sup>a,b</sup>
regression	4	$7.057 \times 10^{-14}$	$1.764 \times 10^{-14}$	530.28**
error	49	$1.630 \times 10^{-15}$	$3.327 \times 10^{-17}$	
total	53	$7.220 \times 10^{-14}$		

<sup>a</sup>\*Significance at the 0.02 level of probability; \*\*significance at the 0.01 level of probability. <sup>b</sup>df, degrees of freedom; SS, sum of squares; MS, mean squares; F, variance ratio.

species in the model calculations. The association constant for the formation of this species was varied until the calculated log IAP values for the 28-day, 0 and 0.01 M ionic strength systems were equivalent. Similar calculations for the 28-day, 0.05 and 0.10 M ionic strength systems produced less negative log IAP values, with log IAP increasing with increasing ionic strength. This suggests that a potassium molybdate ion pair must also be considered in the CaMoO<sub>4</sub>(c) solubility calculations.

Thermodynamic data for calcium and potassium molybdate ion pairs are tabulated only by Wagman et al. (17). They listed a Gibbs standard free energy of formation values ( $\Delta G_f^\circ$ ) of -1389.9 kJ mol<sup>-1</sup> for CaMoO<sub>4</sub>(aq), and a  $\Delta G_f^\circ$  value of -1402.9 kJ mol<sup>-1</sup> for K<sub>2</sub>MoO<sub>4</sub>(aq). However, taking into account the appropriate stoichiometries, these values are simply the summation of the  $\Delta G_f^\circ$  values of Ca<sup>2+</sup>(aq) (-553.54 kJ mol<sup>-1</sup>), K<sup>+</sup>(aq) (-283.26 kJ mol<sup>-1</sup>), and MoO<sub>4</sub><sup>2-</sup>(aq) (-836.38 kJ mol<sup>-1</sup>) from Wagman et al. (17). Free energy values for KMoO<sub>4</sub>(aq) are not available in the literature. Thus, for this study, the required thermodynamic properties of the calcium and potassium molybdate ion pairs must be generated from the solubility data.

The total measured concentrations of Ca and Mo in solution may be written as

$$\sum \text{Ca} = [\text{Ca}^{2+}] + [\text{CaOH}^+] + [\text{CaNO}_3^+] + [\text{Ca}(\text{NO}_3)_2^0] + [\text{CaMoO}_4^0] \quad (3)$$

and

$$\sum \text{Mo} = [\text{MoO}_4^{2-}] + [\text{HMoO}_4^-] + [\text{H}_2\text{MoO}_4^0] + [\text{CaMoO}_4^0] + [\text{KMoO}_4^-] \quad (4)$$

where the brackets denote the molar concentration of the species enclosed. It can be shown from the data used to generate Figure 1 that the CaOH<sup>+</sup>(aq), CaNO<sub>3</sub><sup>+</sup>(aq), Ca(NO<sub>3</sub>)<sub>2</sub><sup>0</sup>(aq), H<sub>2</sub>MoO<sub>4</sub><sup>0</sup>(aq), and HMoO<sub>4</sub><sup>-</sup>(aq) species do not significantly contribute to  $\sum \text{Ca}$  and  $\sum \text{Mo}$ . Thus, the mass balance equations for  $\sum \text{Ca}$  and  $\sum \text{Mo}$  (eq 3 and 4) can be rewritten in terms of activities and activity coefficients ( $\gamma$ s):

$$\sum \text{Ca} = (\text{Ca}^{2+})/\gamma \text{Ca}^{2+} + (\text{CaMoO}_4^0)/\gamma \text{CaMoO}_4^0 \quad (5)$$

and

$$\sum \text{Mo} = (\text{MoO}_4^{2-})/\gamma \text{MoO}_4^{2-} + (\text{CaMoO}_4^0)/\gamma \text{CaMoO}_4^0 + (\text{KMoO}_4^-)/\gamma \text{KMoO}_4^- \quad (6)$$

The following relationships are also defined:

$$K_{\text{sp}} = (\text{Ca}^{2+})(\text{MoO}_4^{2-}) \quad (7)$$

$$Q_1 = (\text{CaMoO}_4^0)/(\text{Ca}^{2+})(\text{MoO}_4^{2-}) \quad (8)$$

$$Q_2 = (\text{KMoO}_4^-)/(K^+)(\text{MoO}_4^{2-}) \quad (9)$$

where  $K_{\text{sp}}$  is the previously defined CaMoO<sub>4</sub>(c) equilibrium solubility product constant (eq 2),  $Q_1$  is the CaMoO<sub>4</sub>(aq) ion association constant, and  $Q_2$  is the KMoO<sub>4</sub>(aq) ion association constant. Multiplying eq 5 by eq 6, substituting eq 7-9 where appropriate, and rearranging yields

$$\sum \text{Ca} \sum \text{Mo} = K_{\text{sp}} X_1 + K_{\text{sp}} Q_2 X_2 + Q_1^2 K_{\text{sp}}^2 X_3 + Q_1 K_{\text{sp}} X_4 + Q_1 Q_2 K_{\text{sp}} X_5 + \epsilon \quad (10)$$

where  $\epsilon$  is the random error associated with the regression model and

$$X_1 = 1/\gamma \text{Ca}^{2+} \gamma \text{MoO}_4^{2-}$$

$$X_2 = (K^+)/\gamma \text{Ca}^{2+} \gamma \text{CaMoO}_4^0$$

$$X_3 = (1/\gamma \text{CaMoO}_4^0)^2$$

$$X_4 = [(\text{Ca}^{2+})/\gamma \text{Ca}^{2+} \gamma \text{CaMoO}_4^0] + [(\text{MoO}_4^{2-})/\gamma \text{MoO}_4^{2-} \gamma \text{CaMoO}_4^0]$$

$$X_5 = (K^+)(\text{MoO}_4^{2-})/\gamma \text{CaMoO}_4^0 \gamma \text{KMoO}_4^- \quad (11)$$

The equilibrium constants ( $K_{\text{sp}}$ ,  $Q_1$ , and  $Q_2$ ) appear as regression parameters in eq 10, which can be least-squares fitted (multiple linear regression analysis) to the solubility data.

A solution to eq 10 can only be obtained by iterative approximation, because the activities and the activity coefficients are a function of the magnitude of the equilibrium constants. The iteration process was initiated with the (Ca<sup>2+</sup>), (MoO<sub>4</sub><sup>2-</sup>), (K<sup>+</sup>), and  $\gamma$  values generated by PHREEQE for elapsed times  $\geq 28$  days without considering the CaMoO<sub>4</sub>(aq) and KMoO<sub>4</sub>(aq) pairs. Multiple-regression analysis provided estimates of  $K_{\text{sp}}$ ,  $Q_1$ , and  $Q_2$ . The analytical data from the solubility experiments and the  $Q_1$  and  $Q_2$  values were then input to the PHREEQE program to yield a new set of activity and activity coefficient data. Linear regression of these data produced a new set of estimated equilibrium constants. The iteration process was complete when successive iterations produced identical equilibrium constant estimates. Note that  $K_{\text{sp}}$  is required to generate  $Q_1$  and  $Q_2$  values, and that  $Q_1$  and  $Q_2$  can be obtained from a number of regression parameters in eq 10. The coefficient of  $X_1$  was combined with the coefficient of  $X_2$  to generate  $Q_2$ . Similarly, the coefficient of  $X_1$  was combined with the coefficient of  $X_4$  to generate  $Q_1$ . The multiple linear regression coefficient for the  $X_3$  term was negative for the first iteration and is, therefore, nonsensical. Further, this term did not significantly contribute to the regression model. The  $X_3$  term was deleted from subsequent regression analyses. The coefficient of  $X_5$  was used as a check. In general,  $Q_1$  or  $Q_2$  values calculated from the  $X_5$  coefficient were not significantly different from those generated from the  $X_4$  and  $X_2$  coefficients. Further, the error (standard deviation) associated with generating either of the association constants from the  $X_5$  coefficient was greater than the error when the constants were generated from  $X_4$  and  $X_2$  coefficients.

Analysis of variance data for the last iteration of eq 10 are listed in Table II. All variables in the equation, with the exception of the error term, are significantly different from zero and, thus, contribute significantly to the model that describes the variability of  $\sum \text{Ca} \sum \text{Mo}$ . The equilibrium constants generated from the regression analysis were  $\log K_{\text{sp}} = -8.06$ ,  $\log Q_1 = 3.09$ , and  $\log Q_2 = 1.29$ . The

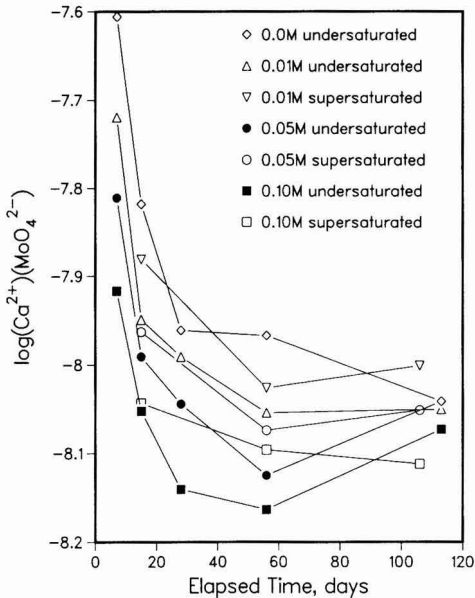


**Figure 2.** Calculated ion activity products as a function of elapsed time for the  $\text{CaMoO}_4(\text{c})$  solubility experiments. The ion pairs  $\text{CaMoO}_4^0(\text{aq})$  and  $\text{KMoO}_4^-(\text{aq})$  are considered in the calculations.

fraction of total soluble Ca occurring as  $\text{Ca}^{2+}(\text{aq})$  and of total soluble Mo occurring as  $\text{MoO}_4^{2-}(\text{aq})$  were recalculated by the PHREEQE model, which included the  $\text{CaMoO}_4^0(\text{aq})$  and  $\text{KMoO}_4^-(\text{aq})$  species and the newly generated ion association constants. The newly generated log IAP values are plotted as a function of elapsed time in Figure 2. The aqueous solutions appear to equilibrate with  $\text{CaMoO}_4(\text{c})$  after a 28-day equilibration period. There still exists some variability in log IAP as a function of background electrolyte concentration. However, the variability in the log IAP values could not be reduced further by independently altering log  $Q_1$  and log  $Q_2$  values. A mean log  $K_{\text{sp}}$  of  $-8.05$  ( $+0.05, -0.06$ ) was determined by averaging over all background electrolyte concentrations, undersaturated and supersaturated initial conditions, and elapsed reaction times of 28 days and greater.

The fraction of total soluble Ca occurring as  $\text{Ca}^{2+}(\text{aq})$  and of total soluble Mo occurring as  $\text{MoO}_4^{2-}(\text{aq})$  in the  $\text{CaMoO}_4(\text{c})$ -spiked spent oil shale systems was calculated by using the chemical equilibrium computer model GEOCHEM. The aqueous species considered for total soluble Ca and Mo included the  $\text{CaMoO}_4^0(\text{aq})$  and  $\text{KMoO}_4^-(\text{aq})$  species. The activity relationships of the spiked spent oil shale systems are illustrated in Figure 3. The spiked spent oil shale aqueous solutions are supersaturated with respect to  $\text{CaMoO}_4(\text{c})$ . The TR8 solutions are supersaturated to a greater degree than are the PPP4 solutions. Correspondingly, the TR8 solutions have higher concentrations of sodium ( $964\text{--}980 \text{ mg L}^{-1}$  at 28 days and  $1080\text{--}1120 \text{ mg L}^{-1}$  at 56 days) than the PPP4 solutions ( $317\text{--}330 \text{ mg L}^{-1}$  at 28 days and  $353\text{--}369 \text{ mg L}^{-1}$  at 56 days). Because  $\text{CaMoO}_4(\text{c})$  is present in these equilibrium systems, the solution activity data should fall on the  $\text{CaMoO}_4(\text{c})$  stability line. The fact that this does not occur, coupled with the observation that solutions highest in sodium are supersaturated to the greatest extent with respect to  $\text{CaMoO}_4(\text{c})$ , suggests that a sodium molybdate ion pair may be forming.

An ion association constant for the formation of  $\text{NaMoO}_4^-(\text{aq})$  was predicted with an iterative estimation

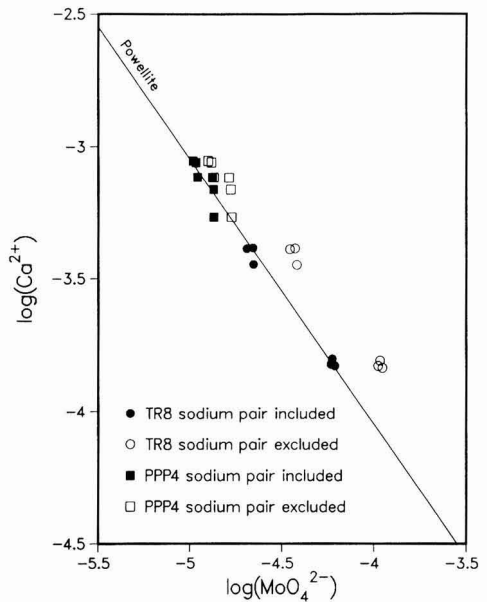


**Figure 3.** Solubility relationships in  $\text{CaMoO}_4(\text{c})$ -spiked spent oil shale systems.

technique similar to that used to generate  $Q_1$  and  $Q_2$ . The total measured concentration of Mo in the equilibrium spiked spent oil shale extracts may be written

$$\sum \text{Mo} = [\text{MoO}_4^{2-}] + [\text{CaMoO}_4^0] + [\text{KMoO}_4^-] + [\text{NaMoO}_4^-] \quad (12)$$

Equation 12 can be expressed in terms of activities, activity coefficients, and ion association constants:

$$\sum \text{Mo} = (\text{MoO}_4^{2-})/\gamma_{\text{MoO}_4^{2-}} + Q_1 K_{\text{sp}}/\gamma_{\text{CaMoO}_4^0} + Q_3(\text{Na}^+)(\text{MoO}_4^{2-})/\gamma_{\text{NaMoO}_4^-} + Q_2(\text{K}^+)(\text{MoO}_4^{2-})/\gamma_{\text{KMoO}_4^-} \quad (13)$$

where

$$Q_3 = (\text{NaMoO}_4^-)/(\text{Na}^+)(\text{MoO}_4^{2-}) \quad (14)$$

If  $(\text{Na}^+)/\gamma_{\text{NaMoO}_4^-} = \sum \text{Na}$  and  $(\text{K}^+)/\gamma_{\text{KMoO}_4^-} = \sum \text{K}$  are assumed, then eq 13 can be rearranged and written as a linear regression equation with  $Q_3$  as the predictor variable:

$$\sum \text{Mo} - Q_1 K_{\text{sp}}/\gamma_{\text{CaMoO}_4^0} - K_{\text{sp}}/(\text{Ca}^{2+})\gamma_{\text{MoO}_4^{2-}} - K_{\text{sp}} Q_2 \sum \text{K}/(\text{Ca}^{2+}) = Q_3 K_{\text{sp}} \sum \text{Na}/(\text{Ca}^{2+}) + \epsilon \quad (15)$$

The initial solution of eq 15 for  $Q_3$ , by linear regression analysis using the parameters generated by GEOCHEM (using the analytical data from all spiked spent oil shale extracts), did not consider  $\text{NaMoO}_4^-(\text{aq})$  in the model calculations. GEOCHEM was rerun using the estimated  $Q_3$  to describe the formation of  $\text{NaMoO}_4^-(\text{aq})$  in the spiked spent oil shale extracts. The iterative process was continued until a constant log  $Q_3$  value of 1.66 was obtained. Linear regression analysis results are presented in Table III.

When  $\text{NaMoO}_4^-(\text{aq})$  is included in the geochemical modeling, the  $\text{CaMoO}_4(\text{c})$ -spiked spent oil shale equilibrium solutions are in equilibrium with  $\text{CaMoO}_4(\text{c})$  (Figure 3). A comparison of spent oil shale and spiked spent oil shale extracts (Figure 4) indicates that the TR8 and PPP4

**Table III. Analysis of Variance for the Linear Regression Analysis of eq 15**

$$\{\sum \text{Mo} - Q_1 K_{sp} / \gamma \text{CaMoO}_4^0 - K_{sp} / (\text{Ca}^{2+}) \gamma \text{MoO}_4^{2-} - Q_2 K_{sp} \sum \text{K} / (\text{Ca}^{2+})\} = Q_3 K_{sp} \sum \text{Na} / (\text{Ca}^{2+}) + \epsilon$$

predictor	coeff	SD	t ratio <sup>a</sup>	
$\epsilon$	-0.00000219	0.00000342	-0.64	
$K_{sp} \sum \text{Na} / (\text{Ca}^{2+})$	45.729	2.293	19.94**	
$R^2 = 0.976$				
source	df <sup>b</sup>	SS <sup>b</sup>	MS <sup>b</sup>	F <sup>a,b</sup>
regression	1	$2.899 \times 10^{-8}$	$2.899 \times 10^{-8}$	398.52**
error	10	$7.273 \times 10^{-10}$	$7.273 \times 10^{-10}$	
total	11	$2.971 \times 10^{-8}$		

<sup>a</sup>\*\*\*Significance at the 0.01 level of probability. <sup>b</sup>See Table II footnote.

**Table IV. Total Soluble Molybdenum Distribution in Spent Oil Shale and CaMoO<sub>4</sub>(c)-Spiked Spent Oil Shale Solutions (Values in % of  $\sum \text{Mo}$ )<sup>a</sup>**

sample	molybdenum species			
	MoO <sub>4</sub> <sup>2-</sup>	CaMoO <sub>4</sub> <sup>0</sup>	KMoO <sub>4</sub> <sup>-</sup>	NaMoO <sub>4</sub> <sup>-</sup>
	Nonspiked			
PPP4-28d	51.6	29.5	1.8	17.2
PPP4-56d	55.4	24.1	2.0	18.5
TR8-28d	45.4	10.9	2.3	41.4
TR8-56d	43.7	5.0	3.1	48.2
	Spiked			
PPP4-28d	52.5	27.8	1.8	17.9
PPP4-56d	56.8	21.8	2.1	19.3
TR8-28d	46.6	9.6	2.2	41.5
TR8-56d	48.7	3.6	2.9	44.8

<sup>a</sup>Mean distributions of triplicate samples.

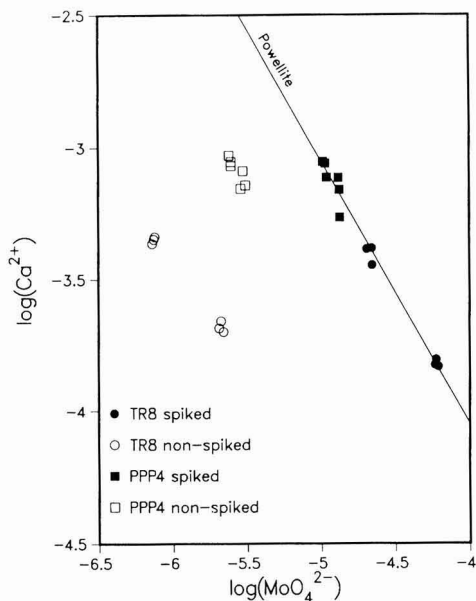


**Figure 4.** Solubility relationships in nonspiked and CaMoO<sub>4</sub>(c)-spiked spent oil shale systems.

equilibrium solutions are undersaturated with respect to CaMoO<sub>4</sub>(c). If CaMoO<sub>4</sub>(c) were present in the spent oil shale samples, the TR8 and PPP4 activities would plot on the CaMoO<sub>4</sub>(c) stability line. Because this does not occur, CaMoO<sub>4</sub>(c) is not controlling the concentrations of Mo in TR8 and PPP4 leachates. Further, these results imply that CaMoO<sub>4</sub>(c) is absent from the TR8 and PPP4 samples.

The results of this study cast doubt on the prediction by previous investigators: Mo concentrations in spent oil shale leachates are controlled by CaMoO<sub>4</sub>(c) precipitation. Stollenwerk and Runnells (9) predicted that molybdenum concentrations in the first pore volume of spent oil shale leachates were controlled by CaMoO<sub>4</sub>(c) precipitation. Similarly, the modeling results of Essington et al. (5) and Essington and Spackman (7) suggested that CaMoO<sub>4</sub>(c) occurred in several spent oil shales. None of these investigators, however, considered the formation of CaMoO<sub>4</sub><sup>0</sup>(aq), KMoO<sub>4</sub><sup>-</sup>(aq), and NaMoO<sub>4</sub><sup>-</sup>(aq) in their geochemical modeling. In the TR8 and PPP4 equilibrium solutions, these ion pairs significantly contribute to the total soluble Mo concentrations (Table IV). Similarly, these molybdate ion pairs should be significant in other

spent oil shale leachates, as such leachates, by their very nature, have elevated concentrations of Ca, Na, and K.

### Summary and Conclusions

The equilibrium solubility of CaMoO<sub>4</sub>(c) was determined in deionized-distilled water and KNO<sub>3</sub> solutions. The equilibrium experiments were carried out under four different background electrolyte concentration conditions for reaction times of up to 113 days. Equilibrium was approached from both undersaturated and supersaturated initial conditions. Solutions were in equilibrium with CaMoO<sub>4</sub>(c) at reaction times of 28 days and greater. The calculated log K<sub>sp</sub> for the dissolution of CaMoO<sub>4</sub>(c) is -8.05. Generation of this constant requires that formation of CaMoO<sub>4</sub><sup>0</sup>(aq) and KMoO<sub>4</sub><sup>-</sup>(aq) ion pairs be considered in the calculations. The ion association constants for the formation of CaMoO<sub>4</sub><sup>0</sup>(aq) and KMoO<sub>4</sub><sup>-</sup>(aq) were determined by an iterative estimation technique. An estimated log Q for the formation of CaMoO<sub>4</sub><sup>0</sup>(aq) is 3.09. Similarly, an estimated log Q for the formation of KMoO<sub>4</sub><sup>-</sup>(aq) is 1.29.

Calcium molybdate solubility in CaMoO<sub>4</sub>(c)-spiked and nonspiked TR8 (combusted) and PPP4 (directly retorted) spent oil shale equilibrium solutions was evaluated. The CaMoO<sub>4</sub>(c)-spiked spent oil shale solutions were initially evaluated as being supersaturated with respect to CaMoO<sub>4</sub>(c). However, the data show that the NaMoO<sub>4</sub><sup>-</sup>(aq) ion pair may significantly contribute to total soluble Mo. The spiked spent oil shale solution data were used to generate a log Q for the formation of NaMoO<sub>4</sub><sup>-</sup>(aq) of 1.66. When this species is included in the geochemical model analyses of the spiked spent oil shale solutions, the solutions are in equilibrium with CaMoO<sub>4</sub>(c). Geochemical model analyses show that CaMoO<sub>4</sub>(c) did not control Mo concentrations in the TR8 and PPP4 (nonspiked) equilibrium solutions. Further, these data suggest that CaMoO<sub>4</sub>(c) may not occur in spent oil shales. Thus, predictions of molybdenum behavior in spent oil shale disposal environments, based on the assumption that CaMoO<sub>4</sub>(c) is present, would be erroneous.

**Registry No.** K-HNO<sub>3</sub>, 7757-79-1; KMoO<sub>4</sub><sup>-</sup>, 12396-30-4; NaMoO<sub>4</sub><sup>-</sup>, 121484-00-2; Mo, 7439-98-7; Calcium molybdate, 37367-98-9; water, 7732-18-5.

### Literature Cited

- (1) Kilkelly, M. K.; Lindsay, W. L. *J. Environ. Qual.* **1982**, *11*, 422-427.
- (2) Schwab, A. P.; Lindsay, W. L.; Smith, P. J. *J. Environ. Qual.* **1983**, *12*, 301-304.
- (3) Reddy, K. J.; Lindsay, W. L. *J. Environ. Qual.* **1987**, *16*, 168-171.

- (4) Reddy, K. J.; Lindsay, W. L.; Boyle, F. W., Jr.; Redente, E. F. *J. Environ. Qual.* **1986**, *15*, 129-33.
- (5) Essington, M. E.; Spackman, L. K.; Harbour, J. D.; Hartman, K. D. *Physical and Chemical Characteristics of Retorted and Combusted Western Reference Oil Shale*; U.S. Dept. of Energy Report DOE/MC/11076-2453; Office of Scientific and Technical Information: Oak Ridge, TN, 1987.
- (6) Essington, M. E. *Environ. Geol. Water Sci.* **1989**, *13*, 59-66.
- (7) Essington, M. E.; Spackman, L. K. *Recarbonation of Retorted Oil Shale: The Influence on Mineralogy and Leachate Chemistry*; U.S. Dept. of Energy Report DOE/FE/60177-2433; Office of Scientific and Technical Information: Oak Ridge, TN, 1986.
- (8) Spackman, L. K.; Essington, M. E. In *Eastern Oil Shale Symposium Proceedings*; Lexington, KY, Nov 30-Dec 2, 1988.
- (9) Stollenwerk, K. G.; Runnells, D. D. *Environ. Sci. Technol.* **1981**, *15*, 1340-1346.
- (10) Stark, J. M.; Redente, E. F. *J. Environ. Qual.* **1986**, *15*, 282-288.
- (11) Zelikman, A. N.; Prosenkova, T. E. *Russ. J. Inorg. Chem. (Engl. Transl.)* **1961**, *6*, 105-107.
- (12) O'Hare, P. A. G.; Jensen, K. J.; Hoekstra, H. R. *J. Chem. Thermodyn.* **1974**, *6*, 681-691.
- (13) Naumov, G. B.; Ryzhenko, B. N.; Khodakovskiy, I. L. *Handbook of Thermodynamic Data*; Trans. G. J. Soleimani; PB-226 722; National Technical Information Service: Springfield, VA, 1974.
- (14) Smith, R. M.; Martell, A. E. In *Inorganic Complexes; Critical Stability Constants, Vol. 4*; Plenum Press: New York, 1976.
- (15) Vlek, P. L. G.; Lindsay, W. L. *Soil Sci. Soc. Am. J.* **1977**, *41*, 42-46.
- (16) Robie, R. A.; Hemingway, B. S.; Fisher, J. R. *Thermodynamic Properties of Minerals and Related Substances at 298.15 K and 1 Bar (10<sup>5</sup> Pascals) Pressure and at Higher Temperatures*. *U.S. Geol. Surv. Bull.* **1978**, No. 1452.
- (17) Wagman, D. D.; Evans, W. H.; Parker, V. B.; Schumm, R. H.; Harlow, I.; Bailey, S. M.; Churney, K. L.; Nutall, R. L. *J. Phys. Chem. Ref. Data* **1982**, *11*, Supplement. No. 2.
- (18) Reddy, K. J.; Drever, J. I. *Geochemical Modeling Research Related to the Surface Disposal of Processed Oil Shale Solid Waste*; U.S. Dept. of Energy Report DOE/MC/11076-2443; Office of Scientific and Technical Information: Oak Ridge, TN, 1987.
- (19) Kittrick, J. A.; Peryea, F. J. *Soil Sci. Soc. Am. J.* **1986**, *50*, 243-247.
- (20) Essington, M. E. *Soil Sci. Soc. Am. J.* **1988**, *52*, 1566-1570.
- (21) Parkhurst, D. L.; Thorstenson, D. C.; Plummer, L. N. *Water-Resour. Invest. (U.S. Geol. Surv.)* **1980**, No. WRI 80-96.
- (22) Merriam, N. W.; Cha, C. Y.; Sullivan, S. *Production of Spent Oil Shale by Simulation of Surface Oil Shale Retorting Processes*; U.S. Dept. of Energy Report DOE/FE/60177-2439; Office of Scientific and Technical Information: Oak Ridge, TN, 1987.
- (23) Sposito, G.; Mattigod, S. V. *GEOCHEM: A Computer Program for the Calculation of Chemical Equilibria in Soil Solutions and Other Natural Water Systems*; University of California, Riverside Publishers: Riverside, CA, 1980.
- (24) Sadiq, M.; Lindsay, W. L. *Selection of Standard Free Energies of Formation for Use in Soil Chemistry*. *Colo. State Univ. Exp. Stn. Bull.* **1979**, No. 134.
- (25) Baes, C. F., Jr.; Mesmer, R. E. *The Hydrolysis of Cations*; Krieger: Malabar, FL, 1986.
- (26) Martell, A. E.; Smith, R. M. *Critical Stability Constants*; First Supplement; Plenum Press: New York, 1982; Vol. 5.
- (27) Santschi, P. H.; Schindler, P. W. *J. Chem. Soc., Dalton Trans.* **1974**, 181-184.

Received for review November 22, 1988. Accepted October 6, 1989. This work was supported by U.S. Dept. of Energy Cooperative Agreement DE-FC21-86MC11076.

## Binding of Metal Ions by Particulate Biomass Derived from *Chlorella Vulgaris* and *Scenedesmus Quadricauda*

Patricia O. Harris and Gerald J. Ramelow\*

Department of Chemistry, McNeese State University, Lake Charles, Louisiana 70609-0455

The metal-binding properties of particulate materials derived from *Chlorella vulgaris* and *Scenedesmus quadricauda* were investigated. The two algae showed very similar binding patterns for silver, copper, cadmium, and zinc. Most metal uptake from aqueous solutions occurred within 1 min. Copper, cadmium, and zinc binding was very pH-dependent; Ag was bound very strongly over a wide pH range. General binding efficiencies decrease in the order Ag > Cu > Cd > Zn. Coincidental metals caused both enhancements and depressions in metal binding. Copper, cadmium, and zinc can easily be stripped from the algae with a pH 2 buffer with little loss of binding efficiency over several binding-stripping cycles. Copper, cadmium, and zinc were retained by a chromatographic column packed with particulate biomass of *S. quadricauda* immobilized in a cross-linked copolymer of ethyl acrylate-ethylene glycol dimethacrylate. Copper was successfully desorbed by using a pH gradient.

### Introduction

The removal of toxic or economically important ions from dilute aqueous solutions is of great importance from an environmental and industrial viewpoint. A number of techniques have been used for removing metals from waste

streams (1). The most generally used is the lime treatment, which removes heavy metals by precipitation as hydroxides. Removal of Cd, Pb, and Hg is not complete, however. Metal recovery is not normally performed but can be accomplished through electrodeposition.

These high-technology processes require expensive equipment and monitoring systems. An alternative treatment system that uses inexpensive materials to remove and reclaim metals could be of technical and commercial interest. Recently the possibilities of using biomass for the cleanup of industrial waste streams and polluted waters has been recognized (2). Research has been focused on the identification of microbial species that can possibly be used to recover metal ions from industrial wastes, radioactive wastes, and mining wastes (3-6).

The accumulation of metals by microorganisms may take place by any or a combination of the following processes: (1) entrapment by cellular components, (2) active transport across the cell membrane, (3) cation exchange or complexation, and (4) adsorption. The first two mechanisms are associated with living cells; the latter two can only occur with dead cells and may be termed "biosorption". The use of dead microbial cells is more advantageous for water treatment in that dead organisms are not affected by toxic wastes.

Metal uptake by microbial cells is quite rapid, occurs to a high degree, and is frequently selective (7-9). *Rhizopus arrhizus* biomass can bind U in excess of 0.5 mmol of U/g of cell dry weight (10) and *Chlorella vulgaris* binds base metals and precious metals with a high affinity for gold—0.5 mmol of Au/g of cell dry weight (11). Biosorption with *C. vulgaris* occurs between pH 5 and 7 with a variety of metals, such as Cu, Pb, Cd, Ni, and U (12).

The immobilization of algae in a polyacrylamide matrix has been used to demonstrate the potential for removal and selective recovery of metals from waste streams (12, 13). Darnall et al. (12) immobilized *C. vulgaris* in a polyacrylamide matrix and demonstrated a successful elution scheme for the binding and selective recovery of Cu, Zn, Au, and Hg from an equimolar mixture. Darnall et al. (14) also developed a technique for immobilizing algae in silica to produce a material superior to polyacrylamide in strength and stability.

The study described herein was initiated to study the biosorption properties of particulate biomass derived from two green algae, *C. vulgaris* and *Scenedesmus quadricauda*, using the metals Ag, Cu, Cd, and Zn. The aim was to thoroughly investigate the adsorption and desorption patterns for each algal biomass and study the effect of time, pH, complexing agents, anions and cations, including coincidental metals, on the biosorption properties of the algae. The two algal species used were chosen because of known differences in size and shape (15) and cell-wall composition (16). The relatively unknown metal-accumulating properties of *S. quadricauda* could be compared with the better understood *C. vulgaris*.

A potentially very important use of algae is in the removal and recovery of metals from waste streams. Another possible application is to concentrate metals from natural waters to increase the sensitivity of existing analytical techniques (17, 18). To study this algal biomass must be immobilized in an inert solid material that can be packed into columns. An effective method of immobilization is to encapsulate the algal cells in a cross-linked polymer network. The retention of metals by adsorption on a polymer containing *C. vulgaris* and *S. quadricauda* in a chromatographic column and subsequent elution is described.

#### Experimental Section

**Growth and Processing of Algae.** Algal cultures were purchased from a commercial supplier (Carolina Biological Supply Co.). Both *C. vulgaris* (no. 15-2075) and *S. quadricauda* (no. 15-2510) were grown as unialgal cultures rather than axenic cultures. Algae were cultivated in separate 10-gal glass tanks with plastic frames with Alga-Gro Freshwater medium and Joubert concentrate (19) as a nutrient enrichment medium. Illumination was provided by either fluorescent lamps or Gro-Lux lamps. The pH of the culture was controlled to within 6.5-7.0 by bubbling 5% CO<sub>2</sub> in air through air stones. Temperature was allowed to vary between 20 and 25 °C. Synchronous growth was maintained by alternating periods of 16 h of light with 8 h of darkness.

Algal cells were harvested from the aquaria by manually syphoning the algae culture and refilling to the original level with fresh nutrients. Approximately 1 L of culture was removed and refrigerated prior to separation of algal cells. The algal cells were separated by centrifugation for 15 min. The concentrated cells were washed by adding twice-demineralized water to the tubes and mixing with a glass stirring rod. This procedure was repeated twice. The resulting concentrated, washed algal samples were pipeted into ampules for freeze-drying or poured into

beakers for oven-drying. Algal samples that could not be dried immediately were frozen.

When drying was completed, the cells were sieved through a 250- $\mu$ m screen (N.B.S. no. 60), mixed, and stored in a freezer. The freeze-dried algae were a low-density material, bright green in color, which easily passed through the sieve. In contrast, the oven-dried material was dark green in color and required mortar and pestle grinding before the material could be passed through the sieve. The homogeneous materials were placed in labeled plastic bottles, capped under nitrogen gas, and stored in a freezer.

**Instrumentation.** Metal analyses were performed on a Perkin-Elmer Model 370A atomic absorption (AA) spectrophotometer, equipped with a Model 2100 graphite furnace atomizer. Flameless atomization was used for metals at concentrations below the optimum conditions of flame AA. Background correction was used with all flameless measurements. The standard additions method was used to eliminate matrix effects. Reagent blank corrections were made for every analysis.

**Chemicals.** Atomic spectral standards (1000 mg/L) were used to prepare all Ag, Cu, Cd, and Zn solutions and working standards. Metal solutions and working standards were prepared fresh daily by dilution of the stock solutions. To eliminate contamination, all glassware and plasticware were cleaned before use with Alconox detergent, followed by an overnight soaking in 50% nitric acid. Reagent blanks were always run for every sample.

The pH 2 buffer was prepared with potassium chloride and hydrochloric acid (20). The pH 4 buffer was prepared from potassium acid phthalate or from color-coded commercial solutions. The pH 7 and 10 buffers were color-coded, commercial buffer solutions. The pH 12.4 buffer was prepared from a calcium carbonate powder of low alkali content (21).

**Immobilization of Algal Biomass in a Cross-Linked Polymer.** A cross-linked polymer was prepared by an emulsion polymerization technique using ethyl acrylate and ethylene glycol dimethacrylate monomers. A 0.5-g sample of freeze-dried *S. quadricauda* was reacted with 26.8 g of ethyl acrylate and 0.775 g of ethylene glycol dimethacrylate to yield 16.47 g of alga-polymer (dry weight). An aqueous suspension of dried alga was added to the polymerization vessel simultaneously with a mixture of the monomers to incorporate algal cells into the polymer. After completion of the polymerization, the alga-polymer was washed, dried, sieved, and loaded into a chromatographic column (Kontes no. K422250; length 250 mm, i.d. 1.2 cm, 125-mL capacity). This column was subsequently used to study metal adsorption and desorption properties of the alga-polymer.

#### Results and Discussion

The natural concentrations of Ag, Cu, Cd, and Zn in acid-digested, freeze-dried samples of both algae grown in aquaria under the conditions described previously are listed in Table I. With the exception of Ag, the concentrations of the metals studied are similar in both species. Copper and Zn were found in the largest amounts within the algal biomass ( $\mu$ g of metal/g of alga). Both of these metals are considered trace nutrients, essential for the growth of algae, that must be present in synthetic growth medium (22).

**Effect of Time on Metal Binding.** The percentage of Cu bound as a function of contact time between the particulate biomass and metal solution is presented in Figure 1. Approximately 90% of the Cu sorption took place within 15 min; the remainder was adsorbed at a slower rate. The kinetics of metal uptake by algae have

**Table I. Natural Concentrations of Ag, Cu, Cd, and Zn in *C. vulgaris* and *S. quadricauda* Grown in Synthetic Medium**

metal	mg of metal/kg of alga	
	<i>C. vulgaris</i>	<i>S. quadricauda</i>
Ag	17.5	2.1
Cu	60.7	67.5
Cd	3.6	1.4
Zn	111.3	110.0

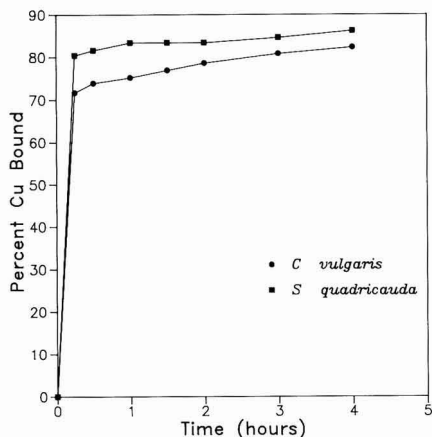


**Figure 1.** Kinetics of copper binding by freeze-dried particulate matter of *C. vulgaris* and *S. quadricauda*. Algal biomass, 5 mg/mL, was mixed with 5 mg/L Cu at pH 5. At intervals, 5-mL aliquots were removed and centrifuged and the supernatants analyzed for Cu content.

been studied and are believed to involve two stages (8). Metal uptake rapidly occurs during the first stage and is thought to be a passive physical adsorption or ion exchange (8, 23, 24). The kinetics of metal uptake by the two species were very similar, with *S. quadricauda* showing more affinity for Cu. A 15-min standard reaction time was selected for all subsequent algal-binding reactions.

**Effect of Particulate Algal Biomass Concentration.** Experiments were conducted with Ag and Cu to determine the binding of these metals with particulate biomass concentrations of 1–5 mg/mL. The results shown in Table II demonstrate the strong affinity of both algae for Ag and Cu. A similar binding pattern was seen with Zn and Cd, except that lower amounts of these metals were bound. A 5 mg/mL algal concentration was chosen as a standard amount for all subsequent experiments.

**Effect of pH.** Several techniques have been used to study biomass systems that are highly pH sensitive. One method is to have no pH control (25); another method is to readjust the solution pH with dilute nitric acid or sodium hydroxide (7, 26), or potassium hydroxide (25). Several workers have used buffer systems such as potassium biphthalate (11), 2-(*N*-morpholine)ethanesulfonic acid (MES) (25), or sodium acetate–acetic acid (1, 26) to regulate pH.

An acetate buffer system was chosen for pH control and to ensure a common medium for all binding experiments. An additional advantage of an acetate buffer is that the metals studied are soluble as acetate salts. Copper adsorption was measured in sodium acetate solutions ranging in concentration from  $1 \times 10^{-5}$  to 1.0 mol/L at pH 5.0. Copper adsorption by both species was strongly affected when the sodium acetate concentration exceeded 0.1 M. Obviously an acetate complex forms that reduces the Cu

**Table II. Effect of Algal Concentration on the Binding of Copper and Silver by Freeze-Dried *C. vulgaris* and *S. quadricauda*<sup>a</sup>**

algal concn, mg/mL	mg/L Ag sorbed	% Ag bound	mg/L Cu sorbed	% Cu bound
<i>C. vulgaris</i>				
1	3.26	86.9	1.77	33.6
2	3.73	99.3	2.87	57.4
3	3.74	99.7	3.63	72.6
4	3.74	99.8	4.12	82.4
5	3.75	99.9	4.36	87.2
6	3.74	99.8	4.63	92.6
<i>S. quadricauda</i>				
1	2.16	60.3	2.77	55.4
2	3.10	82.7	4.01	80.2
3	3.56	94.9	4.41	88.2
4	3.66	97.6	4.64	92.8
5	3.67	97.9	4.71	94.2
6	3.71	98.9	4.75	95.0

<sup>a</sup> Initial silver and copper concentrations were 3.75 and 5.0 mg/L, respectively. All reactions were carried out in 0.05 M sodium acetate at pH 5.

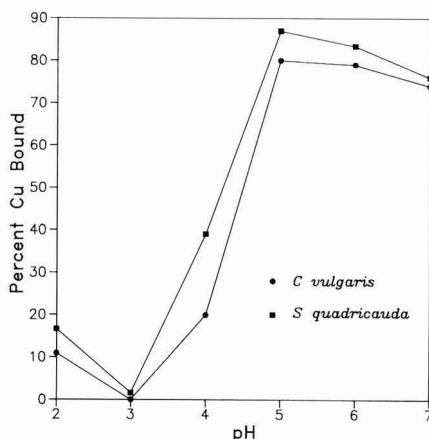


**Figure 2.** Effect of pH on copper binding by freeze-dried *C. vulgaris* and *S. quadricauda*. Algal biomass, 5 mg/mL, was mixed with 5 mg/L Cu at pH 5. After a 15-min reaction time the solution was centrifuged and the supernatant analyzed for Cu content.

available for binding to algae. Silver binding, in contrast, was only slightly depressed. The use of a 0.05 M sodium acetate solution resulted in the highest binding efficiency for both biomasses and was used in the prewashing steps.

The binding of Cu, Cd, and Zn by both types of algal particulate matter was very pH-dependent. The effect was most pronounced for Cu (Figure 2). The binding efficiency of Cu increased rapidly with pH in the range 3–5, with a maximum value seen at pH 5. The decrease in binding after pH 5 may be due to decreased solubility of metal ions. The adsorption edge, the greatest change of adsorption within a narrow pH range (27), occurs between pH 4 and 5. Binding efficiency was near zero at pH 3 and only slightly better at pH 2. Crist et al. (28) suggested that zero-point charge, or isoelectric point, would be found at pH 3. Above this the algal cells would have a net negative charge. This would lead to electrostatic attractions between positively charged cations and negatively charged binding sites, hence the rapid rise in binding efficiency between pH 3 and 5. Below pH 3 the sites would have a positive charge. Since some binding is observed, there must be an additional type of binding that is not electrostatic. This is in accord with recent observations by Crist



**Table III. Effect of Coincidental Metal(s) on Binding of Silver by *C. vulgaris* and *S. quadricauda*<sup>a</sup>**

$\mu\text{g Ag}$ reacted	coincidental metal(s)	<i>C. vulgaris</i>		<i>S. quadricauda</i>	
		$\mu\text{g Ag}$ sorbed	% Ag sorbed	$\mu\text{g Ag}$ sorbed	% Ag sorbed
25	none	24.75	99.00	24.60	98.40
25	25 $\mu\text{g Cu}$	24.60	98.40	23.25	93.00
10	10 $\mu\text{g Cd}$	9.95	99.00	9.80	98.00
5	5 $\mu\text{g Zn}$	4.95	99.00	4.95	99.00
10	10 $\mu\text{g Cu, Cd}$	9.95	99.50	9.90	99.00
5	5 $\mu\text{g Zn, Cd}$	4.95	99.00	4.95	99.00
10	10 $\mu\text{g Cd, Zn}$	9.90	99.00	9.85	98.50
10	10 $\mu\text{g Cu, Cd, Zn}$	9.95	99.50	9.90	99.00

<sup>a</sup> Reactions were carried out in 5 mL of 0.05 M sodium acetate at pH 5 using a freeze-dried algal concentration of 4 mg/mL for Ag-Cu reaction and 5 mg/mL for all other reactions.

**Table IV. Effect of Coincidental Metal(s) on Binding of Copper by *C. vulgaris* and *S. quadricauda*<sup>a</sup>**

$\mu\text{g Cu}$ reacted	coincidental metal(s)	<i>C. vulgaris</i>		<i>S. quadricauda</i>	
		$\mu\text{g Cu}$ sorbed	% Cu sorbed	$\mu\text{g Cu}$ sorbed	% Cu sorbed
25	none	22.10	88.40	22.10	88.40
25	25 $\mu\text{g Ag}$	19.05	76.20	17.70	70.80
10	10 $\mu\text{g Cd}$	8.85	88.50	9.45	94.50
5	5 $\mu\text{g Zn}$	4.50	90.00	4.65	93.00
10	10 $\mu\text{g Ag, Cd}$	9.75	97.50	9.45	94.50
5	5 $\mu\text{g Ag, Zn}$	4.75	95.00	4.85	97.00
10	10 $\mu\text{g Cd, Zn}$	8.70	87.00	9.50	96.00
10	10 $\mu\text{g Ag, Cd, Zn}$	8.60	86.00	9.45	94.50

<sup>a</sup> Reactions were carried out in 5 mL of 0.05 M sodium acetate at pH 5 using a freeze-dried algal concentration of 4 mg/mL for Ag-Cu reactions and 5 mg/mL for all other reactions.

et al. (29) that not all binding sites for Cu in algae are electrostatic in nature.

The pattern of metal binding as a function of pH was similar for Cd and Zn, except that some binding of these metals occurred at pH 3. The adsorption edge for Cd and Zn was also found to lie between pH 4 and 5. The binding efficiencies were greatest at pH 7 and decreased as pH decreased. Silver binding is mainly pH-independent. Binding efficiency was close to 100% in the pH range 3-7. Even at pH 2 binding efficiency still exceeded 80%. Binding patterns of Cd, Zn, and Ag as a function of pH for both algae were very similar.

**Effect of Salts and Complexing Agents.** Samples of algal biomass were exposed to solutions of sodium nitrate and calcium nitrate in a Cu metal solution buffered at pH 5. Both salts decreased binding efficiency; the greatest effect was seen with sodium nitrate. Both algal species were affected in a similar manner by these salts.

Crist et al. (28) studied the adsorption of Cu by the green alga *Vaucheria* sp. in the presence of complexing agents that form positive, negative, or neutral complexes. Silver forms a great variety of soluble complex ions, with the most stable complexes having the L-Ag-L structure that is seen for the silver-ammonium complex ion (30). To study this complex, solutions containing equal concentrations of Ag (5 mg/L) were prepared with increasing concentrations of ammonium hydroxide. The equilibrium was shifted toward the complex ion by increasing the pH of the metal solution (31). Binding of Ag decreased gradually with increasing solution pH, but at pH 12 the binding efficiency was still 80%. In the presence of sodium thiosulfate, the binding efficiency for Ag by *S. quadricauda* was severely decreased.

**Effect of Coincidental Metal(s).** In wastewaters the metal(s) of interest is(are) usually found in a matrix containing other metals as well. To test the binding of each metal in the presence of others, a series of experiments was designed to study the effect of the presence of a second metal or a combination of several metals on the ability of a biomass to adsorb one specific metal. Table III shows that the adsorption of Ag by both algae was not greatly affected by the presence of equal amounts of coincidental metals, either individually or in combination. A slight decrease in Ag binding was seen in both algae for the Ag-Cu combination.

Copper binding by both algae (Table IV) was decreased in the presence of equal amounts of Ag. At lower concentrations of Ag no depression was observed. In reactions involving Cu mixed with Cd, Cd-Zn, and Ag-Cd-Zn, Cu binding by *C. vulgaris* was either slightly enhanced, depressed, or not affected. For these same metal interactions

with *S. quadricauda*, an increase in Cu binding was observed. Both algae showed increased Cu binding in the presence of Ag-Cd and Ag-Zn. Binding sites on the algal cell walls must have a greater affinity for Ag binding compared to that for Cu. Copper binding can be enhanced by the presence of other metals. *S. quadricauda* was able to bind more Cu except when Ag was the only coincidental metal.

Cadmium binding was noticeably affected by the presence of Ag, Cu, and Zn, either alone or in combination. The presence of Ag had the least effect on the Cd binding efficiency. Copper showed a greater effect, but in general, when alone or in combination, the presence of coincidental metals decreased the binding of Cd. *C. vulgaris* showed a greater decrease in Cd binding compared to *S. quadricauda*.

Zinc binding with both algal species was affected in a very similar manner by the presence of coincidental metals. When one coincidental metal was present, Cd had the greatest effect in decreasing Zn binding while Ag had the least effect. When two coincidental metals were present, the combination of Cu-Cd had the greatest effect, and Ag-Cu had the least effect in decreasing Zn binding. The presence of all coincidental metals caused the greater decrease in Zn binding when compared to other combinations. As was observed for Cd, Zn binding is affected much more in *C. vulgaris* than in *S. quadricauda*.

**Metal Binding Capacity.** A set of experiments was devised to determine "binding capacity", the total amount of bound metal per weight of biomass. Washed algal biomass was exposed to an aliquot of a metal solution, mixed for 15 min, centrifuged, decanted, and mixed with a fresh aliquot of metal solution. This procedure was repeated not only to determine the amount of metal load that the biomass could adsorb, but also to determine the pattern of binding. This pattern would be expected to be similar to a breakthrough curve on an ion-exchange column.

For *C. vulgaris* the Ag binding capacity patterns (Figure 3A) were very similar regardless of drying procedures. *S. quadricauda* showed similar patterns (Figure 3B). Thus, the manner in which biomass was processed prior to metal reaction apparently does not have much effect on metal-binding capacity. Silver was biosorbed at the highest level of all metals studied.

Copper was the metal next most strongly adsorbed by both species. Figure 4A shows the Cu-binding capacity patterns seen for *C. vulgaris* biomass that had been processed by different drying methods. Figure 4B demonstrates the higher binding capacity of *S. quadricauda* over *C. vulgaris* for Cu. Drying temperature differences did not

**Table V. Adsorption-Desorption of Silver by *C. vulgaris*<sup>a</sup>**

series	μg Ag bound	% Ag bound	first strip μg Ag	second strip μg Ag	μg Ag desorbed	μg Ag not desorbed
1	18.65	99.47	2.65	1.85	4.50	14.15
2	18.59	99.15	5.40	3.40	8.80	9.79
3	18.47	98.51	6.55	4.10	10.65	7.82
4	18.41	98.19	8.35	4.85	13.20	5.21
5	18.39	98.08	8.20	5.10	13.30	5.09
6	18.45	98.40	7.95	4.65	12.60	5.85
7	18.37	97.97	11.40	4.70	16.10	2.27
8	18.15	96.80	12.64	3.75	16.39	1.76
<b>totals</b>	<b>147.48</b>				<b>95.54</b>	<b>51.94</b>

<sup>a</sup> In each series Ag was bound to algae by mixing 5 mL of 4 mg/mL algal suspension with 3.75 mg/L Ag in 0.05 M sodium acetate at pH 5.0. Algae were stripped of Ag by two successive 5-mL aliquots of 0.05 M sodium acetate at pH 2.0.

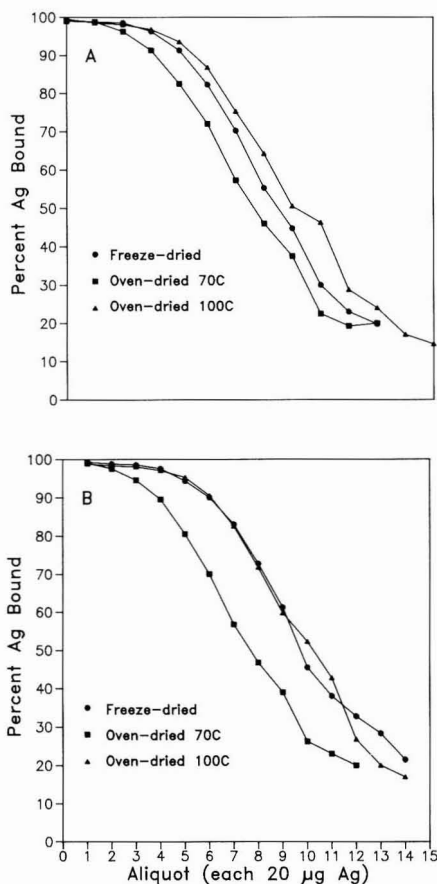


**Figure 3.** Silver binding capacity of (A) *C. vulgaris* and (B) *S. quadricauda*. Algal biomass, 5 mg/mL, was mixed with 4 mg/L Ag at pH 5.

affect binding the same in these two species.

Cadmium was adsorbed to a much lower degree than either Ag or Cu. Zinc was adsorbed to the least degree for all metals studied and showed a pattern similar to Cd. In general, *S. quadricauda* was able to bind metals to a greater degree than *C. vulgaris*. The general binding ability of these organisms for the metals studied, in order of decreasing affinity, was Ag > Cu > Cd > Zn.

**Adsorption-Desorption Series.** Bound metals can be removed from algal biomass with a wash or stripping step

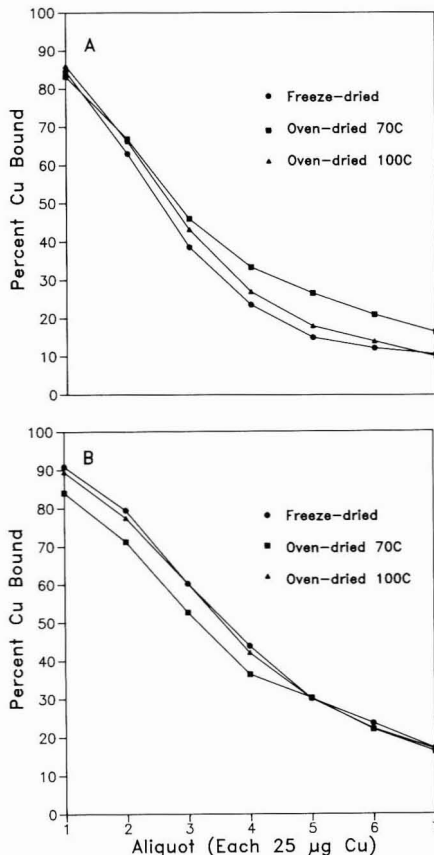


**Figure 4.** Copper binding capacity of (A) *C. vulgaris* and (B) *S. quadricauda*. Algal biomass, 5 mg/mL, was mixed with 5 mg/L Cu at pH 5.

and then subsequently be rebound. This binding-stripping cycle can be described as an adsorption-desorption series. Each biomass was studied with use of an adsorption-desorption series with each metal to determine the stability and reversibility of the binding process. Greene (1) showed that algal binding sites reacted either in a "pH-dependent" or a "pH-independent" manner. The sites that could be acid stripped of bound metals were described as "pH-dependent sites". An adsorption-desorption series can provide information about the number of these sites as well as the predominate type of site at which metals are sorbed.

**Table VI. Adsorption-Desorption of Silver by *S. quadricauda*<sup>a</sup>**

series	μg Ag bound	% Ag bound	first strip μg Ag	second strip μg Ag	μg Ag desorbed	μg Ag not desorbed
1	18.30	97.60	3.80	2.55	6.35	11.95
2	18.50	98.67	6.50	2.95	9.45	9.07
3	18.41	98.19	6.95	4.25	11.20	7.21
4	18.37	97.97	8.55	4.70	13.25	5.12
5	18.37	97.97	8.25	5.00	13.25	5.12
6	18.39	98.08	8.85	4.60	13.45	4.94
7	18.49	98.61	8.74	3.45	12.19	6.30
8	18.23	97.23	9.45	3.75	13.20	5.03
totals	147.06				92.34	54.72

<sup>a</sup> In each series Ag was bound to algae by mixing 5 mL of 4 mg/mL algal suspension with 3.75 mg/L Ag in 0.05 M sodium acetate at pH 5.0. Algae were stripped of Ag by two successive 5-mL aliquots of 0.05 M sodium acetate at pH 2.0.

**Table VII. Adsorption-Desorption of Copper by *C. vulgaris*<sup>a</sup>**

series	μg Cu bound	% Cu bound	first strip μg Cu	second strip μg Cu	μg Cu desorbed	μg Cu not desorbed
3× prewash						
1	21.50	86.00	17.60	2.80	20.40	1.10
2	19.60	78.40	19.15	1.55	20.70	-1.10
3	19.05	76.20	18.20	1.45	19.65	-0.60
totals	60.15				60.75	-0.60
no prewash						
1	17.55	70.20	16.55	1.45	18.00	-0.45
2	20.00	80.00	19.00	1.95	20.95	-0.95
3	19.10	76.40	18.10	1.95	20.05	-0.95
totals	56.65				59.00	-2.35

<sup>a</sup> In each series Cu was bound to algae by mixing 5 mL of 5 mg/mL algal suspension with 5 mL of 5.00 mg/L Cu in 0.05 M sodium acetate at pH 5.0. Algae were stripped of Cu by two successive 5-mL aliquots of 0.05 M sodium acetate at pH 2.0.

**Table VIII. Adsorption-Desorption of Copper by *S. quadricauda*<sup>a</sup>**

series	μg Cu bound	% Cu bound	first strip μg Cu	second strip μg Cu	μg Cu desorbed	μg Cu not desorbed
1	23.40	93.60	14.72	3.88	18.60	4.80
2	22.60	90.40	19.60	3.50	23.10	-0.50
3	22.20	88.80	20.60	3.33	23.93	-1.73
4	22.25	89.00	20.70	2.90	23.60	-1.35
5	22.13	88.52	20.93	1.00	21.93	0.20
6	21.95	87.80	20.35	2.63	22.98	-1.03
7	21.85	87.40	20.25	2.58	22.83	-0.98
totals	156.38				156.97	-0.59

<sup>a</sup> In each series copper was bound to algae by mixing 5 mL of 5 mg/mL prewashed algal suspension with 5 mL of 5.00 mg/L Cu in 0.05 M sodium acetate at pH 5.0. Algae were stripped of Cu by two successive 5-mL aliquots of 0.05 M sodium acetate at pH 2.0.

The results of an adsorption-desorption series for the binding of Ag by freeze-dried *C. Vulgaris* are given in Table V. In the first binding-stripping cycle, approximately 76% of the bound Ag was bound at sites that are pH-independent and remained bound to the biomass. As the series continued, a lower proportion of the Ag was bound at these sites. By the fourth cycle only 28% was bound, and at the eighth cycle less than 10% was bound. As the cycles were continued, a greater proportion of the Ag was removed in the first wash step. *S. quadricauda* (Table VI) bound more Ag at pH-independent sites, but these sites are bound at a much slower rate. By the eighth cycle, approximately 28% of the Ag bound was on pH-independent sites. Both species bind Ag to either pH-independent or pH-dependent sites, with an initial affinity for the pH-independent sites.

*C. vulgaris* biomass prewashed with pH 2 buffer had a larger first series adsorption for Cu (Table VII) than the same biomass that had not been previously washed. There appears to be little difference, however, in the amount of

Cu that was bound in subsequent adsorptions. The prewash may serve as a desorbing step by removing contaminant metals bound to the surface of the biomass. This emphasizes the importance of removal of contaminant metals that may become desorbed during later steps. The general adsorption-desorption pattern for Cu determined with *S. quadricauda* is shown in Table VIII. The binding of Cu occurs primarily at pH-dependent sites. Although two pH 2 washes were used to strip each cycle, the majority of the bound Cu was removed in the first wash step.

Nearly all the bound Cd and Zn was removed with one wash step, even at different pH values, as illustrated for Cd in Figure 5. Zinc was the only metal, of those studied, that desorbed more metal than had been previously adsorbed by the algal biomass. Perhaps Zn, which was found at high concentrations in the acid digest, was not completely removed by the three prewash steps and was leached in small amounts during the desorption steps.

**Immobilization of Algal Biomass.** Techniques to immobilize biomass, while still maintaining the biosorptive

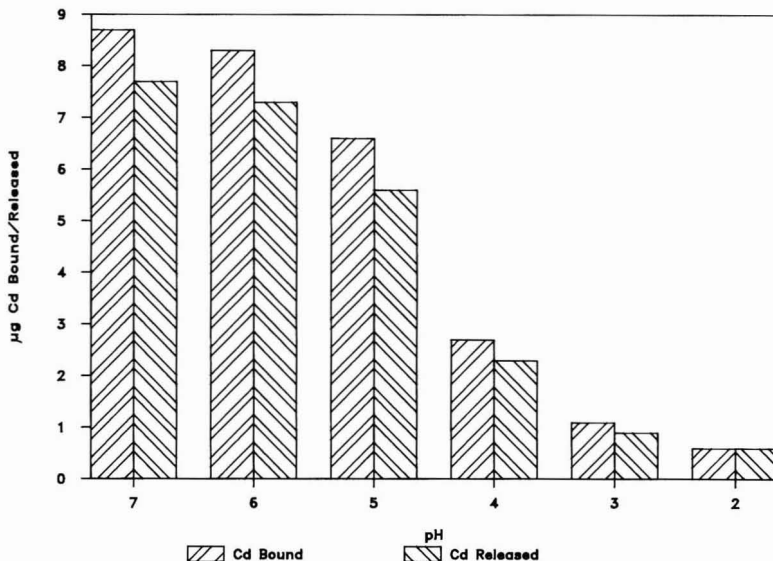


**Figure 5.** Adsorption-desorption series for cadmium by freeze-dried *C. vulgaris* and *S. quadricauda*. Alga solution, 5 mL of 5 mg/mL, was mixed with 5 mL of a 2 mg/L Cd solution at pHs from 2 to 7. Bound metal was stripped from algal cells with two separate 5-mL aliquots of 0.05 M sodium acetate at pH 2.

capacity and selectivity, have generated a new class of biological adsorbents called "biosorbents" (2). Binding and selective recovery of metal ions has been demonstrated with *C. vulgaris* immobilized in a polyacrylamide matrix (12). However, polyacrylamide is far from ideal as an immobilizing medium for algal cells. Control experiments with a polyacrylamide column containing no algal cells showed that Cu(III), Au(II), and Zn(II) were not retained by the column but Hg(II) was retained (12). Also, polyacrylamide gels are not very strong mechanically; since they have high water concentrations (80–95%), leakage occurs through the open network (32).

An ethyl acrylate-ethylene glycol dimethacrylate copolymer, which had a cross-linked network, was developed in the present study to immobilize algal biomass. Separate columns were prepared containing freeze-dried biomass of *C. vulgaris* and *S. Quadricauda* immobilized in a polymer. The alga-polymers were packed into chromatographic columns as described previously.

To test this new type of immobilized algae column, 75 mL of a 4 mg/L solution of Cu, Cd, and Zn in 0.075 M sodium acetate at pH 6.0 were eluted through the *S. quadricauda* column at an average flow rate of 0.7 mL/min. The effluent was collected in 5-mL aliquots and residual metal concentration determined. Figure 6 shows that the maximum capacity of the polymer column to adsorb Cd and Zn was reached immediately, while Cu capacity had not been exceeded. At 70 mL, the polymer column had bound 92.25% of the Cu. At 75 mL, the column had absorbed 1.62 µmol of Cd, and 2.96 µmol of Zn. Binding capacity data with *S. quadricauda* predicted an adsorption of 3.5 µmol of both Cd and Zn. Blank correction for Cd and Zn binding was less than 0.01 µmol of each metal/g of polymer.

Another alga-polymer was prepared in the same manner with *C. vulgaris*. The column was eluted with Cu until the capacity for Cu had decreased. A blank polymer column eluted to determine the blank correction yielded 0.01 µmol Cu/g of polymer. After correcting for the blank, an adsorption of 45 µmol of Cu/g of alga was determined for *C. vulgaris* and 59.5 µmol for *S. quadricauda*. Binding ca-

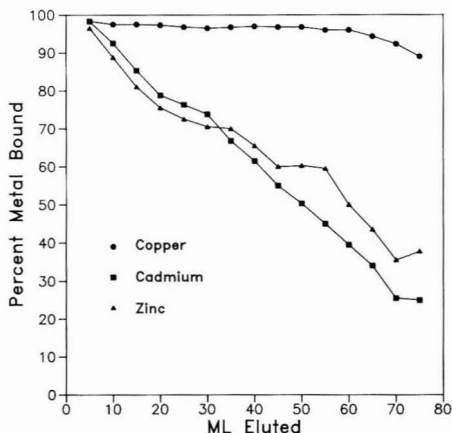


**Figure 6.** Adsorption of copper, cadmium, and zinc by a column of *S. quadricauda* immobilized in ethyl acetate-ethylene glycol dimethacrylate copolymer. A 75-mL sample of a 4 mg/L solution of Cu, Cd, and Zn in 0.05 M sodium acetate at pH 6 was eluted through the column at 0.7 mL/min. Portions (5 mL) were collected and tested for residual metal content.

capacity studies using freeze-dried algae predicted 39 and 54 µmol binding of Cu per g for *C. vulgaris* and *S. quadricauda*, respectively. Copper was bound by both immobilized biomasses to a larger degree than measured in the binding capacity studies. The column was exposed to the metal solution until no further binding of Cu occurred and probably approached the ultimate binding capacity for Cu.

To study desorption properties of the alga-polymer column for Cu, a column of immobilized *S. quadricauda* was rinsed with a 15-mL portion of 0.075 M sodium acetate at pH 7 at a flow rate of 2 mL/per min, and then a pH gradient flow was initiated by eluting 5 mL of 0.075 M sodium acetate at pH 6 through the column. Following this, each 5 mL eluted through the column was 0.5 pH unit less than the pH of the previous solution (i.e., pH 5.5–2.0).

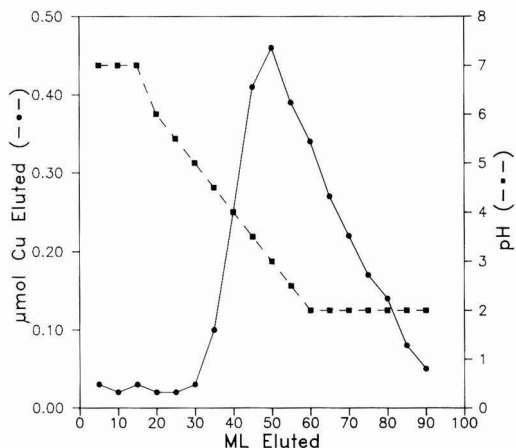


**Figure 7.** Desorption of copper from a column of *S. quadricauda* immobilized in ethyl acetate-ethylene glycol dimethacrylate copolymer. Copper was eluted with 0.075 M sodium acetate by use of a pH gradient from 7 to 2 at a flow rate of 2 mL/min. Portions (5 mL) were collected and tested for pH and Cu concentration.

Elution was continued until a total volume of 30 mL of 0.075 M sodium acetate at pH 2 had been eluted. Each 5 mL of eluent was tested for pH and Cu; the results are plotted in Figure 7. The total Cu desorbed, 3.04 µmol, was approximately 70% of the Cu adsorbed by this polymer. This compares well to the first cycle desorption of 79% seen in the adsorption-desorption series for this alga. The effectiveness of the alga-polymer in binding copper is apparent. Furthermore, the bound Cu could easily be stripped off the column with a pH gradient.

### Summary

*C. vulgaris* and *S. quadricauda* were both able to bind strongly the four metals studied, with particularly strong affinity for Ag and Cu. The metal binding of *S. quadricauda* equaled or exceeded that found for *C. vulgaris* with less effects from coincidental metals. Recently, Mahan et al. (17) observed remarkably similar adsorption patterns for a variety of elements by three different algal strains. It is important to study the metal-accumulating characteristics of many algal species to identify possible individual differences and exploit them. For example, *Eisenia bicyclis* has been shown to have an unusually high affinity for copper (33). There may be other metal-specific species. One source of such organisms might be industrial or mine waste streams. Only organisms that can tolerate high levels of certain metals might be able to live in such an environment and may show an increased metal-binding capacity.

The use of either metal-specific or nonspecific organisms immobilized in columns for the removal of toxic or recoverable metals from waste streams appears very promising. Immobilizing algae in copolymers may lead to a whole new class of biosorbents, which will function like more traditional ion-exchange or chelating resins. As Kubiak et al. (34) recently pointed out, an additional advantage of biosorbent columns is that ions such as the alkali and alkaline-earth elements, which often interfere in analytical procedures, are effectively removed because they are not bound efficiently to algae. The use of algae to concentrate metals from environmental samples with metals at part-per-trillion levels, such as natural waters, and thus increase the sensitivity of existing analytical

techniques will extend the range of environmental analytical chemistry to new low levels of metal detection.

### Acknowledgments

We thank Drs. J. N. Beck, J. D. Tauber, and U. S. Ramelow for their review of the manuscript and constructive criticisms.

**Registry No.** Ag, 7440-22-4; Cu, 7440-50-8; Cd, 7440-43-9; Zn, 7440-66-6.

### Literature Cited

- (1) Greene, B. Recovery of Metal Ions from Aqueous Solutions by Dried *Chlorella vulgaris*. Ph.D. Dissertation, New Mexico State University, Las Cruces, NM, 1985.
- (2) Eccles, H., Hunt, S., Eds. *Immobilization of Ions by Biosorption*; Ellis Horwood Ltd.: Chichester, England, 1986.
- (3) Brierley, C. L. Microbiological mining. *Sci. Am.* **1982**, 44-54.
- (4) Wood, J. M.; Wang, H. K. *Environ. Sci. Technol.* **1983**, 17, 582A-600A.
- (5) Kiff, R. J.; Little, D. R. Biosorption of heavy metals by immobilized fungal biomass. In *Immobilization of Ions by Biosorption*; Eccles, H., Hunt, S., Eds.; Ellis Horwood, Ltd.: Chichester, England, 1986.
- (6) McCready, R. G. L.; Lakshmanan, V. I. Review of bioadsorption research to recover uranium from leach solutions in Canada. In *Immobilization of Ions by Biosorption*; Eccles, H., Hunt, S., Eds.; Ellis Horwood, Ltd.: Chichester, England, 1986.
- (7) Nakajima, A.; Horikoshi, T.; Sakaguchi, T. *Eur. J. Appl. Microbiol. Biotechnol.* **1981**, 12, 76-83.
- (8) Khummongkol, D.; Canterford, G. S.; Fryer, C. *Biotechnol. Bioeng.* **1982**, 24, 2643-2660.
- (9) Les, A.; Walker, R. W. *Water, Air, Soil Pollut.* **1984**, 23, 129-139.
- (10) Tsezos, M.; Volesky, B. *Biotechnol. Bioeng.* **1981**, 23, 583-604.
- (11) Greene, B.; Hosea, M.; McPherson, R.; Henzl, M.; Alexander, M. D.; Darnall, D. *Environ. Sci. Technol.* **1986**, 20, 627-632.
- (12) Darnall, D. W.; Greene, B.; Henzl, M. T.; Hosea, J. M.; McPherson, R. A.; Sneddon, J.; Alexander, M. D. *Environ. Sci. Technol.* **1986**, 20, 206-208.
- (13) Nakajima, A.; Horikoshi, T.; Sakaguchi, T. *Eur. J. Appl. Microbiol. Biotechnol.* **1982**, 16, 88-91.
- (14) Darnall, D. W.; Greene, B.; Hosea, M.; McPherson, R. A.; Henzl, M.; Alexander, M. D. Recovery of heavy metals by immobilized algae. In *Trace Metal Removal from Aqueous Solutions*; Thompson, R., Ed.; Royal Society of Chemistry: London, 1986; Special Publication No. 61.
- (15) Bold, H. C.; Wynne, M. J. *Introduction to the Algae—Structure and Function*, 2nd ed.; Prentice-Hall: Englewood Cliffs, NJ, 1978.
- (16) Loos, E.; Meindl, D. *Planta* **1982**, 156, 270-273.
- (17) Mahan, C. A.; Majidi, V.; Holcombe, J. A. *Anal. Chem.* **1989**, 61, 624-627.
- (18) Zimnik, P. R.; Sneddon, J. *Anal. Lett.* **1988**, 21, 1383-1396.
- (19) Joubert, G. In *Aquatic Toxicology*; O., Nriagu, Ed.; John Wiley & Sons: New York, 1983.
- (20) Weast, R. C. Ed. *Handbook of Chemistry and Physics*, 57th ed. CRC Press: Cleveland, OH, 1976; p D-134.
- (21) *Standard Methods for the Examination of Water and Wastewater*; 14th ed.; Rand, M. C., Greenberg, A. E., Tara, M. J., Franson, M. A., Eds.; American Public Health Association: Washington, DC, 1975; pp 464, 761.
- (22) Manahan, S. E. *Environmental Chemistry*, 2nd ed.; Willard Grant Press: Boston, MA, 1975.
- (23) Sakaguchi, T.; Tsuji, T.; Nakajima, A.; Horikoshi, T. *Eur. J. Appl. Microbiol. Biotechnol.* **1979**, 8, 207-215.
- (24) Hosea, M. *Inorg. Chim. Acta* **1986**, 123, 161-165.
- (25) Townsley, C. C.; Ross, I. S.; Atkins, A. S. Copper removal from a simulated leach effluent using the filamentous fungus *Trichoderma viride*. In *Immobilization of Ions by Biosorption*; Eccles, H., Hunt, S., Eds.; Ellis Horwood, Ltd.: Chichester, England, 1986.

- (26) Ferguson, J.; Bubela, B. *Chem. Geol.* 1974, 13, 163-186.  
 (27) Davis, J. A.; Leckie, J. O. *Environ. Sci. Technol.* 1978, 12, 1309-1315.  
 (28) Crist, R. H.; Oberholser, K.; Shank, N.; Nguyen, M. *Environ. Sci. Technol.* 1981, 21, 1212-1217.  
 (29) Crist, R. H.; Oberholser, K.; Schwartz, D.; Marzoff, J.; Ryder, D.; Crist, D. *Environ. Sci. Technol.* 1988, 22, 755-760.  
 (30) Smith, I. C.; Carson, B. L. In *Silver; Trace Metals in the Environment*; Vol. II; Ann Arbor Science Publishers, Inc.: Ann Arbor, MI, 1977.  
 (31) Hogness, T. R.; Johnson, W. C. *An Introduction to Qualitative Analysis*; Holt, Rinehart and Winston: New York, 1957.  
 (32) *Methods Enzymol.* 1976, 44.  
 (33) Gardea-Torresdey, J.; Darnall, D.; Wang, J. *Anal. Chem.* 1988, 60, 72-76.  
 (34) Kubiak, W. W.; Wang, J.; Darnall, D. *Anal. Chem.* 1989, 61, 468-471.

Received for review September 6, 1988. Revised manuscript received August 28, 1989. Accepted October 5, 1989.

## Mobility of Plutonium and Americium through a Shallow Aquifer in a Semiarid Region

William R. Penrose,<sup>†</sup> Wilfred L. Polzer,<sup>‡</sup> Edward H. Essington,<sup>‡</sup> Donald M. Nelson,<sup>§</sup> and Kent A. Orlandini<sup>\*||</sup>

Transducer Research, Inc., 526 West Franklin Avenue, Naperville, Illinois 60540, Earth and Environmental Science Division, Los Alamos National Laboratory, Los Alamos, New Mexico 87545, Environmental Health and Safety Division, Argonne National Laboratory, Argonne, Illinois 60439, and Environmental Research Division, Argonne National Laboratory, Argonne, Illinois 60439

■ Treated liquid wastes containing traces of plutonium and americium are released into Mortandad Canyon, within the site of Los Alamos National Laboratory, NM. The wastes infiltrate a small aquifer within the canyon. Although laboratory studies have predicted that the movement of actinides in subsurface environments will be limited to less than a few meters, both plutonium and americium are detectable in monitoring wells as far as 3390 m downgradient from the discharge. Between the first and last monitoring wells (1.8 and 3.4 km from the discharge), plutonium concentrations decreased exponentially from 1400 to 0.55 mBq/L. Americium concentrations ranged between 94 and 1240 mBq/L, but did not appear to vary in a systematic way with distance. Investigation of the properties of the mobile actinides indicates that the plutonium and part of the americium are tightly or irreversibly associated with colloidal material between 25 and 450 nm in size. The colloiddally bound actinides are removed only gradually from the groundwater. The fraction of the americium not associated with colloids exists in a low molecular weight form (diameter,  $\leq 2$  nm) and appears to be a stable, anionic complex of unknown composition. The mobile forms of these actinides defeat the forces that normally act to retard their movement through groundwater systems.

### Introduction

Treated waste effluents from the Central Waste Treatment Plant at the Los Alamos National Laboratory have been discharged into Mortandad Canyon since 1963. The canyon drains in an easterly direction from the Parajito Plateau upon which the laboratory complex is located and has been the subject of extensive study (1-5). The shallow alluvium of Mortandad Canyon is composed of lensed sandy to silty clay materials formed by weathering of volcanic rocks (Bandelier Tuff) and contains a small elevated aquifer of  $(20-30) \times 10^3$  m<sup>3</sup> storage capacity (see Figure 1). Annual storm runoff into the canyon ranges from 25 to  $125 \times 10^3$  m<sup>3</sup> per year. Treated waste

effluents are released into the seasonal stream, flow down the canyon and, under ordinary conditions, infiltrate into the tuff within  $\sim 2$  km (1). Surface water may flow as far as 3.4 km beyond the waste outfall during storm events. Subsurface flow represents  $\sim 90\%$  of the water movement in the canyon. Tritium oxide tracer experiments have shown that 85% of the water released from the waste plant is lost through evapotranspiration. Total transit time for the tritium from the waste outfall to a monitoring well 3390 m down the canyon was about a year (2). The water that does not evaporate is assumed to be lost by infiltration into the underlying tuff, because no continuous surface flow exists along the reach of the canyon.

The waste treatment process includes the addition of iron sulfate and lime (6). The precipitation of iron hydroxides and calcium carbonate acts to remove almost all of the actinides from the waste, although traces of <sup>238</sup>Pu, <sup>239,240</sup>Pu, and <sup>241</sup>Am remain in the effluent and are released to the canyon (7, 8).

The shallow aquifer contains a series of monitoring wells. Sampling of these wells has revealed that plutonium and americium are found in the groundwater at distances of 3400 m from the outfall (7, 8). Some of the actinides could be transported to the lower region of the canyon by surface flow during occasional storm events. However, the tritium oxide transit time measurements suggest that the majority of water movement takes place in the subsurface. Reports of plutonium and americium movement in groundwater over distances of even a few meters are rare (9, 10). It was the purpose of this study to determine the true mobility of these actinides in the groundwaters of Mortandad Canyon and to establish the features of either the wastewater or the aquifer that might contribute to enhanced mobility. These studies are part of the United States Department of Energy's Subsurface Science Program, which is developing a better fundamental understanding of contaminant transport in groundwater systems.

Regular monitoring of the effluents and groundwater has confirmed that all effluents are contained within the laboratory boundary, that the concentrations of plutonium and americium have not exceeded the Department of Energy Concentration Guidelines for Controlled Areas, and that no water is derived from Mortandad Canyon for drinking, industrial, or agricultural purposes (11, 12). These trace level actinides, however, act as excellent tracers

<sup>†</sup>Transducer Research, Inc.

<sup>‡</sup>Los Alamos National Laboratory.

<sup>§</sup>Environmental Health and Safety Division, Argonne National Laboratory.

<sup>||</sup>Environmental Research Division, Argonne National Laboratory.

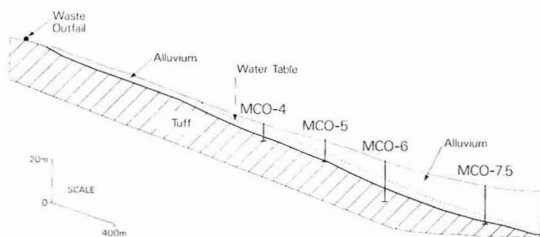


**Figure 1.** Cross-sectional schematic of Mortandad Canyon aquifer system showing the location of the monitoring wells.

**Table I. Surface Sampling Station and Monitoring Wells in Mortandad Canyon (March 1983)<sup>a</sup>**

parameter	surface	MCO-4	MCO-5	MCO-6	MCO-7.5
distance from outfall, m	1900	1807	2235	2660	3390
depth of well, m		5.2	7.3	12.5	18.6
depth to water, m		1.2	4.3	9.1	13.1
pump depth, m		4.4	6.6	11.9	18.0
sampling rate, L/min		4.1	2.8	3.8	1.9

<sup>a</sup> Distances are measured along the stream bed.

to evaluate the potential for colloidal transport of subsurface groundwater contaminants. These contaminants include actinides and other radionuclides, toxic metals, and toxic organic materials.

### Experimental Section

**Sampling.** Sampling took place in May and July 1982 and March 1983, from a series of monitoring wells originally installed by the U.S. Geological Survey. A cross-section diagram of the canyon and the location of the pertinent monitoring wells is shown in Figure 1. Hydrologic characteristics of the sampling stations are listed in Table I. Surface water was sampled from the stream at a location near the first well (MCO-4). An Isco well-sampling pump was used to draw water from the wells at 2–4 L/min. The wells were pumped continuously for 30 min, and then the sample was taken by pumping directly through a 29.3-cm-diameter, 0.45- $\mu\text{m}$  Millipore filter (type HAWP) into 25-L sample bottles, which were completely filled before capping. Measurements of temperature, oxygen, pH, and  $E_h$  were performed by pumping water directly through a series of in-line cells containing the sensors for a dissolved oxygen analyzer (Yellow Springs Instruments, Model 57) and a pH meter (Cole-Parmer Chem-Cadet) with a combination pH electrode and platinum electrode. Subsurface samples were made to 1 M concentration in  $\text{HNO}_3$  and spiked with internal standards of  $^{242}\text{Pu}$  in the reduced (IV) state (13) and  $^{243}\text{Am}$ . For measurements of plutonium oxidation states,  $^{236}\text{Pu}$  was also added in the oxidized (VI) valence state (13). The surface water samples, subsurface samples, and 0.45- $\mu\text{m}$  filters were shipped to Argonne National Laboratory for analysis.

**Actinide Analysis.** The water samples were evaporated to a small volume over low heat and digested with nitric acid. The digest was analyzed for isotopes of plutonium and americium by established methods (14–16). The filters were ashed at 525 °C and the residual ash was weighed. The ash was then dissolved in hydrochloric acid and analyzed for the actinides. The distribution coefficients ( $K_D$ ) were calculated as the ratio of the radioactivity per kilogram of ash to the radioactivity per liter of filtrate.

Contributions of dissolved salts to the ash weights were estimated to be less than 2%.

Oxidation-state distributions of plutonium were measured by the rare-earth fluoride fractionation of Nelson and Lovett (14). The plutonium in the samples was observed to be  $\geq 90\%$  in the reduced, particle-active state.

**Sample Fractionation.** The size distribution of the actinides for a water sample from well MCO-5 was determined by sequential passage of a sample through filters of progressively smaller size. A 15-L sample of water was first filtered through a 0.45- $\mu\text{m}$  Millipore filter. Internal standards of  $^{242}\text{Pu}$  and  $^{243}\text{Am}$  were added to 10 L of the filtrate and 2 days was allowed for exchange with the ambient isotopes. The solution was then filtered through a 0.025- $\mu\text{m}$  (25-nm) Nuclepore polycarbonate filter. Ultrafiltration was carried out with a 100 000 molecular weight (MW) membrane (Amicon Corp., Danvers, MA) under nitrogen pressure in an Amicon Model 2000 apparatus, followed by a 10 000 MW Amicon membrane. The ultrafiltration was not allowed to go to completion because we observed that the concentrated colloidal materials would pass through the filter as the membrane became dry. Near the end of the filtration, the concentrate and the filter were recovered and analyzed separately, and the actinide measurements were combined. The nominal pore sizes of the ultrafiltration membranes were about 5 and 2 nm, respectively.

The filters and concentrates were analyzed as before. In some cases, subsamples of the filtrates were also analyzed as a cross-check on the recovery of the actinides. Since the samples already contained  $^{242}\text{Pu}$  and  $^{243}\text{Am}$ , internal standards of  $^{236}\text{Pu}$  and  $^{244}\text{Cm}$  were used to maintain that actinide recovery was complete. Curium chemical recovery and chemical behavior has been accepted as being indistinguishable from americium.

**Ion-Exchange Properties.** The samples taken for these experiments were pumped from the wells directly through 0.45- $\mu\text{m}$  filters for 10 min into 1-L bottles containing an ion-exchange resin. The liquid was decanted and the resin washed twice with distilled water. The sample and rinse water were combined and evaporated to dryness. The resin was ashed in a muffle furnace and was analyzed for both plutonium and americium. Cationic species were determined with cation-exchange resin (H form, 27 g/L). Anionic forms were similarly detected with anion-exchange resin (Cl form, 27 g/L). Neutral species were determined by contacting samples with mixed cation and anion resins (H and Cl forms, 27 g/L of each) and analyzing the supernatant liquid.

**Other Analyses.** The particulate material was examined using energy-dispersive X-ray fluorescence by the Analytical Chemistry Group of the Chemistry and Laser Science Division of Los Alamos National Laboratory (LANL). Mineralogy of the particulate material was examined using X-ray diffraction, carried out by the Physical Metallurgy Group of the Materials Sciences and Technology Division of LANL. Analyses of ferrous iron and total iron were done by reaction with 1,10-phenanthroline (17). Dissolved silica was determined by the molybdosilicate method (18). Other analytical water chemistry was carried out by the Environmental Science Group at LANL, according to standard methods (19). Waste discharge data were provided by the Waste Management Group of LANL.

### Results and Discussion

**Water Chemistry.** Filtered water samples taken from the surface sampling location and from the four monitoring wells were analyzed for conventional water chemistry parameters (Table II). The most noticeable variations in

**Table II. Chemical and Physical Characteristics of the Waters Sampled in March 1983<sup>a</sup>**

parameter	surface	MCO-4	MCO-5	MCO-6	MCO-7.5
temp, °C		2.8	6.6	7.2	8.0
oxygen	6.5	0.7	0.7	0.3	4.3
pH	10.1	10.0	7.0	6.9	6.4
H <sub>b</sub> , mV	275	205	266	245	303
conductivity, dS/m	1.2	1.2	1.3	1.3	1.4
ammonia	0.6	0.3	0.0	0.0	0.0
fluoride	3.9	6.2	5.5	4.2	0.5
sulfate	137	150	162	161	260
alkalinity (as CaCO <sub>3</sub> )	211	196	167	191	184
carbonate (as CaCO <sub>3</sub> )	141	105	6.6	5.9	0.0
bicarbonate (as CaCO <sub>3</sub> )	63	87	160	185	184
DOC	20	20	21	22	4
nitrate	340	360	430	400	450
nitrite	4.3	4.5	4.6	0.4	0.1
total phosphate (as P)	8.5	19.0	7.4	2.6	0.8
orthophosphate (as P)	6.3	14.3	5.3	2.3	0.5
hydrolyzable P	0.0	0.0	0.0	0.1	0.3
organic P	2.4	4.8	2.1	0.2	0.0
sulfide <sup>b</sup>	nd	nd	nd	nd	nd
silica	3.2	2.5	2.1	2.6	3.0
total iron	2.3	2.7	3.8	2.0	0.1
ferrous iron (% of total iron)	57.8	47.4	27.6	41.1	31.1
aluminum	4.8	4.9	7.0	3.8	0.0
calcium	16.2	8.0	15.9	19.3	60
magnesium	0.6	0.6	3.9	4.9	15.5
potassium	20.4	11.5	5.4	5.5	7.8

<sup>a</sup>All units are in mg/L unless otherwise stated. <sup>b</sup>Sulfide was below limits of detection of 0.004 mg/L.

**Table III. Mineral Phases Predicted To Be Supersaturated in the Surface and Well Water Samples by Using WATEQ<sup>a</sup>**

mineral phase	surface	MCO-4	MCO-5	MCO-6	MCO-7.5
Phases That Remain Supersaturated					
fluoroapatite	xx	xx	xx	xx	xx
iron oxyhydroxides (e.g., goethite, gibbsite, hematite)	xx	xx	xx	xx	xx
Phases That Become Unsaturated with Distance					
calcium carbonate (calcite, aragonite)	x	x	o	o	o
aluminas (boehmite, diaspore)	x	x	xx	x	o
chlorite, prehnite	xx	xx	o	o	o
hydroxyapatite	xx	xx	o	o	o
aluminosilicates (clays, micas, zeolites)	xx	xx	xx	xx	o
silicates (talc, tremolite)	xx	xx	o	o	o
Phases That Are Transient or Become Supersaturated with Distance					
α-alumina	o	o	x	x	o
aluminosilicates	o	o	xx	xx	o
dolomite	o	x	o	o	o
iron phosphates (strengite, vivianite)	o	o	x	x	x

<sup>a</sup>Phases with a positive computed saturation index (CSI) are listed. The codes used in the table are as follows: x, for a CSI ranging from 0 to 3 (slightly supersaturated); xx, for CSI greater than 3 (very supersaturated), and o for negative values (unsaturated).

the water chemistry with distance from the waste outfall were (a) the decreases in phosphate, iron, nitrite, and potassium, (b) the increases in calcium and magnesium, and (c) the decline in pH from the high value in the wastewater to near-neutrality. The alkaline nature of the wastewater could have favored leaching of elements such as silicon and aluminum from the aquifer matrix. As the pH declined with distance, these elements could reprecipitate on immobile surfaces or persist as colloidal materials.

The low oxygen concentrations in the monitoring wells MCO-4, MCO-5, and MCO-6 indicated a situation of potential importance. Under anoxic conditions, we could have expected ferrous iron to be leached from the aquifer matrix. It would have reprecipitated upon encountering oxygen, producing colloidal materials and particulates. In addition, we observed that the measured concentrations of calcium and orthophosphate in surface waters and the MCO-4 well were supersaturated.

To further evaluate these observations, we used the available data in Table II to calculate the predicted

equilibrium concentrations using the WATEQ model (20). Table III lists the mineral phases as identified by WATEQ that could be expected to be supersaturated in the samples. Although the equilibrium model results can only be considered as rough estimates, they do indicate that colloidal materials containing iron oxides, clays, and hydroxy- and fluoroapatites may exist in the subsurface waters and persist as far as the MCO-7.5 well.

Particulate material caught on a 0.45-μm filter was subjected to mineralogical analysis by X-ray fluorescence and X-ray diffraction. X-ray fluorescence analysis confirmed that both calcium and iron were present in the particulate material. The presence of both of these elements in the solid phase was predicted by the WATEQ analysis of the water chemistry data. X-ray diffraction analysis also confirmed that siliceous minerals were present.

**Mobility of Actinides.** The concentrations of <sup>239,240</sup>Pu and <sup>241</sup>Am in water from four selected sampling wells are shown in Figure 2 for May 1982 and March 1983. The



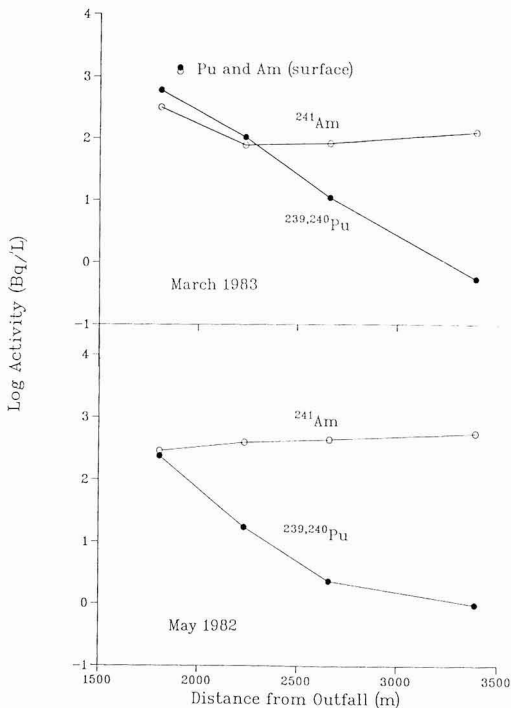


**Figure 2.** Concentrations of plutonium and americium in wells MCO-4, MCO-5, MCO-6, and MCO-7.5 in May 1982 and March 1983. The ordinate is distance in meters from the waste outfall.

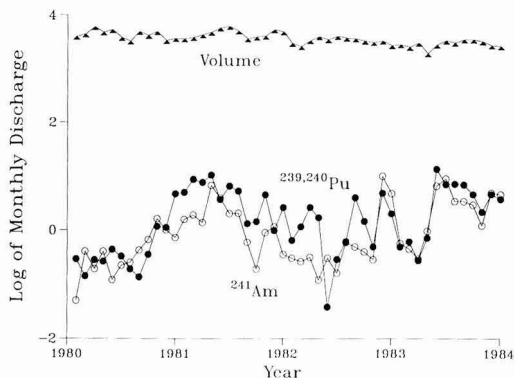


**Figure 3.** Total curies of plutonium and americium and total volumes ( $10^3$  L) of monthly discharges to Mortandad Canyon from January 1980 to April 1983.

concentrations of americium remained relatively constant between the nearest and farthest wells. The plutonium concentration decreased in a nearly exponential fashion with distance. We considered that the variations in the discharge rates of the two elements might explain the different behavior. Discharge data for the years 1980 to 1983 are shown in Figure 3. There were dramatic variations in the relative discharge rates of plutonium and americium. Plutonium concentrations varied as much as 100-fold around the time of the sampling in 1982–1983. The time scale of the fluctuations in the discharges was on the order of weeks, whereas the travel time over the length of the aquifer would be at least a year. We concluded that the systematic decline of the plutonium con-

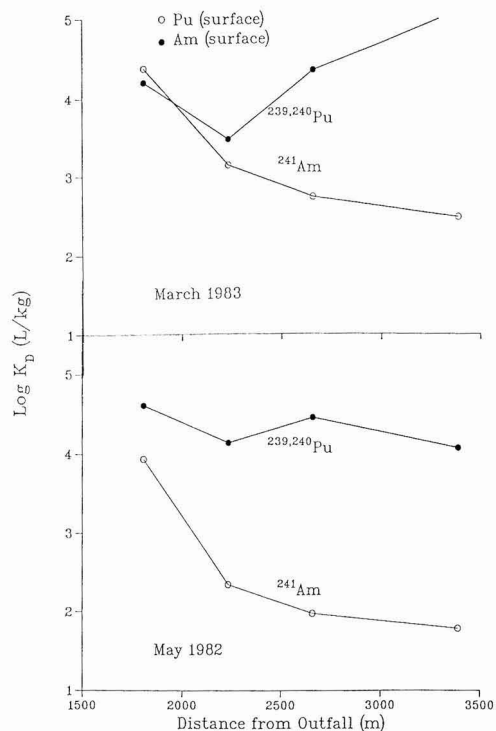


**Figure 4.** Distribution coefficients for actinides in the aquifer in May 1982 and March 1983.

centrations and the different behavior of the two actinides with distance was a consequence of movement through the aquifer and not caused by fluctuations in the discharge.

This conclusion was further supported by isotope ratio data obtained from the Environmental Surveillance Group of LANL (7, 8, 11, 12, 21–25). In 1978, the amount of discharged  $^{239}\text{Pu}$  and  $^{240}\text{Pu}$  increased dramatically relative to the amount of  $^{238}\text{Pu}$ . We calculated the ratio of  $^{239,240}\text{Pu}$  to  $^{238}\text{Pu}$  from available data for each well and the advancing front of  $^{239,240}\text{Pu}$  could be followed. Between wells MCO-4 and MCO-6, a distance of 860 m, the travel time was  $\sim 2$  years. Thus, the rate of movement of the plutonium was  $\sim 1/2$  km per year. We therefore expect that the week-to-week fluctuations of actinide discharges, although appreciable, will be dampened by the much slower movement in the subsurface.

The distribution coefficients ( $K_D$  values) of the plutonium and americium onto particles ( $\geq 0.45 \mu\text{m}$ ) are displayed in Figure 4. The apparent  $K_D$  values for plutonium were relatively constant or increasing over the distance between MCO-4 and MCO-7.5. The plutonium was  $\sim 90\%$  in the reduced state for these experiments. However, the apparent adsorption behavior of americium to  $\geq 0.45\text{-}\mu\text{m}$  particles decreased systematically with distance. In the last well, it was barely adsorbed at all. Such behavior is unexpected for an element that is generally considered to be strongly adsorbed to particles.

The  $K_D$  for plutonium is lower by about an order of magnitude than that observed in many other water bodies (15). In surface waters, the  $K_D$  has been seen to be inversely related to the dissolved organic carbon (DOC) concentration (15, 26). Since the DOC concentrations in the Mortandad Canyon groundwater were found to be elevated (see Table II), it was proposed that this same

**Table IV. Distribution Coefficients ( $K_D$  Values) for  $^{242}\text{Pu}$  onto Sediment from Mortandad Canyon and from Lake Michigan**

water source	sediment source	$K_D, \text{L/kg} \times 10^{-4}$
Mortandad	Mortandad	2
Mortandad	Lake Michigan	10
Lake Michigan	Mortandad	9
Lake Michigan	Lake Michigan	200

**Table V. Concentrations of  $^{239,240}\text{Pu}$  and  $^{241}\text{Am}$  in Size Fractions of Well Water from MCO-5, March 1983<sup>a</sup>**

size class retained, nm	plutonium		americium	
	concn	ratio	concn	ratio
>450	31.8 (0.9)	0.18	21.7 (1.0)	
25-450	141.3 (6.4)	0.18	72.9 (3.3)	0.99
5-25	0.8 (0.1)	6.94	2.0 (0.1)	2.74
2-5	11.3 (0.3)	6.21	68.9 (2.2)	0.78
<2 (filtrate)	8.4 (0.6)	6.94	113.3 (5.0)	0.37
<450 (total)	165.9 (6.4)	1.18	264.8 (9.5)	0.71

<sup>a</sup> Filter sizes and corresponding size fractions are as follows: 0.45  $\mu\text{m}$  (>450 nm), 0.025  $\mu\text{m}$  (25-450 nm), 100 000 MW ultrafilter (5-25 nm), and 10 000 MW ultrafilter (2-5 nm). Standard counting errors are given in parentheses. Also shown is the ratio of added isotope to ambient isotope for the two elements. Concentrations are in mBq/L.

correlation may exist in subsurface waters.  $K_D$  values of added  $^{242}\text{Pu}$  were measured in sediment and water recovered from Mortandad Canyon and compared with water and sediment from Lake Michigan. Lake Michigan materials were chosen because they have been used as reference materials in past work (26) and are low in DOC (1.4 mg/L). The results of this experiment are shown in Table IV. The  $K_D$  values of plutonium onto sediment from either source were notably greater when measured in Lake Michigan water than in Mortandad Canyon water. This suggests that the water chemistry is at least partially responsible for the lower  $K_D$  values.

**Characterization of the Ambient Actinides.** Since the absolute amounts of the actinides in the groundwaters were very small, they were characterized both physically and chemically by using tracer methods. A sample of water from MCO-5 was spiked with  $^{242}\text{Pu}$  and  $^{243}\text{Am}$  and left to stand for 2 days to allow the added actinides to equilibrate with the isotopes originally present. They were then size-fractionated, as described previously, by ultrafiltration techniques. The concentrations of added and ambient isotopes were then determined for each size fraction.

A white material remained insoluble in the filtrate from every size-fractionated sample and, since it was insoluble in nitric or hydrochloric acid, was thought to be silica. Results are given in Table V. Of the ambient plutonium, 85% was found to be retained by the 25-nm filter, corresponding to colloidal materials between 25 and 450 nm in size. The ambient americium was distributed somewhat differently than the plutonium. While 28% of the americium was found in the 25-450-nm size class, 26% was associated with colloidal materials of 2-5-nm size. The largest fraction, ~43%, was small enough to pass through every filter.

An important feature of this experiment was the behavior of the added isotopes,  $^{242}\text{Pu}$  and  $^{243}\text{Am}$ , relative to the ambient ones. If the ambient actinides were readily available to participate in sorption-desorption reactions, they would exchange with their added equivalents. The ratios of added to ambient isotopes would therefore be the same in every fraction. The difference in the ratio between

**Table VI. Relative Distribution (%) of Charged Actinide Species<sup>a</sup>**

water source	anionic	cationic	neutral
	Plutonium		
waste outfall	7	<2	94
surface	3	<2	93
MCO-4	2	<2	99
MCO-5	3	<2	96
MCO-6	4	<2	91
MCO-7.5	8	<2	94
	Americium		
waste outfall	11	11	78
surface	3	<2	97
MCO-4	3	<2	98
MCO-5	17	<2	84
MCO-6	46	<2	63
MCO-7.5	31	<2	93

<sup>a</sup> The radioactivities retained by anion and cation resins, and those not retained by the mixed resins, are expressed as percentages of the total actinide concentration.

the retained and filtered fractions is an inverse measure of the degree of exchange that occurs between the added and ambient isotope over the 2-day equilibration period.

The expected equilibration of plutonium isotopes among the size classes did not occur. Filtration through the 25-nm Nucleopore filter caused a dramatic decrease in the ratio of added to ambient isotope. The ambient  $^{239,240}\text{Pu}$  was preferentially retained by this filter, relative to the added  $^{242}\text{Pu}$ . Therefore ambient plutonium, located in the 25-450-nm size fraction, was bound by colloidal materials in such a way that exchange was not taking place during the time frame of the experiment. The remaining ambient plutonium (approximately 15%) was distributed over the other size classes and was found to be equally exchangeable in each fraction.

The behavior of americium was quite different. The material on the 100 000 MW filter had a higher ratio of added to ambient isotopes than the initial solution. Added americium was therefore retained most effectively in this size range, and this indicates that adsorption sites are still available for binding americium. The other fractions are all reasonably close to the added to ambient ratio expected if the americium is exchanging, with the possible exception of the less than 2-nm fraction. In this fraction the americium is less available for exchange, which would be consistent with the observation of this fraction being quite mobile in the aquifer system, at least as far as well MCO-5.

The 10 000 MW filter, on the other hand, retains material with a decreased ratio, and in the final filtrate, the ratio is lower still. These results may be explained by assuming the ambient americium is bound irreversibly to colloidal materials smaller than 100 000 MW. Added americium would be free to bind to the larger colloidal materials similar to the ambient and would be fractionated similarly.

Results of ion-exchange experiments are shown in Table VI. In natural waters, plutonium(IV) is normally in the anionic form due to complexation with carbonate and humic substances, while americium normally is in cationic forms (15). In Mortandad Canyon surface water and groundwater, plutonium behaved primarily as a neutral species. Americium, on the other hand, exhibited a combination of anionic and neutral behavior in all of the samples that had been in contact with the alluvium. The proportion of anionic americium increased with distance from the source. Cationic americium was only found in the waste outfall, before it has contacted stream sediments or the aquifer matrix. The proportion of anionic ameri-

cium varied from a negligible fraction in the surface sample and MCO-4 to nearly half of the total in the lower wells.

### Conclusions

It is true that the aquifer matrix in Mortandad Canyon is not a particularly effective adsorbent for plutonium. Nevertheless, in the groundwater environments, an apparent  $K_D$  of 20 000 is still large enough to retard the movement of plutonium over a short distance. Other workers, studying the volcanic tuff in the Los Alamos area (27–29) have demonstrated that plutonium and americium do in fact move further through the tuff than through other soils or sediments, but these movements are never more than a few tens of meters. Isotope-exchange experiments demonstrated that the plutonium bound to the colloidal materials of 25–450-nm size is not exchangeable. It is therefore unavailable to exchange among adsorption sites on the immobilized solids in the aquifer and would not be subject to the normally estimated retarding forces.

About half of the americium seemed to be located in a nonexchanging anionic species of a small size ( $\leq 2$  nm). The adsorption ( $K_D$  of ambient americium onto large particles  $\geq 0.45 \mu\text{m}$ ) was seen to decrease with distance down the canyon. This may be due to gradual filtration of americium associated with the larger colloids, leaving only the low molecular weight material in the groundwater. Large fractions of both americium and plutonium were observed to travel in the aquifer over similar distances. This further implies that the high molecular weight fraction of the americium (about half) must have been associated irreversibly with mobile colloids in the same way as the plutonium. It is also likely that the americium associated with large colloids would be removed from the groundwater at about the same rates as plutonium. The reason that the total americium does not become depleted with distance (Figure 2) is because nearly half of it is associated with less than 2-nm material, which is not as rapidly removed as the larger colloidal materials. As well, evaporation of water from the shallow elevated aquifer (2, 3) would act to concentrate this remaining low molecular weight americium complex.

We feel that there is very strong evidence that the actinides, plutonium and americium, are associated with colloidal materials in a way that is effectively irreversible. Even very slow adsorption-desorption reactions, with time constants of months, would allow the actinides to be adsorbed to the aquifer matrix over relatively short distances.

The observation that the apparent  $K_D$  value of americium decreases dramatically with distance helps to resolve the question of surface transport of actinides down the canyon. If storm events had transported the actinides down the reach of the canyon by surface flow, we would have expected all species of americium less than a few microns in size to be transported in the surface flow with about equal efficiency. The apparent  $K_D$  of americium (i.e., the relative amounts of americium in the  $\geq 0.45$ - and  $\leq 0.45$ - $\mu\text{m}$  fractions of the groundwater would have been similar in each sampling well, although the concentration might vary. The systematic change in the  $K_D$ s for americium as a function of distance in the aquifer suggests that it is transported predominantly by subsurface flow at least as far as well MCO-7.5.

Some of the americium was undoubtedly discharged in the same form as the plutonium and was borne by the colloidal material, but the remainder was of very low molecular weight, and its chemical nature is unknown. It is possible that a stable complex of americium was produced by operations within the Los Alamos Laboratory site, or as a result of the waste treatment process, and

discharged from the Laboratory as a low molecular weight complex whose particle reactivity was very slight and whose exchange rate was so slow that it could persist for years under the conditions in the aquifer. It is also possible that the americium could be interacting with natural complexing agents in the aquifer.

These observations have suggested that colloidal materials can be mobile in groundwater systems for great distances and are capable of binding and transporting radionuclide contaminants in subsurface systems. Similar observations of colloid-mediated mobility of radionuclides in groundwater have recently been made (30–32). It is likely that colloid-mediated mobility of radionuclides and other contaminants will be encountered in many other locations once investigators have become aware of its importance. Clearly, as pointed out in a recent feature article (33), colloidal materials may be important means of mobilizing not only actinides, but toxic metals and organics as well. Further information regarding both natural and waste-derived colloidal materials and their physical and chemical properties will be necessary if we are to accurately predict the mobility of groundwater pollutants.

### Acknowledgments

We acknowledge the participation of J. O. Karttunen and D. N. Metta of Argonne for their assistance in the analysis of the actinides. We also thank E. B. Fowler, W. D. Purtymun, and F. R. Roensch of Los Alamos National Laboratory for their valuable contributions to this research. J. F. Schubert, N. C. Sturchio, and P. M. Gschwend read this manuscript and offered many valuable suggestions. Drs. Jeffrey Gaffney and Nancy Marley, of Argonne National Laboratory, were very helpful in the final revision of this paper.

**Registry No.**  $^{239}\text{Pu}$ , 15117-48-3;  $^{240}\text{Pu}$ , 14119-33-6;  $^{241}\text{Am}$ , 14596-10-2.

### Literature Cited

- (1) Abrahams, J. H., Jr.; Baltz, E. H.; Purtymun, W. D. *Geol. Surv. Prof. Pap. (U.S.)* **1962**, No. 450-B, B93-B94.
- (2) Purtymun, W. D. U.S. Atomic Energy Commission Report no. LA-5716-MS; Los Alamos Scientific Laboratory, 1974.
- (3) Purtymun, W. D.; Buchholz, J. R.; Hakonson, T. E. *J. Environ. Qual.* **1977**, *6*, 29–32.
- (4) Environmental Surveillance Group *Environmental Impact Statement: Los Alamos Scientific Laboratory Site, Los Alamos New Mexico*; Department of Energy Report, DOE/EIS-0018; 1979.
- (5) Hakonson, T. E.; Nyhan, J. W. In *Transuranic Elements in the Environment*; Hanson, W. C., Ed.; Department of Energy Report, DOE/TIC-22800; Department of Energy: Washington, DC, 1980; pp 403–419.
- (6) Emelity, L. A.; Buchholz, J. R.; McGinnis, P. E. In *Management of Low-Level Radioactive Waste*; Pergamon Press: New York, 1979; pp 369–392.
- (7) Environmental Surveillance Group *Los Alamos Natl. Lab. [Rep.] LA (U.S.)* **1981**, LA-8810-ENV.
- (8) Environmental Surveillance Group *Los Alamos Natl. Lab. [Rep.] LA (U.S.)* **1983**, LA-9762-ENV.
- (9) Nelson, D. M.; Orlandini, K. A.; Larsen, R. P. *Argonne National Laboratory Annual Report*; 1982; ANL-82-65, pp 49–53.
- (10) Nelson, D. M.; Orlandini, K. A. *Argonne National Laboratory Progress Report*; 1984–1985; ANL-86-15, Chapter 3, pp 7, 12.
- (11) Environmental Surveillance Group *Los Alamos Natl. Lab. [Rep.] LA (U.S.)* **1980**, LA-8200-ENV.
- (12) Environmental Surveillance Group *Los Alamos Natl. Lab. [Rep.] LA (U.S.)* **1985**, LA-10421-ENV.
- (13) Lovett, M. B.; Nelson, D. M. In *Techniques for Identifying Transuranic Speciation in Aquatic Environments*, International Atomic Energy Agency: Vienna, 1981; pp 27–35.

- (14) Nelson, D. M.; Lovett, M. B. *Nature* 1978, 276, 599-601.
- (15) Wahlgren, M. A.; Orlandini, K. A. In *Environmental Migration of Long-Lived Radionuclides*; International Atomic Energy Agency: Vienna, 1982; pp 757-774.
- (16) Nelson, D. M.; Orlandini, K. A. In *Speciation of Fission and Activation Products in the Environment*; Bulman, R. A., Cooper, J. R., Eds.; Elsevier: London, 1986; pp 262-268.
- (17) Stucki, J. W.; Anderson, W. L. *Soil Sci. Soc. Am. J.* 1981, 45, 633-637.
- (18) Taras, M. J.; Greenberg, A. E.; Hoak, R. D.; Rand, M. C., Eds. *Standard Methods for the Examination of Water and Wastewaters*, 13th ed.; American Public Health Association: New York, 1971; pp 303-306.
- (19) American Public Health Association *Standard Methods for the Examination of Water and Wastewater*; American Public Health Association: Washington, DC, 1975.
- (20) Truesdell, A. H.; Jones, B. F. *J. Res. U.S. Geol. Surv.* 1974, 2, 233-248.
- (21) Environmental Surveillance Group Los Alamos Natl. Lab. [Rep.] LA (U.S.) 1977, LA-6801-MS.
- (22) Environmental Surveillance Group Los Alamos Natl. Lab. [Rep.] LA (U.S.) 1978, LA-7263-MS.
- (23) Environmental Surveillance Group Los Alamos Natl. Lab. [Rep.] LA (U.S.) 1979, LA-7800-ENV.
- (24) Environmental Surveillance Group Los Alamos Natl. Lab. [Rep.] 1984, LA-9762-ENV.
- (25) Environmental Surveillance Group Los Alamos Natl. Lab. [Rep.] 1986, LA-10721-ENV.
- (26) Nelson, D. M.; Penrose, W. R.; Karttunen, J. O.; Mehlhoff, P. *Environ. Sci. Technol.* 1985, 19, 127-131.
- (27) Fried, S. M.; Friedman, A. M.; Hines, J. J.; Quarterman, L. A. *Argonne National Laboratory Report*; 1975; ANL-75-64.
- (28) Fried, S. M.; Friedman, A. M.; Hines, J. J.; Atcher, R. W.; Quarterman, L. A.; Volesky, A. *Argonne National Laboratory Report*; 1976, ANL-76-127.
- (29) Nyhan, J. W.; Drennon, B. J.; Abele, W. V.; Wheeler, M. L.; Purtymun, W. D.; Trujillo, G.; Herrera, W. J.; Booth, J. W. *J. Environ. Qual.* 1985, 14, 501-509.
- (30) Buddemeier, R. W.; Hunt, J. R. *Appl. Geochem.* 1988, 3, 535-548.
- (31) Kim, J.-I.; Buckau, G.; Klenze, R. *Mirage II Project Progress Report*; RCM-01687; Institute for Radiochemistry, Technical University of Munich, 1987.
- (32) Short, S. A.; Lowson, R. T.; Ellis, J. *Geochim. Cosmochim. Acta* 1988, 52, 2555-2563.
- (33) McCarthy, J. F.; Zachara, J. M.; *Environ. Sci. Technol.* 1989, 23, 496-502.

Received for review March 9, 1989. Revised manuscript received September 1, 1989. Accepted October 5, 1989. This work was supported by the United States Department of Energy's Office of Health and Environmental Sciences as part of the Subsurface Science Program. The submitted manuscript has been authored by a contractor of the U.S. Government under Contract No. W-31-109-ENG-38. Accordingly, the U.S. Government retains a nonexclusive, royalty-free license to publish or reproduce the published form of this contribution, or allow others to do so, for U.S. Government purposes.

## Kinetic Approach to Trace Metal Complexation in Seawater: Application to Zinc and Cadmium

Francois L. L. Muller and Dana R. Kester\*

Graduate School of Oceanography, University of Rhode Island, Narragansett, Rhode Island 02882

■ Anodic stripping voltammetry (ASV) using a rotating disk electrode, along with ion-exchange procedures in the column and batch modes were used to study the lability characteristics of zinc and cadmium in Narragansett Bay seawater. By combining the three techniques into one single scheme, the effective time of measurement can be varied in a controlled way between  $10^{-2}$  and  $10^6$  s. Application of this procedure to zinc and cadmium showed that the labile fraction of the metal was a function of measurement time over the entire range. The species of a metal in natural waters can be characterized directly on the basis of lability dependence with time.

### Introduction

It is now well established that the total metal concentration in a water sample is rarely adequate to assess the reactivity of that metal in biological or geochemical processes (3, 12). Some characterization of the physicochemical forms of the metal, together with the rates of transformation among these forms, is a prerequisite for understanding global processes. For example, being able to explain the observed distribution of a metal in the sea through fundamental physicochemical principles would open the door to the prediction of future distributions, e.g., given a change in anthropogenic inputs. The investigation of chemical speciation requires measurements of an untreated sample. The composition of the sample with respect to the major elements, pH, organic ligands, redox state, and adsorption sites must be kept as constant as possible, since chemical speciation is dictated by these parameters. In the absence of adequate techniques, pro-

cedures have been used that involve reanalyzing the sample after applying successively harsher chemical steps such as lowering of pH. As the results from these speciation procedures are operationally defined, Davison (1) recommended that the effective time of measurement be reported in all electroanalytical work so that measurements performed by different workers under different experimental conditions could be compared.

The speciation method of Figura and Mc Duffie (2) subdivides the dissolved metal into categories described as labile, moderately labile, slowly labile, and inert, based upon the concentrations measured by anodic stripping voltammetry (ASV) at pH 6.3 and Ca-Chelex ion exchange in successive column and batch procedures. The terminology they used implies a simple kinetic basis for the discrimination between "detectable" vs "undetectable" metal. This approach is based on the premise that the magnitude of each fraction may be controlled by some slowly dissociating species not (or partially) detected by the corresponding technique, and it ignores the possibility of species shifts upon buffering to pH 6.3. These fractions are defined at some arbitrary measurement times and may therefore be only loosely related to the unknown species. This fractionation of total dissolved metal into four identifiable categories is based on operationally defined procedures rather than actual chemical or physical properties.

In this paper we use three techniques to characterize the time scales of exchange for the species comprising the total metal concentration of Zn and Cd in marine systems. With increasing cumulated time, one observes the contributions of progressively more inert species. This scheme distin-

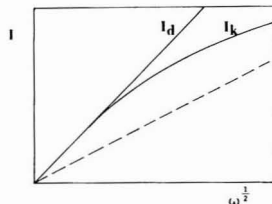
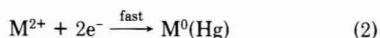
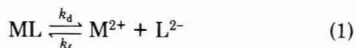
guishes species on the basis of their kinetics of availability to the analytical methods.

### Methods

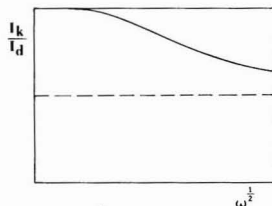
**Sample Collection and Treatment.** Unless otherwise specified, all samples referred to in Results were collected into a 4-L high-density polyethylene jug, ~200 m off the beach at the Graduate School of Oceanography. After a thorough rinse with bay water the bottle was uncapped ~60 cm below the surface (while the researcher was swimming with fins). It was capped again while still immersed so as to avoid contamination from the surface microlayer. The sample was then brought to the laboratory where it was kept at 5 °C in the dark, prior to analysis. In each experiment described below, speciation information was obtained by making measurements in an untreated sample, a filtered subsample, and a subsample subjected to photooxidation. Filtration was performed through 0.40- $\mu\text{m}$  Nuclepore membrane disks (40-mm diameter) at a vacuum of 40 cm of Hg. The difference in zinc or cadmium concentrations between unfiltered and filtered subsamples was taken as a measure of the amount of metal "bound" to particulate material. The UV photooxidation of the sample was performed with a Hanovia (Model 673A-36) 550-W medium-pressure Hg vapor lamp operated within an immersion well of clear fused quartz. The bay water placed in an outer well was then irradiated for 8 h, during which time both the lamp and the sample were cooled by circulation of cold water. In addition, a small but continuous stream of a  $\text{N}_2/\text{CO}_2$  mixture was passed through the sample to maintain the natural pH. Under these conditions, the difference in metal concentrations between UV-irradiated and untreated subsamples provided an estimate of "organically bound" metal.

**DPASV at the Rotating Disk Electrode.** Voltammetric measurements were made with a PAR Model 174A Polarographic Analyser and the sequence of steps programmed with a PAR Model 315 Controller (EG&G Princeton Applied Research). The polarograms were recorded on an X-Y recorder (Hewlett-Packard 705A) and the peak heights determined manually. A 1-L Teflon vessel (Saville Corp.) served as the electrochemical cell: the large capacity minimized any possible effects of the vessel walls on the streamlines when the working electrode was rotated at high speeds (60–100 Hz). This cell was placed inside a Plexiglas-made container, the inlet and outlet of which were connected to a Lauda K-2/RD thermocirculator (Brinkman Instruments) for temperature control at  $25 \pm 0.5$  °C. Use of an AFMR rotator (Pine Instruments Corp.) allowed the mercury thin-film electrode to be rotated up to 100 Hz. After each analysis the mercury film was wiped off with a tissue in order to restore the surface and a new film was then preplated from a stirred  $\text{Hg}^{2+}$  solution ( $5 \times 10^{-4}$  M in 0.01 N  $\text{HNO}_3$ , -0.90 V for 400 s, 5 Hz) for the next analysis. The sequence of steps during analysis was the following: purging (50 min), conditioning (1 min at -0.40 V), plating (25–100 s at -1.20 V).

Florence (3) recently reviewed some of the criteria that have been applied to the definition of labile, quasi-labile, and inert complexes in ASV analysis. The dissociation of a 1:1 complex formed between a divalent metal ion M (M = Zn, Cd) and a ligand L, and the subsequent reduction of  $\text{M}^{2+}$  at the electrode, is described by the overall reaction



theoretical plots of peak current,  $I$ , in the presence ( $I = I_k$ ) or absence ( $I = I_d$ ) of kinetic control



the  $I_k/I_d$  vs  $\omega^{1/2}$  dependence in the presence of kinetic control

**Figure 1.** Illustration of kinetic control in ASV. In each diagram, the contribution from the labile metal is represented by the broken line.

Assuming that the complex ML is not directly reducible, it is clear from eq 1 that the ASV peak current may be affected by slow kinetics of dissociation. When this is the case, the peak current  $I_k$  is said to be kinetically controlled and the ratio  $I_k/I_d$  can be used as an index of the lability of the metal;  $I_d$  represents the diffusion-limited current, i.e., the current that would be observed for the same metal concentration in the absence of ligand (4). The lability of a complex in ASV depends not only on its dissociation rate constant  $k_d$  but also on its residence time in the diffusion layer, which depends on the diffusion layer thickness  $\delta$  (5). Because of the hydrodynamics at the rotating disk electrode, a simple relationship exists between electrode rotation speed  $\omega$  ( $\text{rad s}^{-1}$ ) and diffusion layer thickness  $\delta$  (cm) (6):

$$\delta = 1.61(D/\nu)^{1/3}(\nu/\omega)^{1/2} \quad (3)$$

The values used in this study are as follows: diffusion coefficient  $D_{\text{Zn}} = 0.78 \times 10^{-5}$   $\text{cm}^2 \text{s}^{-1}$ ; kinematic viscosity  $\nu = 0.01$   $\text{cm}^2 \text{s}^{-1}$ . Hence, kinetic control in ASV can be investigated by studying the dependence of the measured current  $I$  on the rotation speed  $\omega$  or the rotation frequency  $f$  (Hz). A linear relationship of  $I$  vs  $f^{1/2}$  is expected in the absence of kinetic control, but the form of this relationship is altered if kinetic effects become important (Figure 1). Even so, a linear region representing the  $I_d$  vs  $f^{1/2}$  relationship will usually be observed at the lower end of the  $f^{1/2}$  range, because the larger the value of  $\delta$  the greater is the opportunity for complete dissociation of the ML complex ( $I_k/I_d \rightarrow 1$ ). Extrapolation of this linear portion to the region of quasi-lability will therefore allow calculation of  $I_d$ , and hence  $I_k/I_d$ , at each rotation frequency. At any rotation frequency, the ratio  $I_k/I_d$  in a seawater sample containing both labile (including the free metal) and quasi-labile forms of a metal M can also be related to the relative concentrations of those forms according to

$$\frac{I_k}{I_d} = \frac{[\text{M}]_{\text{labile}} + x[\text{ML}]}{[\text{M}]_{\text{labile}} + [\text{ML}]} = \frac{R + x}{R + 1} \quad (4)$$

where  $x(t)$  is the fraction of ML dissociated during the time of measurement, and  $R = [\text{M}]_{\text{labile}}/[\text{ML}]$ .

If the dissociation rate is first order with respect to [ML] the degree of dissociation at time  $t$  will be given by

$$1/(1-x) = \exp(k_d t) \quad (5)$$

Davison (1) showed the time of measurement in ASV can be estimated from

$$\delta = (\pi D t)^{1/2} \quad (6)$$

The expressions of  $\delta$  given in eq 3 and eq 6 can be equated to give

$$t = (0.131/f)(\nu/D)^{1/3} \quad (7)$$

Replacing  $\nu$  and  $D$  by their numerical values and substituting into (5) gives

$$1/(1-x) = \exp(1.45k_d/f) \quad (8)$$

which leads to the final result

$$\frac{I_k}{I_d} = 1 - \frac{1}{(R+1)\exp(1.45k_d/f)} \quad (9)$$

A nonlinear curve fitting technique was then used to calculate  $R$  and  $k_d$  from the experimental plot of  $I_k/I_d$  vs  $f$ . Experimental data were also obtained after two additions of a Zn/Cd mixed standard ( $3 \times 10^{-5}$  M/ $0.17 \times 10^{-5}$  M) to produce triplicate measurements of  $k_d$ .

Finally, peak currents  $I_k$  and limiting peak currents  $I_d$  should ultimately be converted to metal concentrations by using a calibration equation of the form  $[M]_{\text{detected}} = I/S$ . For this purpose, the free response  $I/S$  was evaluated at each rotation frequency used from the slope of the  $I_d$  vs  $[M]_{\text{added}}$  relationships. Obviously, the absence of any residual complexing capacity when  $M$  is added should be assessed first, if the measured slope is to represent that of free metal.

**Ion Exchange in the Column Mode.** A 75-g portion of Dowex 50W-X8 resin, 50–100 mesh designation (Bio-Rad Laboratories), was required for the large column, while 2 g was used for the small column (see below for a description of the system). Preconditioning of the 75-g portion proceeded as follows, all reagent quantities being scaled down for the second portion. Impurities (very fine particles) were separated out by decantation followed by wet-sieving through a 100  $\mu\text{m}$  mesh Teflon cloth. Purification and conditioning consisted of sequentially equilibrating the resin with  $1 \times 200$  mL of 1 M  $\text{HNO}_3$  (Ultrex),  $3 \times 200$  mL of 1 M  $\text{NH}_3$  (Ultrex), and  $4 \times 200$  mL of filtered seawater collected off Block Island, Rhode Island (in which zinc and cadmium concentrations determined by atomic absorption were 3.4 and 0.16  $\text{nmol kg}^{-1}$ , respectively). The last step was designed to equilibrate the resin with respect to the major cations of seawater as well as pH to avoid pH and compositional changes upon passage of the sample through the column. The resin/seawater slurry was introduced into the column in small portions in an attempt to achieve a uniformly packed bed. A Teflon cylinder of 4.0-cm inner diameter served as the larger column: it was  $2/3$  filled with resin and  $1/3$  filled with Teflon stones to minimize the dead volume and to ensure a uniform flow across the top section of the column (drawn perpendicular to the average direction of flow). The smaller column was a Teflon sleeve of 1.1-cm inner diameter. A piece of Teflon cloth was stretched over the end of the  $1/4$ -in. tube connecting the bottom of each column to the rest of the system. The complete apparatus also included a 1-L Teflon bottle holding the sample, a peristaltic pump (Varistaltic, Manostat Products), three chemically inert valves (Hamilton), and another Teflon cylinder used as a measuring reservoir for the reacted sample. These elements were connected to each other via  $1/8$ -in.

Teflon tubing. With a void volume among the resin beads of 36.7 mL in the large column and 1.0 mL in the small column and with flow rates over the range of 2–120 mL/min, it was possible to examine a continuous range of contact times between 1 and 1000 s.

The subsamples, each of which resulted from a particular contact time between 1 and 1000 s, were preconcentrated by Co-APDC coprecipitation and subsequently analysed for Zn and Cd by flameless atomic absorption (AA) (Perkin Elmer 5000 AA spectrophotometer with accompanying HGA-500 graphite furnace assembly and AS-40 autosampler). The Co-APDC coprecipitation technique described earlier (7) was modified in three ways: (1) the pH of coprecipitation was 6 instead of 3; (2) the precipitates were collected on 0.4- $\mu\text{m}$  Nuclepore disk filters (25-mm diameter) and not separated out by centrifugation as suggested by Huizenga (7); (3) blank determinations were made on a stock solution of filtered, UV-irradiated, Chelex-stripped seawater, rather than by rerunning previously coprecipitated samples. Blanks for zinc were of the order of 0.4–2.0  $\text{nmol kg}^{-1}$ ; for cadmium, they were below the detection limit of 0.01  $\text{nmol kg}^{-1}$  (expressed as concentration in seawater). The mean recovery of the Co-APDC coprecipitation was determined by spiking the sample at analyte concentrations spanning those expected in the sample (10–40  $\text{nmol kg}^{-1}$  for zinc, 0.5–2.0  $\text{nmol kg}^{-1}$  for cadmium). Spike recovery was 80% complete for zinc and 91% complete for cadmium. All work, including processing of the sample through the column system, coprecipitation of the subsamples, and AA analyses on the concentrates, was carried out in a portable laboratory designed for trace metal research (8) and thermostated at  $22 \pm 1$  °C.

When the first elemental volume of unreacted sample comes into contact with the resin bed, a reaction zone forms that contains all concentrations of metal between some initial value  $[M]_{\text{labile}}$  and zero. The question then arises of how far down the column the near-zero concentration front will move, as more sample is added to the resin bed. A first-order approach consists of assuming that sorption processes involving free metal are sufficiently fast that each elemental layer of ion exchanger is in equilibrium with the seawater passing over it. Taking the smaller column to illustrate our point, we find that the displacement of the zone of near-zero concentration represents only 2.5% of the total capacity (i.e., 2.5% of the length) of the column after 1.5 L of seawater has been fed into it. This means that in a typical experiment, the condition that metal complexes will be subjected to near-zero concentration should be fulfilled 97.5% of the contact time, at the least. Under those conditions, the definition of "effective measurement time" in the column method reduces to that of "contact time", which can easily be computed from a knowledge of void volume and flow rate. The metal concentration determined on the effluent represents a fraction that is inert to the column measurement. An instantaneous decrease in metal concentration with time represents the uptake of labile metal, while a slower, first-order decrease with time represents the kinetically limited uptake of a complex whose dissociation rate constant lies within the rate of accessibility of the column method ( $k_d$  between  $10^{-1}$  and  $10^{-4}$  s; see Figure 2). In practice, however, the uptake of free metal proceeds at a finite rate so that the assumption that instantaneous equilibrium is achieved between the ion exchanger and the moving solution does not hold at fast flow rates. Because of incomplete exchange at fast flow rates, the lower kinetic boundary (solid line in figure) has been drawn for a

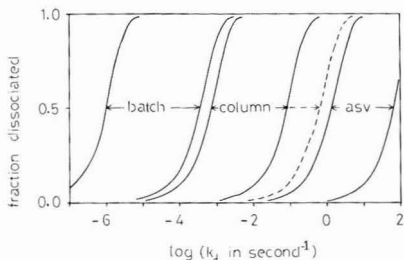


Figure 2. Predicted kinetic boundaries of three methods for the measurement of a complex ML with first-order dissociation rate constant  $k_d$  ( $s^{-1}$ ).

measurement time of 8 s, even though measurements were made at contact times as low as 0.3 s. Such a boundary defines a range of  $k_d$  values that will result in a kinetic control of the rate of uptake and allows calculation of the fraction of the complex dissociated in 8 s (2).

**Chelating Ion Exchange in the Batch Form.** These uptake experiments were conducted in 1-L Teflon reactors, each containing approximately 1 L of bay water at the start of the experiment as well as 10 g (dry weight) of Chelex 100 resin (100–200 mesh designation, Rio Rad Laboratories). The 10-g portion of resin was taken fresh from the bottle and slurried into a 125-mL polyethylene funnel holder used for liquid filtration through a Nuclepore filter. Conditioning took place through successive leaching with  $1 \times 75$  mL of 1 M  $HNO_3$  (Ultrex),  $3 \times 75$  mL of 1 M  $NH_2$  (Ultrex), and  $4 \times 75$  mL of filtered bay water. As mentioned before, the last step was designed to equilibrate the resin with respect to  $Na^+$  (calculated to occupy 1% of the available sites on the resin at  $S = 30\%$ , pH 8.0),  $Mg^{2+}$  (55%),  $Ca^{2+}$  (5%), and  $H^+$  (37%). Since the resin retains considerable  $H^+$ , it may be acting as a pH buffer. In the present experiment, the overall pH change observed after 200 h was +0.10 in reactor 1 and -0.10 in reactor 2, from an initial value of 7.90. Temperature readings taken after 200 h and averaged between the three reactors gave  $24 \pm 1$  °C. The system used magnetic stirrer bars mounted on a fixed frame (Nalge Corp.) to ensure vigorous agitation of the solutions, yet prevent grinding of the resin. The reactors could be connected to each other and to the atmosphere by means of three stopcocks positioned along a common gas line. The solutions were moved along separate lines ( $1/8$ -in. Teflon tubing), the exact pathway being selected by manually switching a combination of three Teflon valves (Hamilton). The fourth Hamilton valve, situated at the top of the measuring reservoir (Teflon sleeve, 1.1 cm i.d.  $\times$  23 cm), was used to direct either  $N_2$  gas or bay water.

Following the introduction of resin into a reactor, the time series experiment for that reactor was begun by turning on the magnetic stirrer ( $t = 0$ ). At designated time intervals the stirring was interrupted and the resin was allowed to settle for 2 min. A pressure of  $N_2$  of 0.4 atm was then applied to the solution, thereby forcing it into the measuring reservoir. As the reservoir overflowed, the valves were switched so as to force the subsample (volume =  $23.8 \pm 0.05$  mL) into a sealed, acid-cleaned Teflon bottle. Total metal determinations were made by Co-APDC coprecipitation followed by AA analysis (see previous section). The reagent blank was  $2.7$  nmol  $kg^{-1}$  for zinc and below the detection limit of  $0.01$  nmol  $kg^{-1}$  for cadmium. Spike recovery was 83% complete for zinc and 93% complete for cadmium. The resolving power of the batch technique was limited by the fact that the solution was left unstirred for  $\sim 3$  min every time a sample was drawn.

Therefore, we did not feel it appropriate to draw any sample during the first 30 min of the experiment. Furthermore, a settling time of 2 min appears to have been insufficient when Dowex 50W-X4 (100–200 mesh) was substituted for Chelex 100 (100–200 mesh) in reactor 3. This conclusion was reached in view of the consistently high values ( $[Zn] = 42\text{--}78$  nmol  $kg^{-1}$ ;  $[Cd] = 0.39\text{--}0.57$  nmol  $kg^{-1}$ ) observed over the 200-h duration of the experiment. Such values could well have been caused by the entrainment with the solution phase of smaller beads or colloidal sulfonates. Consequently, only the results from reactors 1 and 2 are presented and discussed below.

In the batch method, the removal rate of free and labile metal is unmeasurably fast. It follows that the removal rate of a quasi-labile complex is controlled by the rate  $k_d[ML]$  at which the complex dissociates, and hence  $k_d$  can be obtained directly from the removal curve (9). For a single quasi-labile complex ML characterized by a first-order dissociation rate constant  $k_d$  the observed metal concentration is given by

$$[M]_{total} = [M]_{labile} + [ML]_0 \exp(-k_d t) + [M]_{inert} \quad (10a)$$

where  $[M]_{inert}$  accounts for the presence of complexes with unmeasurably slow rates of dissociation. Given the initial rapid removal of  $[M]_{labile}$  from solution, eq 10a reduces to

$$[M]_{total} = [ML]_0 \exp(-k_d t) + [M]_{inert} \quad (10b)$$

in a first step,  $[M]_{inert}$  is estimated by averaging the values observed at long measurement times. In a second step,  $[M]_{quasi-labile}$  ( $= [ML]_0$ ) and  $k_d$  are determined by systematically subtracting  $[M]_{inert}$  from all remaining values of  $[M]_{total}$  and fitting the results to the exponential function of eq 10b. Finally,  $[M]_{labile}$  represents the difference between  $[M]_{total}$  ( $t = 0$ ) and the sum  $[M]_{quasi-labile} + [M]_{inert}$ .

## Results

**Comparison of the Uptake Kinetics of Dowex 50W-X4 and Chelex 100 in the Column Operation.** A Dowex column experiment was performed on a bay water sample collected on 22 November 1986 ( $S = 28.3\%$ , pH 7.86). Since the effluent from the larger column was found to be contaminated with both zinc and cadmium, the only useful results are those obtained with the smaller column for contact times between 0.5 and 25 s. Figure 3 demonstrates in a striking manner the nonquantitative removal of labile metal at contact times less than 8 s or so. The similarities between zinc and cadmium and between untreated vs irradiated samples suggest that this initial removal is limited by the finite rate at which the metal is taken up by the resin. A similar situation was observed with the batch method by Huizenga (9), and by Figura and McDuffie (2); these authors determined a first-order removal rate constant, which was taken as their "batch method constant" for the conditions used (i.e., resin to solution ratio, stirring rate, etc.). However, this comparison cannot be carried through to the extent of deriving a "column method constant" because in the present case the thickness of the effective diffusion layer increases with decreasing flow rate, i.e., with increasing cumulated time. As a result, the instantaneous rate of exchange of zinc or cadmium with the resin cannot be expressed simply as a function of remaining metal concentration so that no simple rate law can be derived. Comparison of the uptake data between the filtered and unfiltered portions of this sample suggested that a kinetic signal from particulate zinc might well be superimposed on the removal of labile zinc in the unfiltered sample (10): indeed, the initial zinc concentrations are 39.3 and 44.4 nmol  $kg^{-1}$  in the filtered and unfiltered samples, respectively, but after a contact time of 24 s,  $\sim 5.0$  nmol

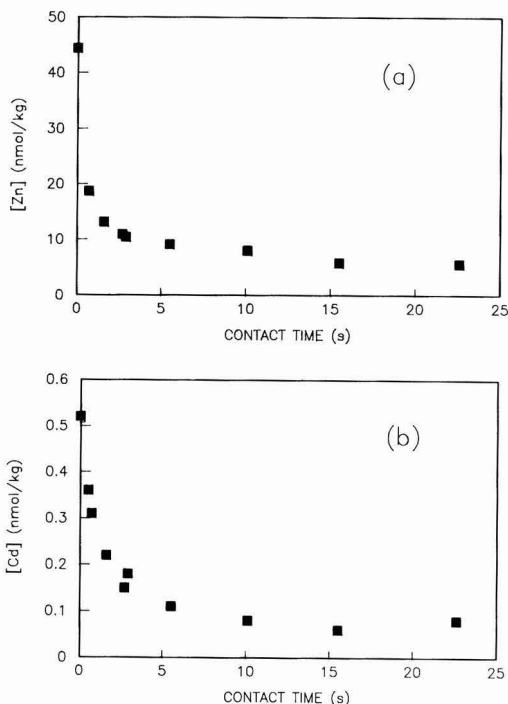


**Figure 3.** Exchange of (a) zinc (b) cadmium from a Narragansett Bay water sample with the Dowex 50W-X8 resin. The total concentration of metal in the effluent is plotted as a function of time.

$\text{kg}^{-1}$  of inert metal remains in both cases. The experimental results of Figure 3a can thus be explained if the dissolved phase of the sample includes both labile ( $34.3 \text{ nmol kg}^{-1}$ ) and inert ( $5.0 \text{ nmol kg}^{-1}$ ) zinc, with particulate zinc contributing a further  $5.0 \text{ nmol kg}^{-1}$  over the time scale of the experiment. The interpretation of the cadmium data shown in Figure 3b was that dissolved cadmium ( $0.41 \text{ nmol kg}^{-1}$ ) was entirely labile, while particulate cadmium ( $0.10 \text{ nmol kg}^{-1}$ ) was definitely inert (10).

Another evaluation of column ion exchange as a useful speciation technique was made on a sample collected at the same location on 26 October 1986 ( $S = 28.0\%$ , pH 7.95). This time, we tested the capacity of Chelex 100 (3 g of dry weight, conditioned as for 2 g of Dowex) to provide accurate kinetic information on complexed forms of zinc and cadmium. The full range of kinetic regimes defined in Figure 2 was explored. As indicated by the results presented in Figure 4a, uptake of labile zinc ( $27.5 \pm 3.5 \text{ nmol kg}^{-1}$ ) occurred completely in less than 1 s. This allows a clear definition of the remaining fractions, i.e., quasi-labile particulate ( $[\text{Zn}] = 7.5 \pm 0.3 \text{ nmol kg}^{-1}$ ;  $k_d = 0.050 \pm 0.004 \text{ s}^{-1}$ ), inert dissolved ( $[\text{Zn}] = 1.5 \pm 0.2 \text{ nmol kg}^{-1}$ ), and inert particulate ( $[\text{Zn}] = 6.5 \pm 0.4 \text{ nmol kg}^{-1}$ ), from a comparison of the removal curves in unfiltered, filtered, and UV-irradiated portions of the sample (10). The fact that two types of surface sites for zinc could be identified shows that a kinetic scheme could be used to understand the behavior of a mixture of surface phases with different adsorption/desorption characteristics. Also, some loss of zinc ( $\sim 6 \text{ nmol kg}^{-1}$ ) to the walls of the irradiation vessel might account for the reduced initial zinc concentration in that sample. But the important message from that experiment is the organic nature of the adsorption sites for zinc. Finally, cadmium ( $0.33 \pm 0.03 \text{ nmol kg}^{-1}$ ) is en-

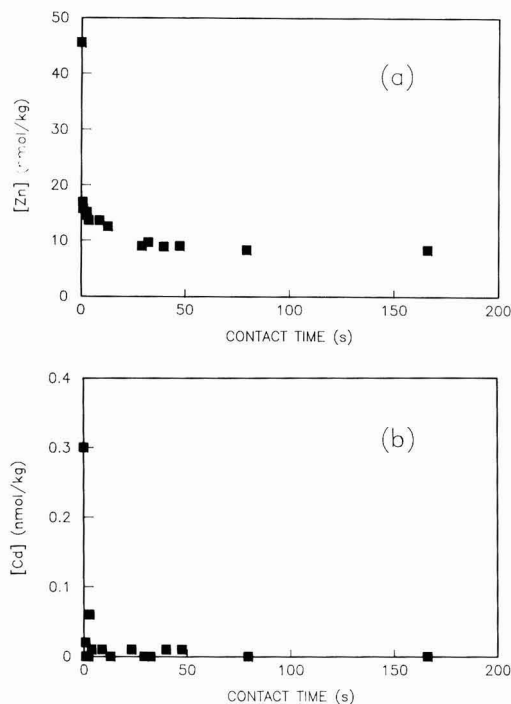


**Figure 4.** Exchange of (a) zinc (b) cadmium from a Narragansett Bay water sample with the Chelex resin. The total concentration of metal in the effluent is plotted as a function of time.

tirely dissolved and labile and therefore drops immediately to undetectable levels (Figure 4b).

On the basis of the above, one might be tempted to favor Chelex 100 for use in the column technique. However, the use of Chelex 100 to characterize the dissociation behavior of metal complexes in solution may have limitations other than the fact that partial dissociation must occur within the time span of the measuring technique. Cox et al. (11) compared the percentages of nonlabile metal measured after Donnan dialysis with those remaining after passage through Chelex and Dowex columns, for a variety of metal-ligand systems. Donnan dialysis gave values very close to Dowex ion exchange but the Chelex column always gave lower values, even though the experimental conditions were made as identical as possible between the two columns. They concluded that the iminodiacetic functional groups on the Chelex resin can effectively compete with the ligands in solution (those were glycine, nitrilotriacetic acid, and humic acid). In view of these results, we opted for the Dowex column even though its useful range of accessible  $k_d$ 's was more limited than anticipated from the available range of contact times.

**Evaluation of the Techniques on an Environmental Sample.** The bay water sample used in this experiment ( $S = 29.4\%$ , pH 7.90) was collected in a 20-L carboy on 16 December 1986. The voltammetric measurements on the filtered and unfiltered portions were completed on the same day while the UV-irradiated portion was analyzed on December 18. The column experiments were run between December 19 and 20. The batch experiment was started on December 23 and was over on December 31.

**Characterization of Kinetic Behavior by DPASV.** The  $I_k$  vs  $t^{1/2}$  plots for zinc clearly departed from the linear relationship expected for labile species only, although the UV-irradiated sample did yield linear plots (10). This



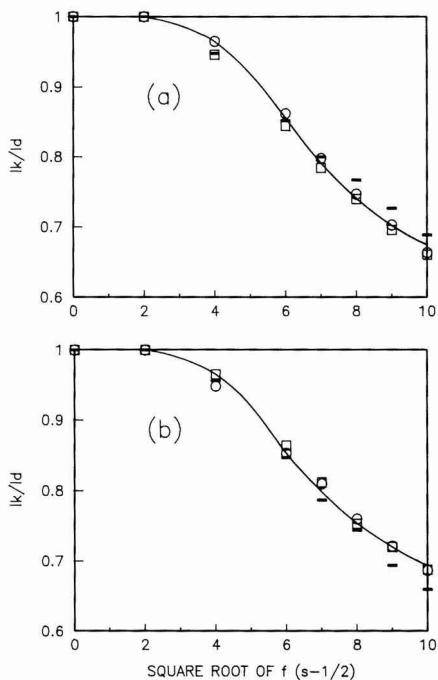


**Figure 5.**  $I_k/I_d$  vs  $f^{1/2}$  for three standard additions of zinc (—, 0; ○, 14; □, 27 nmol kg<sup>-1</sup>) to the bay water sample collected on 16 December 1986. Lines fit the mL according to eq 9. (a) Untreated. (b) Filtered.

demonstrated that some quasi-labile organic complexes of zinc were exercising kinetic control on the observed current, as has previously been reported for copper organic complexes in seawater (4). The data were modeled accordingly (Figure 5) to give for the unfiltered sample,  $R = 1.03 \pm 0.20$  and  $k_d = 29 \pm 3 \text{ s}^{-1}$ ; and for the filtered sample,  $R = 1.04 \pm 0.15$  and  $k_d = 30 \pm 2 \text{ s}^{-1}$ . Thus,  $[\text{Zn}]_{\text{quasi-labile}}/[\text{Zn}]_{\text{labile}} = 1$ , with  $[\text{Zn}]_{\text{quasi-labile}}$  contributing proportionally less than  $[\text{Zn}]_{\text{labile}}$  except at measurement times greater than 0.1 s when the electrode can no longer distinguish between the two forms. We also noted that a plot of  $I_d$  (proportional to  $[\text{Zn}]_{\text{labile}} + [\text{Zn}]_{\text{quasi-labile}}$ ) vs  $[\text{Zn}]$  added was linear (10), thus indicating that no residual complexing capacity was present in the sample. From such plots, the free response was determined to be 50, 58, and 49 nA/nmol kg<sup>-1</sup> in the unfiltered, filtered, and filtered + UV-irradiated samples, respectively. These fluctuations are paralleled by similar fluctuations in the cadmium-free response (52.2, 67.9, and 62.7, respectively) and must be due to the lack of reproducibility noted earlier. In addition to—and consistent with—the lack of available ligands to form inert complexes with zinc, this sample does not seem to contain any inert complexes in the first place: thus, the electroactive zinc measured after irradiation ( $20.7 \pm 0.8 \text{ nmol kg}^{-1}$ ) is no greater than when measured before irradiation at the slowest rotation speed ( $25.9 \text{ nmol kg}^{-1}$ ). The only inert fraction of zinc in that sample must be found in the particulate phase. It will be seen below that it is made up of at least two component phases with different characteristics in terms of zinc desorption reactions. Similarly with zinc, no residual complexing capacity for cadmium is found in this sample; but unlike zinc, no kinetic limitation of the current is observed so that the time of measurement is immaterial in determining the concentration of electroactive cadmium.

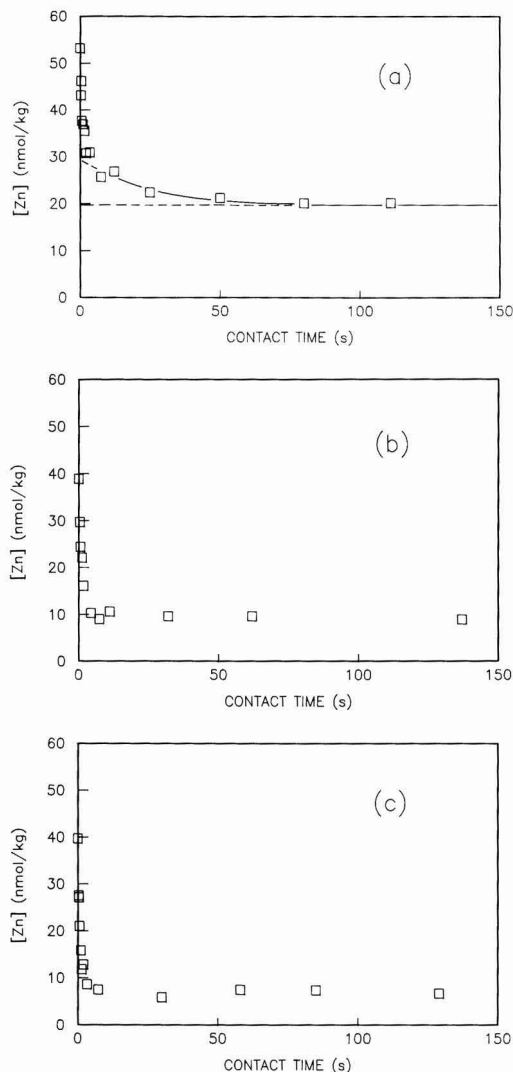


**Figure 6.** Removal of zinc from bay water sample collected on 16 December 1986 by Dowex column method. The total concentration of zinc coming through the column is plotted as a function of the contact time. (a) Untreated. (b) Filtered. (c) UV-irradiated. Contact times longer than 150 s have been omitted for clarity.

**Characterization by Column Ion Exchange.** As seen in Figure 6c, significant desorption of zinc from particles occurred over the time interval 7.5–75 s. Contact times shorter than 7 s were not considered in this calculation since the column-dependent removal rate of labile zinc is superimposed on the desorption signal at shorter contact times. Irradiation of the sample caused this signal to disappear and the labile zinc signal to increase from 25 to 33 nmol kg<sup>-1</sup> (Table I). This result is indicative of an organic surface, either as organic particles proper (live or dead organisms, fecal aggregates, condensed humic material) or as an organic coating on inorganic particles (silicate, carbonate, metal oxides). The remaining inert fraction is comprised of a dissolved organic phase and a particulate inorganic phase (Table I). With cadmium filtration has the effect of removing the inert fraction while UV-irradiation converts it into a labile form, which sug-

**Table I. Summary of the Metal Concentrations (nmol kg<sup>-1</sup>) Seen as Labile by ASV, Dowex Column, and Chelex Batch Methods in the Bay Water Sample Collected on 16 December 1986<sup>a</sup>**

subsample	untreated	UV-irrad	filtered	filtered and UV-irrad
<b>Zinc</b>				
ASV	13 ± 2 <sup>b</sup>		13 ± 2 <sup>b</sup>	21 ± 2 <sup>b</sup>
column	25 ± 4	33 ± 4	29 ± 4	
batch	37 ± 4	42 ± 4		
<b>Cadmium</b>				
ASV	0.39 ± 0.02		0.48 ± 0.05	0.46 ± 0.07
column	0.54 ± 0.05	0.61 ± 0.05	0.47 ± 0.05	
batch	0.53 ± 0.05	0.57 ± 0.05		

<sup>a</sup>Total zinc was 53 ± 4 nmol kg<sup>-1</sup> and total cadmium was 0.57 ± 0.05 nmol kg<sup>-1</sup> (average ± SD). <sup>b</sup>The concentration of inorganic zinc, as obtained by extrapolation of [Zn] to measurement times shorter than 10<sup>-2</sup> s.

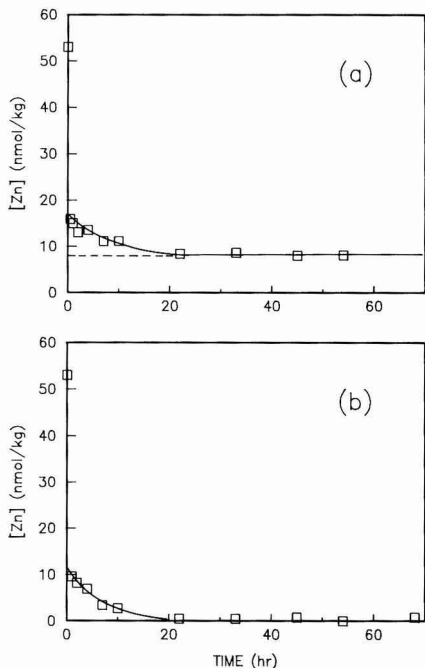


**Figure 7.** Removal of zinc from bay water sample collected on 16 December 1986 by Chelex batch method. (a) Untreated. (b) UV-irradiated. Data points for reaction times longer than 70 h have been omitted for clarity.

gests that cadmium is organically bound in that fraction. When no kinetic signal is present, as in the case for cadmium in the column method, the removal curves will not be presented. All speciation results are nevertheless given for reference in Table I.

#### Characterization by Chelating Batch Adsorption.

Zinc decreased by 37 nmol kg<sup>-1</sup> in the first 0.5 h of the experiment (Figure 7a). As expected, this initial uptake can account for all forms that were sensed as labile or quasi-labile by the column method. It was followed by a slower, first-order decrease, which also could be attributed to the desorption of zinc from some particulate phase (8.3 ± 0.9 nmol kg<sup>-1</sup>;  $k_d = (3.7 \pm 0.3) \times 10^{-5} \text{ s}^{-1}$ ). This result seemingly demonstrates that zinc can adsorb onto inorganic surfaces and that the rate of desorption of the surface complex formed can be slower than for organic surfaces.

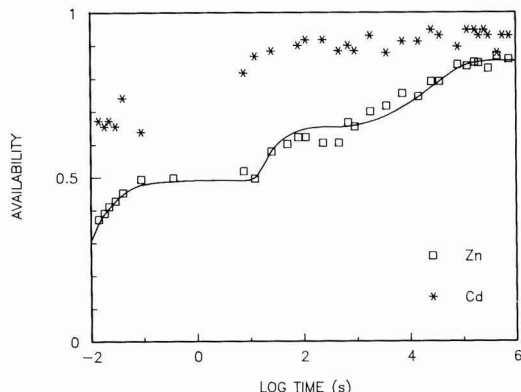


**Figure 8.** Relationship between the availability of zinc and cadmium and the effective time of measurement in the bay water sample collected on 16 December 1986. For zinc, the availability function has been drawn in accordance with the compositional and kinetic parameters extracted from all the individual experiments and listed in Table II; it is defined as follows:  $x_{Zn}(t) = 13/53 + 13/53 [1 - \exp(-31t)] + 9/53 [1 - \exp(-3.8 \times 10^{-2}t)] + 10/53 [1 - \exp(3.9 \times 10^{-5}t)]$ , where  $t$  is the time of measurement in seconds.

When making the comparison, it is implicitly assumed that well-defined coordinative properties (sites) can be assigned to the inorganic surface as well as to the organic surface. The results of the Chelex batch speciation are summarized in Table I. It should be noted that although some zinc (8.0 ± 0.7 nmol kg<sup>-1</sup>) is not accessible to measurement even after 200 h, this inert fraction is made totally available by the UV oxidation treatment. Most of the cadmium is labile with respect to the time scale of the batch method. However, a small inert fraction of organically bound cadmium already detected in the column method was again found (Table I).

#### Overall Kinetic Scheme for Zinc and Cadmium.

In order to have a logical analogy with the term "electrochemical availability" defined by Turner and Whitfield (5), it is proposed to call "availability" of a metal  $M$  the ratio  $[M]/[M]_{\text{total}}$ , where  $[M]$  is the concentration measured by a technique involving diffusion under limiting conditions and  $[M]_{\text{total}}$  is the total metal concentration. Let  $t$  be the characteristic time of the measurement. It is obvious that  $[M]/[M]_{\text{total}} \rightarrow [M]_{\text{free}}/[M]_{\text{total}}$  when  $t \rightarrow 0$  and  $[M]/[M]_{\text{total}} \rightarrow 1$  when  $t \rightarrow \infty$ . The pathway between these two limits will be determined by the kinetics of transformation between the bound forms of the metal and the free metal. In the bay water/zinc system examined here two types of solid phases and one type of complex in solution have been identified and their rates of desorption (or dissociation) measured. Such a characterization proved relatively straightforward because the rate constants were far apart. Consequently, a plot of availability vs time produces a stepwise function where each step is controlled by only one (group of) species: from its height and position the concentration and kinetic behavior of that (group of) species can be determined. In practice, our observations spanned such a broad time range that we chose to present a plot of availability vs log time (Figure 8). In each of the time ranges accessed by the individual techniques the logarithmic scale causes horizontal compression of the data at the longer time scales. Because of this, the zones of time-invariant availability (plateaus) are not as evident as they are when a linear time scale is used. For practical reasons, we did not obtain any overlap between the time domains covered by any two techniques. Yet, the apparent

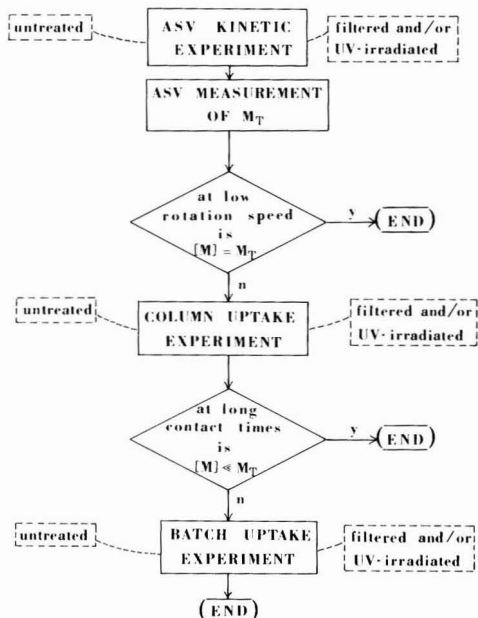


**Figure 9.** Schematic representation of the methodology described in this study.  $[M]$  is the concentration of metal detected at a given time of measurement and  $M_T$  is the total metal concentration.

continuity of the availability function over the whole range of time scales ( $10^{-2}$ – $10^6$  s) suggests that, as practiced here, the ASV as well as column and batch operations are consistent with each other. The results for cadmium seem to confirm this, but also suggest that some (group of) quasi-labile species might have been missed over the time span where no valid measurements of the availability were made (0.1–8.0 s). Yet, even if such a species exists, it certainly cannot be detected from the removal curves of the Dowex column experiments (Figure 6,  $t < 8$  s). More significant, perhaps, is the discrepancy between ASV-labile cadmium measured in the untreated ( $0.39 \pm 0.02$  nmol  $\text{kg}^{-1}$ ) and filtered ( $0.48 \pm 0.05$  nmol  $\text{kg}^{-1}$ ) samples. Indeed, assuming that the former estimate is somehow too low by 0.09 nmol  $\text{kg}^{-1}$  would lead to an average electrochemical availability for cadmium of  $0.84 \pm 0.08$ , i.e., entirely consistent with the  $0.91 \pm 0.03$  measured by the other two techniques.

**Application to Environmental Studies.** Despite the real advantages of this methodology over some empirical speciation schemes, it may not be practical to use it on a routine basis in its complete form, i.e., passing both untreated and treated (filtered and/or UV-irradiated) subsamples through the entire procedure each time. The cadmium results presented here also demonstrate that the column and batch characterization are unnecessary if it can first be established that most of the metal of interest is in fact ASV-labile. Consequently, it may be profitable to measure "total metal" by ASV (see refs 2, 3, and 10) immediately after the ASV experiment, in order to decide whether additional kinetic characterization on the longer time scales is really necessary. This strategy is summarized in Figure 9; it would allow a more reasonable sample throughput and ensure that only "potentially interesting" samples are given the full sequential treatment.

### Discussion

Techniques as unrelated as anodic stripping voltammetry and ion-exchange chromatography (batch or column mode) can be combined to measure the availability of a

**Table II.** Partitioning of Zinc and Cadmium in the Bay Water Sample Collected on 16 December 1986 According to the Kinetic Scheme Developed in This Study [nmol  $\text{kg}^{-1}$  (average  $\pm$  SD)]

	dissolved	particulate (>0.40 $\mu\text{m}$ )
zinc		
inorganic	$13 \pm 2$ ( $k_d$ too high)	$10 \pm 2$ ( $k_d = 3.9 \times 10^{-5} \text{ s}^{-1}$ )
organic	$13 \pm 2$ ( $k_d = 31 \text{ s}^{-1}$ )	$9 \pm 1$ ( $k_d = 3.8 \times 10^{-2} \text{ s}^{-1}$ )
		$8 \pm 1$ ( $k_d$ too low)
cadmium		
inorganic	$0.47 \pm 0.08$	less than 0.05
organic	less than 0.05	$0.05 \pm 0.01$

trace metal under limiting conditions (zero free metal concentration at the electrode or resin bead surface) over a range of time scales (from 10 ms to 8 days). The definition of availability used here is consistent with, and includes, the well-established definition of electrochemical availability (5) and, by analogy with it, is expected to be a function of the time scale of the measurement  $t$ , the diffusion coefficient of the metal species  $D$ , and all the relevant ligand concentrations  $[L_i]$ , complex stability constants  $K_i$ , and dissociation rate constants  $k_{d-i}$ . In the preceding sections, we highlighted the importance of  $t$  and  $k_d$  in determining the availability of zinc in estuarine waters, the other parameters being unknown. The variation of zinc availability with time of measurement was the basis of a new and original speciation scheme, which should be independent of the specific techniques used: apart from a gap between  $t = 0.5$  s and  $t = 5$  s where no observations were made, a continuum of zinc availability was observed over the whole range of time scales. Five distinct groups of zinc species could be distinguished on the basis of their relative labilities, two of which were associated with solid phases Table II). For cadmium, only two groups of species were identified, one dissolved and the other particulate, with a resulting availability that is always greater than that of zinc. This difference is due in part to the greater tendency of cadmium to form chloro complexes in solution and in part to the greater tendency of zinc to adsorb onto the particulate phases present in an estuarine system. The type of species-dependent kinetic information obtainable from such a scheme might be used to assess the role of these species in environmental processes (12). Perhaps the most serious shortcoming comes from the fact that neither Chelex 100 nor Dowex 50W-X8 is able to meet the rather stringent conditions imposed by eqs 1 and 2. In this regard, it would be profitable to develop an ion-exchange resin combining the selectivity of Dowex 50W-X8 (11) with the fast sorption kinetics of Chelex 100.

**Registry No.** Cd, 7440-43-9; Zn, 7440-66-6; water, 7732-18-5.

### Literature Cited

- Davison, W. J. *Electroanal. Chem.* **1978**, *87*, 395.
- Figura, P.; McDuffie, B. *Anal. Chem.* **1980**, *52*, 1433.
- Florence, T. M. *Analyst* **1986**, *111*, 489.
- Shuman, M. S.; Michael, L. C. *Environ. Sci. Technol.* **1978**, *12*, 1069.
- Turner, D. R.; Whitfield, M. J. *Electroanal. Chem.* **1979**, *103*, 43.
- Levich, V. G. *Physicochemical Hydrodynamics*; Prentice-Hall: Englewood Cliffs, NJ, pp 39–72.
- Huizenga, D. L. The Cobalt-APDC Coprecipitation Technique for the Preconcentration of Trace Metal Samples. Technical Report 81-3; University of Rhode Island, Graduate School of Oceanography, 1981.
- Zuehlke, R. W.; Kester, D. R. In *Trace Metals in Sea Water*; Wong, C. S., Boyle, E., Bruland, K. W.; Burton, J. D., Goldberg, E. D., Eds.; NATO Conference Series IV; Vol. 9, pp 773–788.

- (9) Huizenga, D. L. An Examination of Copper Speciation in Sea Water. Ph.D. Thesis, University of Rhode Island, Kingston, RI, 1981.
- (10) Muller, F. L. L. A Kinetic Approach to Zinc Speciation in Marine and Estuarine Waters. Ph.D. Thesis, University of Rhode Island, Kingston, RI, 1988.
- (11) Cox, J. A.; Slovianska, K.; Gatchell, D. K. *Anal. Chem.* **1984**, *56*, 650.
- (12) Kester, D. R. In *The Importance of Chemical "Speciation" in Environmental Processes*; Bernhard, M., Brinkman, F. E., Sadler, P. J., Eds.; Dahlem Konferenzen: Berlin, 1986; pp 275-299.

Received for review June 29, 1988. Revised manuscript received October 6, 1989. Accepted October 6, 1989.

## Kinetics of Trace Metal Complexation: Ligand-Exchange Reactions

Janet G. Hering<sup>†</sup> and François M. M. Morel\*

Ralph M. Parsons Laboratory, Massachusetts Institute of Technology, 48-425, Cambridge, Massachusetts 02139

■ Ligand-exchange reactions of copper–nitrilotriacetate (CuNTA) and copper–humate complexes with a fluorescent ligand, calcein, were examined and compared. The reverse reactions of copper–calcein with ethylenediaminetetraacetate (EDTA) and NTA were also studied; the correspondence of equilibrium constants and kinetic rate constants is discussed. Reactions with model ligands proceeded both by complete dissociation of the initial complex (disjunctive pathway) and by direct attack of the incoming ligand on the initial complex (adjunctive pathway). Reactions of humate-bound copper were also consistent with this mechanistic interpretation. The contributions of the adjunctive and disjunctive pathways depended on the Cu-to-humate loading; both pathways were important at the Cu-to-DOC loadings typical of natural waters. At higher values, disjunctive ligand exchange predominated. This pathway could be interpreted in terms of dissociation of Cu from a humate-binding site and the rate constant related to the conditional stability constant for Cu–humate binding.

### Introduction

The speciation of trace metals in natural waters is controlled by the interaction of the metals with a complex and varying mixture of inorganic anions, organic ligands, reducible or oxidizable dissolved chemical species (e.g., H<sub>2</sub>O<sub>2</sub>), surfaces, and organisms. Filterable concentrations of metals may include fine colloidal particles as well as organic and inorganic metal complexes.

Both metal speciation and biological availability or toxicity are functions of the tendency of the metal to react, as quantified by the free metal ion activity, under pseudo-equilibrium conditions (1–3). For metals occurring as organic complexes, pseudo-equilibrium conditions among dissolved species may be maintained only if the rates of metal complexation reactions are fast compared with rates of metal uptake. If, however, complex dissociation and ligand-exchange rates are slow compared to biological uptake, the rate of metal incorporation into the biota will be limited by abiotic chemical kinetics (3).

The apparent rate of other processes, such as precipitation, reduction, or adsorption, will be similarly influenced by the rates of metal complexation reactions if (i) the reacting metal occurs predominantly as an organic complex and (ii) the process of interest requires removal of the metal from the initial complex.

In this study, we have investigated rates of complex dissociation and ligand exchange for copper under environmentally relevant conditions of pH and metal and ligand concentrations. We have determined the predominant mechanistic pathways for exchange reactions with model ligands under such conditions, focusing on the effects of the relative concentrations of the competing ligands and of the metal-to-ligand ratios. We then examined the kinetics of ligand-exchange reactions of humate-bound copper. These reactions can be described in terms of the mechanisms applicable to the model ligands.

### Background and Theory

Studies of the kinetics of ligand-exchange reactions of transition metals (reviewed in ref 4) have shown the reactions to proceed by direct attack of the incoming ligand on the initial metal complex usually with rate-determining dissociation of the intermediate ternary complex thus:



The overall rate constants are influenced by steric and electrostatic factors and by protonation of the incoming ligand.

In contrast, Shuman and co-workers have observed that ligand-exchange reactions of Cu–DOC complexes involve dissociation of the initial copper complex and have reported rate constants for the dissociation of these complexes (5–7). Other studies of reactions of humate- or fulvate–metal complexes or of reactions of metals with humic or fulvic acids have focused on different metals—Fe (8–11), Al (12, 13), Ni (14), and Th (15, 16).

On the basis of previous work (vide supra), we consider two mechanistic pathways for the overall ligand-exchange reaction: an adjunctive pathway, which proceeds by direct attack of the incoming ligand on the initial complex, and a disjunctive pathway, which proceeds by dissociation of the initial complex. [We use this terminology, introduced in Hering and Morel (17), to emphasize that these pathways are stoichiometric mechanisms inferred from rate laws and do not imply any characterization of the transition state of the substitution reaction: terms and definitions are given in Table I.] The mechanisms for the overall (forward) reaction



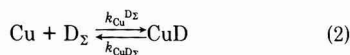
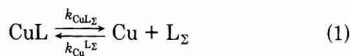
are written below with reaction of the protonated ligands included in the overall rate constants, which are thus pH-dependent. Rate expressions are derived by assuming steady-state concentrations of intermediate species (i.e., Cu and LCuD) and neglecting back-reaction of the product

<sup>†</sup>Current address: Institute for Water Resources and Water Pollution Control (EAWAG), CH-8600 Dübendorf, Switzerland.

**Table I. Terms and Definitions**

$k_{CuL}$ or $k_{CuD}$	intrinsic rate constants for dissociation of complex CuL or CuD
$k_{CuL}^H$ or $k_{CuD}^H$	intrinsic rate constant for acid-catalyzed dissociation of complex CuL or CuD or for dissociation of the protonated complex CuLH or CuDH
$k_{Cu}^L$ or $k_{Cu}^D$	intrinsic rate constant for formation of the complex CuL or CuD by reaction of Cu with D or L
$k_{Cu}^{HL}$ or $k_{Cu}^{HD}$	intrinsic rate constant for formation of complex CuL or CuD by reaction of Cu with HL or HD ( $H^+$ is displaced by the incoming metal)
$k_D^{CuL}$ or $k_{HD}^{CuL}$	intrinsic rate constant for direct attack of D or HD on complex CuL to give the product CuD
$k_{CuD_2}$ or $k_{CuL_2}$	apparent rate constant (at fixed pH) for dissociation (including acid-catalyzed dissociation) of complex CuD or CuL
$k_{D_2}^{CuL}$	apparent rate constant for reaction of all D species with complex CuL to give the product CuD (rate constant for adjunctive pathway)
$k_{Cu}^{L_2}$ or $k_{Cu}^{D_2}$	apparent rate constant (at fixed pH) for formation of complex CuL or CuD by reaction of Cu with all L or D species (including protonated ligand species)
$\alpha$	ratio of rate constants for reaction of Cu with $D_2$ and $L_2$ , $k_{Cu}^{D_2}/k_{Cu}^{L_2}$
$k_{CuHum\Sigma}$	apparent rate constant (at fixed pH) for dissociation of CuHum
$k_{Cu}^{Hum\Sigma}$	apparent rate constant (at fixed pH) for reaction of Cu with Hum
$k_{overall}$	overall rate constant describing dependence of the rate, usually $-d[D]/dt$ , on reactant concentrations as specified in the text
$k_{dis}$	component of the overall rate constant attributed to reaction via disjunctive pathway
$k_{adj}$	component of the overall rate constant attributed to reaction via adjunctive pathway
$k^{H1}$	rate constant for reaction of CuHum1 with $D_2$
$k_{dis}^{H1}$ or $k_{adj}^{H1}$	rate constant for reaction of CuHum1 with $D_2$ by disjunctive or adjunctive pathway
$k^{H2}$	rate constant for reaction of CuHum2 with $D_2$
$K_{HD}$ or $K_{HL}$	equilibrium stability constant for complex HD or HL
$K_{CuD}^{cond}$	conditional stability constant (pH-dependent) for complex CuD
$P_m$	fitting parameter used to account for imperfect mixing in kinetics experiments
$Y_T$	total concentration of species Y ( $Y = D, L, Hum, Cu$ )
$D_2$ or $L_2$ or $Hum_2$	concentration of free or protonated species D, L, or Hum (e.g., $L_2 = HL + L = L_T - CuL$ )
[HumX] or [CuHumX]	concentration of humate binding site X or of Cu bound at humate site X ( $X = 1, 2$ for two binding sites)
[X] <sub>0</sub> or [X] <sub>t</sub>	concentration of species X ( $X = D, L, Hum, CuD, CuL, etc.$ ) at time $t = 0$ or at some later time, $t$
S	site density of Cu humate binding sites/mg of humic acid

CuD. For each mechanism, contributions of the protonated species to the rate constants can be expressed explicitly if equilibration of protonated species is assumed to be rapid. Thus, for the disjunctive mechanism



$$\frac{-d[D_2]}{dt} = \left[ \frac{k_{CuL_2} k_{Cu}^{D_2}}{k_{Cu}^{D_2} [D_2] + k_{Cu}^{L_2} [L_2]} \right] [CuL][D_2] \quad (3)$$

where

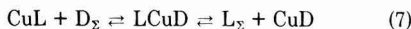
$$k_{CuL_2} = k_{CuL} + k_{CuL}^H [H^+] \quad (4)$$

$$k_{Cu}^{L_2} = \frac{k_{Cu}^{HL} K_{HL} [H^+] + k_{Cu}^L}{1 + K_{HL} [H^+]} \quad (5)$$

$$k_{Cu}^{D_2} = \frac{k_{Cu}^{HD} K_{HD} [H^+] + k_{Cu}^D}{1 + K_{HD} [H^+]} \quad (6)$$

[N.B.,  $k_{CuD_2}$  is neglected in consideration of the reaction as written above. It is shown here for future discussion on the reverse reaction (i.e.,  $CuD + L \rightarrow D + CuL$ ).

For the adjunctive reaction



$$\frac{-d[D_2]}{dt} = k_{D_2}^{CuL} [CuL][D_2] \quad (8)$$

where

$$k_{D_2}^{CuL} = \frac{k_D^{CuL} + k_{HD}^{CuL} K_{HD} [H^+]}{1 + K_{HD} [H^+]} \quad (9)$$

In this study, the rate constants for the formation and

dissociation of the ternary complex, which is assumed to be at steady state, were not resolved and so are expressed as a single term ( $k_{D_2}^{CuL}$ ).

These two types of mechanisms can be distinguished experimentally based on the effect of the free (excess) L concentration on the overall rate. The apparent rate constants (that is, for the reaction considered as first order in both [CuL] and  $[D_2]$ ) for the disjunctive pathway should be strongly influenced by the relative concentrations of D and L. For  $[L] \gg [D]$ , competitive behavior is predicted and the rate should be inversely proportional to [L]. For  $[L] \ll [D]$ , "trapping" behavior is predicted and the rate should be dependent only on the rate constant for dissociation of the initial metal complex at fixed pH ( $k_{CuL_2}$ ). In contrast, the apparent rate constant for the adjunctive pathway should be unaffected by the concentration of free L or the L:D ratio.

### Experimental Section

**Materials.** Analytical-grade reagents were used without further purification, except for NaCl. Solutions of 5 M NaCl, prepared with analytical-grade salts, were treated with Chelex 100 to remove trace metals and then diluted with Milli-Q water. (Chelex 100 resin was cleaned with 3 M  $NH_4OH$ , rinsed extensively, and then reconverted to the Na form before use to minimize leaching of organic chelators from the resin.) Humic acid (Aldrich) was obtained as the Na salt and cleaned before use by reprecipitation from acid solution (as described in ref 18). The fluorescent reagent calcein, 3',6'-dihydroxy 4',5'-bis[N,N'-(dicarboxymethyl)aminomethyl]fluoran, (herein referred to as dye or D) was used as received from Sigma.

All kinetics experiments (except for the study of the reverse reaction of NTA with CuD) were performed in 0.1 M NaCl and  $10^{-3}$  M  $(PO_4)_T$  (pH =  $7.4 \pm 0.2$ ) at room temperature. The experiment on the reverse reaction was done in 0.1 M NaCl buffered to pH 7.3 with 5 mM HEPES [N-(2-hydroxyethyl)piperazine-N'-2-ethanesulfonic acid]. Experiments were routinely conducted using acid-washed

(dilute HCl) polyethylene and sample handling was done in a laminar flow hood.

**Use of the Fluorescent Reagent.** Calcein, the condensation product of fluorescein with aminodiacetate and formaldehyde, is fluorescent over the pH range of ~3–11. The fluorescence is quenched on formation of complexes with paramagnetic transition metals, in this case Cu(II) (ref 19 and references cited therein). The structure, based on proton NMR and acidity constants for calcein, has been determined by Markuszewski (20). Metal complexation with calcein occurs through the aminodiacetate functionalities and the phenolic hydroxy groups of the parent compound fluorescein. Both 1:1 and 2:1 metal-calcein complexes have been reported. The conditional stability constant for the 1:1 complex at pH = 7 reported by Saari and Seitz (21) is  $10^{12.3}$ . The overall stability constants for the 2:1 complex range from  $10^{20.8}$  in 50% ethanol (20) to  $10^{29.0}$  (22). Our best estimates for conditional stability constants at pH = 7.3, based on fluorescence quenching, are  $K_{CuL} = 10^{12.8}$  and  $\beta_{Cu_2L} = 10^{24.5}$ . Equilibrium fluorescence quenching experiments in the presence of NTA also suggest the formation of a fluorescent ternary complex, calceinNTACu (23).

Fluorescence was measured with a Perkin-Elmer LS-5 fluorescence spectrophotometer at an excitation wavelength of 492 nm and an emission wavelength of 511 nm. Fluorescence signals were integrated over 4 s. The fluorescence-dye concentration relationship was calibrated for all kinetics experiments in the presence of NTA or EDTA. For experiments with humic acid, the dye fluorescence was calibrated at each humic acid concentration. The decrease in apparent dye fluorescence at high concentrations of humic acid is attributed to light absorption by the humic acid in solution. Fluorescence quenching arising from dye-humate association is unlikely due to the hydrophilic nature of the fluorescent reagent.

**Kinetics Experiments.** All kinetics experiments (again excepting the NTA reverse-reaction experiment) were performed by mixing approximately equal volumes of the two reagent solutions (one a solution of the initial Cu-ligand complex and the other of the incoming ligand), using a dual-syringe assembly to deliver the mixed reagent solutions into a fluorescence cuvette. The first fluorescence reading was obtained at ~20 s and thereafter at ~10-s intervals. Fluorescence was measured over 10–30 min. The extent of reaction occurring over this time varied considerably depending on the reaction conditions. For the NTA reverse reaction (performed in duplicate), the reaction was initiated by spiking a solution of the dye preequilibrated with Cu in 100-mL volumetric flasks with a small aliquot of 0.01 M NTA to give a total NTA concentration of 10  $\mu$ M. The solutions were mixed and aliquots removed for fluorescence measurements. The first fluorescence measurement was obtained at ~4 min. Each flask was sampled at ~10-min intervals for the first hour and the reaction was followed to equilibrium (~4 h).

**Data Treatment and Modeling.** In all kinetics experiments, measured fluorescence was related to free dye concentration by calibration curves obtained immediately following the kinetics experiments. Only the free or protonated dye species were considered to contribute to observed fluorescence. The quenching of fluorescence in the forward reaction was attributed solely to the formation of a 1:1 CuD species. Thus, from the total concentrations of reagents, the (assumed) stoichiometry of the complexes, and the observed fluorescence, the concentrations of free D and CuD over time could be calculated. For the reverse reaction (i.e., reaction of NTA or EDTA with CuD species),

formation of Cu<sub>2</sub>D was also considered in calculating initial dye speciation. However, the reaction of Cu<sub>2</sub>D + L → CuD + CuL was neglected in the kinetic analysis as it does not result in any fluorescence change.

Kinetic rate constants were extracted from the data (observed concentration of free dye over time at varying initial reactant concentrations) based on the models for the ligand-exchange reactions described above. For kinetics experiments performed with the dual-syringe assembly, the imperfect initial mixing affects the initial concentrations of the reagents. A fitting parameter  $P_m$ ,  $P_m$  = apparent [D]<sub>0</sub>/undiluted [D], was introduced in the data analysis to account for this imperfect mixing ( $P_m$  = 0.5 corresponds to ideal mixing). The method of extraction of rate constants is described in detail in Appendix I. Briefly, for the forward reaction of CuNTA with dye with NTA in excess, the reaction was analyzed as first order in both [CuNTA] and [D]. For [CuNTA] ≫ [D], the [CuNTA] was constant over time and a pseudo-first-order rate constant was obtained from an exponential fit to [D] vs time. For [CuNTA] ≈ [D] (again with NTA in excess), the second-order rate constant was obtained explicitly from the expression

$$\frac{1}{a-b} \ln \left[ \frac{b(a-x)}{a(b-x)} \right] = kt \quad (10)$$

where  $a$  and  $b$  are the initial reactant concentrations and  $x$  is the amount reacted (24). Rate constants thus obtained for the disjunctive ( $k_{CuL_2}k_{Cu}^{D_2}/k_{Cu}^{L_2}$ ) and adjunctive ( $k_{D_2}^{CuL}$ ) pathways were then used in modeling the forward reaction of CuNTA with dye where NTA was *not* in excess. In this case the data was interpreted such that

$$\text{rate} = \frac{-d[D_2]}{dt} = \left[ \frac{k_{CuL_2}k_{Cu}^{D_2}}{k_{Cu}^{L_2}[NTA] + k_{Cu}^{D_2}[D]} + k_{D_2}^{CuL} \right] [CuNTA][D_2] \quad (11)$$

and the parameter  $\alpha$  (the ratio of  $k_{Cu}^{D_2}/k_{Cu}^{L_2}$ ) was obtained.

For the reverse reaction of CuD with excess ligand (either NTA or EDTA), the data were analyzed as pseudo first order in [CuD]. Rate constants for the adjunctive ( $k_{L_2}^{CuD}$ ) and disjunctive ( $k_{CuD_2}$  for [L] ≫ [D]) pathways were calculated from the dependence of the pseudo-first-order rate constant on the concentration of the incoming ligand L.

## Results

**Mechanisms and Rates for Ligand-Exchange Reactions with Model Ligands.** Ligand-exchange reactions between the fluorescent dye and synthetic ligands were studied for the forward reaction, CuL + D → L + CuD, with L = NTA. Ligand exchange was inhibited in the presence of an excess concentration of the outgoing ligand, free NTA, as shown in Figure 1. For experiments with a sufficient excess of NTA (free NTA:dye > 5), rate constants for the disjunctive pathway (NTA-dependent) and adjunctive pathway (NTA-independent) were extracted from a plot of overall second-order rate constant (i.e., rate = -d[D]/dt =  $k_{overall}[CuNTA][D]$ ) as a function of 1/[free NTA] as shown in Figure 2. The nonzero intercept indicates that at high free NTA concentrations the dominant pathway for ligand exchange does not involve complete dissociation of the CuNTA complex. From Figure 2, the following rate constants are obtained: an NTA-dependent rate constant of  $(1.31 \pm 0.07) \times 10^{-3} \text{ s}^{-1}$  and an NTA-in-

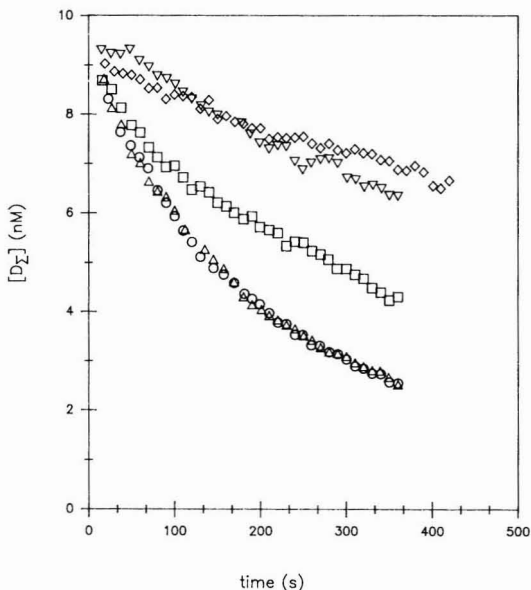


**Figure 1.** Dye concentration,  $[D_z]$ , over time for forward reaction,  $\text{CuNTA} + \text{D} \rightarrow \text{NTA} + \text{CuD}$ , at varying NTA concentrations for  $D_T \approx 10$  nM,  $\text{Cu}_T \approx 50$  nM,  $\text{NTA}_T \approx 60$  nM (O,  $\Delta$ ), 80 nM ( $\square$ ), 120 nM ( $\nabla$ ), or 200 nM ( $\diamond$ ).

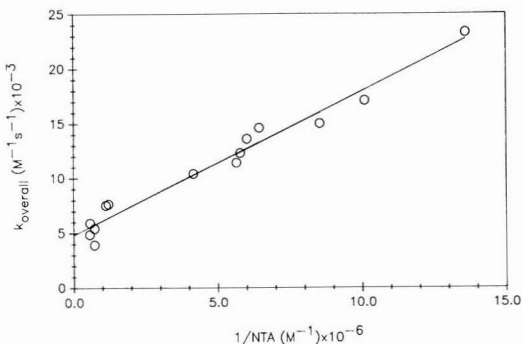


**Figure 2.** Overall (second-order) rate constants for forward reaction,  $\text{CuNTA} + \text{D} \rightarrow \text{NTA} + \text{CuD}$ , (i.e.,  $k_{\text{overall}}$  for rate  $= -d[D]/dt = k_{\text{overall}}[\text{CuNTA}][D]$ ) vs  $1/[\text{NTA}]$ . The slope corresponds to the NTA-dependent rate constant for the disjunctive pathway and the intercept to the NTA-independent rate constant for the adjunctive pathway.

dependent rate constant of  $(4.8 \pm 1.0) \times 10^3 \text{ M}^{-1} \text{ s}^{-1}$ . For these conditions (i.e., excess free NTA), the contributions of the two pathways are equal at a free NTA concentration of  $\sim 270$  nM.

The reverse reaction,  $\text{CuD} + \text{L} \rightarrow \text{D} + \text{CuL}$ , was studied in the presence of excess concentrations of the incoming ligand, for  $\text{L} = \text{NTA}$  with a very large excess of NTA and for  $\text{L} = \text{EDTA}$  over a range of EDTA concentrations. For the reaction of  $\text{CuD}$  with EDTA (EDTA in excess), contributions of disjunctive and adjunctive pathways to the overall rate could be assessed by plotting an overall pseudo-first-order rate constant (i.e., for rate  $= d[D]/dt = k_{\text{overall}}[\text{CuD}]$ ) against EDTA concentration (Figure 3). In this case, the EDTA-independent rate constant of  $(4 \pm 2) \times 10^{-5} \text{ s}^{-1}$  is due to the contribution of the disjunctive pathway (under "trapping" conditions) and the EDTA-dependent rate constant of  $33 \pm 4 \text{ M}^{-1} \text{ s}^{-1}$  to the contribution of the adjunctive pathway. (Note that this de-

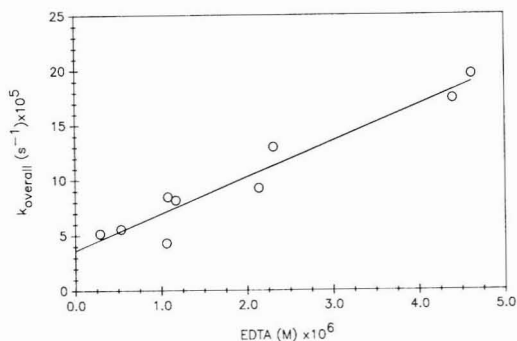


**Figure 3.** Overall (pseudo-first-order) rate constant for reverse reaction,  $\text{CuD} + \text{EDTA} \rightarrow \text{D} + \text{CuEDTA}$ , (i.e.,  $k_{\text{overall}}$  for rate  $= -d[\text{CuD}]/dt = k_{\text{overall}}[\text{CuD}]$ ) vs  $[\text{EDTA}]$ . The slope corresponds to the EDTA-dependent rate constant for the adjunctive pathway and the intercept to the EDTA-independent rate constant for the disjunctive pathway under "trapping" conditions of excess incoming ligand.

pendence on ligand concentration arises from treatment of the reverse reaction as pseudo first order in the concentration of the initial complex rather than as first order in both concentrations of the initial complex and of the incoming ligand.) On the basis of the value of the disjunctive rate constant obtained from the EDTA experiments, this pathway can be neglected for the reaction of  $\text{CuD}$  with a very large excess of NTA. In this case, only the adjunctive pathway was considered to contribute to the observed rate constant of  $25 \pm 2 \text{ M}^{-1} \text{ s}^{-1}$ .

**Interpretation of Rate Constants for Reactions of Model Ligands.** The various ligand-dependent and ligand-independent rate constants obtained for the forward reaction,  $\text{CuL} + \text{D} \rightarrow \text{CuD} + \text{L}$  ( $\text{L} = \text{NTA}$ ), and the reverse reaction,  $\text{CuD} + \text{L} \rightarrow \text{CuL} + \text{D}$  ( $\text{L} = \text{NTA}, \text{EDTA}$ ), can be related to the rate constants for the adjunctive and disjunctive pathways (as summarized in Table II).

Thus, for the forward reaction in the presence of excess  $\text{L}$ , the NTA-dependent rate constant for the disjunctive pathway corresponds to the term  $k_{\text{CuL}_2} k_{\text{Cu}}^{D_z} / k_{\text{Cu}}^{L_z}$ . Since the inverse of the ratio  $k_{\text{CuL}_2} / k_{\text{Cu}}^{L_z}$  equals the conditional stability constant for  $\text{CuNTA}$  ( $K_{\text{CuNTA}}^{\text{cond}} = 10^{10.6}$ ,  $\text{pH} = 7.3$ ,  $\mu = 0.1$ ; ref 25), the intrinsic rate constant  $k_{\text{Cu}}^{D_z}$  can be calculated. Thus

$$k_{\text{Cu}}^{D_z} = \frac{k_{\text{CuL}_2} k_{\text{Cu}}^{D_z}}{k_{\text{Cu}}^{L_z}} K_{\text{CuNTA}}^{\text{cond}} = (5.2 \pm 0.3) \times 10^7 \text{ M}^{-1} \text{ s}^{-1}$$

For ligand-exchange experiments under conditions for which the free NTA was not in excess of the dye, the value of  $\alpha$  (i.e., the ratio of  $k_{\text{Cu}}^{D_z} / k_{\text{Cu}}^{L_z}$ ) was obtained from the NTA-dependent (disjunctive) rate constant (defined in eq 11). Due to the difficulties with imperfect mixing (and the necessity for the additional mixing parameter  $P_m$ ), the value of  $\alpha$  is not well constrained by the experimental data. The experimental results are consistent with a value of this ratio of  $0.6 \pm 0.3$  (shown for a sample data set in Figure 4).

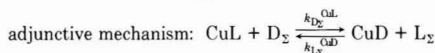
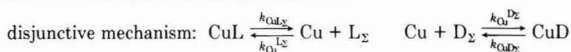
Based on this value for  $\alpha$ , the rate constants  $k_{\text{Cu}}^{L_z}$  and  $k_{\text{CuL}_2}$  can be estimated. Thus

$$k_{\text{CuL}_2} = \frac{k_{\text{CuL}_2} k_{\text{Cu}}^{D_z}}{k_{\text{Cu}}^{L_z} \alpha} = \frac{1.31 \times 10^{-3}}{0.6} = (2 \pm 1) \times 10^{-3} \text{ s}^{-1}$$

and

$$k_{\text{Cu}}^{L_z} = K_{\text{CuNTA}}^{\text{cond}} k_{\text{CuL}_2} = 10^{10.6} (2 \times 10^{-3}) = (9 \pm 4) \times 10^7 \text{ M}^{-1} \text{ s}^{-1}$$

**Table II. Summary of Rate Constants for Ligand-Exchange Reactions**



(a) Rate Constants for Forward Reaction

description of rate constant or parameter obtained (value)	interpretation	value
NTA-dependent ( $1.31 \times 10^{-3} \text{ s}^{-1}$ )	$k_{\text{CuL}_{\Sigma}} k_{\text{CuD}_{\Sigma}} / k_{\text{CuL}_{\Sigma}}^{\text{D}_2}$	$k_{\text{CuD}_{\Sigma}} = 5.2 \times 10^{-1} \text{ s}^{-1}$ (for $k_{\text{CuL}_{\Sigma}} / k_{\text{CuL}_{\Sigma}}^{\text{D}_2} = K_{\text{CuL}_{\Sigma}}^{\text{cond}}$ )
$\alpha$ (0.6)	$k_{\text{CuD}_{\Sigma}}^{\text{D}_2} / k_{\text{CuL}_{\Sigma}}^{\text{D}_2}$	$k_{\text{CuL}_{\Sigma}}^{\text{D}_2} = 9 \times 10^7 \text{ M}^{-1} \text{ s}^{-1}$
NTA-independent	$k_{\text{D}_{\Sigma}\text{CuL}}$	$k_{\text{CuL}_{\Sigma}} = 2 \times 10^{-3} \text{ s}^{-1}$ $4.8 \times 10^3 \text{ M}^{-1} \text{ s}^{-1}$

(b) Rate Constants for Reverse Reaction

description of rate constant or parameter obtained (value)	interpretation	value
EDTA-independent	$k_{\text{CuD}_{\Sigma}}$	$4 \times 10^{-5} \text{ s}^{-1}$
EDTA-dependent	$k_{\text{L}_{\Sigma}\text{CuD}}$	$33 \text{ M}^{-1} \text{ s}^{-1}$
(assumed) NTA-dependent	$k_{\text{L}_{\Sigma}\text{CuD}}$	$25 \text{ M}^{-1} \text{ s}^{-1}$

(c) Values of Equilibrium Stability Constants Obtained from Kinetic Rate Constants

$$K_{\text{CuD}}^{\text{cond}} = k_{\text{CuD}_{\Sigma}} / k_{\text{CuD}_{\Sigma}} = 10^{12.1}$$

$$K_{\text{CuD}}^{\text{cond}} = [k_{\text{D}_{\Sigma}\text{CuL}} / k_{\text{L}_{\Sigma}\text{CuD}}] K_{\text{CuL}}^{\text{cond}} = 10^{12.9}$$

for L = NTA,  $K_{\text{CuL}}^{\text{cond}} = 10^{10.6}$

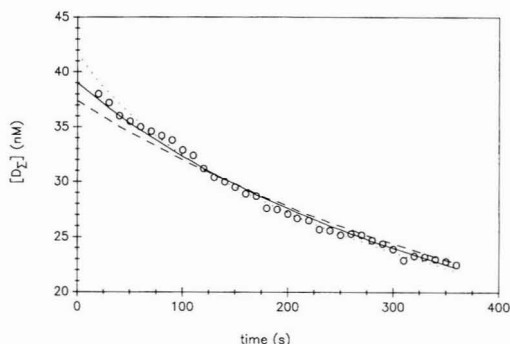


**Figure 4.** Dye concentration,  $[\text{D}_2]$ , over time for forward reaction of CuNTA with  $\text{D}_2$  (for  $\text{D}_T \approx 40 \text{ nM}$ ,  $\text{Cu}_T \approx 50 \text{ nM}$ ,  $\text{NTA}_T \approx 60 \text{ nM}$ ). Model fit to data for (—)  $\alpha = 0.7$ ,  $P_m = 0.49$ ; (---)  $\alpha = 1.1$ ,  $P_m = 0.47$ ; (---)  $\alpha = 0.3$ ,  $P_m = 0.52$ .

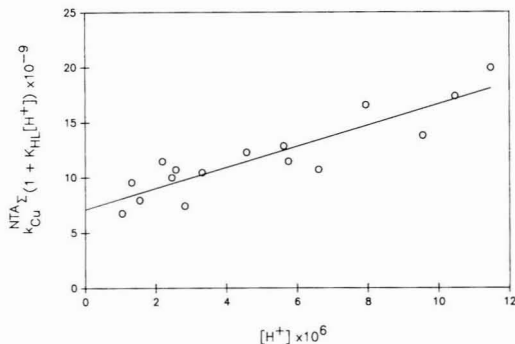
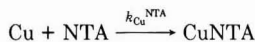
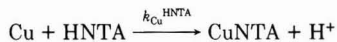


**Figure 5.** Effect of pH on formation of CuNTA based on work of Maguire (26). For the reaction  $\text{Cu} + \text{NTA}_{\Sigma} \rightarrow \text{CuNTA}$ ,  $k_{\text{CuNTA}} = (k_{\text{CuNTA}} + k_{\text{CuHNTA}} K_{\text{HNTA}} [\text{H}^+]) / (1 + K_{\text{HNTA}} [\text{H}^+])$ . Thus, the intrinsic rate constants  $k_{\text{CuNTA}}$  and  $k_{\text{CuHNTA}}$  can be obtained from a plot of  $k_{\text{CuNTA}} / (1 + K_{\text{HNTA}} [\text{H}^+])$  vs  $[\text{H}^+]$ .

An independent estimate of  $k_{\text{CuL}_{\Sigma}}$  may be obtained from the work of Maguire (26) in which the effect of pH on the rate of CuNTA formation was studied. For the reactions



and



the overall rate constant for reaction of Cu with both NTA species is

$$k_{\text{CuNTA}_{\Sigma}} = \frac{k_{\text{CuNTA}} + k_{\text{CuHNTA}} K_{\text{HNTA}} [\text{H}^+]}{1 + K_{\text{HNTA}} [\text{H}^+]} \quad (12)$$

Values for the rate constants  $k_{\text{CuNTA}}$  ( $7.1 \times 10^9 \text{ M}^{-1} \text{ s}^{-1}$ ) and  $k_{\text{CuHNTA}}$  ( $1.0 \times 10^5 \text{ M}^{-1} \text{ s}^{-1}$ ) were obtained from a plot of  $k_{\text{CuNTA}_{\Sigma}} / (1 + K_{\text{HNTA}} [\text{H}^+])$  vs  $[\text{H}^+]$  as shown in Figure 5. The predicted value for  $k_{\text{CuNTA}_{\Sigma}}$  at pH = 7.3 of  $2.0 \times 10^7 \text{ M}^{-1} \text{ s}^{-1}$  is in reasonable agreement with our value for  $k_{\text{CuL}_{\Sigma}}$  of  $9 \times 10^7 \text{ M}^{-1} \text{ s}^{-1}$ .

For the reverse reaction under "trapping" conditions (i.e., excess EDTA), the EDTA-independent rate constant (disjunctive pathway) corresponds to the rate constant for dissociation of the CuD complex,  $k_{\text{CuD}_{\Sigma}}$ , and the EDTA-dependent rate constant to the rate constant for adjunctive exchange,  $k_{\text{L}_{\Sigma}\text{CuD}}$ . The consistency of the kinetic data may be assessed by comparison of kinetic and equilibrium constants. The ratio of disjunctive rate constants,  $k_{\text{CuD}_{\Sigma}}$  (obtained from the forward reaction of CuNTA) and  $k_{\text{CuD}_{\Sigma}}$  (from the reverse reaction of CuD with EDTA), is the conditional stability constant for CuD; then

$$\frac{k_{\text{CuD}_{\Sigma}}}{k_{\text{CuD}_{\Sigma}}} = k_{\text{CuD}}^{\text{cond}} = \frac{5.2 \times 10^7}{4 \times 10^{-5}} = 10^{12.1 \pm 0.2}$$

This value for  $K_{\text{CuD}}^{\text{cond}}$  is somewhat less than the best estimate from equilibrium studies ( $K_{\text{CuD}}^{\text{cond}} = 10^{12.8}$ ). Some of the discrepancy between estimates for  $K_{\text{CuD}}^{\text{cond}}$  may be due to the involvement of minor species (see Discussion).

The value of  $K_{\text{CuD}}^{\text{cond}}$  can also be obtained from the ratio of the adjunctive rate constants for forward and reverse



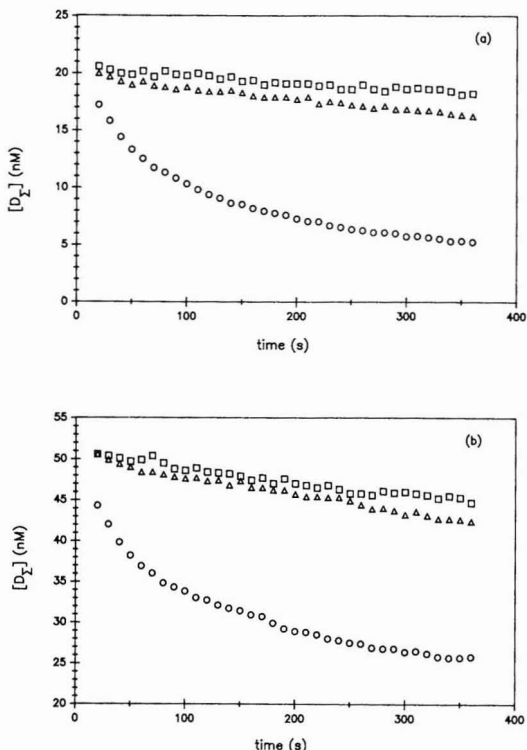


**Figure 6.** Dye concentration  $[D_2]$ , over time for  $\text{CuHum} + \text{D} \rightarrow \text{Hum} + \text{CuD}$  for  $\text{Cu}_T \approx 50 \text{ nM}$  and  $\text{D}_T \approx 20 \text{ nM}$  (a) or  $50 \text{ nM}$  (b). Total humic acid:  $1.1 \text{ mg/L}$  (O),  $5.4 \text{ mg/L}$  ( $\Delta$ ), and  $10.8 \text{ mg/L}$  ( $\square$ ).

reactions with  $\text{L} = \text{NTA}$ . The ratio of  $k_{D_2}^{\text{CuL}}$ , the NTA-independent rate constant for the forward reaction, and  $k_{L_2}^{\text{CuD}}$ , the rate constant for the reverse reaction with a large excess of NTA, corresponds to the ratio of the conditional stability constants for  $\text{CuD}$  and  $\text{CuNTA}$ . Thus

$$\frac{k_{D_2}^{\text{CuL}}}{k_{L_2}^{\text{CuD}}} = \frac{K_{\text{CuD}}^{\text{cond}}}{K_{\text{CuNTA}}^{\text{cond}}} = \frac{4.8 \times 10^3}{25} = 190 \pm 40$$

Then for  $K_{\text{CuNTA}}^{\text{cond}} = 10^{10.6}$ ,  $K_{\text{CuD}}^{\text{cond}} = 10^{12.9 \pm 0.1}$  in good agreement with the value from equilibrium studies of  $10^{12.8}$ .

**Ligand-Exchange Reactions of Humate-Bound Copper.** The reaction of the dye with Cu-humate complexes was studied at several humic acid concentrations. For the forward reaction  $\text{CuHum} + \text{D} \rightarrow \text{Hum} + \text{CuD}$ , a decrease in the ligand-exchange rate was observed with increasing humic acid concentrations (Figure 6). For the ligand-exchange reaction with 5.4 or 10.8 mg/L humic acid, each reaction could be described with a single rate constant as shown in Figure 7a. However, for lower concentrations of humic acid (1.1 mg/L), two rate constants were required (Figure 7b). Values obtained for the rate constants are summarized in Table III. As discussed for the model system, the contributions of the disjunctive and adjunctive mechanisms may be estimated from the dependence of the overall (second-order) rate constants on the free humic acid concentration (i.e.,  $[\text{Hum}_T] - [\text{CuHum}]$ ). For 5.4 and 10.8 mg/L humic acid, the humic acid Cu-binding sites appear to be sufficiently in excess of  $\text{Cu}_T$  (50 nM) that  $[\text{free humic}] \approx [\text{total humic}]$ . However, for 1.1 mg/L humic acid, the necessity for two kinetic rate constants suggests that the Cu concentration is not negligible compared to the concentration of strong binding sites. Thus, the data

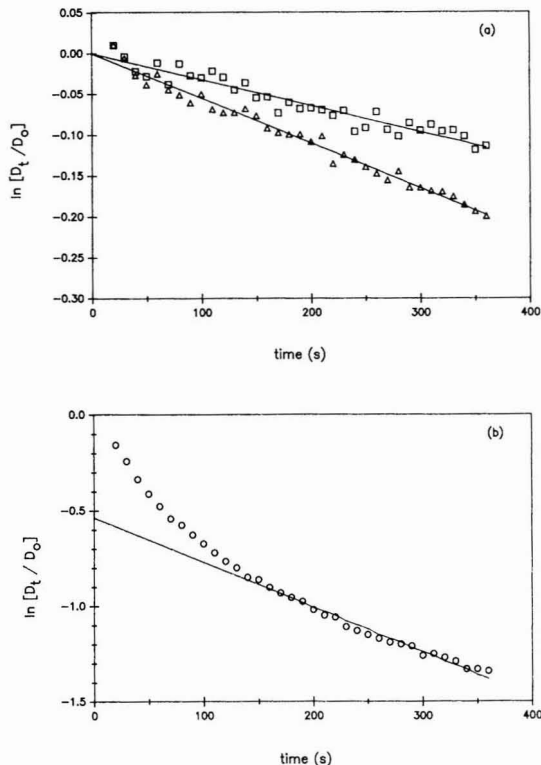


**Figure 7.** Logarithmic transform of the free dye over time (normalized to apparent  $[D]_0$ ) for  $\text{CuHum} + \text{D} \rightarrow \text{Hum} + \text{CuD}$  for  $\text{Cu}_T \approx 50 \text{ nM}$ ,  $\text{D}_T \approx 20 \text{ nM}$ , (a)  $\text{Hum}_T \approx 5.4 \text{ mg/L}$  ( $\Delta$ ), and  $10.8 \text{ mg/L}$  ( $\square$ ) and (b)  $\text{Hum}_T \approx 1.1 \text{ mg/L}$ . With  $[\text{CuHum}] > [\text{D}]$ , the reaction is pseudo first order in  $[\text{D}]$ .

**Table III.** Summary of Overall Rate Constants for Ligand-Exchange Reactions with Humate-Bound Cu,  $\text{Cu}_T \approx 50 \text{ nM}$  (i.e.,  $k_{\text{overall}} \text{ for Rate} = -d[\text{D}]/dt = k_{\text{overall}}[\text{CuHum}][\text{D}]$ )

$\text{D}_T$ , nM	$\text{Hum}_T$ , mg/L	overall (second-order) rate constant, $\text{M}^{-1} \text{ s}^{-1}$
20	10.8	$6.6 \times 10^3$
50	10.8	$7.4 \times 10^3$
20	5.4	$1.1 \times 10^4$
50	5.4	$1.0 \times 10^4$
20	1.1	(early) $9 \times 10^3$
		(late) $6.0 \times 10^4$

for 1.1 mg/L are omitted from Figure 8a, which shows the second-order rate constant vs the reciprocal of the humic acid concentration (in mg/L). Again by analogy with the model system, we expect that the disjunctive and adjunctive rate constants may be obtained from the observed dependence of the overall rate constant (for rate =  $-d[\text{D}]/dt = k_{\text{overall}}[\text{CuHum}][\text{D}]$ ) on the free humate concentration, that is

$$k_{\text{overall}} = k_{\text{dis}} \frac{1}{[\text{Hum}]} + k_{\text{adj}} \quad (13)$$

From Figure 8a,

$$k_{\text{dis}} = (3.95 \pm 0.63) \times 10^4 \text{ mg} \cdot \text{mol}^{-1} \text{ s}^{-1}$$

and

$$k_{\text{adj}} = (3.3 \pm 0.6) \times 10^3 \text{ M}^{-1} \text{ s}^{-1}$$

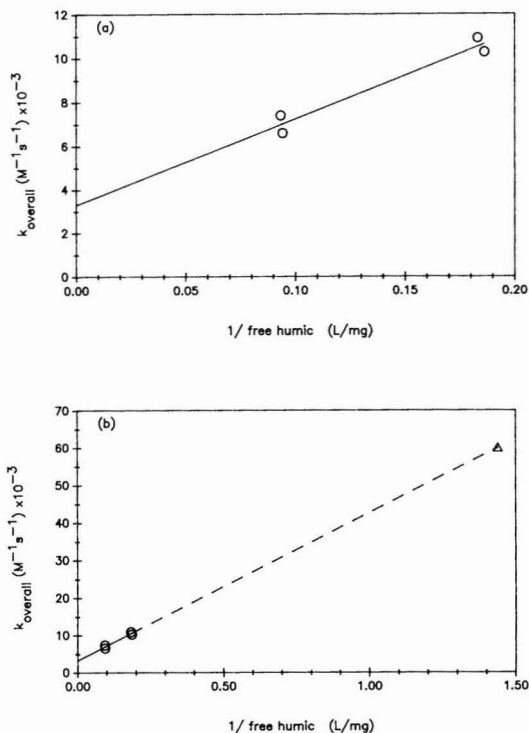


**Figure 8.** Plot of overall (second-order) rate constant (i.e.,  $k_{\text{overall}}$  for rate  $= -d[D]/dt = k_{\text{overall}}[\text{CuHum}][D]$ ) vs  $1/[\text{free humic}]$  for  $\text{CuHum} + D \rightarrow \text{Hum} + \text{CuD}$ , where  $k_{\text{overall}} = k_{\text{dis}}/[\text{free humic}] + k_{\text{adj}}$ . (a) Experimental results for 5.4 and 10.8 mg/L of humic acid (with the assumption that  $[\text{free humic}] \approx [\text{total humic}]$ ). (b) Experimental values for 5.4 and 10.8 mg/L (O) and extrapolated value for 1.1 mg/L  $\text{Hum}_T$  (Δ) used in calculations for Figure 9.

These results indicate the contribution of the disjunctive pathway (predominant at low [free humate]) and the adjunctive pathway (predominant at high [free humate]) to the observed reaction. Under these reaction conditions, the contributions of the two pathways are equal at a free humate concentration of  $\sim 13$  mg/L, that is, at a Cu-to-humate ratio of  $\sim 4$   $\mu\text{mol}$  of Cu/g of humate.

For the experiments with 1.1 mg/L humic acid, the apparent change in the rate constants over the course of the reaction indicated that the amount of Cu bound was not negligible compared to the concentration of strong Cu-binding sites. If, for the reaction with 20 nM dye, it is assumed that the observed rate constant for the later part of the reaction conforms to the equation determined for the reaction at higher humic acid concentrations, i.e.,  $k_{\text{overall}} = 3300 + 39500(1/[\text{free humic}])$ , then the concentration of free humic at 1.1 mg/L total humic acid and 50 nM  $\text{Cu}_T$  can be calculated. As shown in Figure 8b, for  $k_{\text{overall}} = 60000$ , the calculated free humic concentration is 0.7 mg/L. Thus, by difference, the Cu-bound humic concentration is 0.4 mg/L. The amount of Cu bound at this site is  $\sim 42$  nM (since some of the total 50 nM of Cu is bound at the faster reacting site; see Appendix II). Thus, the site density is

$$\frac{42 \text{ nM Cu}}{0.4 \text{ mg/L}} \approx 10^{-7} \frac{\text{mol Cu-binding site}}{\text{mg humic acid}}$$

For the experiment with 50 nM dye and 1.1 mg/L humic acid, rate constants could not be obtained directly because

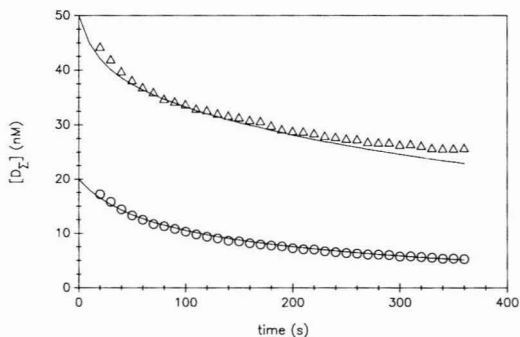
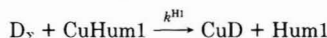
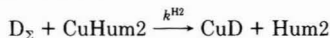


**Figure 9.** Model fit for reaction of dye with two Cu-humate species (solid lines) and data for ligand-exchange reaction of dye with Cu/humic acid ( $\text{Cu}_T \approx 50$  nM,  $\text{Hum}_T \approx 1.1$  mg/L) and  $D_T \approx 20$  nM (O) or 50 (Δ) nM.

the change in Cu-humate concentration is significant compared to the change in the dye concentration. Instead, for these conditions, we compared the observed reaction rates predicted based on the rate constants obtained in other ligand-exchange experiments with humic acids using the following model. (A complete description of the model is given in the Appendix II.) In this model, the dye reacts with Cu bound at two humate sites (i.e., with  $\text{CuHum1}$ , the slow-reacting species, and  $\text{CuHum2}$ , the fast-reacting species). The initial concentrations of these Cu-humate species (for  $\text{Cu}_T \approx 50$  nM,  $\text{Hum}_T \approx 1.1$  mg/L) were obtained from the experiments with 20 nM dye. The reaction of the dye with  $\text{CuHum1}$  is described with two rate constants, for ligand exchange via disjunctive and adjunctive pathways, obtained from Figure 8a. The reaction of the dye with  $\text{CuHum2}$  is described with a single rate constant. The value for this rate constant was optimized from the model fit for the experiment with 20 nM dye, 1.1 mg/L humic acid. Then for



$$\text{where } k^{H1} = \frac{k_{\text{dis}}^{H1}}{[\text{Hum1}]} + k_{\text{adj}}^{H1}$$

$$\frac{-d[D_T]}{dt} = k^{H2}[\text{CuHum2}][D_T] + \left( \frac{k_{\text{dis}}^{H1}}{[\text{Hum1}]} + k_{\text{adj}}^{H1} \right) [\text{CuHum1}][D_T] \quad (14)$$

where

$$[\text{Hum1}] \text{ (mg/L)} = \text{Hum}_T \text{ (mg/L)} - \frac{[\text{CuHum1}] \text{ (mol/L)}}{\text{site density (mol/mg)}} \quad (15)$$

The site density ( $10^{-7}$  mol/mg) was obtained from the 20 nM  $D_T$ , 1.1 mg/L  $\text{Hum}_T$  experiment as described above. The model fit to the data is shown for experiments with 1.1 mg/L  $\text{Hum}_T$ , 50 nM  $\text{Cu}_T$ , and both 20 and 50 nM  $D_T$  in Figure 9. (Note that there are no adjustable parameters in the fit to the 50 nM dye experiment.) The deviation of the model fit from the data at longer times may indicate that the system is approaching equilibrium. The general agreement of the model with the data demonstrates the consistency of ligand-exchange experiments with 1.1, 5.4, and 10.8 mg/L  $\text{Hum}_T$ .

**Table IV. Cu-to-DOC Loadings in Natural Waters**

water type	$\mu\text{mol}$ of Cu/g of C	ref
oceanic (Sal 36.1)	3.8	27
coastal (Sal 32)	4.7–9.7 <sup>a</sup>	
	7.0 <sup>b</sup>	28
coastal (Sal 26.8–36.4)	1.9–5.6 <sup>a</sup>	
	3.7 <sup>b</sup>	27
estuarine (Sal 5.4)	6.5	29
estuarine (Sal 10.9)	14	29
estuarine (Sal 13.9)	13	29
tidal pond (Sal 23–28)	3.7–12.1 <sup>a</sup>	
	7.3 <sup>b</sup>	28
four lakes (pH 5.5–6.5)	6–26 <sup>a</sup>	
	16 <sup>b</sup>	30
ten lakes (pH 4.6–6.3)	1.1–32 <sup>a</sup>	
	9.2 <sup>b</sup>	31
two ponds	27, 61	32
two rivers (pH 5.8)	5.7	31
stream	60	32
lake sediment pore waters	5.2 <sup>b</sup>	33

<sup>a</sup> Range. <sup>b</sup> Average.

### Discussion

The results obtained in model systems (with well-defined ligands) demonstrate that the kinetics of ligand-exchange reactions are consistent with a relatively simple interpretation. In this interpretation, ligand-exchange reactions at high concentrations of the out-going ligand are dominated by direct attack of the incoming ligand on the initial metal-ligand complex (adjunctive pathway). This result is consistent with previous observations. However at low concentrations of the outgoing ligand (in this case NTA), a disjunctive pathway becomes important. Based on this model, kinetic constants can be derived from the data. The agreement of the rate constant for the formation of CuNTA (at pH = 7.3) derived from ligand-exchange experiments with the value predicted from the work of Maguire (26) as well as the coherence of kinetic rate constants and equilibrium stability constants supports our interpretation of the ligand-exchange kinetic data.

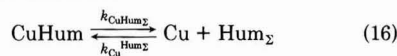
Although this mechanistic model for ligand-exchange reactions is reasonably consistent with kinetic and equilibrium observations, it is nonetheless an oversimplification of the actual system. Equilibrium experiments show that some minor species, particularly the dinuclear species Cu<sub>2</sub>D, are not negligible. The presence of a stable ternary complex, NTACuD, is also suggested by equilibrium experiments (23). However, with only the available information on the concentration of reacting species, a more detailed mechanism cannot be defined.

Based on results from the model system, ligand-exchange reactions of the fluorescent reagent with Cu-humate may be interpreted by using the same models. These results suggest both disjunctive and adjunctive pathways for the ligand-exchange reactions. The contributions of the two mechanisms to the overall reaction are approximately equal at a free humic acid concentration of  $\sim 13 \pm 4$  mg/L with 50 nM Cu<sub>T</sub> or at a Cu-to-humate loading of  $\sim 4$   $\mu\text{mol}$  of Cu/g of humic acid (or  $\sim 8$   $\mu\text{mol}$  of Cu/g of humic C).

To assess the contributions of these pathways in natural waters, this value for Cu-to-humate loading may be compared with Cu<sub>T</sub>/DOC ratios measured in the environment (Table IV). The Cu-to-humate carbon loading for which the disjunctive and adjunctive mechanisms are equally important in ligand-exchange reactions falls within the range of Cu-to-DOC loadings in natural waters. This comparison must be regarded with some caution. Although similar metal-humate interactions have been observed for

commercial (soil-derived) and aquatic humic materials (18), there are significant structural differences between the commercial and natural materials (34). In addition, the normalization to DOC for natural waters may overestimate the proportion of the DOC involved in metal binding. Comparisons of whole waters with isolated fulvic acids suggest that approximately 50% of the DOC is important in metal binding (35), though the lower apparent metal binding for whole waters might also result from higher ambient metal concentrations (36). Nonetheless, the comparison in Table IV suggests that both of these types of mechanisms may be important under natural conditions. In contrast, only a disjunctive pathway for ligand exchange was observed in the experiments of Shuman et al. (6), as would be expected for their much higher Cu-to-DOC loadings (340  $\mu\text{mol}$  of Cu/g of DOC).

The rate constant for ligand-exchange reactions by the disjunctive pathway of Cu-humate complexes with the fluorescent dye provides information on Cu-humate binding. By analogy with the model system, for the ligand-exchange reaction, CuHum + D  $\rightarrow$  Hum + CuD, by a disjunctive mechanism



the observed humic-dependent rate constant is

$$k_{\text{dis}} = \frac{k_{\text{CuHum}_2} k_{\text{CuD}_2}}{k_{\text{CuHum}_2}} = (3.95 \pm 0.63) \times 10^4 \text{ mg}\cdot\text{mol}^{-1} \text{ s}^{-1}$$

From the model study,  $k_{\text{CuD}_2} = (5.2 \pm 0.3) \times 10^7 \text{ M}^{-1} \text{ s}^{-1}$ , then

$$\frac{k_{\text{CuHum}_2}}{k_{\text{CuHum}_2}} = \frac{3.95 \times 10^4}{5.2 \times 10^7} = (7.6 \pm 1.3) \times 10^{-4} \text{ mg/L}$$

or  $k_{\text{CuHum}_2}/k_{\text{CuHum}_2} = (1.3 \pm 0.2) \times 10^3 \text{ L/mg}$ . This ratio is related to a more conventionally expressed conditional stability constant for CuHum by the Cu-binding site density (in mol/mg of humic acid). Thus

$$k_{\text{CuHum}_2}/k_{\text{CuHum}_2} = 10^{3.12} = \frac{K_{\text{CuHum}_2}^{\text{cond}} [\text{L/mol}] \text{ site density} [\text{mol/mg}] (18)$$

For the calculated site density of  $\sim 10^{-7} \text{ mol/mg}$ , the corresponding stability constant for Cu binding at this site ( $K_{\text{CuHum}_2}$ ) is  $10^{10.1}$ . Although equilibrium Cu-humate interactions (determined by complexometric titrations) have also been described in terms of Cu binding at discrete humate-binding sites, comparison of model parameters obtained from kinetic and equilibrium studies would be misleading. It has clearly been shown that the discrete ligand model (derived from equilibrium studies) does not uniquely describe complexometric titration data and thus physical-chemical significance cannot necessarily be attributed to model parameters, i.e., stability constants and concentrations of binding sites (37–39). It remains to be seen whether alternative models for metal-humate interactions are also consistent with kinetic data.

The results of ligand-exchange experiments with humic acids demonstrate the crucial role of metal-to-humate loading in kinetics experiments. Only at low Cu-to-humate loadings (approximately environmental values) can the contribution of the adjunctive mechanism be discerned. At higher Cu-to-humate loadings, more than one rate constant is required to describe the exchange reaction. Several rate constants were also required to model the reactions of CuDOC with 4-(2-pyridylazo)resorcinol (PAR)

at 340  $\mu\text{mol}$  of Cu/g of DOC (6), of Ni-fulvate with PAR at 120–1100  $\mu\text{mol}$  of Ni/g of fulvic acid (14), and of Th-humate with arsenazo(III) at 50  $\mu\text{mol}$  of Th/mequiv of humic acid or 250  $\mu\text{mol}$  of Th/g of humic acid, assuming 5 mequiv/g of humic acid (16).

For ligand-exchange reactions at low Cu-to-humate ratios, the requirement for only a single rate constant for the disjunctive mechanism does not necessarily indicate involvement of only one type of humate binding site. The apparent "saturation" of the site(s) by Cu at 1.1 mg/L humic acid puts an upper bound on the site density and thus a lower bound on the Cu-humic stability constant. However, the involvement of stronger sites at correspondingly lower site densities cannot be excluded.

### Conclusion

The ligand-exchange reactions of Cu-humate species with the fluorescent reagent can be interpreted on the basis of the model used for the reaction of this reagent with CuNTA. Experiments with well-defined ligands demonstrate that the concentration range and relative concentrations of the reactants chosen for study determines whether the contributions of different mechanisms can be discerned. Ligand-exchange reactions of Cu complexes with well-defined ligands and with humic acid proceed by mechanisms involving dissociation of the initial Cu complex (disjunctive pathway) and direct attack of the incoming ligand on the initial complex (adjunctive pathway). Both pathways are likely to be important at Cu-to-humate loadings occurring in natural waters. The rate constants observed for the disjunctive reaction of Cu-humate species may be further interpreted to provide information on equilibrium stability constants for Cu-humate interactions.

### Appendix I

#### Extraction of Rate Constants from Kinetic Data.

**A. Forward Reaction,  $\text{CuL} + \text{D} \rightarrow \text{L} + \text{CuD}$ . 1. Excess L.** (a) For  $[\text{CuNTA}] \gg [\text{D}]$ , a pseudo-first-order rate constant,  $k$  ( $\text{s}^{-1}$ ), (for rate  $= -d[\text{D}]/dt = k[\text{D}]$ ) was obtained from an exponential fit to the concentration of free dye over time. The extrapolated value of  $[\text{D}]_0$  was used to calculate the mixing parameter  $P_m$ ,  $P_m = [\text{apparent } [\text{D}]_0 / (\text{undiluted } [\text{D}])]$  where the apparent  $[\text{D}]_0$  is obtained by extrapolation of the observed  $[\text{D}]$  vs  $t$  to  $t = 0$  and the undiluted  $[\text{D}]$  is the known dye concentration before mixing. Then the second-order rate constant,  $k$  ( $\text{M}^{-1} \text{s}^{-1}$ ), (for rate  $= -d[\text{D}]/dt = k[\text{CuNTA}][\text{D}]$ ) was calculated such that

$$\text{second-order } k \text{ (M}^{-1} \text{s}^{-1}) = \frac{\text{pseudo-first-order } k \text{ (s}^{-1})}{[\text{CuNTA}]} \quad (1)$$

where the concentration of CuNTA is corrected for the mixing inefficiency [where apparent  $[\text{CuNTA}] = (1 - P_m)$  undiluted  $[\text{CuNTA}]$ ].

(b) For  $[\text{CuNTA}] \approx [\text{D}]$ , the second-order rate constant was obtained explicitly by plotting

$$\frac{1}{[\text{CuNTA}]_0 - [\text{D}]_0} \ln \left[ \frac{[\text{D}]_0([\text{CuNTA}]_0 - x)}{[\text{CuNTA}]_0([\text{D}]_0 - x)} \right] \quad (2)$$

vs time, where  $x$  is the amount reacted (24). The mixing parameter  $P_m$  in this case was also obtained from the ratio of the apparent initial dye concentration (again extrapolated from a simple exponential fit) to the expected initial concentration.

2.  $[\text{L}] \approx [\text{D}]$ . For the reaction of CuNTA with dye (NTA not in excess), the data were modeled by applying

the rate constants for the disjunctive ( $k_{\text{CuL}_2} k_{\text{Cu}}^{\text{D}_2} / k_{\text{Cu}}^{\text{L}_2}$ ) and adjunctive ( $k_{\text{D}_2}^{\text{CuL}}$ ) mechanisms obtained (as described above) from experiments with NTA in excess. For each data set, the fit was optimized with two fitting parameters,  $\alpha$  (the ratio of  $k_{\text{Cu}}^{\text{D}_2} / k_{\text{Cu}}^{\text{L}_2}$ ) and  $P_m$ , by comparing the observed  $[\text{D}]$  over time with the predicted values based on the following model. For  $\text{CuNTA} + \text{D} \rightarrow \text{NTA} + \text{CuD}$ ,

$$\frac{-d[\text{D}_2]}{dt} = \left[ \frac{k_{\text{CuL}_2} k_{\text{Cu}}^{\text{D}_2}}{k_{\text{Cu}}^{\text{L}_2} [\text{NTA}] + k_{\text{Cu}}^{\text{D}_2} [\text{D}]} + k_{\text{D}_2}^{\text{CuL}} \right] [\text{CuNTA}][\text{D}_2] \quad (3)$$

Let  $[\text{D}]_t = y$ ; then the amount reacted is  $[\text{D}]_0 - y$  and from stoichiometry

$$[\text{CuNTA}]_t = [\text{CuNTA}]_0 - [\text{D}]_0 + y$$

$$[\text{NTA}]_t = [\text{NTA}]_0 + [\text{D}]_0 - y$$

then

$$\frac{-dy}{dt} = \left[ \frac{k_{\text{CuL}_2} k_{\text{Cu}}^{\text{D}_2}}{k_{\text{Cu}}^{\text{L}_2} ([\text{NTA}]_0 + [\text{D}]_0 - y) + k_{\text{Cu}}^{\text{D}_2} y} + k_{\text{D}_2}^{\text{CuL}} \right] [([\text{CuNTA}]_0 - [\text{D}]_0 + y)y] \quad (4)$$

or

$$\left[ \frac{\alpha k_{\text{CuL}_2}}{(\alpha - 1)y + [\text{NTA}]_0 + [\text{D}]_0} + k_{\text{D}_2}^{\text{CuL}} \right] \times [([\text{CuNTA}]_0 - [\text{D}]_0)y + y^2] \quad (5)$$

and

$$[y]_{t+\Delta t} = [y]_t - \left[ \left[ \frac{\alpha k_{\text{CuL}_2}}{(\alpha - 1)y + [\text{NTA}]_0 + [\text{D}]_0} + k_{\text{D}_2}^{\text{CuL}} \right] [([\text{CuNTA}]_0 - [\text{D}]_0)y + y^2] \right] \Delta t \quad (6)$$

The mixing parameter  $P_m$  affects the initial values of all concentrations such that

$$\text{apparent } [\text{D}]_0 = \text{undiluted } [\text{D}](P_m)$$

$$\text{apparent } [\text{NTA}]_0 = \text{undiluted } [\text{NTA}](1 - P_m)$$

$$\text{apparent } [\text{Cu}]_0 = \text{undiluted } [\text{Cu}](1 - P_m)$$

Because there are two fitting parameters in this model,  $\alpha$  and  $P_m$ , there is a large uncertainty in the value of  $\alpha$ .

**B. Reverse Reaction,  $\text{CuD} + \text{L} \rightarrow \text{D} + \text{CuL}$ .** For the reaction of CuD with excess ligand (either NTA or EDTA), the data were analyzed as a pseudo-first-order reaction in  $[\text{CuD}]$ . Thus, for  $\text{CuD} + \text{L} \rightarrow \text{D} + \text{CuL}$  (excess L), the pseudo-first-order rate constant for the indirect pathway is

$$\frac{k_{\text{CuD}_2} k_{\text{Cu}}^{\text{L}_2} [\text{L}]}{k_{\text{Cu}}^{\text{L}_2} [\text{L}] + k_{\text{Cu}}^{\text{D}_2} [\text{D}]} = k_{\text{CuD}_2} \text{ for } [\text{L}] \gg [\text{D}] \quad (7)$$

and the pseudo-first-order rate constant for the direct pathway is

$$k_{\text{L}_2}^{\text{CuD}} [\text{L}_2]$$

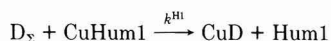
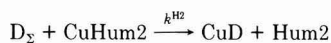
for

$$\frac{-d[\text{CuD}]}{dt} = [k_{\text{CuD}_2} + k_{\text{L}_2}^{\text{CuD}}[\text{L}_2]][\text{CuD}] \quad (8)$$

For experiments with EDTA, a value for  $P_m$  based on the apparent concentration of  $[\text{D}]_0$  was applied as a correction to all concentrations. In these cases the effect of the formation of  $\text{Cu}_2\text{D}$  on the expected  $[\text{D}]_0$  was also included in the calculation. However, the reaction of  $\text{Cu}_2\text{D} + \text{L} \rightarrow \text{CuD} + \text{CuL}$  is neglected in the kinetic analysis as it does not result in any fluorescence change.

## Appendix II

**Model Used for Reaction of Dye with Cu-Humic Acid (50 nM  $\text{Cu}_T$ , 1.1 mg/L Humic Acid).** Dye reacts with Cu bound at two humate sites (i.e.,  $\text{CuHum1}$ , slow-reacting species, and  $\text{CuHum2}$ , fast-reacting species).



where

$$k^{\text{H1}} = \frac{k_{\text{dis}}^{\text{H1}}}{[\text{Hum1}]} + k_{\text{adj}}^{\text{H1}}$$

Then species concentrations over time are predicted from

$$[\text{D}]_{t+\Delta t} = [\text{D}]_t - \left[ k^{\text{H2}}[\text{CuHum2}]_t[\text{D}]_t + \left[ \frac{k_{\text{dis}}^{\text{H1}}}{[\text{Hum1}]} + k_{\text{adj}}^{\text{H1}} \right] [\text{CuHum1}]_t [\text{D}]_t \right] \Delta t$$

$$[\text{CuHum2}]_{t+\Delta t} = [\text{CuHum2}]_t - [k^{\text{H2}}[\text{CuHum2}]_t[\text{D}]_t] \Delta t$$

$$[\text{CuHum1}]_{t+\Delta t} = [\text{CuHum1}]_t - \left[ \frac{k_{\text{dis}}^{\text{H1}}}{[\text{Hum1}]} + k_{\text{adj}}^{\text{H1}} \right] [\text{CuHum1}]_t [\text{D}]_t \Delta t$$

and

$$[\text{Hum1}]_{t+\Delta t} = \text{Hum1}_T - \frac{[\text{CuHum1}]_{t+\Delta t}}{S}$$

The input parameters to this model are as follows:  $k_{\text{dis}}^{\text{H1}} = 39\,500 \text{ mg}\cdot\text{mol}^{-1} \text{ s}^{-1}$ ;  $k_{\text{adj}}^{\text{H1}} = 3300 \text{ M}^{-1} \text{ s}^{-1}$ ;  $k^{\text{H2}} = 9 \times 10^9 \text{ M}^{-1} \text{ s}^{-1}$ ;  $\text{Hum}_T = 1.1 \text{ mg/L}$ ;  $[\text{D}]_0 = 20 \text{ or } 50 \text{ nM}$ ;  $[\text{CuHum1}]_0 = 42 \text{ nM}$ ;  $[\text{CuHum2}]_0 = 8 \text{ nM}$ ;  $S = 10^{-7} \text{ mol/mg}$ ;  $\Delta t = 10 \text{ s}$ .

The rate constants  $k_{\text{adj}}^{\text{H1}}$  and  $k_{\text{dis}}^{\text{H1}}$  are obtained from analysis of ligand-exchange experiments conducted with high humic acid concentrations, as shown in Figure 8a. The rate constant  $k^{\text{H2}}$  is optimized from the model fit for the experiment with 20 nM dye, 50 nM  $\text{Cu}_T$ , and 1.1 mg/L  $\text{Hum}_T$ .

The initial concentrations of  $\text{CuHum1}$  and  $\text{CuHum2}$  and the site density  $S$  are calculated as follows: For the experiment with 20 nM dye, 50 nM  $\text{Cu}_T$ , and 1.1 mg/L,  $\ln[\text{D}]$  is plotted vs time (shown in Figure 6b). The extrapolation of the line fit to these data (for  $t \geq 130 \text{ s}$ ) to zero time gives the concentration of dye reacting with  $\text{CuHum1}$  (the slow-reacting Cu-humate species). The remainder of the dye is taken to have reacted with  $\text{CuHum2}$ . Thus

$$D_T - \text{extrapolated value of } [\text{D}]_0 = [\text{CuHum2}]_0$$

$$\text{Cu}_T - [\text{CuHum2}]_0 = [\text{CuHum1}]_0$$

The site density,  $S$  is calculated as described in the text under Results.

## Literature Cited

- Sunda, W. G.; Guillard, R. R. J. *Mar. Res.* **1976**, *34*, 511-29.
- Anderson, D. M.; Morel, F. M. M. *Limnol. Oceanogr.* **1978**, *23*, 283-95.
- Anderson, M. A.; Morel, F. M. M. *Limnol. Oceanogr.* **1982**, *27*, 789-813.
- Margerum, D. W.; Cayley, G. R.; Weatherburn, D. C.; Pagenkopf, G. K. In *Coordination Chemistry*; Martell, A., Ed.; ACS Monograph 174; American Chemical Society: Washington, DC, 1978; Vol. 2, pp 1-220.
- Shuman, M. S.; Michael, L. C. *Environ. Sci. Technol.* **1978**, *12*, 1069-72.
- Shuman, M. S.; Collins, B. J.; Fitzgerald, P. J.; Olson, D. L. In *Aquatic and Terrestrial Humic Materials* Christmann, R. F., Gjessing, E. T., Eds., 1983, Ann Arbor, MI: Ann Arbor Science.
- Olson, D. L.; Shuman, M. S. *Anal. Chem.* **1983**, *55*, 1103-7.
- Langford, C. H.; Khan, T. R. *Can. J. Chem.* **1975**, *53*, 2979-84.
- Langford, C. H.; Kay, R.; Quance, G. W.; Khan, T. R. *Anal. Lett.* **1977**, *10*, 1249-60.
- Langford, C. H.; Wong, S. M.; Underdown, A. L. *Can. J. Chem.* **1981**, *59*, 181-6.
- Waite, T. D.; Morel, F. M. M. *Anal. Chim. Acta* **1984**, *162*, 263-74.
- Mak, M. K. S.; Langford, C. H. *Can. J. Chem.* **1982**, *60*, 2023-8.
- Plankey, B. J.; Patterson, H. H.; Cronan, C. S. *Environ. Sci. Technol.* **1986**, *20*, 160-5.
- Lavigne, J. A.; Langford, C. H.; Mak, M. K. S. *Anal. Chem.* **1987**, *59*, 2616-20.
- Choppin, G. R.; Nash, K. L. *J. Inorg. Nucl. Chem.* **1981**, *43*, 357-9.
- Cacheris, W. P.; Choppin, G. R. *Radiochim. Acta* **1987**, *42*, 185-90.
- Hering, J. G.; Morel, F. M. M. *Environ. Sci. Technol.* **1988**, *22*, 1469-78.
- Hering, J. G.; Morel, F. M. M. *Environ. Sci. Technol.* **1988**, *22*, 1234-7.
- Pribil, R. *Applied Complexometry*; Pergamon Press: Oxford, UK, 1982.
- Markuszewski, R. Ph.D. Thesis, Iowa State University, Ames, IO, 1976.
- Saari, L. A.; Seitz, W. R. *Anal. Chem.* **1984**, *56*, 810-3.
- Miyahara, T. *Bunseki Kagaku* **1977**, *26*, 615-20; *Chem. Abstr.* **1978**, *88*, 28490a.
- Hering, J. G. Ph.D. Thesis, Massachusetts Institute of Technology—Woods Hole Oceanographic Institution Joint Program in Oceanography. Cambridge, MA, 1988.
- Moore, J. W.; Pearson, R. G. *Kinetics and Mechanism*, 3rd ed.; Wiley-Interscience: New York, 1981.
- Martell, A. E.; Smith, R. M. *Critical Stability Constants*; Plenum Press: New York, 1974; Vol. 1.
- Maguire, J. *Can. J. Chem.* **1974**, *52*, 4106-8.
- Sunda, W. G.; Ferguson, R. L. In *Trace Metals In Sea Water*; Wong, C. S., Boyle, E., Bruland, K. W., Burton, J. D., Goldberg, E. D., Eds.; Plenum Press: New York, 1983; pp 871-91.
- Anderson, D. M.; Lively, J. S.; Vaccaro, R. F. *J. Mar. Res.* **1984**, *42*, 677-95.
- Newell, A. D.; Sanders, J. G. *Environ. Sci. Technol.* **1986**, *20*, 817-21.
- Hutchinson, N. J.; Sprague, J. B. *Environ. Toxicol. Chem.* **1987**, *6*, 755-65.
- Giesy, J. P.; Briese, L. A.; Leversee, G. J. *Environ. Geol.* **1978**, *2*, 257-68.
- Giesy, J. P. *Environ. Toxicol. Chem.* **1983**, *6*, 203-24.
- Piemontessi, D.; Baccini, P. *Environ. Technol. Lett.* **1986**, *7*, 577-92.
- Malcolm, R. L.; MacCarthy, P. *Environ. Sci. Technol.* **1986**, *20*, 904-11.
- McKnight, D. M.; Feder, G. L.; Thurman, M.; Wershaw, R. L.; Westall, J. C. *Sci. Total Environ.* **1983**, *28*, 65-76.

(36) Cabaniss, S. E.; Shuman, M. S. *Geochim. Cosmochim. Acta* 1988, 52, 195-200.  
 (37) Dzombak, D. A.; Fish, W.; Morel, F. M. M. *Environ. Sci. Technol.* 1986, 20, 669-75.  
 (38) Turner, D. R.; Varney, M. S.; Whitfield, M.; Mantoura, R. F. C.; Riley, J. P. *Geochim. Cosmochim. Acta* 1986, 50, 289-97.

(39) Cabaniss, S. E.; Shuman, M. S. *Geochim. Cosmochim. Acta* 1988, 52, 185-93.

Received for review June 9, 1989. Accepted October 5, 1989. Financial support from the National Science Foundation (Grant OCE 8317532) and the Office of Naval Research (Contract N-00014-80-C-0273) is gratefully acknowledged.

## A Conceptual Model of Organic Chemical Volatilization at Waterfalls

Michael McLachlan, Donald Mackay,\* and Philip H. Jones

Institute for Environmental Studies, University of Toronto, Toronto, Ontario, Canada M5S 1A4

■ A conceptual model of volatilization of organic chemicals at waterfalls is presented. It is suggested that the extent of volatilization may be controlled by diffusion limitations (as is the case with oxygen and chemicals with large air-water partition coefficients), by the flow rate of air into the plunge pool (for chemicals with low air-water partition coefficients), or both. The model is applied to 11 organic contaminants present in the water of Niagara Falls. The results suggest that volatilization is significant for chloroform, chlorinated benzenes, and PCBs, but negligible for 2,3,7,8-TCDD,  $\gamma$ -HCH, and PAHs. The model can generate only order of magnitude estimates. Model validation is required for more exact predictions.

### Introduction

The exchange of gases and vapors between air and water plays an important role in the fate of many organic contaminants in the environment (1-3). It has been established that dams and weirs significantly enhance river reaeration, i.e., the diffusion of oxygen from air into water (4). It is expected that volatilization, the diffusion of compounds from water to air, is also enhanced by these hydraulic disturbances. It is thus possible that waterfalls significantly affect the fate of many organic compounds in rivers and act as "point sources" of atmospheric contaminants. In the course of a study of organic chemical fate in the Niagara River (5) a conceptual model of mass transfer at Niagara Falls was assembled to evaluate this possibility. In this paper we present this model, discuss the factors that may influence the rate of volatilization, and suggest that the process is fundamentally different in nature from volatilization at water surfaces.

### Background

Early efforts to describe diffusive mass transfer between air and water in the environment focused on reaeration in rivers. From mass balances for dissolved oxygen and later for various tracers a number of predictive equations have been developed for oxygen diffusion into rivers as a function of river depth, gradient, and flow velocity (6). These equations have been extended to describe the volatilization of organic chemicals from rivers (2, 7, 8). Whitman's two resistance diffusion concept has gained widespread acceptance as the appropriate model for mass transfer across the air-water interface (9-11) by quantifying liquid "film" and gas "film" resistances in series at the air-water interface. The values of the mass-transfer coefficients for the two films are a function of the air and water turbulence, temperature, and molecular diffusivities.

Considerable research has also been directed toward quantifying reaeration at waterfalls and dams usually in the form of correlations for the deficit ratio ( $r$ ), the ratio

of the oxygen deficit above the falls to that below the falls, namely

$$r = (C_s - C_i)/(C_s - C_o) \quad (1)$$

where  $C$  is oxygen concentration, subscripts referring to saturation  $s$ , upstream or inflow  $i$ , and downstream or outflow  $o$ . A value of unity for  $r$  implies no transfer; a value of infinity implies attainment of equilibrium.

The following correlations have been proposed for  $r$  as a function of fall height ( $h$ ) and other parameters describing water quality ( $a$ ), weir structure ( $b$ ), temperature ( $T$ , °C), flow rate per unit crest length ( $q_w$ ), and depth of plunge pool ( $d$ ):

$$r = 1 + 0.38abh(1 - 0.11h)(1 + 0.046(T + 273)) \quad (12)$$

$$r_{25} = e^{0.525h} \quad (25 \text{ }^\circ\text{C}) \quad (13)$$

$$r_{15} = 2.05h^{0.434} \quad (15 \text{ }^\circ\text{C}) \quad (\text{Jarvis in ref 13}) \quad (4)$$

$$r_{20} = 1 + 0.21h \quad (20 \text{ }^\circ\text{C}) \quad (\text{Holler in ref 13}) \quad (5)$$

$$\ln(r_{20}) = 5.92h^{0.816}q_w^{-0.363}d^{0.310} \quad (14) \quad (6)$$

These correlations were developed from measurements on laboratory-scale structures or small weirs or falls with a maximum height of 3 m. As is shown in Figure 1, they are in fair agreement in the 1-3-m height range, but for greater heights the correlations diverge and become unreliable. Measurements at the 21 m high Great Falls, NJ, in which  $r$  ranged from 4 to infinity (i.e., 80-100% approach to equilibrium), give an indication of the mass-transfer efficiency of higher waterfalls (15).

Another approach for predicting reaeration at higher waterfalls is the use of semiempirical dimensionless equations based on the theory of "solid" jets. Two such equations using the Reynolds number ( $R$ ) and the Froude number ( $F$ ) have been developed from laboratory-scale and small-weir reaeration measurements.

$$r_{15} = 1 + 0.627 \times 10^{-4}R_j^{0.53}F_j^{1.787} \quad (4) \quad (7)$$

where

$$R_j = q_j/v \quad F_j = (gh^3/2q_j^2)^{0.25}$$

$$r_{15} = 1 + f_{wq}(0.1F_j^{1.2}) \text{ for } R > 5 \times 10^5 \quad (16) \quad (8)$$

where

$$R = q_w/v \quad F = (8gh^3/q_w^2)^{0.25}$$

Here  $q_w$  is flow rate per unit crest length,  $q_j$  is the flow rate per unit wetted jet perimeter ( $m^2/s$ ),  $g$  is the gravitational constant, and  $v$  is the kinematic viscosity of water.

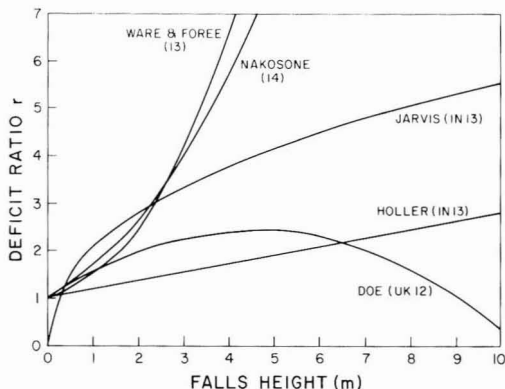


Figure 1. Comparison of correlations for deficit ratio  $r$  as a function of fall height.

There is some theoretical justification for extrapolating these equations to other falls, provided that the nature of the reaeration phenomena does not change significantly. The data on reaeration at large falls is scarce, but for the three large river dams of heights 3.7, 4.6, and 8.4 m cited by Avery and Novak (4) both correlations give reasonable results, with Avery and Novak's tending to overpredict, and Markofsky's (16) tending to underpredict, mass transfer.

To our knowledge, the extension of these findings to the volatilization of other compounds has not been undertaken to date, although gas tracer studies at dams have been used to estimate the volatilization of organic chemicals (17). However, air-water transfer at waterfalls is not simply a surface phenomenon as occurs at river and lake surfaces. Laboratory studies indicate that mass transfer occurs primarily between entrained air bubbles and water in the plunge pool, and not between the sheet of falling water or "nappe" and the surrounding air (18). The quantity of air entrained could thus be the limiting factor controlling mass transfer, as opposed to control by diffusive resistances as applies at relatively quiescent surfaces.

We develop and discuss a model, which is essentially a hypothesis, which addresses this and other questions concerning the fate of organic chemicals at waterfalls. The following section describes the model concept, equations, their solution, and a sample application using Niagara Falls. The results are then presented, along with a discussion of their implications and a proposal for validation.

#### The Model

It is assumed that the only significant fate phenomenon occurring at waterfalls is volatilization. The trapping of particles from entrained air is ignored but may be important for aerosol-associated chemicals. A key hypothesis of the model is that volatilization occurs primarily between the entrained air and the water in the pool below the falls. There is evidence that particles present in the water accumulate on the skin of entrained air bubbles, and that when the bubbles burst, a significant fraction of this matter is ejected into the atmosphere (19). This could be an important process contributing to air-water mass transfer, but due to a lack of understanding of this phenomenon, it is not included. There is also a possibility that the surface organic layer or "scum", which frequently forms immediately downstream of falls, can act as a reservoir or trap for hydrophobic organic chemicals, thus hindering their volatilization. Again, this is not included in the model because of lack of data.

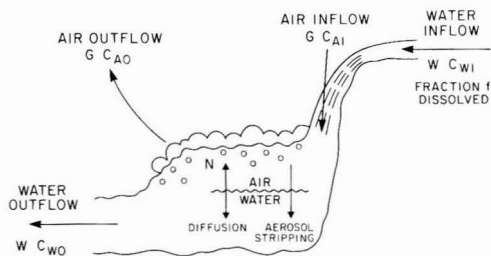


Figure 2. Schematic diagram of air, water, and chemical flows at a waterfall.

The waterfall is treated as a completely mixed steady-state air-water contactor (Figure 2). The water inflow and outflow are equated to the water flow rate over the fall. The air inflow and outflow rates are equal to the equivalent amount of air entrained in the plunge pool. Changes in volumetric flow of water arising from spray loss or of air gas absorption are assumed to be negligible.

The diffusion rate from water to air in the contactor can be expressed as the product

$$KA(fC_W - C_A/H) \quad (\text{mol/s}) \quad (9)$$

and

$$1/K = 1/k_L + 1/Hk_G \quad (10)$$

where  $K$  (m/s) is the overall water side mass-transfer coefficient and can be further defined in terms of water and air side "film" coefficients  $k_L$  and  $k_G$  as shown in eq 10;  $A$  ( $\text{m}^2$ ) is area and may include a contribution from the area of the nappe. The quantity in parentheses is the driving force for diffusion and is the difference between the truly dissolved water concentration of the chemical  $fC_W$  ( $\text{mol}/\text{m}^3$ ) and the water concentration in equilibrium with the gaseous concentration, i.e.,  $C_A/H$ .  $H$  is the dimensionless air-water partition coefficient, and  $f$  is the fraction of the substance in water present in dissolved form, a fraction  $(1-f)$  being sorbed and unavailable for volatilization.

Mass balance equations may be written for the air and for the water phases in terms of the air flow rate  $G$  ( $\text{m}^3/\text{s}$ ), the water flow rate  $W$  ( $\text{m}^3/\text{s}$ ), and the concentrations, subscript  $W$  applying to water,  $A$  to air,  $i$  to inflow, and  $o$  to outflow,  $N$  being the flux from water to air.

$$\text{air: } N = G(C_{Ao} - C_{Ai}) = KA(fC_{Wo} - C_{Ao}/H) \quad (\text{mol/s}) \quad (11)$$

$$\text{water: } N = W(C_{Wi} - C_{Wo}) = KA(fC_{Wo} - C_{Ao}/H) \quad (\text{mol/s}) \quad (12)$$

These two linear equations may be directly solved for the two unknowns:  $C_{Ao}$ , the concentration ( $\text{mol}/\text{m}^3$ ) in the outflowing air, and  $C_{Wo}$ , the concentration in the outflowing water.

$$C_{Ao} = [fHC_{Wi} + C_{Ai}(fGH/W + GH/KA)] / (1 + fGH/W + GH/KA) \quad (13)$$

$$C_{Wo} = [(C_{Ai}G/W) + C_{Wi}(1 + GH/KA)] / (1 + fGH/W + GH/KA) \quad (14)$$

This solution is more easily understood with the help of a graph. If the inlet air concentration  $C_{Ai}$  is assumed to be negligible, then the fraction of the river load of chemical that volatilizes at the falls  $(1 - C_{Wo}/C_{Wi})$  may be plotted as a function of two dimensionless parameters as in Figure 3. The first parameter  $(fGH/W)$  can be regarded as the ratio of the capacity of air for chemical to

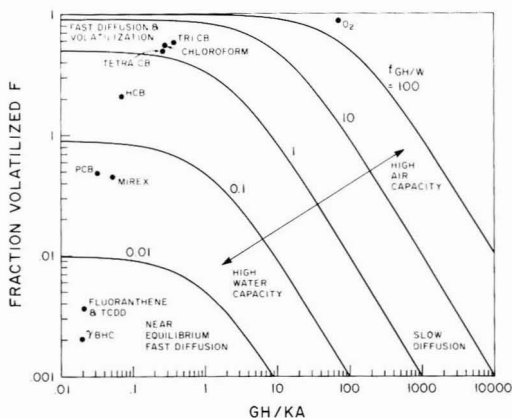


**Figure 3.** Plot of the dimensionless parameters ( $fGH/W$ ), the ratio of air to water "capacities", and  $GH/KA$ , the ratio of air to diffusive "capacities", with specific chemicals located assuming values of 2500  $m^3/s$  for  $W$ , 50000  $m^3/s$  for  $G$ , and 7.1 for  $r$  the deficit ratio.

that of the water. The second parameter ( $GH/KA$ ) is the ratio of the air capacity to the diffusive capacity. When  $W/f$  is large compared to  $GH$  (i.e., the parameter  $fGH/W$  is small), the capacity of the water phase dominates, and the water-phase concentration tends to be unchanged, and the fraction evaporated is small. If, in addition,  $KA$  is large compared to  $GH$  (i.e., the parameter  $GH/KA$  is small) the air will achieve equilibrium with the water (lower left region in Figure 3). If  $KA$  is small with respect to  $GH$ , diffusion is also slow, and the air is also unchanged (lower middle). When  $GH$  is large compared to  $W/f$ , the capacity of the air phase dominates, and the air phase tends to be unchanged; the water tends to achieve equilibrium with the air (upper left), or if  $KA$  is small, it is unchanged (lower right). River-transfer conditions correspond to the lower right of the diagram.

Clearly the fraction evaporated may be affected or controlled by the mass-transfer limitation ( $GH$ ) or by the capacity of the air to accept chemical ( $KA$ ) relative to that of the water to provide chemical. Sorption (reduced  $f$ ) tends to reduce the fraction volatilized.

It is interesting to examine the relationship between the deficit ratio  $r$  and these parameters. For oxygen it can be assumed that the concentration in air (e.g., 240  $g/m^3$ ) is unaffected by the river (e.g., 10  $g/m^3$ ), thus  $C_{A_i}$  equals  $C_{A_0}$ . Substituting eq 12 into eq 1 and setting  $f$  as 1.0, it can be shown that

$$r - 1 = (KA)_{ox} / W \quad (15)$$

where  $(KA)_{ox}$  is for oxygen. Since  $W$  is known and the order of magnitude of  $r$  is known, i.e., typically 4, the magnitude of  $KA$  can be established for oxygen as approximately  $3W m^3/s$ .

It is noteworthy that oxygen has a very large value of  $H$ , typically 24, corresponding to an air concentration of 240  $mg/L$  and a water concentration of 10  $mg/L$ . If it is assumed that  $G$  and  $W$  are of the same order of magnitude, then  $GH$  is much larger than  $W/f$  and  $KA$ , and diffusion controls. The capacity of the water to accept oxygen is much less than the capacity of the air to deliver it. This is not the case with other chemicals, which typically have  $H$  values in the range 0.1–0.001 and even lower.

Unfortunately, neither  $k_G$  or  $k_L$  are known, but  $k_G$  is typically 100–200 times that of  $k_L$  because of the approximate square root dependence on molecular diffusivities, which differ for air and water by a factor of approximately

10000. For oxygen,  $Hk_G$  thus greatly exceeds  $k_L$  in eq 10; thus,  $K$  equals  $k_L$  and transfer is water-phase controlled. For chemicals of lower  $H$ , this is not necessarily the case.

Little information is available on  $k_G$ , but we can postulate it to be of the order of 150  $k_L$ . Thus, eq 10 can be rewritten to include area as

$$1/KA = (1 + 1/150H)/(KA)_{ox} \quad (16)$$

$KA$  can be estimated from the deficit ratio by substituting eq 15 to give

$$KA = W(r - 1)/(1 + 1/150H) \quad (17)$$

It is acknowledged that there is a dependence of  $K$  on diffusivity, probably to the power 0.5, but the effect is small compared to the errors in  $r$  and the assumed ratio of 150. If desired, a diffusivity or Schmidt number correction can be included. Equation 17 shows that only when  $H$  is below 0.01 does volatilization become impeded by the gas film resistance. Ultimately, as  $H$  tends to zero,  $KA$  also tends to zero and no volatilization takes place.

There are two further simplifying assumptions in the model that should be noted. First, in the definition of eq 11 and 12 it is implicitly assumed that the fraction of the substance present in dissolved form  $f$  remains constant during depletion of the water phase. This could lead to overestimation of volatilization for substances that are present primarily in sorbed form and desorb slowly. If a kinetic limitation is suspected, the best approach is to define  $C_{w_i}$  as the dissolved chemical and ignore the sorbed form in the calculation.

Second, it is assumed that all diffusion occurs across the final concentration gradient between the air bubbles and water. A more accurate approach is to integrate the diffusion over the changing concentration gradient experienced by a rising air bubble. It was decided to present the simpler solution to facilitate understanding and interpretation of the equations. The differences in results are confined to a slight underestimation of volatilization in the transition region between diffusion and gas flux control of mass transfer.

Equations 14 and 17 permit the estimation of volatilization of organic compounds at a waterfall. The waterfall characteristics of water flow, entrained air flow, and deficit ratio must be defined. The chemical's air-water partition coefficient, the suspended-matter-water partitioning, and the regional air and inflowing water chemical concentrations must also be specified.

#### Application to the Horseshoe Falls at Niagara

There is a substantial chemical industry along the Niagara River above Niagara Falls, as well as a large urban population. This has resulted in extensive contamination of the river with organic chemicals (20). Consequently, Niagara Falls is an appropriate and interesting subject for the application of this model.

Eleven organic chemicals were selected for examination using the model. They are listed in Table I along with the required physical-chemical properties. These compounds are among those that are of concern along the Niagara River, and they represent a range of properties.

Niagara Falls consists of two waterfalls: the Horseshoe Falls, and the American Falls. The Horseshoe Falls plunge 51.8 m in a generally unbroken 732 m wide curtain into a deep pool, while the water that passes over the American Falls has a free drop of between 21 and 33 m on to talus slopes and then runs down over this rock, which extends 120 m horizontally out from the falls' face (21). During normal daytime flow the Horseshoe Falls receives ~90%



**Table I. Estimated Physical Chemical Properties of Selected Chemicals at 10 °C<sup>a</sup>**

chemical	molec mass, g/mol	vapor pressure, Pa	water solub, g/m <sup>3</sup>	air-water part. coeff <i>H</i>	log <i>K</i> <sub>ow</sub>	<i>f</i>	<i>KA</i>	<i>fGH/W</i>	<i>GH/KA</i>	<i>F</i>	loadings, kg/day	
											NOTL	volat
chloroform	119.4	13000	8900	7.4 × 10 <sup>-2</sup>	1.97	1.00	14000	1.48	0.26	0.54	43	23
1,2,4-trichloro-benzene	181.5	12	11	0.084	4.0	1.00	14000	1.68	0.30	0.56	1.03	0.58
1,2,3,4-tetrachloro-benzene	215.9	3	4.0	0.069	4.5	0.99	14000	1.37	0.25	0.52	0.64	0.33
hexachlorobenzene	284.8	2.6 × 10 <sup>-4</sup>	0.002	0.016	5.5	0.94	11000	0.30	0.07	0.21	0.179	0.04
γ-BHC	291.0	8.1 × 10 <sup>-4</sup>	0.9	1.1 × 10 <sup>-4</sup>	3.7	1.00	250	0.0022	0.022	0.0021	1.54	0.0032
<i>p,p'</i> -DDE	318.0	7 × 10 <sup>-5</sup>	0.018	5.3 × 10 <sup>-4</sup>	5.7	0.91	1100	0.0095	0.023	0.0092	0.03	0.0003
mirex	545.6	9 × 10 <sup>-7</sup>	3 × 10 <sup>-5</sup>	7.0 × 10 <sup>-3</sup>	6.9	0.34	7800	0.053	0.045	0.048	0.014	0.0007
2,2',5,5'-tetrachloro-biphenyl	292.0	3.5 × 10 <sup>-4</sup>	0.013	3.3 × 10 <sup>-3</sup>	6.1	0.79	5100	0.053	0.032	0.049	1.03	0.050
benzo[ <i>a</i> ]pyrene	252.0	6 × 10 <sup>-8</sup>	0.002	3.2 × 10 <sup>-6</sup>	6.0	0.83	7	5.3 × 10 <sup>-5</sup>	0.022	5 × 10 <sup>-5</sup>	0.66	3 × 10 <sup>-5</sup>
fluoranthene	202.0	2 × 10 <sup>-4</sup>	0.09	1.9 × 10 <sup>-4</sup>	5.2	0.97	423	0.0037	0.022	0.0036	2.44	0.009
2,3,7,8-TCDD	322.0	1 × 10 <sup>-7</sup>	1.9 × 10 <sup>-5</sup>	7 × 10 <sup>-4</sup>	6.8	0.44	1500	0.0063	0.024	0.00361		

<sup>a</sup> Model parameters and results assuming the deficit ratio *r* to be 7.1 (eq 17), the water flow *W* to be 2500 m<sup>3</sup>/s, the air flow *G* to be 20*W*, the fraction dissolved *f* calculated from eq 18 and the fraction volatilized *F* from eq 14. Volatilization rates are based on loadings at Niagara-on-the-Lake (NOTL).

of the total flow. The selection of parameters for a model of the Horseshoe Falls is described below.

**Water Flow (*W*).** The water flow in the Niagara River is relatively constant throughout the year, but there is a strong diurnal flow variation as a result of hydroelectric power diversions. A typical daytime value of 2500 m<sup>3</sup>/s was used.

**Air Flow (*G*).** Although there have been laboratory investigations of air entrainment into water jets (15, 22), the work has concentrated on solid and near-solid jets. Entrainment ratios (i.e., flow of entrained air/flow of water in jet) as high as 6 have been recorded (22). However, no work was found on entrainment into completely disintegrated high-speed water curtains such as Niagara Falls.

One approach would be to apply the observation from the laboratory studies above that all air trapped within the plunging jet is entrained. Assuming frictionless free fall, the velocity of the water as it enters the plunge pool below Horseshoe Falls is ~30 m/s. Photographs show the curtain to be several meters thick. If an average value of 3 m is assumed, the air to water ratio in the curtain is ~27.

A large plume of mist is generated at Horseshoe Falls. The air that is drawn into the pool by the Falls is driven back up into the air in the middle of the horseshoe as a result of the confining geometry of the Falls. An attempt was made to measure the air flow in the visible portion of this plume and to assume that all this air was entrained once into the water of the Falls. The plume was filmed on a clear autumn day giving a measured air-water flow ratio of 20. This value was adopted for the model. There is a large degree of uncertainty associated with the assumption that the visible plume flux represents the entrained air flow, but the ratio appears to be reasonable. In our judgement it almost certainly lies between 5 and 30.

**Deficit Ratio (*r*).** The plunging water at the Horseshoe Falls is a fully disintegrated jet, but unfortunately the literature search yielded no correlations and very few data on re-aeration for disintegrated jet flow. There was no choice but to use one of the relationships for solid jets. Of the various correlations for deficit ratio, only those of Markofsky and of Avery can reasonably be applied to large waterfalls. Avery's equation predicts a very high value of 31.9 for *r*, while Markofsky's equation predicts a value of 7.1, which is more in accord with measured values for large falls (4, 22) and is adopted here. A Froude number extrapolation of factor 2 beyond the maximum value of *F*

given by Markofsky is required, but this is surprisingly little in view of the scale of the Falls.

**Air-Water Partition Coefficient (*H*).** The air-water partition coefficient can be calculated from vapor pressures and solubilities, estimated values being given for the chemicals of interest at 10 °C in Table I. The treatment of PCBs as one substance is justified since the Henry's law constants for the different congeners are similar. There is, of course, a seasonal dependence on temperature; thus, the data in Table I have been rounded-off and represent only typical values, the present aim being only to estimate volatilization characteristics rather than exact rates.

**Dissolved-Phase Fraction (*f*).** The partitioning between water and organic matter in the water was calculated by using Karickhoff's model (25). The resulting equation for fraction dissolved is

$$f = 1 / (1 + 0.41\phi K_{OW}S) \quad (18)$$

The concentration of the suspended sediment *S* (kg/L) was set equal to 5 mg/L (i.e., 5 × 10<sup>-6</sup> kg/L), the average value measured by Oliver and Charlton (26). The fraction organic carbon content of the sediment (*φ*) selected was 0.1, the average value measured by Oliver (27). The octanol-water partition coefficients *K*<sub>ow</sub> are included in Table I.

**Air Concentration (*C*<sub>Aj</sub>).** Air concentration data were not available for most of the chemicals examined. Measurements were found for PCBs (28) and fluoranthene and benzo[*a*]pyrene (29) in the Niagara Falls area. For these compounds the calculated equilibrium concentration in the water was well below the measured water concentration, indicating that the air concentration could be set to zero in the mass-transfer equation. For the remaining compounds the air concentration was assumed to be zero.

**Water Concentration (*C*<sub>wj</sub>, *C*<sub>w0</sub>).** It is difficult to select reliable contaminant concentrations in the Niagara River. These concentrations vary considerably with time as a result of episodic emissions. River loadings at the entrance and mouth of the river have, however, been deduced by integrating flow and concentration measurements (30). Since most of the significant contaminant sources are upstream of the Falls and volatilization in the upper river is also suspected to be significant, the loading at Niagara-on-the-Lake (NOTL) at the river mouth is believed to give a better estimate of the loading at the Horseshoe Falls. Further, about half of the daytime flow

is typically diverted around the Falls through the powerhouses.

### Model Results and Discussion

The results are summarized in Table I. The model predicts that about half of the chloroform and about one-third of the chlorinated benzenes flowing over the Horseshoe Falls will volatilize, along with ~5% of the PCBs and mirex, and 1% of the DDE. Only very small fractions, i.e., less than 1%, of the other chemicals are expected to volatilize. As expected, the value of  $H$  controls the volatilization potential.

The process controlling mass transfer is indicated by the value of the dimensionless parameter  $GH/KA$ . For the chemicals studied this value is always less than 0.3, and for most of the compounds it is less than 0.1. Referring to Figure 3, it is apparent that the chemicals studied fall on the left-hand edge of the plot, indicating that the quantity of air entrained is limiting volatilization rather than mass-transfer kinetics. This quantity is the model parameter with the most uncertainty. Clearly, application of river-transfer models to falls is erroneous since river models usually assume infinite air volume.

A sensitivity analysis can be undertaken easily by varying parameters such as  $r$ ,  $KA$ , or the air to water ratio. For example for chloroform with 54% volatilized, halving  $r$  reduces  $KA$ , resulting in 47% volatilization, i.e., both kinetics and equilibrium control. Halving  $G/W$  gives 39% volatilized. For PCB (4.9% evaporated), halving  $r$  only causes a reduction to 4.7%, but halving  $G/W$  gives 2.5%, i.e., volatilization is almost entirely controlled by the volume of available air. The sensitivities of these factors thus vary with  $H$ , but generally  $G/W$  is the most critical factor. This is not the case with oxygen, which is entirely kinetically controlled.

Validation of the model is clearly required to reduce this and other uncertainties. The model predictions can only be considered to be order of magnitude estimates. They provide some indication of whether volatilization is significant for a particular compound and worthy of further investigation. In general it appears that this is the case for chloroform, chlorinated benzenes, PCBs, and mirex, while volatilization of  $\gamma$ -HCH, the larger PAHs, and PCDDs at Horseshoe Falls is negligible. Niagara Falls is behaving like a headspace analysis system with an air to water ratio of 20. Any chemicals with an appreciable  $H$ , i.e., exceeding 0.005, are expected to volatilize appreciably.

One approach to model validation would be to simultaneously analyze water and air samples at Niagara Falls, or indeed other falls. However, there are severe difficulties in obtaining representative samples at Niagara Falls. There are large temporal and spatial variations in water concentration, and the air is inaccessible and subject to rapid dilution. A promising strategy would be to conduct tracer experiments involving chemicals not found in the river. A series of compounds with varying  $H$  values could be mixed with a conservative tracer and released into the river upstream of the Falls. The difference between the chemical to conservative tracer concentration ratio upstream and downstream of the Falls would be a measure of the volatilization between the sampling points. Several compounds are required if both the liquid and gas film mass-transfer coefficients are to be estimated. A complementary approach is to study volatilization from simulated waterfalls in the laboratory, varying height and flow rate under controlled conditions.

This study shows that transfer of oxygen and other chemicals of large  $H$  is always diffusion limited, and for chemicals of lower  $H$ , transfer is air flow limited. Failure

to include this effect could result in overprediction of transfer rates. It is also suspected that the air supply may have a limiting effect on volatilization from rapids and other highly turbulent areas where air is entrained into the water. The appropriate model in this case would be a combination of the bubble and surface mass-transfer models.

**Air Concentration.** The publication of the early results of this study caused considerable controversy because of new media reports that the mists of Niagara Falls were "toxic". The model can estimate these concentrations ( $\text{g/m}^3$ ) simply as the (river loading  $\text{g/s}$ )/(fraction evaporated)/(air flow  $\text{m}^3/\text{s}$ ). The large air flow fortunately results in considerable dilution. The largest air concentration that can be achieved is that in equilibrium with the water, i.e.,  $HC_w$ .

Taking chloroform and PCBs as examples, the model estimates 54% and 5% evaporation, respectively. If the loading figures in Table I are used, the evaporation rates will be approximately 23 and 0.05 kg/day, respectively. Assuming a water flow of 2500  $\text{m}^3/\text{s}$  and an air flow 20 times this, the concentrations in the mist will be ~5400  $\text{ng/m}^3$  (chloroform) and 12  $\text{ng/m}^3$  (PCB). These values are well below air quality guidelines; thus, there is no concern about conditions being "toxic", especially given the substantial dilution of the plume by dispersion.

Hoff et al. (31) measured the concentration of these chemicals in the vicinity of the plume and obtained chloroform concentrations ranging from 100 to 800  $\text{ng/m}^3$  and estimated total PCBs from 2 to 11  $\text{ng/m}^3$ . Typical regional concentrations are respectively 200 and 0.1  $\text{ng/m}^3$  (25). Similar levels were determined by the Ontario Ministry of the Environment (32). The total PCB concentration is in fair agreement, while the observed chloroform concentrations are lower than predicted by the model. Possible reasons for this include (i) error in the model, (ii) introduction of the chemical downstream of the Falls, (iii) evaporation of the chemical upstream of the Falls, (iv) sampling at times of unusually low loadings, (v) dispersion of the plume arising from the practical infeasibility of measuring air directly in the plume, and (vi) retardation of evaporation by the organic "scum" formed in the plunge pool.

### Conclusions

We conclude that given the intimate contact between air and water at this and other falls, there must be appreciable volatilization of chemicals with high air-water partition coefficients. Waterfalls can act as significant point sources affecting local air concentrations, although dilution fortunately mitigates this concern. The extent of volatilization may be controlled by diffusion limitations, by air supply, or both. The model presented can be used to estimate volatilization, but several uncertainties remain and validation is necessary. Accurate determination of rates of chemical loss at waterfalls is best done by measuring water concentrations upstream and downstream, using air analyses only for semiquantitative confirmation of rates. Where the chemical loadings display high temporal and/or spatial variability, tracer chemicals normally not found in the river may be needed. Estimation of differential loadings in rivers such as the Niagara River, which contain waterfalls and which assume conservative behavior, could be in serious error for volatile chemicals.

### Acknowledgments

We gratefully acknowledge W. D. Baines, M. Brooksbank, R. Findlay, R. Hoff, B. Kerman, J. Kingham, H.

Kobus, H. J. Leutheusser, D. J. O'Connor, B. G. Oliver, and W. Y. Shiu for their contributions to this project.

#### Literature Cited

- (1) Mackay, D.; Shiu, W. Y. In *Gas Transfer at Water Surfaces*; Brutsaert, W., Jirka, G. H., Eds.; D. Reidel, The Netherlands, 1984; p 3.
- (2) Mackay, D.; Yuen, T. K. *Water Pollut. Res. J. Can.* **1980**, *15*, 83.
- (3) Mackay, D. In *Environmental Exposure from Chemicals*; Neely, W. B., Blau, G. E., Eds.; CRC: Bata Raton, FL, 1985; Vol. I, p 91-108.
- (4) Avery, S. T.; Novak, P. *J. Hydraul. Div., Am. Soc. Civ. Eng.* **1978**, *104*, 1521.
- (5) McLachlan, M. A Model of the Fate of Organic Chemicals in the Niagara River. A Master of Applied Science Thesis, University of Toronto, 1987.
- (6) Rathbun, R. E. *J. Hydraul. Div., Am. Soc. Civ. Eng.* **1977**, *103*, 409.
- (7) Mackay, D.; Shiu, W. Y.; Bobra, A.; Billington, J.; Chau, E.; Yeun, A.; Ng, C.; Szeto, P. Volatilization of Organic Pollutants from Water. EPA Report No. 600/63-82-019, NTIS No. PB 82-830-934, Athens, GA, 1982.
- (8) Rathbun, R. E.; Tai, D. Y. *Water Res.* **1981**, *15*, 243.
- (9) Liss, P. S.; Slater, P. G. *Nature* **1974**, *247*, 181.
- (10) Mackay, D.; Leinonen, P. *J. Environ. Sci. Technol.* **1975**, *9*, 1178.
- (11) Mackay, D.; Yeun, T. K. *Environ. Sci. Technol.* **1983**, *17*, 211.
- (12) Department of the Environment (UK) *Notes on Water Pollution*; London, UK, 1973; No. 61.
- (13) Ware, R.; Foree, E. G. Reaeration Characteristics of Low-Level In-Channel Dams and Waterfalls in Kentucky Streams, UKY TR97-76-CE25; University of Kentucky, 1976 Report.
- (14) Nakasone, H. *J. Hydraul. Div., Am. Soc. Civ. Eng.* **1979**, *105*, 1211.
- (15) Uchirin, C. G.; Ahlert, W. K.; Park, S. S.; Schneck, S. R. *Water Resour. Bull.* **1985**, *21*, 475.
- (16) Markofsky, M.; Kobus, H. *J. Hydraul. Div., Am. Soc. Civ. Eng.* **1978**, *104*, 562.
- (17) Tofflemire, T. J.; Shen, T. T.; Buckley, E. H. *Volatilization of PCB from Sediment and Water: Experimental and Field Data*; Technical Paper No. 63; N.Y. State Department of Environmental Conservation: Albany, NY, 1981.
- (18) Van der Kroon, G. T. M.; Schram, A. H. *H<sub>2</sub>O* **1969**, *2*, 528.
- (19) Kerman, B. R. *Atmos.-Ocean* **1986**, *24*, 329.
- (20) Niagara River Toxics Committee Report of the Niagara River Toxics Committee. Environment Canada, Ontario Ministry of the Environment, N.Y. State Department of Environmental Conservation, and U.S. Environmental Protection Agency, 1984.
- (21) International Joint Commission *Regulation of Great Lakes Water Levels Appendix G: Regulatory Works*; Windsor, Ontario, 1973.
- (22) Van de Sande, E.; Smith, J. M. *Chem. Eng. Sci.* **1973**, *28*, 1161.
- (23) Irvine, D. A.; McKeogh, E.; Elsway, E. M. *Proc. Inst. Civ. Eng.* **1980**, *69*, Part 2, 425.
- (24) Mackay, D.; Bobra, A.; Chan, D. W.; Shiu, W. Y. *Environ. Sci. Technol.* **1982**, *16*, 645.
- (25) Karickhoff, S. W. *Chemosphere* **1981**, *10*, 833.
- (26) Oliver, B. G.; Charlton, M. N. *Environ. Sci. Technol.* **1984**, *18*, 903.
- (27) Oliver, B. G. In *QSAR in Environmental Toxicology II*; Kaiser, K. L. E., Ed., D. Reidel: Dordrecht, The Netherlands, 1987; p 251.
- (28) Singer, E.; Jarv, T.; Sage, M. In *Physical Behavior of PCBs in the Great Lakes*, Mackay, D., Paterson, S., Eisenreich, S. J., Simmons, M. S., Eds.; Ann Arbor Science: Stoneham, MA, 1983; p 367.
- (29) Hoff, R. M.; Chan, K. W. *Environ. Sci. Technol.* **1987**, *21*, 556.
- (30) Data Interpretation Group *Joint Evaluation of the Upstream/Downstream Niagara River Monitoring Committee of Environment Canada, USEPA, Ontario Ministry of Environment and NY State Dept. of Environmental Conservation*; Environment Canada: Ottawa, Ontario, 1988.
- (31) Hoff, R. M.; Bottenheim, J.; Niki, H.; Forsyth, P.; Khouw, B.; Barnett, S.; Fellin, P. Vapour Phase Air Concentrations of PCBs and Chloroform at Niagara Falls. Report ARD 87-4; Atmospheric Environment Service of Environment Canada: Downsview, Ontario, 1987.
- (32) Bell, R. W.; DeBrou, G. B. *Niagara 1987: Air Quality Survey in the Vicinity of the Mist of Horseshoe Falls*; Report ARB-130-87-ARSP; Ontario Ministry of Environment, Toronto, Ontario, 1987.

Received for review April 13, 1989. Accepted October 10, 1989. This project was funded by Environment Canada and NSERC.

# Characterization of Mercury, Arsenic, and Selenium in the Product Streams of a Bench-Scale, Inert-Gas, Oil Shale Retort

K. B. Olsen,\* J. C. Evans, D. S. Sklarew, J. S. Fruchter, D. C. Girvin, and C. L. Nelson

Pacific Northwest Laboratory, Richland, Washington 99352

■ The purpose of this study was to determine the effects of heating rates and maximum temperatures on the redistribution of mercury, arsenic, and selenium into the shale oil, retort water, and offgas of a 6-kg bench-scale retort. A Green River shale (western) from Colorado and a New Albany shale (eastern) from Kentucky were heated at 1–2 °C/min to a maximum temperature of 500 °C. The eastern and western shales were also heated at 2 °C/min to 750 °C and at 10 °C/min to 750 °C. Real-time monitoring of the offgas stream for mercury was accomplished with Zeeman atomic absorption spectroscopy or a microwave-induced helium plasma spectroscopy. Microwave-induced helium plasma spectroscopy was also used to monitor for arsenic in the offgas stream. Raw and spent shales, retort water, and shale oil were analyzed by X-ray fluorescence, instrumental neutron activation analysis, and mercury cold vapor atomic absorption. Most of the mercury volatilized into the offgas during retorting; little or no arsenic was observed in the offgas. Mass balance calculations for arsenic and selenium accounted for essentially 100% of those elements in the spent shale, shale oil, and retort water. The mass balance calculations suggest little offgas component for arsenic and selenium. This agrees with the results of the MPD monitoring of the offgas. These results indicate the potential pathway for mercury to enter the environment is from the offgas. Arsenic and selenium preferential redistribution into the shale oil may present problems during the upgrading process. Furthermore, the tendency for arsenic and selenium to redistribute into the retort water should be considered when selecting a water treatment process to prevent the release of these elements into the environment.

## Introduction

Previous studies of trace element redistribution during retorting of U.S. oil shale have shown that most of the trace elements (including beryllium, chromium, cobalt, fluorine, lead, manganese, molybdenum, nickel, vanadium, and zinc) are largely retained in the retorted shale (1–3). However, several elements of environmental interest (i.e., mercury, arsenic, selenium, and cadmium) can be redistributed in significant quantities to other product streams including oil, water, and offgas.

Different types of retorts affect the partitioning of these elements. For example, in the Paraho surface retort, 28% of the mercury was found in the oil, 0.01% in the water, and 23% in the offgas (4–6). The arsenic and selenium were redistributed to a lesser extent, with 5.3% and 3.8% in the oil, 0.04% and 1.9% in the water, and 0.1% and <0.8% in the offgas, respectively. In contrast to the Paraho surface retort, a bench-scale inert-gas retort released approximately 70% of the mercury present in the raw shale to the offgas (7, 8). Previously indirect measurements of mercury in the offgas (obtained by mass balance calculation or by collection on sorption beds in gas-sampling trains) have been confirmed by direct measurement using Zeeman atomic absorption (ZAA) spectroscopy. Quenched runs of a simulated laboratory-scale in situ retort indicated that the mercury accumulated in unretorted shale ahead of the reaction zone. This phenomenon caused the mercury to travel down the length of the retort ahead of the reaction zone and to be released

in a relatively concentrated pulse toward the end of the retort zone (9).

Under still different conditions, viz. Fischer assay conditions, oil shale from the Julia Creek deposit in Queensland, Australia, was recently retorted at temperatures ranging from 250 to 550 °C (10). Elements found to be significantly mobilized included mercury, selenium, arsenic, chlorine, and bromine. The arsenic and selenium partitioned into the retort water and shale oil. However, analysis of the offgas was not carried out to determine if there were any gas-phase components of mercury, arsenic, or selenium.

Many of the previous retorting and redistribution studies have obtained trace element mass balances for various types of retorts without direct measurements in the offgas stream. Finally, little work has been done directly comparing the behavior of mercury, arsenic, and selenium in western (Green River) and eastern (New Albany) oil shales. Therefore, a study to determine the concentrations of mercury, arsenic, and selenium in raw shale, spent shale, and product streams from an instrumented 6-kg laboratory-scale retort using both types of shales was undertaken.

## Experimental Section

**Retort Description.** An in-depth description of the design and operation of the PNL 6-kg retort (Figure 1) was published earlier (11). The main component of the system is a three-zone Thermocraft furnace and its temperature controller unit. The furnace controller allows the furnace to be uniformly heated at various rates ranging from 0.1 to 10 °C/min. The furnace is designed to house a 10-cm-diameter stainless steel retort containing approximately 6 kg of shale.

The nitrogen sweep gas, flowing at 1.5 L/min, enters the top of the vessel and flows down through the shale bed. From the oil/water receiver below the retort, the output gases and condensable vapors are routed to two 0.75-m-long glass condensers connected in series and cooled to –5 °C with a refrigerated bath.

Temperatures at various points were monitored with in-line thermocouples. Gas flow was monitored by a heat-capacity mass flowmeter, which was recalibrated periodically with a wet-test meter. The thermocouples, mass flowmeter, wet-test meter, ZAA, and microwave plasma detector (MPD) were all monitored by a data logger; the data were stored on magnetic tape for further analysis.

**Raw Oil Shale Samples.** Samples of the Green River shale were obtained from the Mahogany Zone in the Anvil Points Mine in Colorado. Its Fischer assay yield was 25.6 gal/ton (92 kg/tonne). Samples of eastern shale were obtained from the lower 5 ft of the Clegg Creek Member of the New Albany Shale (Upper Devonian) from Bullitt County, KY. Its Fischer assay yield was 12.4 gal/ton (44 kg/tonne). Raw oil shale was allowed to air dry at room temperature and then crushed with a Morse jaw crusher. Material less than 0.64 cm but greater than 550 μm (30-mesh screen) was homogenized by using a twin-shell V-blender. Grab samples were pulverized and analyzed by energy-dispersive X-ray fluorescence (XRF) to demonstrate homogeneity.

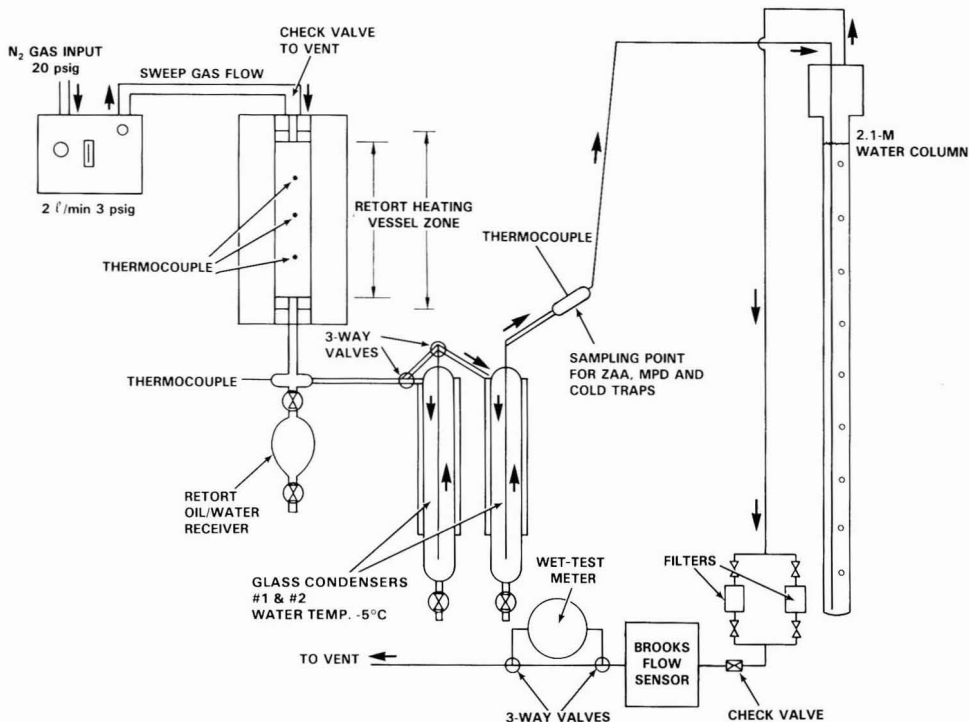


Figure 1. Schematic diagram of PNL 6-kg retort.

**Sample Collection.** Shale oil and retort water samples were collected immediately after the maximum programmed temperature of the retort was reached. The retort water and shale oil were separated, similarly to a separatory funnel separation, placed in Teflon bottles, and stored at 4 °C. A 100-g aliquot of spent shale was removed for further analysis after the retort was cooled to room temperature under a N<sub>2</sub> flow and passed through a Gibson splitter.

**Zeeman Atomic Absorption Spectroscopy.** Mercury in the offgas was monitored by ZAA during the first retort run (PNL-2) because ZAA has successfully detected mercury in an oil shale offgas (12, 13). Offgas from the retort was diverted through the ZAA system from the sampling point (Figure 1) through a 6.2-mm-o.d. Teflon tube. The gas passed into a heated 30-cm-long quartz tube filled with loosely packed quartz wool and then into a heated 10-cm-long absorption cell. The entire quartz assembly was maintained at 800–900 °C during the run to pyrolyze organically associated mercury compounds in the offgas and to atomize the mercury. Unfortunately, this temperature also caused polymerization of volatile offgas compounds and resulted in a tar deposit on the windows of the cell, which eventually caused premature termination of the mercury monitoring by the ZAA. The retort gas did not cause any measurable suppression of signal during the period of mercury evolution from the retort demonstrated by using standard additions of mercury to the offgas (14).

**Microwave-Induced Helium Plasma Detector.** A plasma emission technique was used for real-time monitoring of mercury and arsenic in the offgas during retort runs PNL-3–PNL-8. The microwave-induced helium plasma sources were mounted on either an MPD-850 spectrometer (Applied Chromatography Systems, Luton, Bedfordshire, England) or a Spectraspan IIIB 0.75-m

echelle spectrometer (MPD) (15). The microwave cavities were obtained from Applied Chromatography Systems (ACS) and J&D Industries (Lexington, MA) and were constructed in accordance with the description of Beenakker (16). The ACS system was modified by using a tuning arrangement adapted from their low-pressure Evenson source. All retort runs after the second run used the ACS source at atmospheric pressure.

Offgas was sampled from a point immediately after the second and last condenser in the offgas stream (Figure 1). At this sampling point, most of the constituents still remaining in the gas phase could be considered noncondensable species. The offgas sample stream was routed through a 1.6-mm Teflon tube to an all-glass-Teflon low-flow rotameter followed by an uncoated fused-silica capillary tube (7 cm long by 50 μm diameter) used as a critical orifice. The flow of offgas into the plasma was accurately measured at 3.3 mL/min for both plasma systems. At the point where the capillary tube terminated, a four-way cross fitting allowed the addition of a helium make-up gas containing oxygen as a scavenge gas, and a calibration gas when necessary.

Mercury concentration in the offgas was monitored on the 253.7-nm emission line with both the MPD-850 and the Spectraspan IIIB spectrometer systems. Arsenic concentration in the offgas was monitored on the 228.8-nm emission line on the Spectraspan system.

**Routine Analytical Methods.** A Kevex energy-dispersive XRF system (17, 18) was used to analyze the raw shale, spent shale, shale oil, and retort water for total arsenic and selenium. Other major and trace elements were also analyzed by using the XRF system, with the exception of mercury.

Selected samples of raw shale, spent shale, shale oil, and retort water were analyzed for total arsenic and selenium

**Table I. Retorting Parameters for Retort Runs PNL-2-PNL-8**

retort run	shale	$T_{max}$ , °C	heating rate, °C/min	comments
PNL-2	western	500	1	
PNL-3	western	750	2	
PNL-4	western	750	10	terminated early
PNL-5	eastern	500	2	
PNL-6	eastern	750	2	
PNL-7	western	750	10	
PNL-8	eastern	750	10	

by standard instrumental neutron activation analysis techniques (INAA) (19); the shale oil and retort water samples were also analyzed for mercury by INAA. In addition, a neutron multiplier system was used on selected shale oil samples specifically for selenium analysis.

Oil shale, spent shale, and shale oil were analyzed for mercury by cold vapor atomic absorption spectroscopy (19).

**Extraction of Organomercury Compounds from Raw Oil Shale.** One-gram samples of the pulverized shale were extracted with methylene chloride according to the U.S. Environmental Protection Agency's (EPA) SW-846 method 3550 (ultrasonication). Extract samples were reduced to a 10-mL volume with a Buchi Rotovap. Extracted samples were analyzed with an HP 5880 gas chromatography (GC) interfaced to an atmospheric pressure Beenakker cavity and a Spectraspan IIIB echelle spectrometer (Beckman Instruments) according to procedures previously published (18).

*Results and Discussion*

**Retort Conditions.** Variations in heat rate and maximum temperature affect the mobilization and relative partitioning of mercury, arsenic, and selenium from the raw oil shale matrix into product streams. A Green River shale from Colorado and a New Albany shale from Kentucky were heated at 1-2 °C/min to a maximum temperature of 500 °C. The eastern and western shales were also heated at 2 °C/min to 750 °C and 10 °C/min to 750 °C. Using this approach, we were able to determine the individual effect of heating rates and maximum temperatures on the redistribution of mercury, arsenic, and selenium into the products of spent shale, shale oil, retort water, and offgas.

The results of seven retort runs are included in this paper. Table I is a list of the retorting parameters and shales used in retort runs PNL-2-PNL-8.

**Comparison of Eastern and Western Shale Retorting.** A comparison of western oil shale retorted at three different heating rates and two different maximum

temperatures reveals different trends (Table II). When the shale is heated at a slow heating rate to a maximum temperature of 500 °C (PNL-2), the oil and water yields are approximately 95% and 68% of the Fischer assay results, respectively. When the maximum temperature is 750 °C (PNL-3), the oil yield remains at 95%; however, the water yield increases to approximately the Fischer assay value. At the faster heating rate of 10 °C/min (PNL-7), the oil yield is reduced slightly to 87% of the Fischer assay yield, while the water yield remains close to the Fischer assay number. Apparently, the significant increase in water yield at the 750 °C maximum temperature results from the increased loss of water of hydration from minerals in the shale.

Similar though more pronounced trends are evident with the eastern shale (Table II). When the shale is heated to a maximum temperature of 500 °C (PNL-5), the oil and water yields are approximately 86% and 98% of the Fischer assay values, respectively. When the maximum temperature is increased to 750 °C, the oil yield remains at 87% of the Fischer assay value; however, the water yield increases dramatically to 169% of the Fischer assay yield. As with the western shale, the significant increase in water yield at a maximum retorting temperature of 750 °C, compared with 500 °C, was attributed to the increased loss of water from minerals in the shale. The oil and water yields noticeably decrease to 78% and 152% of the Fischer assay values, respectively, when heating at the faster rate of 10 °C/min. This decrease in oil yield with increased heating rates may be due to the inability of the oil to migrate out of the shale matrix and out of the retort before being pyrolyzed. The increased pyrolyses of the shale oil may also account for the decreased water yield.

**Organomercury Compounds in Raw Shale.** The analysis of the extract from the raw shale for three organomercury compounds (dimethyl-, diethyl-, and *n*-propylmercury) failed to identify any of those species above the 2, 5, and 10 ppb (in the raw shale) detection limit for the organomercury compounds, respectively. These detection limits for the individual organomercury compounds are well below the total mercury quantities of 40.4 and 95.1 ppb in the western and eastern shales, respectively. These results suggest that the mercury is not bound in raw shales as a readily labile organic form, or if it is bound with these organomercury compounds, it may be complexed with other minerals within the shale matrix.

**Offgas Measurement of Mercury, Arsenic, and Selenium. Mercury.** Mercury was monitored in the offgas during retort runs PNL-2, -3, -6, -7, and -8. During retort run PNL-2, mercury in the offgas was monitored and quantified by ZAA. On subsequent retort runs, mercury evolution was monitored by either the Spectraspan MPD or the MPD-850. The mercury concentration in the offgas

**Table II. Comparison of Oil and Water Yields from PNL Retort Runs**

retort run	$T_{max}$ , °C	heating rate, °C/min	oil yield		water yield	
			gal/ton	% of Fischer assay	gal/ton	% of Fischer assay
Western Shale						
Fischer assay			25.6	≈100	3.4	≈100
PNL-2	500	1	24.2	95	2.3	68
PNL-3	750	2	24.1	95	3.8	112
PNL-7	750	10	22.2	87	3.9	115
Eastern Shale						
Fischer assay			12.4	≈100	5.4	≈100
PNL-5	500	2	10.6	86	5.3	48
PNL-6	750	2	10.8	87	9.1	169
PNL-8	750	10	9.7	78	8.2	152

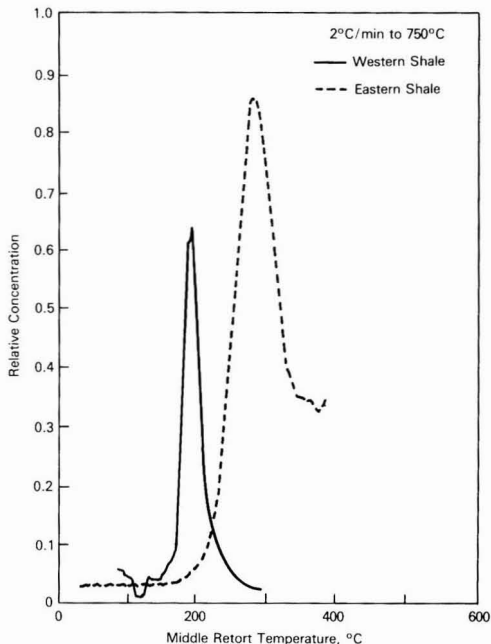


**Figure 2.** Relative concentration of mercury in the offgas during the retorting of western and eastern shale at 2 °C/min to 750 °C.

was calculated only for retort runs PNL-2 and -6; however, qualitative data on time-dependent release patterns for the volatilization of mercury from the shale were determined for retort run PNL-3. The amount of information obtained from retort runs PNL-7 and -8 (10 °C/min heating rate) was limited because mercury volatilization overlapped oil production at these higher heating rates.

During the ZAA monitoring of retort run PNL-2, mercury first appeared in the offgas at 160 °C, peaked at 220 °C, and approached base line by 260 °C. In addition, the area under the mercury release curve (concentration vs time) was integrated. Approximately 220 µg of mercury was measured with a ±50% uncertainty. This number, when compared with 204 µg in the raw shale, accounted for a 108% recovery in the offgas.

The MPD-850 output from retort run PNL-3 showed that mercury first appeared in the offgas by 160 °C, peaked at 220 °C, and approached base line by 260 °C (Figure 2). This agreed with the results first observed during retort run PNL-2 monitored by the ZAA. These results showed that mercury was released from the shale matrix well before oil production began in the retort.

The behavior of mercury in the eastern shale was significantly different from its behavior in the western shale. Mercury first appeared at 220 °C, which was 50–60 °C higher than in a similar run using western shale. The peak concentration of mercury in the offgas was observed at 280 °C, with the approach toward the base line by 360–380 °C (Figure 2). At this time, the plasma was overwhelmed by hydrocarbons from oil production, which obscured the tail of the mercury peak. An integration of the area under the curve accounted for 180 µg, or 35% of the mercury in the raw shale. However, this concentration should be considered a lower limit because of considerable quenching of the plasma by the hydrocarbons in the offgas.

The 160 °C temperature at which mercury was first observed in the offgas during the retorting of western shale is considerably lower than the 304 °C temperature reported

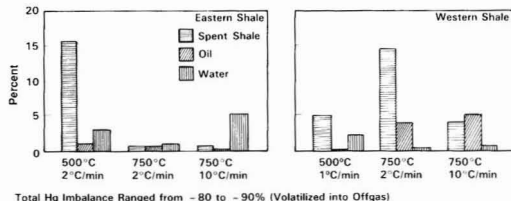


**Figure 3.** Comparison of mercury distribution for eastern and western shales as a function of retorting parameters (percent of total in raw shale).

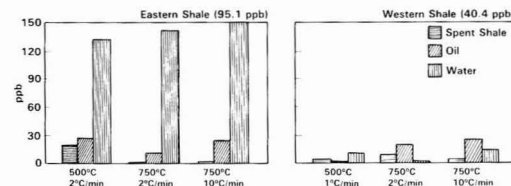


**Figure 4.** Concentration of mercury in retort products as a function of retorting parameters.

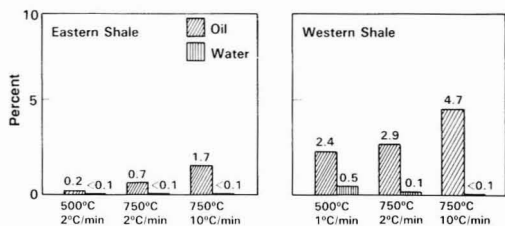
by others (9); however, the 160 °C temperature agrees with the 79–185 °C (9) and 160–320 °C (8) temperatures when mercury was first released from the oil shale matrix during retorting. The difference between release profiles from the eastern and western shales is not well understood, but may result from different geochemical forms of mercury in the shale matrix.

**Arsenic.** Arsenic in the offgas was monitored by the Spectraspan MPD during retort run PNL-5, -6, and -7; however, no arsenic was detected during any of these runs. A detection limit of 93 µg/L for arsenic in the retort offgas was calculated by using an arsine/gas mixture.

**Selenium.** Periodic checks for selenium in the offgas of retort run PNL-6 with the Spectraspan MPD have not detected any gaseous selenium component at a detection limit of 122 µg/L, based on a hydrogen selenide gas standard. Analysis for selenium in the offgas is a challenge because selenium is not sensitively detected by emission spectroscopy.

**Distribution of Mercury, Arsenic, and Selenium in the Product Streams as a Function of Retorting Parameters.** **Mercury.** The eastern shale had a mercury concentration of 95.1 ppb, compared with 40.4 ppb in the western shale. Upon retorting, 80–98% (determined by difference) of the mercury in the eastern and western raw shales was volatilized into the offgas and was not recovered in either the spent shale, shale oil, or retort water. For eastern shale, the amount of mercury in the spent shale dropped from 15.6% to 0.6% of the total mercury in the raw shale when the maximum retort temperature was increased from 500 to 750 °C (Figure 3). Mercury in eastern shale preferentially migrates to the retort water rather than the shale oil (Figures 3 and 4). For western shale, the amount of mercury in the spent shale ranged from 14.2% to 3.9%. Mercury in western shale preferentially migrated to the shale oil except at a maximum temperature of 500 °C. The percentage of mercury remaining in the western shale after heating to 500 °C was comparable to the 13% found during another study of western shale (9). However, the percentage range of mercury (normalized to the quantity in the raw shale) in the shale oil and retort water of this study was consistently lower than the 9% and 3% previously reported (9).

**Arsenic.** The eastern and western shales contained similar levels of arsenic, at 51.0 and 43.4 ppm, respectively.



Total As in Spent Shale Ranged from 89.4 to 105.4% of Raw Shale

**Figure 5.** Comparison of arsenic distribution for eastern and western shale as a function of retorting parameters (percent of total in raw shale).

Most of the arsenic remained in both the eastern and western shales following retorting, with concentrations in the spent shales accounting for 89–105% of the arsenic in the raw shales. The comparison of eastern and western shales under identical retorting conditions demonstrates that the arsenic in the western shale is considerably more mobile (Figure 5): the arsenic distribution in shale oil ranged from 0.2% to 1.7% of the amount in the raw shale for eastern shale oil and from 2.4% to 4.7% for western shale oil. Redistribution into retort water was <0.1% for eastern shale compared with a range of <0.1–0.5% for western shale. The arsenic preferentially redistributed into the shale oil of the liquid products during the retorting of both eastern and western shales. As the shale was heated to higher temperatures and at more rapid heating rates, more of the arsenic was distributed into the liquid products (Figure 5).

Comparison of this study's results to three Australian shales (i.e., Julia Creek, Condor, and Rundle retorted under Fischer assay conditions) showed many similarities in the behavior of arsenic (10, 20). For example, at a maximum temperature of 500 °C, 84–99% of the arsenic was found in the spent shale. The mobility of arsenic into the liquid products was found to increase as maximum retort temperatures increased and the arsenic preferentially redistributed into the shale oil for Julia Creek, Condor, and Rundle shales.

**Mass Balance for Arsenic.** The average recovery for arsenic in eastern and western shales was 103.4% with a 1σ standard deviation (SD) of 9.0% for the three retort runs. The average range of analytical uncertainty for each individual retort run was ±6.9% (Figure 6). The data strongly suggest that when these shales are retorted under the conditions of this study, little arsenic is lost to the offgas. This conclusion agrees with the results from the monitoring of the offgas by the MPD for gas-phase arsenic, which failed to observe any arsenic above the detection limit of the analytical method.

**Selenium.** The relative distribution of selenium into the various product streams is shown in Figure 7. After retorting, most of the selenium remains in the spent shale (78.2–110.2% of the original amount in the raw shale). The redistribution of selenium into the retort water ranged from 0.5% to 2.0% for eastern retort water and 0.5% to 0.8% for western retort water. The redistribution of selenium into the liquid products appears to be independent of the retorting parameters used. Selenium in the eastern liquid products slightly favors partitioning into retort water. Selenium in the western liquid products is preferentially distributed into shale oil.

Comparing these results to those observed during the retorting of the three aforementioned Australian shales revealed some differences and some similarities. The selenium in Julia Creek (10), Condor, and Rundle shales

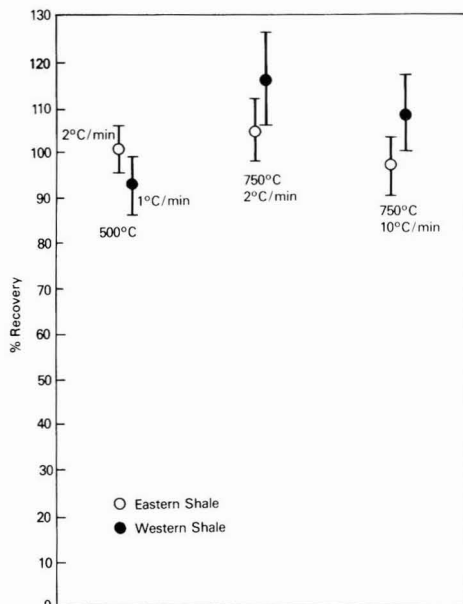
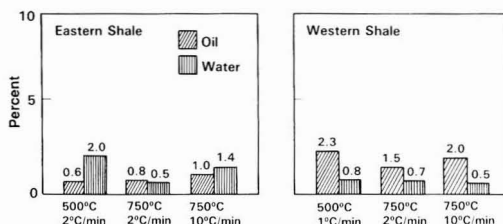


**Figure 6.** Mass balance for arsenic in eastern and western shales under various retorting conditions.



Total Se in Spent Shale Ranged from 78.2 to 110.2% of Raw Shale

**Figure 7.** Comparison of selenium distribution for eastern and western shales as a function of retorting parameters (percent of total in raw shale).

(19) had a tendency to distribute almost equally into the shale oil and the retort water in a manner similar to the behavior in this study's eastern shale; however, contrary to the Australian study findings (10, 19) that selenium was progressively mobile as temperatures increased in the Julia Creek, Condor, and Rundle oil shales, this study found little dependency on heating rates or maximum temperatures.

**Mass Balance for Selenium.** The average recovery for selenium in both eastern and western retort runs was 101.4%, with a 1σ SD of 11.7% for the three retort runs (Figure 8). The average analytical uncertainty for each individual retort run was ±8.7%. These data strongly suggest that the Green River and New Albany shales have little, if any, gas-phase selenium component.

### Conclusions

During the retorting of Green River shale (western), mercury first appeared in the offgas at 160 °C, peaked at 220 °C, and approached base line by 260 °C, all before oil production. For New Albany shale (eastern), mercury first appeared in the offgas at 220 °C, peaked at 280 °C, and approached base line by 360–380 °C. This release of mercury from the eastern shale overlapped with the be-



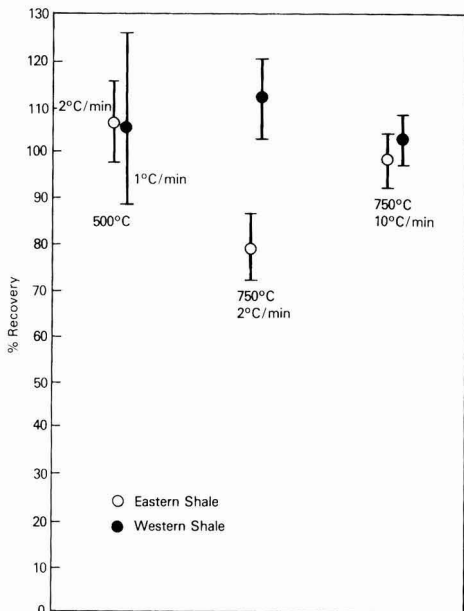


**Figure 8.** Mass balance for selenium in eastern and western shales under various retorting conditions.

gining of oil production. However, this overlap failed to cause significant differences in the mercury concentration in the eastern and western shale oils. Furthermore, the distinctly different temperatures at which the mercury was released from the eastern and western shales during retorting strongly suggest that the mercury exists in different chemical forms within the shale matrix. However, attempts to extract the raw shale failed to find any dimethyl-, diethyl-, and di-*n*-propylmercury that was easily extractable.

Redistribution of mercury into the liquid products appeared to be independent of heating rate and maximum temperature and more dependent on the shale. The mercury in eastern shale preferentially redistributed into the retort water. In western shale, the redistribution of mercury into the liquid products was less consistent; however, mercury appeared to slightly favor redistribution into the shale oil.

In general, more than 90% of the arsenic remained in the shale after retorting. The arsenic in the western shale demonstrated a greater tendency to mobilize into the liquid products than did the arsenic in the eastern shale under similar conditions. More of the arsenic is redistributed into the liquid products as higher maximum temperature and/or higher heating rates occur. The arsenic that mobilized preferentially redistributed into the shale oil rather than the retort water during retorting of eastern and western shales. No arsenic was observed in the offgas above the detection limit of the analytical method during any of the three retort runs monitored, agreeing with the mass balance results.

In general, more than 80% of the selenium remained in the shale after retorting. Redistribution of the selenium into the liquid products appeared to be independent of heating rate and maximum temperature and more dependent on the shale type. The selenium in the eastern shale slightly favored partitioning into the retort water. Selenium in the western shale preferentially partitioned into the shale oil.

## Acknowledgments

We would like to thank Elwood A. Lepel, David E. Robertson, and Ronald W. Sanders of Pacific Northwest Laboratory for their assistance with the analysis of the many samples generated during this program.

**Registry No.** Mercury, 7439-97-6; arsenic, 7440-38-2; selenium, 7782-49-2.

## Literature Cited

- (1) Fox, J. P. Ph.D. Dissertation, University of California, Berkeley, CA, 1981.
- (2) Fruchter, J. S.; Laul, J. C.; Petersen, M. R.; Ryan, P. W.; Turner, M. E. In *Proceedings of the American Chemical Society Symposium on Analytical Chemistry of Tar Sands and Oil Shale*; New Orleans, LA, 1978.
- (3) Shendrikar, A. D.; Faudel, G. B. *Environ. Sci. Technol.* **1978**, *12*, 332.
- (4) Fruchter, J. S.; Wilkerson, C. L.; Evans, J. C.; Sanders, R. W. *Environ. Sci. Technol.* **1980**, *14*, 1374.
- (5) Fruchter, J. S.; Wilkerson, C. L.; Evans, J. C.; Sanders, R. W.; Abel, K. H. Source Characterization Studies at the Paraho Semiworks Oil Shale Retort. PNL-2945; Pacific Northwest Laboratory, Richland, WA, 1979.
- (6) Fruchter, J. S.; Wilkerson, C. L. In *Oil Shale the Environmental Challenges*; Petersen, K. K., Ed.; Colorado School of Mines: Golden, CO, 1980; pp 31-63.
- (7) Girvin, D. C.; Hodgson, A. T.; Doyle, S. Energy and Environmental Division 1979 Annual Report. LBL-11486; Lawrence Berkeley Laboratory, Berkeley, CA, 1980.
- (8) Hodgson, A. T.; Pollard, M. J.; Harris, G. J.; Girvin, D. C.; Fox, J. P. Mercury Mass Distribution During Laboratory Oil Shale Retorting. LBL-12908; Lawrence Berkeley Laboratory, Berkeley, CA, 1982.
- (9) Fox, J. P. *Environ. Sci. Technol.* **1985**, *19*, 316.
- (10) Patterson, J. H.; Dale, L. S.; Chapman, J. F. *Environ. Sci. Technol.* **1987**, *21*, 490.
- (11) Olsen, K. B.; Evans, J. C.; Girvin, D. C.; Sklarew, D. S.; Nelson, C. L. Testing and Performance of the Pacific Northwest Laboratory 6-kg Retort. PNL-5055; Pacific Northwest Laboratory, Richland, WA, 1984.
- (12) Fox, J. P.; Duval, J. J.; Mason, K. K.; McLaughlin, R. D.; Bartke, T. C.; Poulson, R. E. In *Proceedings of the 11th Oil Shale Symposium*; Golden, CO, 1978.
- (13) Girvin, D. C.; Fox, J. P. *On-Line Zeeman Atomic Absorption Spectroscopy for Mercury Analysis in Oil Shale Gases*; U.S. Environmental Protection Agency, U.S. Government Printing Office: Washington, DC, 1980; EPA-600/7-80-130.
- (14) Nelson, G. O. *Rev. Sci. Instrum.* **1970**, *41*, 776.
- (15) Olsen, K. B.; Sklarew, D. S.; Evans, J. C. *Spectrochim. Acta* **1985**, *40B*, 357.
- (16) Beenakker, C. I. M. *Spectrochim. Acta* **1976**, *31B*, 483.
- (17) Sanders, R. W.; Olsen, K. B.; Weimer, W. C. *Anal. Chem.* **1983**, *55*, 1911.
- (18) Nielson, K. K.; Sanders, R. W. SAP3 Computer Program for Quantitative Multielement Analysis by Energy Dispersive X-Ray Fluorescence. PNL-4173; Pacific Northwest Laboratory, Richland, WA, 1982.
- (19) Olsen, K. B.; Evans, J. C.; Sklarew, D. S.; Girvin, D. C.; Nelson, C. L.; Lepel, E. A.; Robertson, D. E.; Sanders, R. W. Characterization of Mercury, Arsenic, and Selenium in the Product Streams of the Pacific Northwest Laboratory 6-kg Retort. PNL-5658; Pacific Northwest Laboratory, Richland, WA, 1985.
- (20) Patterson, J. H.; Dale, L. S.; Chapman, J. F. *Environ. Sci. Technol.* **1988**, *22*, 532.

Received for review July 19, 1989. Accepted October 10, 1989. This program was funded by the U.S. Department of Energy (DOE), Office of Fossil Energy through the Morgantown Energy Technology Center, Laramie Project Office, under Contract DE-AC06-76RLO 1830. Special thanks to Doug Uthus, Arthur Hartstein, Jerry Ramsey, Ted Bartke, and Carl Rosmaggi of DOE for supporting this effort.

# Effect of Hydrogen Peroxide on the Alkaline Hydrolysis of Carbon Disulfide

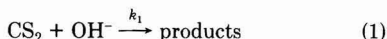
Scott Elliott\*

Department of Chemistry, University of California, Irvine, California 92717

■ The stability of carbon disulfide in aqueous alkaline solutions has been compared in the absence and presence of hydrogen peroxide, by a headspace gas chromatography technique. Reactant decay is first order in CS<sub>2</sub> and OH<sup>-</sup> in solutions containing sodium hydroxide alone. At room temperature, the second-order rate constant  $1 \times 10^{-3} \text{ M}^{-1} \text{ s}^{-1}$  matches previous measurements for basic hydrolysis and, along with the activation energy  $22 \text{ kcal mol}^{-1}$ , is consistent with rate control in a carbonate-like hydration step. In alkaline hydrogen peroxide solutions, loss is also first order in H<sub>2</sub>O<sub>2</sub>, suggesting reaction between CS<sub>2</sub> and the HO<sub>2</sub><sup>-</sup> anion with a second-order rate constant in the range  $10\text{--}100 \text{ M}^{-1} \text{ s}^{-1}$ .

## Introduction

Carbon disulfide is a raw material in xanthation, and its hydrolysis



has received attention both as a secondary step in rayon manufacture (1-3) and as a means for removal from industrial wastewater effluents (4). Hydrolysis of the related species carbonyl sulfide (OCS) has been recognized as the first quantifiable source of the hydrogen sulfides (H<sub>2</sub>S, SH<sup>-</sup>, S<sup>2-</sup>) to the open ocean (5-7), and this development has led directly to the detection of sulfide in open ocean seawater (8, 9). CS<sub>2</sub> is also a trace seawater constituent (10, 11) and, by analogy with OCS, should be evaluated as an additional sulfide source.

A recent major study of the kinetic properties of aqueous carbon disulfide over the pH range 8-11 included hydrogen peroxide as an oxidizing agent in order to convert hydrogen sulfide products to sulfate (4). CS<sub>2</sub> loss rates in ref 4 were equal to or greater than those traditionally observed at much higher pH (13-14 in ref 1-3), with characteristic decay lifetimes (*e*-folding times;  $t_{1/2}/0.69$ ) of <10 000 s. The indication is that H<sub>2</sub>O<sub>2</sub> opens carbon disulfide oxidation and removal channels alternate to hydroxide attack. In the current work, I have investigated this possibility by monitoring CS<sub>2</sub> disappearance from solutions covering a wide range of pH and peroxide concentrations. The well-known basic hydrolysis shown as eq 1 is first order in both carbon disulfide and hydroxide ion (12, 13), while a faster CS<sub>2</sub> removal process is first order in hydroxide and H<sub>2</sub>O<sub>2</sub> and likely involves the peroxide anion HO<sub>2</sub><sup>-</sup> as a nucleophile. I conclude that neither hydrolysis of carbon disulfide nor its reaction with HO<sub>2</sub><sup>-</sup> can be competitive with carbonyl sulfide as an open ocean sulfide source.

## Experimental Section

**Reagents.** All aqueous solutions were prepared from distilled deionized water saturated with helium for several hours to remove oxygen. In situations with hydroxide ion present in large excess over carbon disulfide (generally pH 12 and above), unbuffered systems were created by dilution of Fischer 10 normal sodium hydroxide. An 0.05 M potassium carbonate/borate/hydroxide mixture from Fischer Scientific was employed as a buffer in some of the pH 10

experiments. Other buffers were provided by Micro Essential Laboratories (Brooklyn, NY) and included a combination of potassium phosphate monobasic and sodium borate at pH 9, a sodium carbonate/bicarbonate mixture at pH 10, and at 11, sodium carbonate/phosphate dibasic. Detailed buffer compositions constitute proprietary information, but can be obtained on an individual basis from the manufacturer. Fischer 30% H<sub>2</sub>O<sub>2</sub> was diluted to produce the desired hydrogen peroxide concentrations. Liquid carbon disulfide was degassed on a vacuum line before the generation of vapor-phase gas chromatographic calibration curves for the quantification of CS<sub>2</sub> in the reactor headspace.

**Vessels.** Reactions were carried out in sealed, blackened 300-mL Pyrex round-bottom flasks equipped with ports for half-hole septa. Before each run, the bulbs were acid washed and rinsed several times with the deoxygenated water. In parallel with all the experiments described below, control reactions conducted in the absence of the reagents of interest ensured that CS<sub>2</sub> is stable with respect to wall losses. In fact, under conditions in the present work, no degradation was apparent over 24-h periods at any pH up to 11. A typical example of carbon disulfide stability is incorporated into Figure 1.

In setting up the runs, reactors were filled to capacity with the helium-saturated water, capped, then water removed, and reagents added with a syringe in amounts arranged to leave a 5-mL gas headspace. During these manipulations, occasional injections of helium preserved a slight internal overpressure and minimized the entry of air. Even at the highest temperatures involved in the study (41 °C in the activation energy determinations), the ratio of total CS<sub>2</sub> in the liquid to that in the vapor phase was 50, so that the headspace served only as an indicator of losses in solution and could not act as a kinetic source by replenishing the aqueous phase. Most of the runs proceeded at ambient in the laboratory (22.5 ± 0.5 °C). Other temperatures were maintained in an oven with thermostat, or in water baths.

**Procedure.** Reactions were initiated with the addition of hydroxide, peroxide, or both. The vessels were shaken at regular intervals and 500-μL samples of the headspace injected onto a gas chromatograph with thermal conductivity detection. Separation of carbon disulfide from products, including carbonyl sulfide and hydrogen sulfide, was achieved on a 5 ft × 0.25 in. stainless steel column packed with Chromosorb 102. The vapor-phase sensitivity limit corresponded to 10<sup>-5</sup> M aqueous CS<sub>2</sub>. Headspace concentrations were calibrated by comparison with vapor-phase CS<sub>2</sub> standards prepared fresh twice daily at 0.5, 1.0, 5.0, and 10.0 Torr. Prior to each sample removal, 500 μL of humidified helium was injected into the headspace, again to prevent the entry of oxygen.

Except as specified in Table I, the initial carbon disulfide concentration in all experiments was under 10<sup>-3</sup> M. Hovenkamp (3) showed that side reactions leading to the byproduct trithiocarbonate (CS<sub>3</sub><sup>2-</sup>) are restricted to ~1% at this level. All CS<sub>2</sub> decay curves were tracked over at least 1 full kinetic lifetime (until concentration had decreased by more than a factor of *e*), and in most cases 2-3, with at least five samples taken per lifetime, and in most cases, well over a dozen total. Rate constants were ex-

\* Present address: Dept. of Atmospheric Sciences, University of California, Los Angeles, CA 90024.

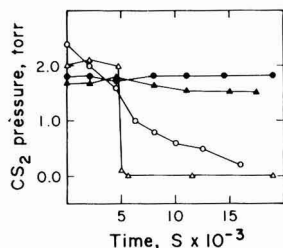


**Figure 1.** Preliminary examination of CS<sub>2</sub> loss in water alone (solid circles), 0.1 M hydrogen peroxide (solid triangles; H<sub>2</sub>O<sub>2</sub> added at time zero), 0.1 M sodium hydroxide (open circles; OH<sup>-</sup> added at time zero), and both 0.1 M hydrogen peroxide and sodium hydroxide (open triangles; H<sub>2</sub>O<sub>2</sub> and OH<sup>-</sup> added simultaneously at 5000 s).

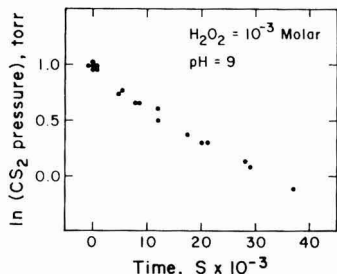


**Figure 2.** Sample CS<sub>2</sub> decay plot for hydrogen peroxide concentration 10<sup>-3.05</sup> M, in a pH 9 buffer, as tracked by the natural logarithm of headspace pressure.

**Table I.** Initial Concentrations and Reactions Rates for CS<sub>2</sub> Decay with Various Combinations of Reactants, and Rate Constants for Equations 1 and 2 in the Text<sup>a</sup>

init concn, log <sub>10</sub> M				init rate, log <sub>10</sub> M/s	rate, log <sub>10</sub> M <sup>-1</sup> s <sup>-1</sup>	
CS <sub>2</sub>	OH <sup>-</sup>	pH	H <sub>2</sub> O <sub>2</sub>		k <sub>1</sub>	k <sub>2</sub>
-3.77	-1.0	13.0		-7.73	-2.96	
-3.26	-1.0	13.0		-7.30	-3.04	
-2.77	-1.0	13.0		-6.86	-3.09	
-2.26	-1.0	13.0		-6.30	-3.04	
-3.77	-1.5	12.5		-8.14	-2.87	
-3.77	-1.0	13.0		-7.76	-2.99	
-3.77	-0.5	13.5		-7.34	-3.07	
-3.77	-0.0	14.0		-6.66	-2.89	
-3.77	-4.0	10.0	-3.36	-7.53		1.30
-3.77	-4.0	10.0	-2.88	-7.15		1.20
-3.77	-4.0	10.0	-2.50	-6.73		1.24
-3.77	-4.0	10.0	-2.36	-6.58		1.24
-3.77	-4.0	10.0	-2.05	-6.30		1.22
-3.77	-5.0	9.0	-3.05	-8.22		1.30
-3.77	-4.0	10.0	-3.05	-7.04		1.48
-3.77	-3.0	11.0	-3.05	-6.10		1.50

<sup>a</sup> All runs performed at room temperature.

tracted by interpreting CS<sub>2</sub> loss over the first *e*-folding period in pseudo-first-order terms. Linear regression was applied to plots, such as the sample shown in Figure 2, and first-order decay translated into bimolecular rate constants. Hydroxide was either buffered or present in large excess, so that its concentrations remained essentially unchanged. Nevertheless, all vessels were checked for final pH on a pH meter. Hydrogen peroxide levels exceeded those of carbon disulfide but were not always sufficient to be considered invariant. For some of the peroxide experiments, rate constants are based on H<sub>2</sub>O<sub>2</sub> concentrations averaged over 1 carbon disulfide lifetime and falling several percent below the initial values in Table I. Within this simple analysis framework, there were no significant de-

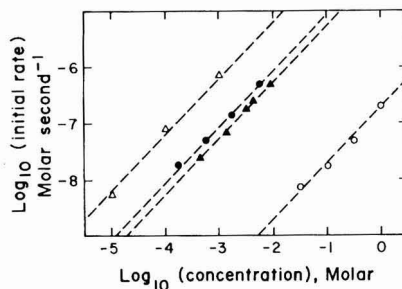


**Figure 3.** Initial carbon disulfide removal rates as functions of concentration of CS<sub>2</sub> (solid circles), hydroxide ion (open circles), hydrogen peroxide at pH 10 (solid triangles), and hydroxide ion at [H<sub>2</sub>O<sub>2</sub>] = 10<sup>-3</sup> M (open triangles). Data are from Table I.

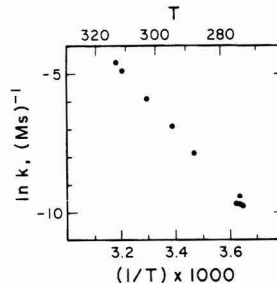


**Figure 4.** Arrhenius plot of rate constant measured for reaction 1 as a function of reciprocal temperature (Kelvin).

**Table II.** Reaction Order Determined from the Initial Rate Data in Table I

init concn, -log <sub>10</sub> M			reaction order for species varied
CS <sub>2</sub>	OH <sup>-</sup>	H <sub>2</sub> O <sub>2</sub>	
3.77-2.26	1.0		0.94 ± 0.04 (CS <sub>2</sub> )
3.77	1.5-0.0		0.97 ± 0.10 (OH <sup>-</sup> )
3.77	4.0	3.36-2.05	0.96 ± 0.04 (H <sub>2</sub> O <sub>2</sub> )
3.77	5.0-3.0	3.05	1.06 ± 0.07 (OH <sup>-</sup> )

viations from first-order kinetic behavior.

### Results and Discussion

It was readily demonstrated in a series of preliminary orientation experiments that hydrogen peroxide and the hydroxide ion operating together can remove CS<sub>2</sub> faster than either by itself. As shown in Figure 1, the disulfide survived on the order of 3-30 h in 0.1 M NaOH or 0.1 M H<sub>2</sub>O<sub>2</sub>, but disappeared instantaneously when they were combined.

**Reaction Order and Rate Constants.** In Table I, initial reaction rates are reconstructed for the headspace experiments by extrapolating the measured second-order rate constant values to time zero. A standard initial rates display is given in Figure 3. Slopes for regression of rate against varying reactant concentrations were calculated in the SPSS statistical software package. The results are summarized in Table II. None of the values differs by more than 6% from unity, and the dashed lines in Figure 3 have been fixed at unit slope to emphasize this point.

Earlier studies have implied that uptake of carbon disulfide by pure hydroxide solution is first order in CS<sub>2</sub> and OH<sup>-</sup> (e.g., ref 12 and 13). Table II verifies the conclusion over wide concentration ranges. The simplest choice for rate-determining step is eq 1 leading to the dithiocarbonate species (CS<sub>2</sub>OH<sup>-</sup>, CS<sub>2</sub>O<sup>2-</sup>; ref 3 and 4). In both this work

**Table III. Temperature Dependence of Rate Constant for Hydroxide Attack on CS<sub>2</sub>**

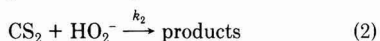
T, °C	init concn, log <sub>10</sub>		k <sub>1</sub> , log <sub>10</sub> M <sup>-1</sup> s <sup>-1</sup>
	CS <sub>2</sub>	OH <sup>-</sup>	
41.0	-3.77	-1.0	-1.99
39.0	-3.77	-1.0	-2.12
30.5	-3.77	-1.0	-2.56
22.5	-3.77	-1.0	-2.96
15.0	-3.77	-1.0	-3.42
2.0	-3.77	-1.0	-4.22
2.0	-3.77	-1.0	-4.27
2.0	-3.77	-1.0	-4.20
2.0	-3.77	-1.0	-4.10

**Table IV. Selected Rate Constants and Activation Energy (E<sub>a</sub>) Measurements for Hydration of Carbon Dioxide, Carbonyl Sulfide, and Carbon Disulfide**

	k(298)	E <sub>a</sub> range, kcal	ref
CO <sub>2</sub> + H <sub>2</sub> O	0.03 s <sup>-1</sup>	16-19	14-17
CO <sub>2</sub> + OH <sup>-</sup>	10 <sup>4</sup> M <sup>-1</sup> s <sup>-1</sup>	5-13	14-17
OCS + H <sub>2</sub> O	2 × 10 <sup>-5</sup> s <sup>-1</sup>	20-23	6, 18
OCS + OH <sup>-</sup>	13 M <sup>-1</sup> s <sup>-1</sup>	12-14	6, 19
CS <sub>2</sub> + H <sub>2</sub> O	<<10 <sup>-5</sup> s <sup>-1</sup>		4, this work
CS <sub>2</sub> + OH <sup>-</sup>	10 <sup>-3</sup> M <sup>-1</sup> s <sup>-1</sup>	20-23	1-3, 12, this work

(Table I) and Hovenkamp (3), the rate constant  $k_1$  (referring to eq 1) is near  $1 \times 10^{-3} \text{ M}^{-1} \text{ s}^{-1}$  at room temperature. Some temperature-dependent data are listed in Table III, and the Arrhenius diagram in Figure 4 yields an activation energy of  $22.0 \pm 0.5 \text{ kcal mol}^{-1}$ . Several related investigations have been conducted on the two-phase liquid system of water/CS<sub>2</sub>, making direct comparisons difficult, but  $k_1$  values seem to fall in the range  $10^{-4}$ – $10^{-2} \text{ M}^{-1} \text{ s}^{-1}$  (1, 2), and the energy barrier between 20 and 21 kcal mol<sup>-1</sup> (1, 12). In Table IV the rate constant and its temperature dependence are placed in the context of hydration along the sequence CO<sub>2</sub>, OCS, and CS<sub>2</sub> (14–19). Carbon dioxide and carbonyl sulfide are known to hydrate to carbonate and monothiocarbonate, respectively (14, 19). The regularity in  $k$  decrease and energy increase with the addition of sulfur atoms along the sequence is thus consistent with rate control by eq 1, and with carbonate-like initial products. It is interesting to note that activation energy differences alone are sufficient to account for the spread in Table IV rate constants for hydroxide attack (CO<sub>2</sub>, OCS, or CS<sub>2</sub> + OH<sup>-</sup>). This may simply be a reflection of electrophilicity changes at the carbon center.

The hydrogen peroxide runs are also collected in Tables I and II and Figure 3. Initially, pH was fixed at 10 and the peroxide concentration varied; then in separate experiments at pH 9, 10, and 11, the peroxide concentration was set at  $8.8 \times 10^{-4} \text{ M}$ . In all these cases, the contribution from the eq 1 basic hydrolysis was negligible. In the presence of a combination of hydrogen peroxide and hydroxide, the rate of CS<sub>2</sub> loss is proportional to both. The rate law  $-d[\text{CS}_2]/dt = k[\text{CS}_2][\text{H}_2\text{O}_2][\text{OH}^-]$  suggests an elementary interaction between CS<sub>2</sub> and the hydrogen peroxide conjugate base HO<sub>2</sub><sup>-</sup>



via the acid-dissociation  $\text{H}_2\text{O}_2 = \text{H}^+ + \text{HO}_2^-$  ( $K_{a1} = 2 \times 10^{-12}$ , ref 20). The rate constants listed for reaction 2 in Table I are calculated from the rate expression  $k_2[\text{CS}_2] - ([\text{H}_2\text{O}_2]K_{a1}/[\text{H}^+])$ , and range from 15 to  $30 \text{ M}^{-1} \text{ s}^{-1}$ . The speed of the HO<sub>2</sub><sup>-</sup> attack relative to hydroxide should not

be surprising. Peroxide anion is the archetypal  $\alpha$  nucleophile (21, 22), and is 1–3 orders of magnitude more reactive than OH<sup>-</sup> in organic substitutions (23, 24).

Adewuyi and Carmichael (4) did not monitor carbon disulfide loss directly, but rates can be estimated through a sulfur mass balance from data on intermediates such as sulfide or dithiocarbonate or from their Table I. An intermediate  $k_2$  value of  $20 \text{ M}^{-1} \text{ s}^{-1}$  for eq 2 yields a CS<sub>2</sub>  $e$ -folding period on the order of 5–5000 s in their room-temperature experiments ( $[\text{H}_2\text{O}_2] = 0.05 \text{ M}$ ; pH 8–11), roughly comparable to the observed turnover. It therefore seems likely that the reaction with HO<sub>2</sub><sup>-</sup> played an important role in the ref 4 experiments. I have not attempted to identify products in the present work, but by analogy with the hydration series in Table IV, dithiopercarbonate (CS<sub>2</sub>O<sub>2</sub>H<sup>-</sup>, CS<sub>2</sub>O<sub>2</sub><sup>2-</sup>) might be expected initially, and stoichiometries also point to sulfide, elemental sulfur, or perhaps polysulfides. It does not seem to be mechanistically obvious that dithiocarbonate should be included in the list. Reaction 2 may not be capable of explaining an absorption maximum obtained at 272 nm and corresponding to that of dithiocarbonate (4).

**Application to Seawater.** At 20 °C and the seawater pH of 8, Adewuyi and Carmichael (4) reported a CS<sub>2</sub> lifetime ( $e$ -folding time) of  $\sim 5 \text{ h}$ , roughly equivalent to time scales estimated by Elliott et al. (6) for hydrolysis of carbonyl sulfide to the hydrogen sulfides in open seawater. If reaction 1 were responsible with sulfide as product, CS<sub>2</sub> and OCS would hold similar significance as oceanic sulfide sources, because their concentrations in seawater are both on the order of 10 pM (10). However, hydrogen peroxide concentrations in the surface ocean are generally below micromolar (25), so that the specific rate constants  $k_1$  and  $k_2$  derived in this work give oceanic time scales of years or longer for both eq 1 and 2. The channels converting CS<sub>2</sub> to dithiocarbonate in the Adewuyi and Carmichael experiments may be distinct and remain to be considered.

**Summary.** Several groups have now investigated the reaction between aqueous carbon disulfide and the hydroxide ion (1–4). An elementary step which is first order in both species has the rate constant  $10^{-3} \text{ M}^{-1} \text{ s}^{-1}$  (22.5 °C) and an activation energy of 20–23 kcal mol<sup>-1</sup>. Analogy with Arrhenius parameters for hydration of CO<sub>2</sub> and OCS supports the unit reaction orders, and also the assignment of dithiocarbonate as an initial metastable product. Decay of the disulfide is augmented when peroxide is added to the system. I have observed a reaction between CS<sub>2</sub> and the HO<sub>2</sub><sup>-</sup> anion with a rate constant on the order of  $10$ – $100 \text{ M}^{-1} \text{ s}^{-1}$ , consistent with the  $\alpha$  nucleophile effect. Neither OH<sup>-</sup> nor HO<sub>2</sub><sup>-</sup> attack occurs rapidly enough in the sea to compete with hydrolysis of carbonyl sulfide as a source of the hydrogen sulfides.

**Registry No.** CS<sub>2</sub>, 75-15-0; H<sub>2</sub>O<sub>2</sub>, 7722-84-1; NaOH, 1310-73-2.

#### Literature Cited

- (1) Cherkasskaya, P. M.; Pakshiver, A. B.; Kargin, V. A. *J. Appl. Chem. USSR* 1953, 26, 55–60.
- (2) Schmiedeknecht, H. H.; Claus, W. *Z. Phys. Chem. (Leipzig)* 1969, 240(5–6), 411–416.
- (3) Hovenkamp, S. G. *J. Polym. Sci., Part C* 1963, No. 2, 341–355.
- (4) Adewuyi, Y. G.; Carmichael, G. R. *Environ. Sci. Technol.* 1987, 21, 170–177.
- (5) Johnson, J. E. *Geophys. Res. Lett.* 1981, 8(8), 938–940.
- (6) Elliott, S.; Lu, E.; Rowland, F. S. *Geophys. Res. Lett.* 1987, 14(2), 131–134.
- (7) Dyrssen, D. Sulfide Complexation in Surface Seawater. Submitted for publication in *Mar. Chem.*
- (8) Krahforst, C. F.; Cutter, G. A. *EOS Trans. AGU* 1987, 68(16), 339.

- (9) Cutter, G. A.; Oatts, T. J. *Anal. Chem.* **1987**, *59*, 717-721.
- (10) Andreae, M. O. In *The Role of Air-Sea Exchange in Geochemical Cycling*; Buat-Menard, P., Ed.; Reidel: Dordrecht, The Netherlands, 1986; pp 331-356.
- (11) Toon, O. B.; Kasting, J. F.; Turco, R. P.; Liu, M. S. *J. Geophys. Res.* **1987**, *92*(D1), 943-963.
- (12) Philipp, B. *Faserforsch. Textiltech.* **1955**, *6*, 433.
- (13) Vermaas, D. *Chem. Weekbl.* **1958**, *54*, 33.
- (14) Kern, D. M. *J. Chem. Educ.* **1960**, *37*, 14-23.
- (15) Johnson, K. S. *Limnol. Oceanog.* **1982**, *27*(5), 849-855.
- (16) Magid, E.; Turbeck, B. O. *Biochim. Biophys. Acta* **1968**, *165*, 515-524.
- (17) Pinsent, B. R.; Pearson, L.; Roughton, F. J. *Trans. Faraday Soc.* **1956**, *52*, 1512-1520.
- (18) Thompson, H. W.; Kearton, L. F.; Lamb, S. A. *J. Chem. Soc.* **1935**, 1033-1037.
- (19) Philipp, B.; Dautzenberg, H. Z. *Phys. Chem. (Leipzig)* **1965**, *229*, 210-224.
- (20) Evans, M. G.; Uri, N. *Trans. Faraday Soc.* **1949**, *45*, 224.
- (21) Edwards, J. O.; Pearson, R. G. *J. Am. Chem. Soc.* **1962**, *84*, 16.
- (22) Aubort, J. D.; Hudson, R. D. *Chem. Commun.* **1970**, 937.
- (23) Jencks, W. P.; Carriuolo, J. *J. Am. Chem. Soc.* **1960**, *82*, 1778.
- (24) Pearson, R. G.; Edgington, D. N. *J. Am. Chem. Soc.* **1962**, *84*, 4608.
- (25) Moffett, J. W.; Zika, R. G. *Mar. Chem.* **1983**, *13*, 239-251.

*Received for review February 3, 1988. Revised manuscript received August 9, 1988. Accepted June 29, 1989. This study was supported by United States Department of Energy Grant ATO3-73ER-70126.*

## CORRESPONDENCE

### Comment on "Homogeneous Hydrolysis Rate Constants for Selected Chlorinated Methanes, Ethanes, Ethenes, and Propanes"

SIR: The comprehensive study of the reactions of C<sub>1</sub>-C<sub>3</sub> chloroaliphatic compounds with OH<sup>-</sup> and H<sub>2</sub>O by Jeffers, Ward, Woytowitch, and Wolfe (1) represents a substantial contribution to our understanding of the rates and pathways by which these compounds undergo dechlorination in aqueous solution. However, we are writing to clarify an apparent discrepancy (1) between some of the data from the Jeffers et al. study and data from our own work (2).

In discussing their results, Jeffers et al. (1) compare their kinetic data on the dehalogenation of 1,2-dichloroethane (1,2-DCA) in water at neutral pH with ours (2). In their paper, Jeffers et al. (1) state, "For the neutral reaction, Barbash and Reinhard found ... [a] 37-year half-life at 25 °C [which] is about half our 72-year calculated value". The estimated half-life obtained by Jeffers et al. for 1,2-DCA at 25 °C was based on experiments conducted in dilute HCl (3). The data that they quote from our work, however, include the effect of 0.05 M phosphate buffer (0.025 M Na<sub>2</sub>HPO<sub>4</sub> + 0.025 M KH<sub>2</sub>PO<sub>4</sub>) on the reaction rate. When

we extrapolated our rate constants to zero buffer concentration, we obtained an estimated half-life for 1,2-DCA at 25 °C of 64 years (2), in close agreement with the 72-year estimate calculated by Jeffers et al. (1) and the 72-year value computed (2) from the data of Ehrenberg et al. (4).

The foregoing example illustrates the importance of accounting for the potential influence of phosphate buffers on the rates of dehalogenation of haloaliphatic compounds in aqueous solution.

**Registry No.** 1,2-DCA, 107-06-2; chloromethane, 74-87-3; chloroethene, 75-01-4; chloropropane, 26446-76-4.

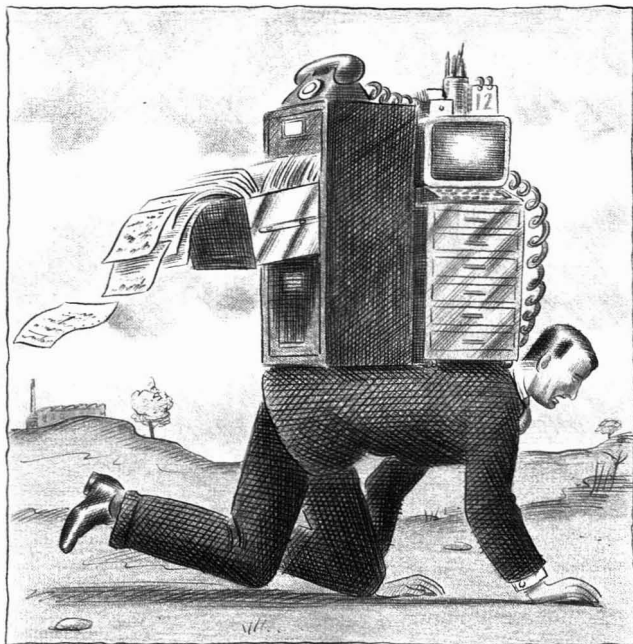
#### Literature Cited

- (1) Jeffers, P. M.; Ward, L. M.; Woytowitch, L. M.; Wolfe, N. L. *Environ. Sci. Technol.* **1989**, *23*, 965-969.
- (2) Barbash, J. E.; Reinhard, M. *Environ. Sci. Technol.* **1989**, *23*, 1349-1358.
- (3) Jeffers, P. M., personal communication (9/18/89).
- (4) Ehrenberg, L.; Osterman-Golkar, S.; Singh, D.; Lundqvist, U. *Radiat. Bot.* **1974**, *15*, 185-194.

**Jack E. Barbash,\* Martin Reinhard**

Department of Civil Engineering  
Stanford University  
Stanford, California 94305

# How to make your reporting requirements less of a burden



Compiling OSHA and EPA reports can be back-breaking work — though not if you have a Bruel & Kjaer gas monitor with hard-copy output.

Our Multi-gas Monitor Type 1302 is ideal for occupational hygiene applications. It monitors up to five toxic gases simultaneously and calculates values like TWA and STEL automatically. At 9 kg (20 lbs), it's half the weight of similar monitors — perfect for spot checks on the shop floor or in storage areas. What's more, an extensive

memory and computer interface make it equally useful for area and emission monitoring.

For larger monitoring networks, there's the Bruel & Kjaer Toxic-gas Monitor Type 1306, which offers both high reliability and unattended operation. Software is available to let you control up to 31 of these single-gas monitors from a personal computer.

Detection thresholds for both units are low: typically less than 1 ppm. Their wide dynamic range lets you monitor continuously, even during peak emission periods. And with both systems, data can be stored, printed or

plotted to meet your reporting requirements.

Call today for full details.



Type 1306



Type 1302

**Brüel & Kjær**   
Brüel & Kjær Instruments, Inc.

HEAD OFFICE: 185 Forest Street · Marlborough · MA 01752-3093 · (508) 481-7000 · TWX: 710-347-1187 · Fax.: (508) 485-0519

WORLD HEADQUARTERS: DK-2850 Nærum · Denmark · Telephone: +45 42 80 05 00 · Telex: 37316 bruks dk · Fax: +45 42 80 14 05 / +45 42 80 21 63

Australia (02) 450-2066 · Austria 02235/7550\*0 · Belgium 02-242 97 45 · Brazil (011) 246-8149/246-8166 · Canada (514) 695-8225 · Finland (90) 80 17 044  
France (1) 64 57 20 10 · Federal Republic of Germany 04106/70 95-0 · Great Britain (01) 954-2366 · Holland 03402-39994 · Hong Kong 5-487486 · Hungary (1) 133 83 05/133 89 29  
Italy (02) 52 44 141 · Japan 0423-62-3631 · Republic of Korea (02) 554-0605 · Norway 02-90 44 10 · Portugal (1) 65 92 56/65 92 80 · Singapore 225 8533 · Spain (91) 268 10 00  
Sweden (08) 711 27 30 · Switzerland (042) 65 11 61 · Taiwan (02) 713 9303 · USA (508) 481-7000 · Local representatives and service organisations world-wide

CIRCLE 1 ON READER SERVICE CARD

# P.E.T. ORGANICS. NOW YOU CAN FINALLY SEE HOW YOUR LAB COMPARES.

Only the new P.E.T. Organics Program from APG gives you a measure of importance. For the first time, Analytical Products Group, who has operated the only interlaboratory Performance Evaluation Program in the country for the past seven years, is extending this valuable service to include the GC and GC/MS 600 Series Methods.

By using the P.E.T. Organics standards, you can evaluate the performance of your laboratory against other labs throughout the country. With blind samples at two levels, the P.E.T. Program has the ability to evaluate your



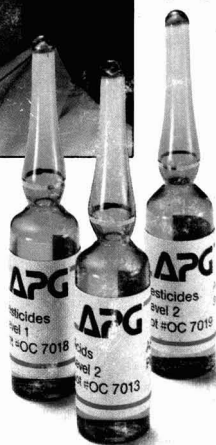
laboratory fairly and impartially. Our summary reporting format gives you the answers you need while maintaining complete confidentiality.

The P.E.T. Program works. More than 500 laboratories throughout the U.S. and Canada use this program as their external QA source. The addition of P.E.T. Organics for Volatiles, Acids, Base/Neutrals, and

Pesticides brings you a new level of control in the important area of Quality Assurance for Organic Analysis.

To put the P.E.T. Organics Program to work for you, order your first standards set today. Contact Analytical Products Group, Inc., 2730 Washington Blvd. Belpre, OH 45714.

**Toll-free**  
1-800-272-4442  
(In Ohio:  
1-614-423-4200,  
FAX: 1-614-423-5588)



**APG**  
Analytical Products Group, Inc.

The measure of quality

CIRCLE 7 ON READER SERVICE CARD

**APG Analytical Products Group, Inc.**

Customer Code: 9736  
parameter: Benzene

your Result:  
Spike Value:  
Mean of Reporting Laboratories:  
Actual Standard Deviation:  
Number Reporting Laboratories:  
Average Reporting Deviation:  
Your % Recovery:  
Your Result was:  
Deviations from the Mean:  
Comment:

parameter: 1,2 Dichlorobenzene

your Result:  
Spike Value:  
Mean of Reporting Laboratories:  
Actual Standard Deviation:  
Number Reporting Laboratories:  
Average Reporting Deviation:  
Your % Recovery:  
Your Result was:  
Deviations from the Mean:  
Comment:

Spike Compounds

Level	ug/L	Level 2
10.000		56.000
8.960		54.280
9.501		58.112
2.073		15.159
52		48
106.040		107.060
111.607		103.169
0.241		0.139

Page: 1